Functional Plasma Treatments for Nylon 6 and Regenerated Cellulose

Richard Harry Thompson

Submitted in accordance with the requirements for the degree of
Doctor of Philosophy

The University of Leeds
Department of Colour Science, School of Chemistry

September 2020

The candidate confirms that the work submitted is his own and that appropriate credit has been given where reference has been made to the work of others.

Acknowledgements

I would like to thank my supervisor, group members, friends, and family for their endless support, encouragement, and kindness throughout my PhD studies.

Firstly, I am extremely thankful and pay my gratitude to my supervisor Prof. Long Lin for his continued generous support and guidance. I would like to thank Long for providing me with a wealth of opportunities, knowledge, and exposure to invaluable research experiences.

I express my sincere gratitude to the University of Leeds for providing the funding for my project and making the entire PhD possible through the Henry Ellison Scholarship.

I would like to thank all of my colleagues in the Department of Colour Science, including Dr Daniel Hall and Dr Qi Meng for their regular friendly chats, optimism, and advice. Additionally, thanks to Trevor Lambourne for initially introducing me to the Department and providing continual support throughout my time at Leeds, Algy Kazlauciunas for helping with some technical analyses, and Dr Natalia Sergeeva for her suggestions and guidance.

I would like to show my appreciation to Prof. Anne Neville and Dr Chun Wang in the Institute of Functional Surfaces (School of Mechanical Engineering), Dr Ben Johnson in the School of Physics, Dr Mark Isaacs and Dr David Morgan at HarwellXPS, and Dr Chris Pask in the School of Chemistry for kindly assisting with the surface analysis in my project. I would also like to thank and acknowledge the hard work and patience of Dr Alexander Kulak in helping me with microscopy.

Finally, a special thanks to my family and girlfriend Yue, for their endless encouragement, inspiration, and unconditional support throughout my studies.

Abstract

Three plasma processes and their corresponding surface modifications to nylon 6 plastic sheets and regenerated cellulose films have been studied extensively in this research: plasma activation, plasma etching, and the surface grafting of functional monomers via plasma-enhanced chemical vapour deposition. The study has enabled the effects of plasma-surface interactions to be explored for different polymer structures, gaining insight into the mechanisms of plasma action occurring, and for the control of parameter over the different processes to be achieved.

Through the use of capacitively coupled, low-frequency, low-pressure oxygen plasma, plasma activation was shown to incorporate polar oxygen functionalities into the surface structures of the nylon 6 sheets, and to a lesser extent the regenerated cellulose films, increasing the surface wettability. Examples of such functional groups included -C-OH, -C=O and -COOH. However, plasma activation did not alter the surface morphology. In comparison, it was found that the plasma etching process led to an increase in surface roughness of both studied materials, alongside a simultaneous surface-chemical activation process, resulting in a substantial increase in surface wettability for both substrates. Furthermore, the grafting of the versatile functional monomer hexamethyldisiloxane (HMDSO) onto nylon 6 and regenerated cellulose substrates via plasma-enhanced chemical vapour deposition was achieved and characterised, having used HMDSO directly in comparisons to gaseous mixtures of HMDSO:O_2 in the ratio of 1:6. Grafted co-polymer films with both hydrophobic (HMDSO) and hydrophilic (HMDSO:O_2) properties were obtained.

In addition to these activation, etching, and surface grafting processes, the phenomenon known as post-plasma treatment “hydrophobic recovery” or “ageing” was also investigated for the nylon 6 and regenerated cellulose materials, both in terms of wettability and surface-chemistry. The wettability and surface energies of the sample surfaces were shown to decrease over time due to a reduction in surface-oxygen concentration.

Table of Contents

List of Figures

List of Tables

List of Equations

List of Terms and Acronyms

ZDHC	Zero Discharge of Hazardous Chemicals
LPP	Low-Pressure Plasma
DBD	Dielectric Barrier Discharge
APPJ	Atmospheric-Pressure Plasma Jet
CCP	Capacitively Coupled Plasma
ICP	Inductively Coupled Plasma
HMDSO	Hexamethlydisiloxane
WCA	Water Contact Angle
FWHM	Full Width Half Maximum
DPPH	2,2-diphenyl-1-picrylhydrazyl
FT-IR	Fourier Transform Infrared
SEM	Scanning Electron Microscopy
EDX	Energy Dispersive X-ray
XPS	X-ray Photoelectron Spectroscopy
AFM	Atomic Force Microscopy
SSIMS	Static Secondary Ion Mass Spectrometry
DSC	Differential Scanning Calorimetry
XRD	X-ray Diffraction
TGA	Thermogravimetric Analysis
RF	Radio Frequency

1. Introduction

Currently, processing and manufacturing industries for plastic and textile products are facing increasing challenges to produce more resource-efficient processes. This is necessary due to industrial demands to reduce costs, coupled with increasingly restrictive legislative requirements, particularly when considering the environmental impacts of material processing.[1] For these reasons, there is a push towards finding 'greener' procedures and avoiding the use of water, chemicals and energy; the waste from processing needs to be minimised as much as possible, or preferably, completely eradicated. For example, in the textile industry, the Zero Discharge of Hazardous Chemicals (ZDHC) foundation is pushing for these changes, with aims to advance towards zero discharge of hazardous chemicals (particularly fluorocarbons), to improve the environment and to protect consumers and workers.[2] In addition to these challenges, the textile industry is seeing greater demands in providing innovative, high quality products with technical advantages. Such products involve textiles with functional properties such as flame retardancy, hydrophobicity/stain resistance, hydrophilicity/wettability and anti-microbial capabilities.[1] Likewise, there is an equally prevalent desire to produce a wide variety of plastics with these functional properties, for example in the packaging, electronics, construction and automotive industries.[3-5]

Plasma treatment methods are existing technologies that show promise within the plastic and textile industries to be used in the modification of a range of materials with various synthetic and bio-derived origins; they are often considered as "substrate-independent".[6] Plasma treatments can impart desired characteristics onto material substrates without the use of water and with minimal use of chemicals.[7] However, there are still gaps of knowledge in current studies about the specific surface chemistry taking place on the plasma-treated materials, particularly when considering quantitative models of plasma action, and the effects of different plasma discharges on material surfaces. In part, these gaps in the knowledge exist due to the rapid development of innovative, commercially available plasma systems with

unique setups. Furthermore, much of the work that has so far been carried out on surface modifications has had issues with reproducibility, due to the variable nature of plasma generation amongst many plasma systems, particularly in terms of gas flow (this is discussed further in Section 1.1). Therefore, significant improvements are required in the fundamental understandings of the surface chemistry taking place.

In this research, a range of methods utilising different plasma treatments were designed and employed in the surface modifications of nylon 6 plastic sheets and regenerated cellulose films, to provide a range of desired properties that can be applied to both the plastic and textile industries. The surface chemistry of modified nylon 6 and regenerated cellulose was investigated extensively, and quantitative characterisations of the chemical and physical changes induced by plasma processes were undertaken to provide a mechanistic study of plasma action. The extent to which plasma-treatments can be considered as “substrate-independent” was also explored.

1.1 Plasma

Often considered ‘the fourth state of matter’, plasma has unique properties which make it ideal to be used for activating and modifying material surfaces.[8] The term plasma refers to an ionised gas, containing a mixture of reactive species (including radicals), electrically charged particles that are not bound to either an atom or a molecule, and UV radiation. Within a typical plasma, the electron density is balanced by positive ions; it is considered electrically neutral.[9] The abundance of free electrically charged particles make plasma electrically conductive and responsive to electric fields. Plasma is generated from the exposure of a substance in the gaseous state to high energy from either heating, or more commonly the presence of an electric field.[9] It is extremely versatile due to its ability to process a range of different gases/reagents/precursors. Unlike more traditional wet-chemical methods, plasma processing is not limited by the reactivity of different substances at given temperatures/conditions, and does not require any pre-treatment to the surface. Typically, gases used in the plasma treatment of polymers are either classified as ‘polymerising’ or ‘non-polymerising’; polymerising gases are

typically monomeric precursors, which induce a graft-polymerisation process onto the surface of textiles during plasma treatment.[10] Commonly used examples include fluorocarbons, hydrocarbons and silicones. Non-polymerising gases can either be reactive, with the ability to functionalise polymer surfaces through the attachment of new functional groups, or non-reactive, whereby chemically inert gases are used to etch samples without incorporating new functional groups. Both reactive and non-reactive non-polymerising gases etch the surface through particle bombardment, with examples of reactive gases including oxygen and nitrogen, and non-reactive gases including argon and helium.[10]

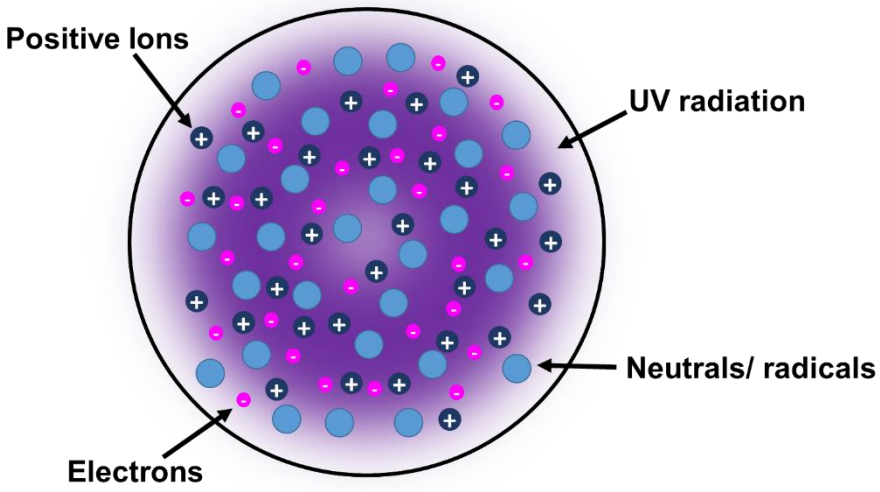

Figure 1-1. The typical species within a plasma gas.

Plasma can generally be categorised into one of two groups: thermal or non-thermal/non-equilibrium/low-temperature/cold. Thermal plasmas can be artificially generated using laser, radiofrequency (RF) or microwave discharges at near atmospheric pressure, but require significantly high temperatures (often above 1000°C).[11] Polymer/textile materials cannot withstand these conditions, therefore non-thermal plasmas are employed due to their non-destructive nature. Non-thermal (or cold) plasmas are formed when a thermodynamic equilibrium is not reached between the electrons and other higher mass reactive species present. They are useful for treating

plastics and textiles, which are essentially heat sensitive polymers, as they can activate and induce morphological changes to the surface without causing any changes in the bulk properties of the material.[10]

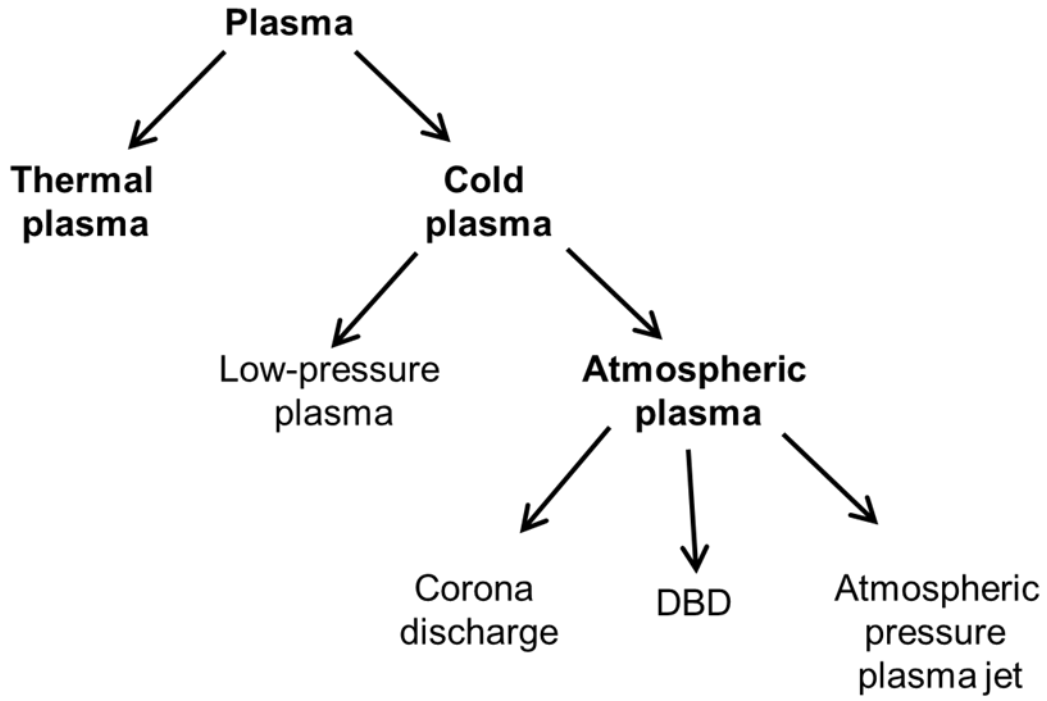

Figure 1-2. The classifications of plasma type.[12]

One of the main types of non-thermal/non-equilibrium plasma technologies utilised in the textile industry is low-pressure plasma (LPP). The low-pressure method offers various distinct advantages such as uniform glow, the ability to generate non-thermal plasma, and the ability to generate a high concentration of reactive species in a set treatment chamber.[7] The major disadvantage of low-pressure plasma is that it is a batch process, so the continuous processing of polymer materials is not possible, with the vacuum systems required also being expensive to generate and difficult to scale-up.[13]

Atmospheric plasma is another non-thermal plasma technology that can be used to modify textile surfaces, and has three common methods of plasma generation:[14] (1) Corona discharge uses two electrodes of differing shapes and sizes, with an applied high voltage of 10-15 kV and a low-frequency used to generate the plasma.[14] (2) Dielectric barrier discharge (DBD) is a method

in which one of the electrodes is covered in a dielectric layer which accumulates a charge on its surface. This gives an even distribution of charge over the electrode during the plasma generation.[15] (3) Atmospheric pressure glow discharge or atmospheric pressure plasma jet (APPJ) generates plasma through a nozzle using a low voltage and high frequency.[15] Each of the atmospheric plasma technologies have several advantages, including the ability to work at atmospheric pressure, and the ability to process materials continuously. However, acquiring an even finish on polymers can be difficult due to the inability to generate uniform gas flow, and even though the process is non-thermal, relatively high temperatures (between 200 - 300°C) are still required for atmospheric plasmas, meaning that they are often unsuitable for plastics/textiles.[14] The type of treatment used for each process varies depending on the desired function of the material.

1.1.1 Oxygen plasma

The species present in oxygen plasma have been well established through the use of optical emission spectroscopy in previously reported studies.[16-18] Oxygen plasma gas typically consists of free electrons, neutral O radicals, excited species, metastables, and UV radiation. More specifically, these include neutral oxygen molecules in the metastable states $a^1\Delta_g$ and $b^1\Sigma_g^+$, (with excitation energies of 0.98 and 1.63 eV respectively[18]), neutral oxygen atoms in the $O(^3P)$ ground state, and neutral oxygen atoms in the excited states, $O(^1D)$ and $O(^1S)$, with excitation energies of 1.96 and 4.17 eV respectively.[19] Additionally, oxygen plasma also contains positively charged O_2^+ ions (the ionisation energy of O_2 is 12.07 eV)[20], and negatively charged O^- and O_2^- ions. Ozone (O_3) is also produced in plasma discharges, but is generally less reactive than the O atoms, which are more important in the surface functionalisation of polymers.[21] Reported rate constants for reactivity of ozone with polypropylene surfaces were 10^{-22} cm^3 s^{-1} compared with O atoms which had a rate constant of 10^{-11} cm^3 s^{-1}. These rate constants were determined through the use of computational modelling of phase kinetics.[22]

In addition to neutral O radicals, species that are suitable for altering the surface structures of polymers that are exposed to oxygen plasma are singly-

charged O_2^+ ions, negatively charged free electrons (e^-) and O^-/O_2^- anionic species. The density of negatively charged oxygen ions tends to be similar to that of the free electrons.[23] Both the cationic and anionic reactive particles diffuse into the gaseous plasma and collide with other gaseous particles, with collisions between the positive and negative ions leading to neutralisation; these collisions can either happen in the gas phases, or on surfaces. The predominant charge neutralisation mechanism at high pressure is three-body collisions in the gas phase, whereby the energy is shared between the colliding particles.[17] At low pressures, there are multiple neutralisation mechanisms. These include dissociative collisions between positively charged O_2^+ ions and electrons, and radiative neutralisation between positively charged molecules colliding with electrons. These neutralisations mechanisms can be described as[24]:

Three-body recombination:	$O^+ + e^- + M \rightarrow O + M$
Dissociative recombination:	$O_2^+ + e^- \rightarrow (O_2^*)_{unstable} \rightarrow O + O$
Radiative recombination:	$O^+ + e^- \rightarrow O + hv$

Where *M* represents a third body such as an electron or ion. These mechanisms are also visualised in Figure 1-3. When the pressure is decreased below 100 pa, the dominant mechanism is based on reactions between the charged species and (polymer) surfaces through heterogeneous surface recombination. The excess energy is absorbed by the material during these collisions, which can lead to heating of the substrate.[25] Under these low-pressure conditions, the probability for the neutralisation of positively charged species by collisions with the surface is close to 100%, and the gas-phase reactions become negligible as the mean-free path of the gaseous plasma species approaches the dimension of the plasma chamber.[16] The $a^1\Delta_g$ and $b^1\Sigma_g^+$ metastable states mentioned earlier are either quenched or pumped away from the plasma system before relaxation by radiation occurs.

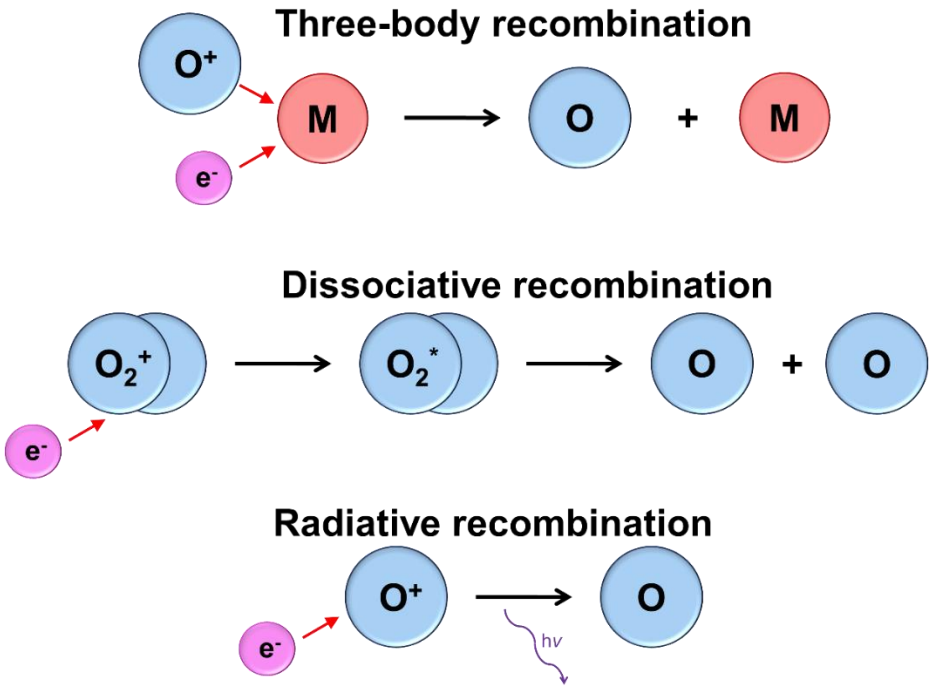

Figure 1-3. The three main recombination/neutralisation mechanisms for oxygen plasma species.[24]

At atmospheric pressure, the gas-phase collisions become the predominant mechanism of neutralisation, meaning that a large proportion of the reactive species are lost before they can react with the surface. These reactive species are lost through three-body collisions that fulfil the requirements for energy and momentum conservation.[26] This means that there is a general inability to form uniform atmospheric plasmas, hence, they are not suitable for providing reproducible surface finishes for polymers/textiles.[27]

For non-thermal/non-equilibrium plasmas, the concentration of oxygen species present depends on the type of discharge used, the discharge power, frequency, gas pressure, volume/shape of plasma chamber and type of material being exposed to the plasma.[28] Direct current (DC) glow discharges are often avoided due to non-uniformity at pressures that are suitable for treating polymers, with the exception of corona DC discharges, which are operated at ambient pressure. However, non-uniformity of surface treatments is still an issue with these treatments.[29] Alternating current (AC) discharges are more suitable for polymers, and generally produce more uniform plasmas.

In non-equilibrium plasma systems, the fluence (dose) of O atoms typically ranges between 10^{20} and 10^{23} m^{-2} s^{-1}. Fluence can be defined as the product of the exposure time and flux of reactive particles onto a material surface, where the flux is defined according to Equation 1.1.[30]

$$j_a = \frac{1}{4} n_n \langle v \rangle$$

Equation 1.1. The flux of oxygen atoms onto a polymer surface.[30]

Whereby j_a is the flux of neutral O atoms onto a polymer surface, n_n is the density of neutral particles in the plasma and $\langle v \rangle$ is the average random velocity of the O atoms, according to the Boltzmann distribution. The atom density, n_n, can be measured experimentally using catalytic probes, while $\langle v \rangle$ is assumed to be:

$$\langle v \rangle = \sqrt{\frac{8 k_B T}{\pi m}}$$

Equation 1.2. The average random velocity of oxygen atoms in a non-equilibrium plasma.[30]

Where k_B is the Boltzmann constant, T is the gas temperature and m is the mass of the gas particle (16 Da for oxygen). Both the flux and exposure time can have an effect on the different reactions observed between oxygen plasma and polymer surfaces.[16]

1.1.2 Plasma system configurations

A/C high-frequency generators operate from a few kHz (radiofrequency) to several GHz (microwave), and "electrodeless" discharges where the electrodes are placed outside of the plasma chamber are usually preferred in plasma processing, as they prevent sputtering of the electrode material that can contaminate the polymers during treatment.[31] Radiofrequency (RF) discharges are popular for the treatment of polymers as they have been shown to provide desired surface finishes such as enhanced wettability.[32]

Classical discharge configurations incorporate a powered electrode and grounded electrode into the walls of the plasma chamber. When an asymmetric discharge is applied, an electric field develops across the sheath next to the powered electrode and differences in the mobility of the ions and electrodes cause the powered electrode to DC self-bias. This means that the powered electrode has a negative bias for the majority of the RF cycle, but becomes positive for a small portion of this cycle. This causes the positive ions to accelerate in the field next to the powered electrode, hence causing the unwanted sputtering effect when the electrode is inside the plasma chamber.[29] For this reason, RF “electrodeless” configurations are superior. They tend to have either capacitive configurations (CCP), with two electrodes outside of the plasma chamber, or with inductive (ICP) configurations, whereby a coil (or two coils connected serially) is connected to the outside of the plasma chamber. Both CCP and ICP configurations have a limited voltage applied to either the electrodes or the coils, to avoid pronounced heating of the dielectric chamber.[33]

Microwave discharges are formed in metallic cavities, but the electromagnetic field generated does not penetrate deep into the electrically conductive plasma. This is because electromagnetic waves propagate perpendicularly to the metallic vessel walls, and attenuate rapidly from the source. This means that microwave discharges are generally limited to small volumes unless the gas pressure is low enough to enable diffusion of charged particles - therefore, they are generally unsuitable for treating and processing polymers.[17]

1.1.3 Low-frequency plasma

The use of low-frequency (40 kHz) plasmas for the treatment of polymer and textile materials under low-pressure have a range of advantages, but have generally not been employed extensively in previous studies due to the systems having only been developed and sold commercially in recent years, with few reports of the surface-chemical modifications induced by low-frequency plasmas. A major advantage of low-frequency plasma is that it is the most inexpensive form of plasma generation, as it requires the lowest

amount of energy to generate, hence being the most environmentally friendly.[34] The treatments are also robust, multiple electrodes/carrier racks can be fitted into the systems to achieve high throughput, and systems also have lower coating rates in plasma polymerisation processes compared to more commonly applied 13.56 MHz (RF) or 2.45 GHz (MW) frequencies, enabling the formation of thinner functional films.[35] The low-frequency plasmas also generate a higher ion density than do the higher RF or MW frequencies, which increases the uniformity of the plasma treatments.[36]

Current studies that have reported the use of low-frequency plasmas concern the plasma treatment of poly(methyl methacrylate) foil, nylon 6 foil and polypropylene foil with oxygen and nitrogen gas for the immobilisation of biomolecules (a further application of plasma treatments). The immobilised biomolecules included mouse immunoglobulin G antibodies labelled with both gold nanoparticles and latex beads. The study showed that both oxygen and nitrogen plasmas increased the surface roughness, and mainly focussed on the optimisation of plasma parameters (power, time, gas composition) in achieving the highest immobilisation efficiency. However, the study did not consider the surface-chemical modifications induced by the different plasma gas treatments in great detail. It was also reported that all of the polymer materials degraded upon exposure to the oxygen and nitrogen plasmas for more than 10 min.[37] A separate reported application of low-frequency plasma was in the treatment of multi-walled carbon nanotube fillers with low-pressure oxygen plasma, to increase the surface free energy of the material surfaces for better compatibility with rubbers, leading to better dispersion. The carbon nanotube fillers can be used to improve the mechanical and electrical properties of these elastomer materials. The low-frequency oxygen plasma treatment resulted in an increase in surface energy compared to the untreated nanotubes, due to the incorporation of polar moieties (C=O, O-H) into the surface structure of the carbon nanotubes that was determined through XPS. The parameters selected in this report also resulted in modifications to the microstructures of the nano-fillers.[38] The low-frequency plasma treatment of polyester and polyamide fabrics with acrylic acid monomer vapour plasma was also reported, with the treatment increasing the hydrophilicity and wrinkle-

recovery angles of the fabrics; there was no reported surface-chemical analysis to rationalise these observations.[39] A similar report of the increase in hydrophilicity of wool fabric following low-frequency oxygen plasma was also presented, again without analysis of the functional groups incorporated by the plasma species.[40] Much of the focus of low-frequency plasmas has been placed on the applications of the treatments, with little emphasis placed on the specific surface chemical and morphological modifications, and their corresponding mechanisms of action. This provided an opportunity to provide insights into the mechanism taking place through the plasma treatments of some common polymers in this research.

1.1.4 Plasma activation

Plasma activation, also known as 'plasma functionalisation' or 'plasma grafting', refers to the alteration of (polymer) surfaces, through the incorporation of hydrophilic functionalities into the surface structure; this procedure is typically used as a prerequisite for applying coatings or paints to plastics, and can also be applied in the textile industry as a pre-treatment before the application of functional coatings. This has the effect of increasing the surface energy, hence increasing the affinity of coatings and adhesives to the surface.[41] Both atmospheric and low-pressure cold plasmas are suitable for activating textile surfaces, due to both processes having the ability to create reactive bonding sites on substrate surfaces from the highly reactive plasma species containing electrons, atoms, ions, and radicals.[42] The generation of these reactive bonding sites can enable functional groups from the gaseous species to be grafted onto the surface, whilst also producing bond scission and cross-linking effects. The extent to which each of these effects occurs largely depends upon the choice of plasma gas.[43]

Non-polymerising gases are used to achieve plasma activation, and in many cases oxygen plasma gas is employed. The surface molecules of the polymer/textile substrate react with the oxygen plasma to form functionalities such as carbonyl, carboxyl and hydroxyl groups. Gas molecules are adsorbed onto the surface, where they react with surface radicals to form these polar

groups, which increase the surface energy of the substrate.[44] Other gases such as air, nitrogen, ammonia and fluorine and can also be used to functionalise polymer/textile surfaces, all of which attach different functionalities to the surface, hence providing opportunity to a range of potential treatments for material surfaces.[45]

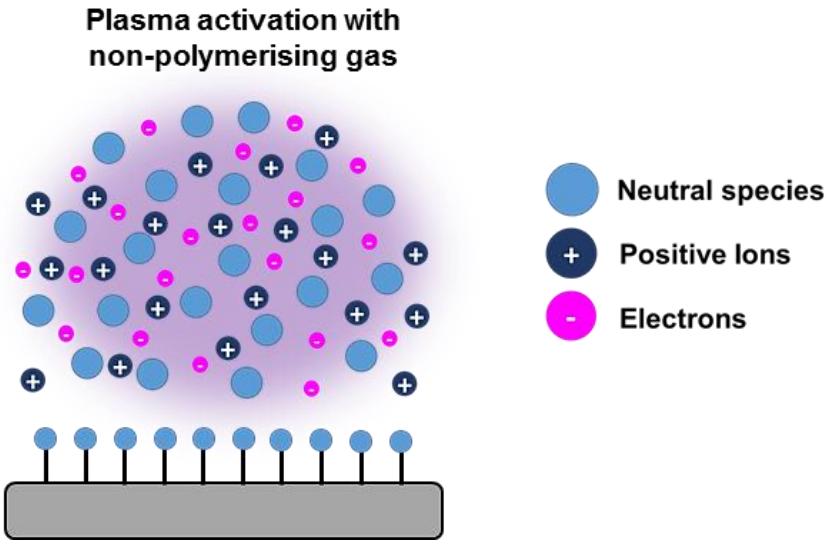

Figure 1-4. General schematic showing the surface plasma activation of a polymer using a reactive non-polymerising gas plasma.[10]

There have been reports of an atmospheric-pressure plasma jet being used to achieve surface activation, avoiding any undesired etching/bombardment of the surface, whilst providing an optimum surface wettability.[29, 45-47] A high-impedance, low-frequency atmospheric discharge plasma in wet argon was used on PET surfaces, with oxygen-rich carbonyl, carboxylic acid, and hydroxyl groups being incorporated into the polymer chains, hence activating the surface (the specific positions of the newly-incorporated groups on the PET polymer chains were not elucidated). It was shown that increasing the distance between the PET samples and the glowing plasma discharge resulted in the level of surface activation being reduced by up to two orders of magnitude.[47] This highlights the problems associated with APPJ plasmas, with simple variations in treatment such as the increase in distance between the plasma nozzle and the substrate having a dramatic effect on the resultant surface modification. This inability to provide uniform treatments onto the surface emphasises the suitability of the low-pressure plasma method over

the APPJs for producing reproducible treatment conditions, which are essential for developing fundamental mechanisms of plasma action.[29, 47]

There is a ‘shelf-life’ associated with activated polymeric materials, meaning that upon exposure to atmospheric conditions the material undergoes an ageing process following plasma treatment. This is generally attributed to the oxygen being released or reoriented away from the surfaces of the material; however, the mechanism of action of this process is not widely understood.[48] Theories relating to this release and the so-called “ageing” effects are discussed in more detail in Section 1.2.

1.1.5 Plasma activation of polymers with oxygen plasma

With regard to functionalisation of polymers with oxygen plasma, numerous authors have studied the activation of polyolefins such as polyethylene and polypropylene, due to their simple structures with no oxygen-containing functional groups in the untreated material.[22] Treatments involving plasma activation with oxygen initially occur through functionalisation of the uppermost layer of the polymer surface with polar oxygen groups such as -OH, -C=O and –C-C=O, with the subsequent penetration of the oxygen species to deeper layers of the polymer substrate.[27] Such processes have reported an increase in oxygen content on polyolefin surfaces of up to 24%, as detected by XPS.[49] Functionalisation is faster with atmospheric plasmas when compared to low-pressure plasmas, while plasma jets have a tendency to deposit traces of metal oxides due to sputtering of the electrode material.[32]

It is generally accepted that the functionalisation process with oxygen plasma proceeds through initiation, propagation and termination steps. Initiation starts through hydrogen abstraction from the surface polymer chain by the gaseous oxygen plasma radical species, which leads to the generation of free radicals on the surface. These free radicals then further react with the oxygen species (including O_2 and O_3) to form peroxy or alkoxy radicals. Peroxy radicals have the ability to subtract hydrogen from neighbouring sites on the same polymer chain, or from different polymer chains to form hydroperoxides, which can then decompose to form various oxidised functionalities. Alkoxy radicals can

produce alcohol groups, or induce chain scission that can lead to the formation of ketones, aldehydes or carboxylic acids. Termination occurs by reactions between hydrogen atoms and OH from the gas phase with other radicals, as they form more stable end products.[22]

1.1.6 Plasma etching

Plasma etching is the result of bombarding polymer surfaces with charged plasma species; typically, non-polymerising gas plasmas are used in these processes.[11] The bombardment of these particles etches the material surface on the nanoscale, through a physical sputtering process to increase the surface roughness. Low-pressure plasma has the ability to etch materials using this method, through generating a high plasma density in the chamber, converting outer layers of the material surface into the gas phase. The etched material is sucked up and removed by the vacuum system, while fresh gas is introduced. This can be considered as a “continuous extraction”.[50] The plasma gas consists of a mixture of highly reactive species, with the majority of the energy generated by the plasma field being transferred to electrons. These high energy electrons undergo collisions with molecules in the plasma system to form atoms, ions and radicals through processes including ionisation, excitation and fragmentation. The high energy of these reactive species enables the plasma to undergo further reactions, including the dissociation and scission of a wide variety of chemical bonds.[51] Unlike plasma activation, etching occurs when adsorbed plasma species react with the surface to form volatile molecular fragments (etch products), which subsequently desorb from the surface, convert back into the plasma gas phase and are eliminated out of the chamber through pumping alongside the process gases.[52] Plasma etching generally requires longer treatment times than plasma activation procedures, due to etching being intended for the removal of several hundreds of nanometres of surface material, rather than just chemically functionalising the surface.[53]

When considering the mechanism of plasma etching, it is important to distinguish between physical etching and chemical etching, which is governed

by the plasma gas/gas combinations utilised. Physical etching is achieved when using inert gases such as argon, and results in the ion bombardment of the polymer surfaces through directional momentum transfer that causes physical sputtering of atoms, with poor selectivity. Chemical etching involves the use of reactive gas plasmas such as oxygen, and proceeds through the transport of the reactive species through diffusion, with subsequent reactions with substrate atoms.[54] Chemical etching is isotropic because the diffusion of reactive species occurs in all directions, with good selectivity. At higher pressures, plasma etching is primarily controlled by the neutral plasma species (excited atoms, excited molecules and metastables) as the ion energies are low. In comparison, in low-pressure conditions, etching is also controlled by the ions, whereby the reactive ions can react with, and subsequently remove the surface material. The evenness or "spread" of surface etching obtained across a polymer surface is largely determined by the uniformity of the plasma composition, the gas flow and the geometry of the reactor/plasma chamber. Any variation in the degree of etching across a surface can be overcome by maintaining a constant gas flow and uniform plasma density, which prevents the localised depletion of gas phase radicals.[55] A general schematic of the plasma etching of a polymer surface is presented in Figure 1-5.

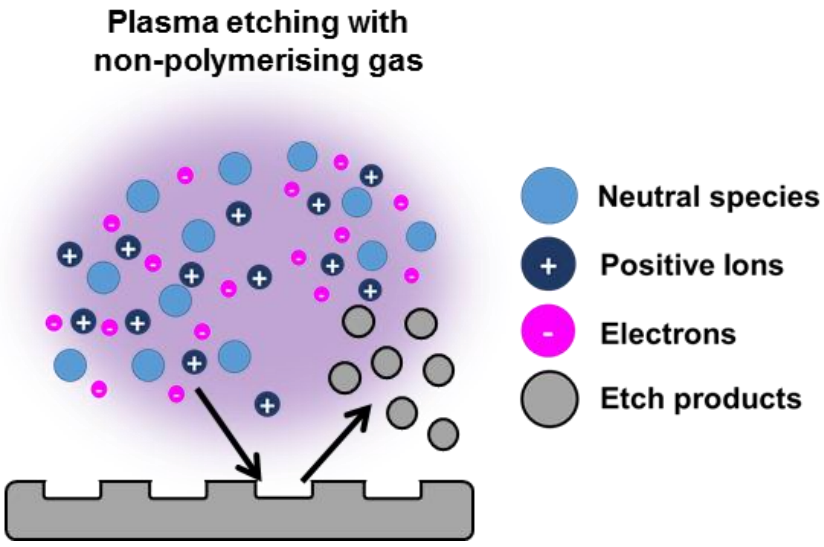

Figure 1-5. The effects of plasma etching using a non-polymerising gas plasma.[10]

1.1.7 Plasma etching of polymers with oxygen plasma

When polymers are exposed to oxygen plasma, there are several effects that the sample can be subjected to, all of which are dependent on the parameters such as gas flow, discharge type, discharge power and treatment time. These effects include attachment of polar groups containing oxygen (such as hydroxyl/carbonyl), destruction of the polymer sub-surface by UV and or VUV (vacuum ultraviolet) radiation, chemical etching by O atoms (molecular and atomic), and physical effects caused by the heterogeneous surface recombination of oxygen atoms and bombardment of positively charged ions. These effects are all exothermic, which results in the treated polymer being heated during the process, hence making over-treatment a possibility.[30]

Oxygen plasmas are commonly employed in the etching of polymer materials, due to their abilities to simultaneously functionalise the substrate whilst also removing some of the surface material. The main species that are responsible for the etching process in oxygen plasmas are atomic oxygen free radicals that have the ability to initiate etching through breaking bonds and abstracting hydrogen from the hydrocarbon backbones of polymers. When reacting with saturated hydrocarbons, atomic oxygen forms hydroxyl groups and radical sites, and forms unsaturated hydrocarbons and phenols when reacting with aromatic hydrocarbons. The newly formed radical sites can then react with molecular oxygen which leads to bond scission of polymer backbone chains, rather than forming new functional groups.[56]

In addition to oxygen radicals, other energetic species such as ions, metastables and photons can also etch polymer surfaces. The typical energies of ions range from 20 eV to several hundred eV, which is high enough to induce chain rupture of polymer backbones. The energies of metastable species are also typically several times higher than most polymer bond energies, and UV and VUV radiations both have higher energies than ionisation potentials of polymers, meaning that these species can also break bonds within polymer structures, leading to etching of the surface.[54]

1.1.8 Grafting of functional monomers via plasma polymerisation

Through the use of low-pressure plasma systems, thin polymer films can be coated onto material surfaces through surface grafting by plasma polymerisation. This process is also known as plasma-enhanced chemical vapour deposition. Generally, volatile monomer gases are dosed into the plasma chamber as precursor molecules, which can polymerise when they are exposed to plasma, converting the gaseous monomers into solid coatings through crosslinking. These precursor monomer gases are fragmented when exposed to the plasma, forming radicals which react with each other and are deposited on the material surface to form a thin film.[57] Often, secondary carrier gases such as oxygen or nitrogen are also used in conjunction with the monomer to ensure that the monomer is spread evenly throughout the plasma chamber, hence forming a homogenous thin film across the substrate surface.[58] A general schematic of this grafting process is displayed in Figure 1-6.

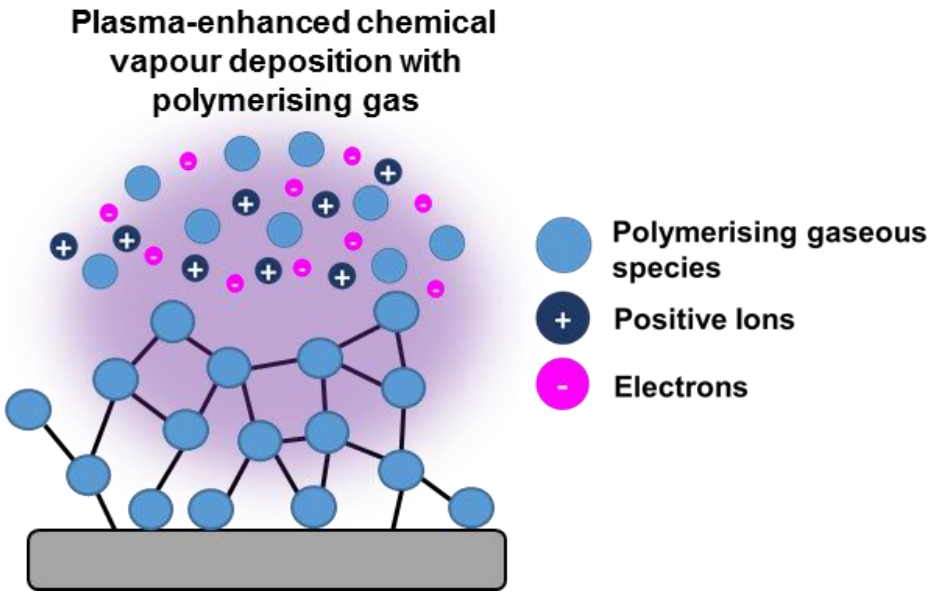

Figure 1-6. The grafting of monomers via polymerising gas plasma.[10]

Atmospheric plasma jets containing mixtures of carrier gas/monomer can also be used to impart functional properties onto material structures, but typically require higher temperatures around 150°C.[59] The properties and potential applications of the thin films formed are determined by the chemical structure and nature of the monomers gases used. Examples of such monomer gases and their various applications are discussed in Section 1.5. The thickness of the films formed is typically in the range of 10-50 nm, (5-30 molecular layers).[60]

1.1.9 Plasma polymerisation utilising hexamethyldisiloxane (HMDSO) plasmas

The use of plasma polymerisation for depositing HMDSO organo-silicon thin films is an increasingly attractive method for functionalising surfaces, due to their wide-ranging practical applications, including generating/improving hydrophobicity, transparency, high scratch resistance and anti-corrosive properties.[61] In the textile industry, plasma polymerised silicon-based films offer an opportunity to replace fluoropolymer treatments for hydrophobicity, as fluoropolymer coatings can break down easily into carcinogenic/toxic compounds such as perfluorooctane sulphonic acid (PFOS) and perfluorooctanoic acid (PFOA).[62] The siloxane coatings can exhibit superhydrophobicity on textiles, with contact angle values of up to 150°. This superhydrophobicity occurs when the non-polar methyl groups of siloxane films are coated on the inherently rough microstructures of knitwear and non-woven surfaces, giving them a comparable performance to fluorinated coatings.[63] HMDSO deposited coatings also generally have good resistance to washing, making them a suitable candidate for textile finishing.[64] The chemical structure of HMDSO is shown in Figure 1-7.

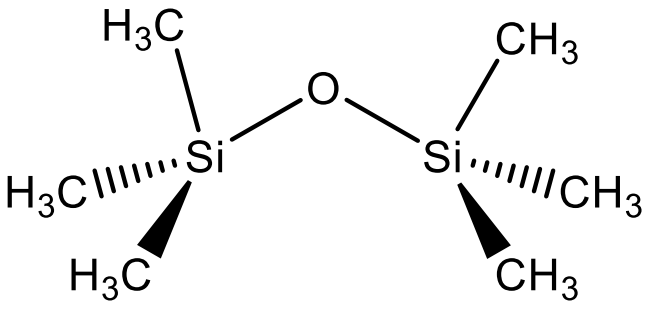

Figure 1-7. The chemical structure of hexamethyldisiloxane (HMDSO).

Traditionally, organosilicon films are prepared through wet chemical methods, such as hydrolysis and ring-opening polymerisations of dimethyltrichlorosilane and hexamethylcyclotrisiloxane. However, these processes typically yield films that are thick and lack uniformity.[65] HMDSO is a liquid precursor that is frequently employed in plasma treatments due to its high vapour pressure and low toxicity. Hence, it serves as a model precursor for studying plasma polymerisation processes, for better understandings of plasma-surface interactions with polymerising gases. Upon ignition of the plasma, hydrogen abstraction from the C-H bonds (with an energy of 3.5 eV) and to a lesser extent abstraction of the methyl groups from the Si-CH_3 bonds (with an energy of 4.6 eV) occur. These abstractions arise due to electron impact dissociation in the HMDSO molecules.[66] This dissociation has activation energies that are greater than the C-H and Si-C bond energies due to the excitation of the HMDSO molecules. However, many of the fragments formed from these abstractions are found in the gas phase, but have a low reactivity with surfaces in the formation of films, as they form stable volatile compounds. Dissociation of the higher energy Si-O bond (8.3 eV) produces $(CH_3)_3$–Si–O· radicals that have a high affinity for film growth on surfaces. Additionally, the dissociation of the Si-O bond also yields a second $(CH_3)_3$–Si· radical.[67] These radicals are generally less reactive, as studies using tetramethylsilane (TMS) in which the $(CH_3)_3$–Si· radical is prevalent have shown the radical to have lower deposition rates than the $(CH_3)_3$–Si–O· radical.[68] Furthermore, it is assumed that the $(CH_3)_3$–Si· radicals are displaced by the $(CH_3)_3$–Si–O· radicals at the deposited growing film surface due to its stronger bond formation. These radicals are largely responsible for the growth of siloxane films on polymer

surfaces, with the retention of the methyl groups resulting in hydrophobic properties.[66]

The use of pure HMDSO in plasma processes leads to the formation of soft, polymer-like coatings due to an increased content of methyl and methylene groups in the siloxane films. Adding non-reactive carrier gases such argon or helium has the effect of increasing homogeneity and stability of the plasma species, hence resulting in more homogenously deposited films; they are considered as energy-carrying gases.[69] On the other hand, co-reactive gases to the HMDSO such as oxygen can reduce the amount of C and H content through the formation of volatile H_2O and CO_2 molecules, with resultant transparent and hard films with inorganic SiO_x structures being deposited.[70] To form inorganic SiO_2 quartz like deposits, a HMDSO:O_2 ratio of 1:12 would generally be expected, to satisfy the equation[66]:

$$(CH_3)_3–Si–O–Si–(CH_3)_3 + 12O_2 \rightarrow 2SiO_2 + 6CO_2 + 9H_2O$$

For this reason, there is an interest in investigating the properties of films deposited from different gas ratios of HMDSO:O_2 mixtures. One study varied the HMDSO:O_2 from 1:18 (excess oxygen) to 1:3 (oxygen deficiency) using a capacitive radiofrequency discharge (13.56 MHz), with the higher oxygen content mixtures (>1:6) forming hard, quartz-like deposits, with the oxygen deficient mixtures forming more polymer-like structures with higher carbon content.[61] Oxygen can be considered as an energy consuming co-monomer. Increasing the atomic oxygen content can result in ion bombardment of the hydrocarbons within the HMDSO structures, hence etching the deposited films. The HMDSO plasma species undergo fragmentation due to electron and oxygen radical collisions during the treatments. However, there are still gaps in the knowledge of how co-reactive gases such as oxygen affect the plasma polymerisation process, and resultant films obtained.[71]

1.2 Ageing of plasma-treated materials

A major disadvantage of reactive gas plasma treatments (such as oxygen, nitrogen or air) of polymer materials is the deterioration of treatment level/functionalisation level of the materials over time; this is known as the ageing phenomenon, or hydrophobic recovery. This effect can limit the practical applications of the plasma treatments that are used in the hydrophilisation of polymers. Several theories have been postulated to explain this phenomenon, including the thermodynamically driven reorientation of polar groups away from the surface and into the bulk material, through rotations of the polymer chains. This has the effect of reducing the surface from a high energy state to a lower energy state.[72]

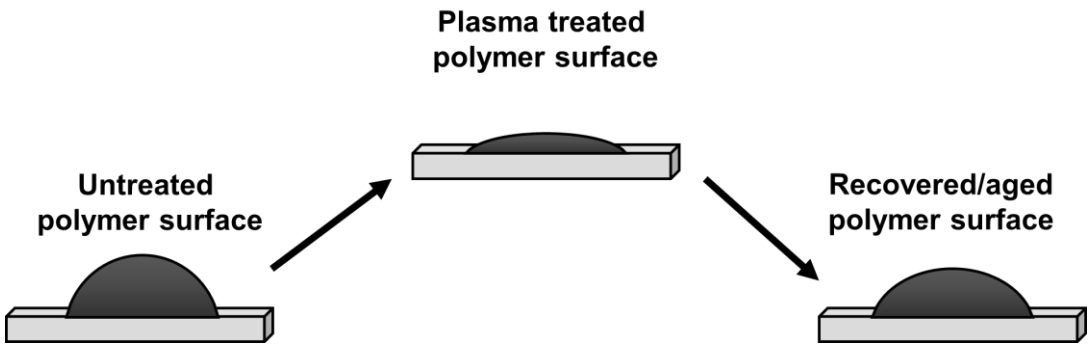

Figure 1-8. Schematic showing the plasma treatment and subsequent ageing of a treated polymer surface through contact angle measurements.[73]

Further explanations for the ageing phenomenon include the migration of low molecular weight, non-polar species from the bulk material to the surface of the polymer, airborne surface contamination, the desorption of low molecular weight oxidised materials into the atmosphere, or contamination due to improper storage conditions.[74] The ageing can be considered as a relaxation process, in which the surface functionalities rearrange to lower the surface energy to a thermodynamically favourable lower energy state. Contact angle measurements prove to be an effective technique in monitoring the hydrophobic recovery of polymers, due to the resulting changes in surface energy caused by the migration and rotations of polymer chains. Following

plasma activation or etching processes with non-polymerising gases such as oxygen or nitrogen, the general decrease in contact angle (and increase in hydrophilicity) observed for treated polymers tends to increase with time following this ageing process, due to this thermodynamically driven lowering of the surface energy of the substrate. This process is shown in the schematic in Figure 1-8.[73]

Previous studies have shown that the composition of plasma gas employed influences the degree of ageing observed, with treatments of poly(ethylene terephthalate) (PET) being commonly reported. One study observed that oxygen functional groups (-C=O, -COOH, -C-OH) formed on the surface of plasma-treated PET polymers treated with oxygen plasma (DBD atmospheric discharge) tended to decay when stored under ambient conditions. 10 days of ageing led to a decrease in oxygen concentration of up to 8%, with an increase in water contact angle of 15.9°. Longer treatment times resulted in better stability in the PET surfaces, hence a lower rate of surface hydrophobic recovery. It was postulated that this could be attributed to a better penetration of oxygen into the subsurface layers of the material when exposed to plasma for prolonged periods.[46] Other reports of treatments for PET included using both helium and oxygen RF plasmas (CCP discharge). These treatments showed an initial increase in O/C ratio for both gases following treatment, with the oxygen plasma treated samples showing a significant hydrophobic recovery with a rapid decrease in O/C ratio in the first few days following treatment. This hydrophobic recovery was also observed in the helium plasma treated PET, but interestingly, the rate of ageing was much slower than that of the oxygen plasma-treated samples.[46] Contradictory to these previously mentioned articles, it was also reported that when PET samples were treated with oxygen RF plasma (CCP discharge), samples that had shorter treatments times underwent slow ageing/hydrophobic recovery processes. When stored under ambient conditions, the measured WCA measurements for these treated PET samples reached that of the original untreated PET (73°) after storage for approximately one month, rather than a number of days. However, when the samples were stored in distilled water, the ageing was significantly reduced over long periods of time, with a maximum contact angle of 33°

reached.[75] These results have proven to be inconsistent with other findings, whereby the hydrophobic recovery of PET was actually reported to have accelerated when stored in distilled water following treatment with oxygen RF plasma.[28]

1.3 Nylon 6

1.3.1 Properties and uses

Nylon 6/polyamide 6/poly(hexano-6-lactam)is a polymer consisting of aliphatic polyamide repeat units, with characteristic -NHCO- linkages (Figure 1-9).[76] It is produced from the hydrolytic or catalytic ring opening polymerisation of caprolactam to produce epsilon-aminocaproic acid. This then condenses to form high-molecular weight polymers of nylon 6 repeating units at high temperatures under vacuum.[77] Nylon 6 has a glass transition temperature of 48°C and a melt temperature of 214°C.

Worldwide demand for nylon 6 has been increasing in recent years, due to growth in several markets including packaging, textiles, and engineering plastics, that utilise the desirable properties of the material including high tensile strength, wrinkle/abrasion resistance, and high elasticity.[78] However, unmodified nylon 6 cannot meet all demands for some modern applications such as technical textiles that require functional coatings. This is often due to problems such as poor surface wettability, which leads to difficulties when applying coatings, in addition to issues with conventional applications involving painting, printing, and bonding.[79] Therefore, understanding the fundamental interactions between plasma gases and popular processing/textile materials such nylon 6, and the extent of the modifications attained are crucially important to the development and optimisation of plasma treatments for industrial processing.[80]

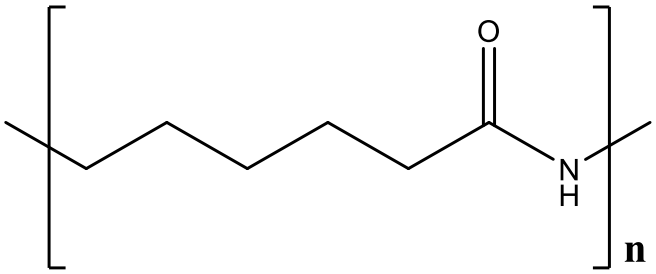

Figure 1-9. The chemical structure of the nylon 6 repeating unit.

1.3.2 Plasma treatments of nylon 6

Generally, across the literature there are few detailed reports of the plasma treatment of nylon 6, particularly with the use of CCP low-frequency, low-pressure oxygen plasma. Previous studies of plasma treatments on nylon 6 have primarily focused on fibres, with emphasis placed on modifications to mechanical (tensile, shearing, bending, compression), air permeability, and thermal properties.[81] Similarly, parameter optimisations for the use of plasma activation in applications such as preparing nylon 6 foil surfaces for the immobilisation of proteins have been performed, but with little focus on the modifications to the chemical structures of the nylon 6 surface polymer chains on the surface.[37] Reports of oxygen plasma being used in combinations with other gases such as helium in atmospheric pressure plasma jets have shown modifications to the surface morphology and surface chemistry of nylon 6 fibres and films, demonstrating the general abilities of oxygen/helium plasma combinations to increase the surface roughness and attach polar groups to the surface. These studies of atmospheric plasma treatments provided more insight into the surface-chemical modifications obtained through XPS analysis.[82-83] However, the lack of available literature providing detailed surface-chemical and morphological analyses of oxygen plasma treated nylon 6 for mechanistic understandings of plasma action on the polymer structure made it a suitable candidate for studying plasma action in this research. Furthermore, the simple aliphatic polyamide structure of nylon 6 provided an ideal material for studying surface-chemical modifications induced by the oxygen plasma, with the opportunity to treat ideal, flat nylon 6 plastic sheet surfaces with low-frequency oxygen plasma.

1.4 Regenerated cellulose

1.4.1 Properties and uses

Regenerated cellulose polymers are made up of repeating glucose units that are connected through β-1, 4 covalent glycosidic linkages (Figure 1-10). They are manufactured by dissolving cellulose in carbon disulphide in the presence of sodium hydroxide to obtain sodium cellulose xanthate. The sodium cellulose xanthate is then neutralised using sulphuric acid, giving regenerated cellulose or viscose.[84] The regenerated cellulose polymers can then be processed in different ways to give rise to several applications. For example, polymer spinning can form fibres that can be used for textiles, and polymer casting can produce films that can be subsequently used for food packaging or medical devices.[85] Interestingly, in the field of materials science, cellulose is often used as a reference material in XPS analysis, as it is non-contaminating and has a spectroscopically well-defined structure.[86]

Regenerated cellulose proves to be an inherently versatile material, due to its properties such as mechanical strength and chemical stability.[85] Furthermore, the biodegradability and wide availability of cellulose also make it an environmentally attractive material for commercial use.[87] However, due to the complexity of the cellulose polymeric network, and the amphiphilic character of the structure, the material is notoriously difficult to process using chemicals,[88] which gives way for solvent-free, dry processing methods such as plasma treatments to be introduced, for the aforementioned applications in textiles, food packaging and medical devices.[89] The majority of research that has been carried out on the plasma treatment of cellulosic materials has focused on cotton fabrics. However, fibre surfaces are notoriously difficult to analyse, as they are non-ideal and variable in nature, making films a better choice for mechanistic studies of plasma action.

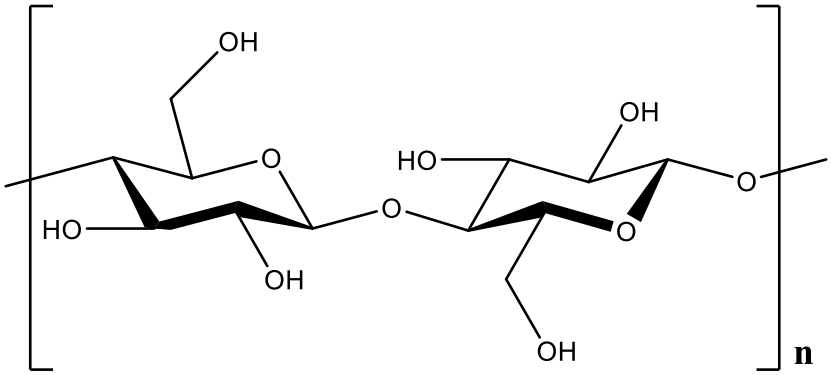

Figure 1-10. The chemical structure of the regenerated cellulose repeating unit.

1.4.2 Plasma treatments of cellulose

Similarly to nylon 6, there are few studies reporting the effects of treating regenerated cellulose with oxygen plasma, particularly with low-frequency plasma. However, there have been numerous reports studying the oxygen plasma treatment of cellulosic materials such as cotton, primarily focussing on specific applications of the treatments such as an increase in wicking ability, air permeability and improvements in dyeing efficiency.[90-91] The use of different gas combinations with oxygen have also been described, with surface-chemical analyses of air plasma treated cotton fabrics with a glow discharge having reported the incorporation of C–O, C=O, and O–C=O groups using XPS analysis, with SEM imaging also showing the formation of cracks and nanopores on the surfaces of the fibres. Mass loss measurements of the cotton samples also showed that plasma treatment resulted in a mass loss of 4.5 % following 10 mins of treatment.[92] A study on the microwave (2.46 GHz) oxygen plasma treatment of cellophane foils revealed that the surface roughness of the samples increased with increasing treatment time through SEM and AFM imaging, and also noted that surface decomposition of surface macromolecules led to the formation and nucleation of crystals on the surfaces of the samples that were exposed for treatment times between 480 s and 640 s. XPS analysis of the plasma-treated cellophane foils also showed that the polymer chains had decomposed and underwent oxidation reactions, forming aldehyde carboxylic acid groups.[93] Regenerated cellulose provides an opportunity to study an ideal model surface for studying plasma processes,

in which fundamental understandings of low-frequency plasma processing can be developed through studying the chemical and morphological modifications obtained. The observed principles can be subsequently transferred onto cellulosic textiles such as cotton or viscose.

1.5 Applications of plasma treatments for polymers and textiles

1.5.1 Fire/flame retardancy

Incorporating fire/flame retardant properties into both polymer (for building materials) and textile materials is desirable for general public safety, in addition to many specific applications such as safety workwear. The effective plasma treatment of cotton fabrics has been reported utilising an atmospheric plasma jet with helium as a carrier gas and oxygen as a reactive gas at a radio frequency of 13.56 MHz. The plasma jet was used to graft a formulation containing the well-known fire retardant organic phosphorous compound N-methylol dimethylphosphonopropionamide to the cotton surface. The plasma surface activation process was carried out in the presence of a phosphoric acid catalyst, a melamine resin cross linking agent and a nano-titanium dioxide co-catalyst, which promoted the grafting procedure.[9]

Further methods of applying fire retardant finishes to cotton have also been reported. They involve the plasma induced graft polymerisation of various acrylate monomers containing phosphorous to cotton fibres, using low-pressure plasma with argon gas.[94] Generally, monomers containing both phosphorous and nitrogen have been shown to have the best fire retardant properties when grafted onto cotton. Examples include diethyl (acryloyloxymethyl) phosphonate (DEAMP) and dimethyl (acryloyloxymethyl) phosphonate (DMAMP).[94] The structures of these molecules are shown in Figure 1-11.

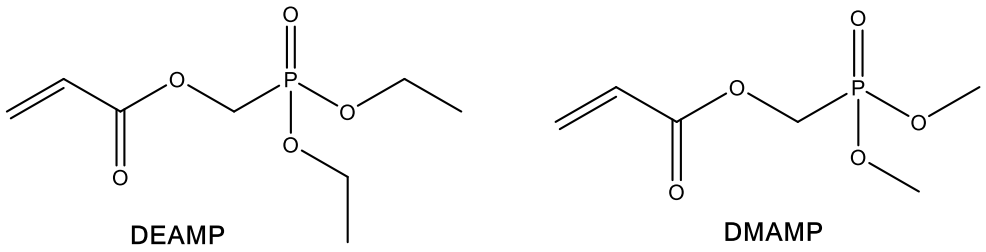

Figure 1-11: The chemical structures of DEAMP and DMAMP

The grafted flame retardant agents promoted the formation of a solid char through pyrolysis, which effectively prevented the flame from spreading by providing an insulating layer on the surface of the textile.[94] This layer prevented the diffusion of oxygen through the fabric, hence limiting combustion and avoiding the formation of potentially reactive free-radicals on the surface.[95] These results showed the treatment to be particularly effective when compared against untreated cotton, which typically burns to ashes at a speed of approximately 30.24 m/hr.[94] However, there is still a need to improve the treatment; upon examination of the cotton surface fibres using scanning electron microscopy (SEM), the surface roughness was shown to be greater on the fibres treated for flame retardancy than the untreated cotton, which could ultimately impact the handle of the textile.[94] Furthermore, the treatment is currently limited to cotton, meaning that the development of treatments on a wider range of both natural and synthetic textiles are necessary.

1.5.2 Hydrophobicity and stain repellence

Within the textile industry, there is a desire to impart hydrophobic properties onto both natural and synthetic textile fibres for a large variety of applications, such as outdoor wear, protective clothing, general stain resistance and in the healthcare industry. The wettability of these textile substrates is governed by chemical properties, and can be altered using plasma treatments.[96] Such methods include the introduction of hydrophobic functional groups through grafted co-polymer coatings onto the fibres. This direct deposition of hydrophobic polymers onto textile surfaces during the plasma process is also effective, in which vaporised hydrophobic monomers are dosed into a low-

pressure plasma chamber (sometimes with a carrier gas such as nitrogen, helium or argon), and fragmented by electron impact dissociation.[66] This forms reactive radical species (with hydrophobic groups) that undergo free radical reactions with the textile surfaces, leading to growth of polymer films, essentially grafting the hydrophobic properties onto the textile.[96]

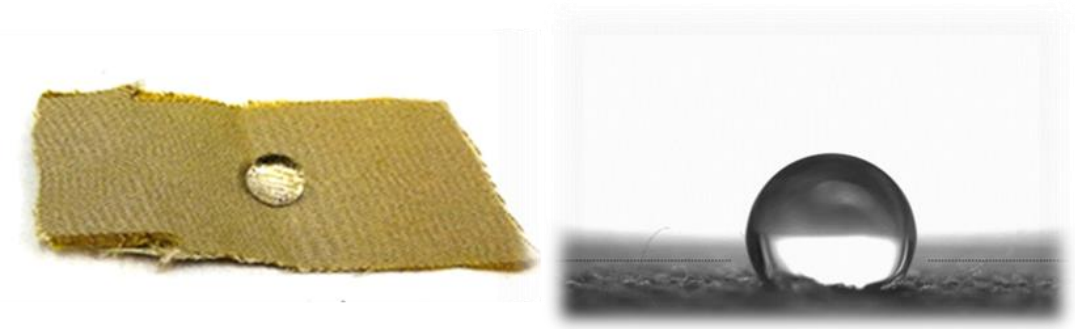

Figure 1-12. An example of a siloxane plasma-treated cotton sample and corresponding two-dimensional side view image of a water droplet on the material surface used to determine the contact angle (value of 112°).

Fluorocarbons can also be grafted onto textile surfaces directly during the plasma treatment process through the use of plasma with polymerising fluorocarbon gases. These gases graft onto the textile surface upon the plasma induced surface activation. Examples of such gases include hexafluoropropylene and tetrafluoromethane.[58] The grafting of fluorocarbon polymers onto textile substrates provides a desirable increase in contact angle, typically of values above 90°, hence increasing the hydrophobicity of the textile. Successful hydrophobic coatings have been applied onto a wide range of textile materials, including cotton, silk, wool and polyethylene terephthalate (PET).[58] This method is generally effective at providing a uniform finish across the textile surface.[13] However, fluorocarbons are undesirable for use in the textile industry due to their associated toxicity (and potential carcinogenic) concerns, and their relatively high cost. For this reason, alternative polymeric coatings have been explored (such as siloxanes).[63] An example of a siloxane plasma-treated cotton sample is shown in Figure 1-12, with the corresponding water droplet image used to determine

the contact angle (112°) demonstrating the hydrophobic properties of the coating.

1.5.3 Hydrophilicity

Hydrophilic properties are required for a range of applications in the plastics, packaging, and textile industries, for coating, bonding, dyeing, and printing. Specifically in the textile industry, there is a desire for synthetic fibres such as polyester, polypropylene and nylon to have improved wettability. These fabrics require hydrophilic surfaces to be able to provide adhesive properties for coatings and increase the printability for applications involving surgical clothing, smart textiles and technical textiles. Hydrophilic textiles are generally characterised by their low contact angle values below 90°.[97]

To improve the wettability/adhesive capabilities of polymer or textile surfaces, plasma treatments are used to either alter the surface composition, to lower the contact angle of the substrate, or to increase the number of hydrophilic functionalities present within the polymer structures such as the carbonyl, carboxylic acid, amine and hydroxyl groups.[98] The most frequently tested plasma gases used to impart these functionalities have been air, nitrogen, oxygen and ammonia.[17-19] These gases have been tested to be effective, both in low-pressure plasma systems and atmospheric systems. Inert gases such as argon initiate the activation of the polymer surfaces through H-abstraction and chain scission, generating free radicals which react to alter the polymer's morphological and chemical surface composition, lowering the contact angle.[99] Non-polymerising but reactive plasma gases such as air, nitrogen, oxygen and ammonia also activate surfaces, in addition to incorporating nitrogen and oxygen functional groups into the surface structures.[100] Examples of the characteristic groups incorporated into polymer surfaces using oxygen plasma are shown in Figure 1-13. Both inert and reactive non-polymerising plasma gases have been shown to have the ability to reduce the contact angle of non-polar textiles below the desired 90°.[100] Factors such as discharge power, exposure time and nature of the substrate can also have a major effect on the surface modification achieved during plasma treatments. Generally, increasing the discharge power and exposure time increases the

degree of plasma action, inducing the formation of more functional groups on the polymer surface.[101]

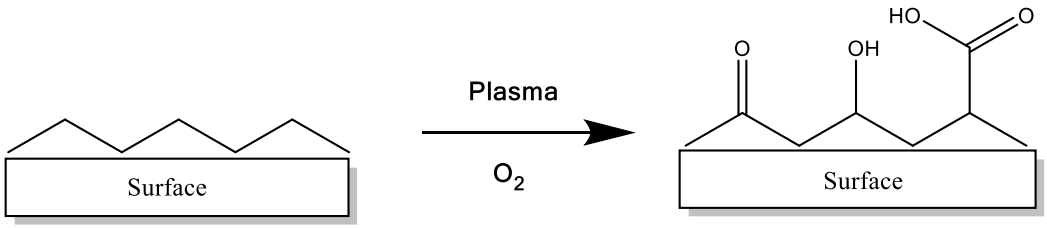

Figure 1-13: The introduction of functionalities containing oxygen using oxygen gas and plasma[1]**.**

1.5.4 Anti-microbial

Anti-microbial textiles have proven to be a promising area of development within the textile industry, with a range of suitable applications in preventing the spread of diseases and potentially damaging effects of textile materials. Cellulosic textile fibres such as cotton are particularly absorbent to water, meaning that they are susceptible to attack from bacteria.[102] Attempts have been made to use plasma treatment procedures to impart anti-microbial agents into the cellulosic structure. N-halamines are well known antibacterial compounds, and it has been possible to graft the organic reagent 5, 5 dimethylhydantoin (DMH) to the surface of cotton fibres.[102] An atmospheric plasma jet of 13.56 MHz was utilised, in conjunction with helium as a carrier gas, and nitrogen as a reactive gas. The process involved immersing the cotton fabric in DMH before treating it with plasma at 160°C for 5 minutes.[102] Surface analysis (FT-IR spectroscopy) confirmed the successful grafting of DMH to cotton, through the characteristic absorbance band of the amide group found within the molecules structure, while bacterial inactivation testing on the fabrics confirmed durable antimicrobial activity.[103]

There have been reports of the synthetic fibre PET, and biologically-derived cotton being treated effectively with plasma to impart anti-microbial properties using an inorganic finishing agent containing silver chloride.[104] Similarly to the N-halamine treatment of cotton, general methods have involved the atmospheric plasma jet treatment of the fibres, with a range of gases including air, oxygen and nitrogen. The presence of a cross linker and mixed catalyst

such as ($MgCl_{2\times}6H_2O$)/citric acid is also required within the process, enabling the grafting of the antibacterial silver compound onto the textile matrix.[104] Testing the rate of bacterial inactivation of treated textiles using agar diffusion test methods in accordance to AATCC standards has shown the treated fabrics to have increased antimicrobial activity.[105] Although the antibacterial mechanism of the grafted silver is not yet fully understood, it is largely accepted that silver ions bind with proteins inside and outside of the bacteria cell wall, inhibiting any further cell reproduction or respiration.[105]

1.5.5 Colouration

Currently, the utilisation of plasma technology within textile dyeing procedures has primarily focussed on pre-treatment/surface modifications of fibres to increase dye uptake in dyeing procedures. This is necessary due to current inefficient dyeing processes, whereby up to 50% of dye molecules are lost in effluents,[106] with an estimated 24 billion tons of effluents containing these dyes being released in China in 2010.[107] Examples of these treatments include the plasma induced removal of waxes, fats and greases from natural fibres such as wool.

For synthetic hydrophobic textiles, the dyeability can be dramatically improved with plasma treatment. For example, the low-pressure plasma treatment of polyester and polyamide with both air and argon plasmas has shown to increase the dye uptake of the fibres.[108] The plasma treatment facilitates the introduction of polar functionalities to the fibre surface, increasing the hydrophilicity, hence leading to a more effective dyeing process with an increase in dye exhaustion when compared against non-plasma dyeing.[109]

In the case of natural fibres, low-pressure systems using oxygen plasma have shown to enhance the dyeability of cotton. The oxygen plasma increases the water absorbency and capillarity of the fibres through increasing the number of polar surface functional groups, which leads to an increase in the rate of diffusivity of the dyes into the fibres.[110] For wool, the use of low-pressure

plasma with nitrogen gas has been shown to remove the outer layer surface fats and greases through ablation, whilst also introducing polar amine functionalities which improve their wettability and enhance their dye exhaustion.[111] For both natural and synthetic fibres, the increase in dye exhaustion in the plasma pre-treatment dyeing processes enables an increase in the colour strength (higher K/S value) to be achieved with significantly reduced quantities of dye, electrolyte and water. Furthermore, the K/S value of the treated textiles are shown to generally increase with plasma treatment time, until a point in which the colour strength starts to decrease. This decrease can be attributed to the plasma degrading the outer layer of the textile surface to such an extent, that it no longer possesses the ability to absorb dye molecules efficiently.[112]

A further reported application of plasma regarding colouration involves a direct plasma dye-coating method to covalently attach dye molecules onto polymer substrates.[113] The method covalently immobilises pre-absorbed dyes that are functionalised with a radical sensitive group; the radical sensitive group is a double bond that acts as an antenna for the radical species generated by the plasma, facilitating the covalent linking of the dyes to the polymer surface. This leads to a reduction in dye leaching. A general schematic of this plasma dye-coating method is shown in Figure 1-14. The research reported the successful plasma-dye coating of polypropylene, polyethylene, nylon 6, cellulose and polytetrafluoroethylene substrates, using a dielectric discharge plasma that was activated with a RF generator (100 W), using argon plasma to promote cross-linking (and reduce any additional surface-chemical modifications). The method is suitable for continuous processing of textile and polymer materials through the use of large-scale atmospheric plasma reactors. The treatment times for the dye-coating method were optimised between 0.5 - 10 minutes, with the shorter treatment time of 1 minute being shown to be the optimum. Longer treatment times appeared to result in dye degradation due to the excess energy induced by the plasma species.[113]

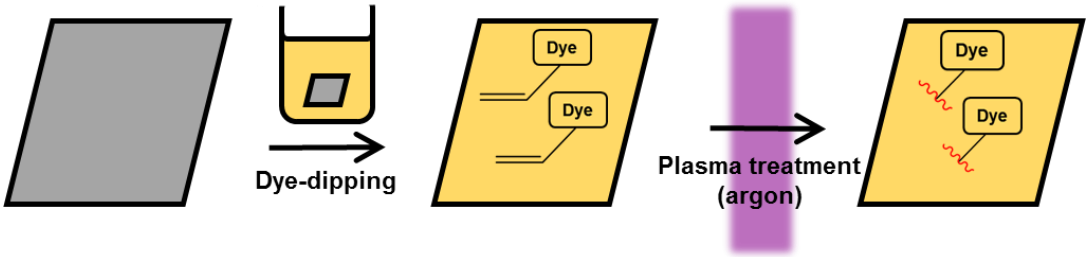

Figure 1-14. Schematic of the plasma dye coating procedure.[113]

2. Aims of the research

The aims of the research reported in this thesis include:

- To fully analyse and characterise the chemical and morphological changes induced by different capacitively-coupled, low-frequency (40 kHz), low-pressure oxygen plasma gas treatments on different polymer surfaces, providing insights into the fundamental principles of plasma-surface interactions. The specific modes of plasma treatments that were investigated included oxygen surface plasma activation/functionalisation and oxygen plasma etching, with the ageing phenomenon of post-plasma activated and etched polymers also being examined through their hydrophobic recoveries.
- To investigate the plasma-enhanced chemical vapour deposition process on polymer substrates utilising HMDSO and HMDSO:O_2 gas mixtures as example precursors. The investigation aimed to provide detailed understandings of the deposition process, whilst also demonstrating the versatility of the process by grafting both hydrophobic and hydrophilic siloxane coatings onto polymer substrates.

More specifically, the research focussed on the plasma treatments of two widely used polymer substrates: nylon 6 and regenerated cellulose. Through studying the chemical and morphological modifications to the polymer surfaces, mechanisms of plasma action were able to be developed to explain the fundamentals of the plasma treatment processes. The extent to which

plasma treatments can be considered as “substrate-independent” was also explored through comparisons between the materials.

3. Experimental

In order to obtain reliable data for the mechanistic studies of different modes of plasma action on nylon 6 and regenerated cellulose samples, the experiments in this work were all designed with a focus on reproducibility. Due to the variation in plasma system configurations and methods of plasma generation across the literature, in addition to the limited availability on studies specifically focussing on low-frequency (40 kHz), low-pressure plasma systems, the parameters required to achieve different plasma effects had to be determined empirically.[114] Established procedures used for a range of previously reported plasma systems were adapted to suit the system utilised in this research, ensuring that the data were reliable and comparable to previous studies. Additionally, all work described in this research was designed in consultation with risk assessments and Material Safety Data Sheets (MSDS) for all chemicals used. General safety precautions including the use of ventilated fume cupboards and safety goggles/gloves were adopted at all points in which the experimental work was undertaken.

3.1 Materials, instruments and methods

3.1.1 Plastic/polymer film samples

All nylon 6 materials used in the plasma treatments (nylon 6 natural plastic sheets, 1.00 mm thickness, 1.14 g cm^{-3} density, extruded) were provided by Direct Plastics Ltd (UK). Regenerated cellulose (film, 0.031 mm thickness, 1.50 - 1.55 g cm^{-3} density) was purchased from Goodfellow Cambridge Ltd (UK), which was manufactured through the xanthate process.

3.1.2 Pre-cleaning of samples

The nylon 6 plastic sheet and regenerated cellulose film samples were cleaned via ultrasonic cleaning with acetone prior to the plasma treatments, to remove any surface impurities, dusts or hydrocarbon contaminants. Thus, the samples were fully submerged in a beaker containing acetone that was then placed in a Branson 1510 ultrasonic cleaning bath (USA) filled with deionised water, operating at a power of 160 W for 10 minutes. The efficiency of these cleaning procedures were verified further by XPS and SEM/EDX analysis in Section 4.1, confirming that they had removed surface contaminants without altering the chemical or physical structures of the polymers.

3.1.3 Chemicals

Owing to the “dry” nature of plasma treatments, minimal chemicals were required during this research. The chemicals that were utilised were primarily for sample preparation/cleaning and analysis. Oxygen gas was provided by BOC (UK), and was supplied through a portable GENIE gas cylinder (20 litres) of purity 99.99%. Hexamethyldisiloxane (≥98%) was purchased from Sigma-Aldrich (UK) and 2,2-Diphenyl-1-picrylhydrazyl (95%) was purchased from Fisher Scientific (UK). Dermotec 70 resin (based on methyl methacrylate and electrically conductive carbon) was purchased from Agar Scientific (UK). All solvents (acetone, toluene) used in the project were AR grade, and were purchased from Sigma-Aldrich (UK). All contact angle measurements were carried out using doubly-distilled, deionised water.

3.1.4 Plasma

All plasma treatments in this research were carried out using a commercially available Diener Zepto Low-Pressure Plasma Laboratory Unit, supplied by Diener electronic GmbH & Co KG (Germany). The system comprised a cylindrical borosilicate glass chamber of 1.7 L volume, two semi-arc electrodes assembled axis-symmetrically on the outer wall of the chamber, two needles valves with mass flow controllers for controlling process gas flow,

a Pirani gauge for chamber pressure measurement, an analogue timer and a Pfeiffer Duo 3 rotary-vane vacuum pump (Germany) with an exhaust outlet for the process gas. The system had a working frequency of 40 kHz and an adjustable power ranging from 0 - 100 W. The low-frequency plasma was generated by a capacitively-coupled plasma (CCP) discharge. All samples were placed in the centre of the plasma chamber, so that they were directly between the ground electrode and biased electrode. An image of the plasma unit and schematic of the plasma setup are shown in Figure 3-1 and Figure 3-2 respectively.

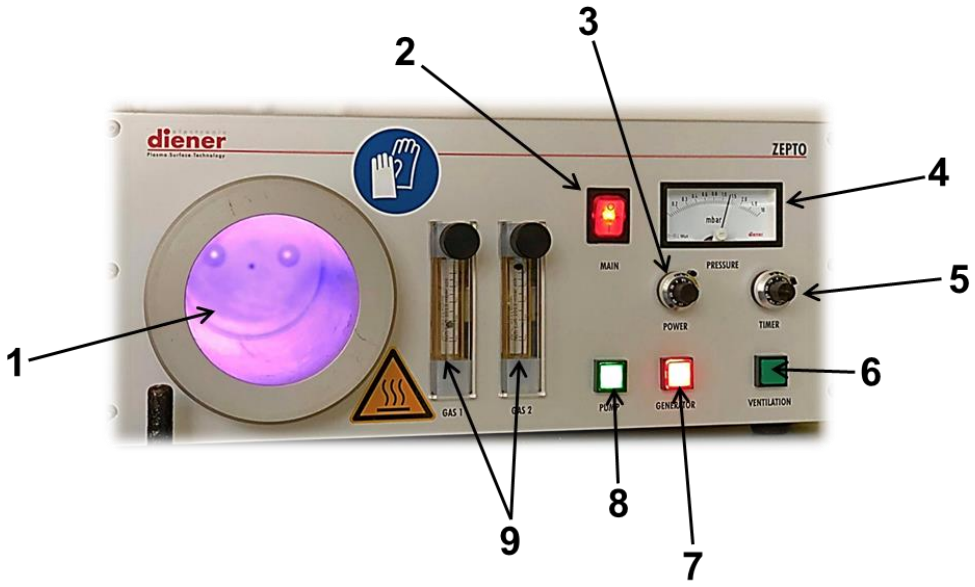

Figure 3-1. The front panel of the Diener Zepto low-pressure plasma unit, showing the: (1) plasma chamber; (2) mains power switch; (3) plasma power selector toggle; (4) display for pressure measurement (from Pirani gauge); (5) timer; (6) ventilator switch; (7) generator switch (to ignite plasma); (8) pump switch and (9) mass-flow controllers for gas inlet (×2).

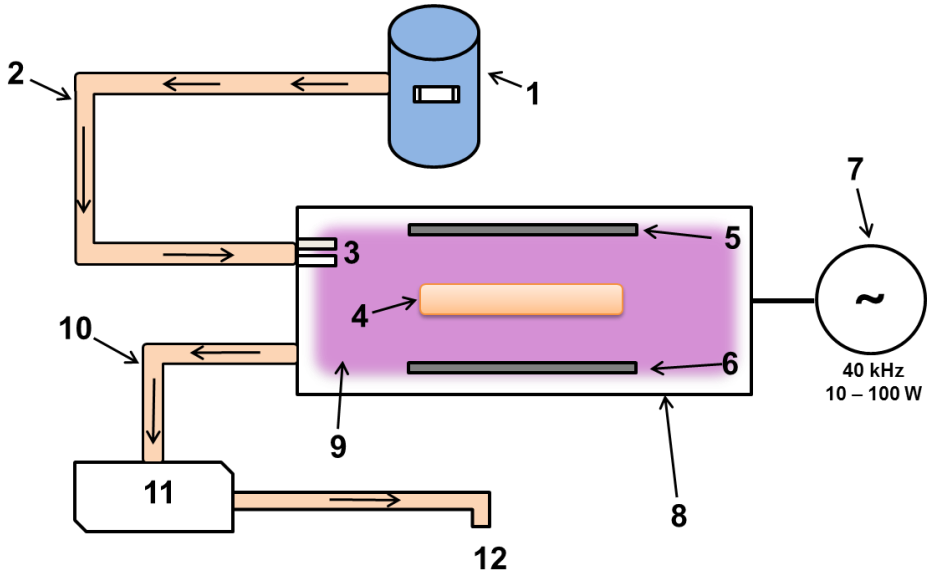

Figure 3-2. Schematic of the low pressure plasma setup equipped with: (1) gas cylinder/source; (2) tubing for gas inlet; (3) mass flow controllers; (4) polymer sample; (5) ground electrode; (6) biased electrode; (7) low-frequency (40 kHz) generator operating at 10 – 100 W; (8) plasma chamber; (9) plasma gas; (10) tubing for gas outlet; (11) rotary-vane vacuum pump and (12) exhaust.

3.1.5 Statistical factorial experimental design using the design of experiments (DOE) approach

Factorial designs were constructed in this research using Minitab 17 software, to determine the different processing parameters/conditions that would induce different corresponding plasma processes, namely plasma functionalisation/activation and plasma etching. Further studies on these processes then formed the basis of Chapters 4 and 5 respectively. Mass loss measurements were used as the response in the experimental design, to determine the point at which etching of the polymer surfaces began to occur; any loss of mass was indicative of a plasma etching process. This method was used to maximise efficiency in the determination of parameters to study plasma activation and etching as separate phenomena in more depth, with minimum expenditure of time and resources. More specifically, it allowed the surface functionalisation/activation process to be isolated through parameter control, preventing additional interfering effects such as plasma etching from influencing the study.

It is well documented that plasma power, treatment time and pressure all influence the resultant surface modifications induced by the plasma treatment of polymers. Due to the operational setup of the low-pressure system utilised in this research, it was not feasible to significantly alter the operating pressure, so it was held constant in all plasma treatments. Therefore, plasma power and treatment time were the two factors that were identified as potentially having a significant influence on the response (mass loss) of the polymer samples. A factorial design based around these two parameters was generated for treatments with powers ranging between 10 and 100 W, and treatment times ranging from 10 s to 600 s. The number of experiments required by the full factorial design at two levels was given by:

$$n = 2^k$$

Equation 3.1. The required experimental runs at 2 levels.

Where *n* = the number of observations and *k* = the number of factors to be considered. In the experiments performed, there were two factors, therefore yielding $2^2 = 4$ observations to be considered. These four observations are shown in the experimental design matrix in Figure 3-3. The matrix shows that the 2^2 matrix was an orthogonal design, which was based on the two investigated variables *A* (plasma power) and *B* (treatment time), in addition to the interaction effect *AB.* An additional centre point was also included in the matrix. The 2^2 orthogonal design proved to be a simple and efficient way in monitoring the initial effects to the plasma parameters, to screen for suitable conditions to study the mechanisms of plasma activation and plasma etching. Furthermore, by including a centre point replicate in the design matrix, it was possible to check for the presence or absence of curvature in the model, to aid in confirming whether the relationship between the factors was linear.

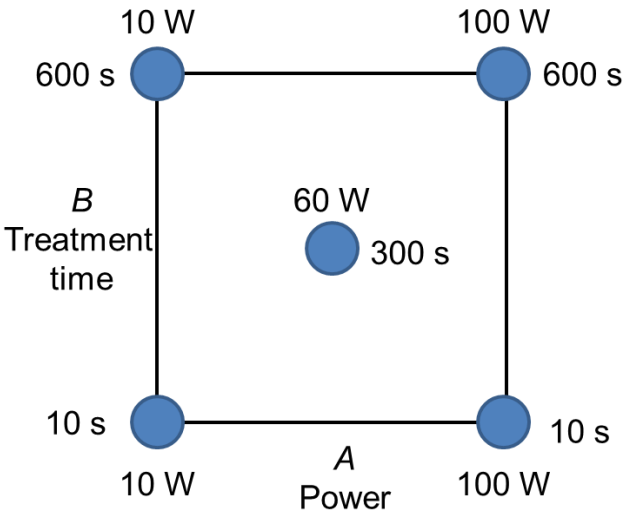

Figure 3-3. Design matrix for the two factor (plasma power and treatment time) 2^2 factorial design used in the DOE experiments to measure mass loss (response).

3.1.6 Gravimetric measurements

The mass loss of the nylon 6/regenerated cellulose samples was determined by gravimetry using a Kern ALJ 200-5 analytical microbalance (accuracy of 0.01 mg), through recording the masses of the samples before and immediately after plasma exposure. The mass loss experiments were repeated three times for each of the plasma treated samples in order to obtain average mass loss values, with uncertainties expressed as the standard deviations between the different measurements. The etch rates for the nylon 6/regenerated cellulose samples treated with oxygen plasma under the specific parameters utilised were calculated using:

$$\xi = \frac{\Delta m/p}{At}$$

Equation 3.2. The calculation for etch rates of the plasma treated polymer samples[115].

Where ξ is the etch rate, Δm is the average change in mass, p is the polymer density, A is the area of the polymer surface exposed to the plasma and t is the plasma exposure time. When determining the rates of deposition of the

plasma-enhanced chemical vapour deposited polymer films, mass gain measurements were used to plot the mass deposited against plasma treatment time. From these plots, it was possible to determine the deposition rates from the slopes of the graph, due to the linear plots obtained.

3.1.7 Infrared spectroscopy

FT-IR is a spectroscopic technique that uses infrared radiation to detect the molecular chemistry of samples, and could potentially be used to study the surface functionalities of plasma treated polymers. Using the attenuated total reflection (ATR) mode of FTIR allows the polymer samples to be studied directly in the solid state without any prior sample preparation that may interfere with the surface chemistry, and is advantageous due to its relatively non-destructive nature. The ability to detect surface functional groups should in theory have enabled the chemical effects of the plasma treatments to be observed.[116] However, the penetration depth of FT-IR is typically 1 - 5 µm, meaning that it may not have the sensitivity to detect the modifications induced by the plasma treatments.[117] On the other hand, some reports of plasma treated polymers have suggested that FT-IR is capable of detecting the surface modification.[118-119] Consequently, this technique was reported in this thesis.

Thus, the untreated and plasma treated nylon 6 plastic sheets and regenerated cellulose were analysed by infrared spectroscopy using a PerkinElmer Spectrum One FT-IR Spectrometer (ATR mode, 100 scans), with the scanning range between 500 and 4000 cm^{-1}. The spectra obtained for the nylon 6 samples and regenerated cellulose samples are shown in Figure 3-4 and Figure 3-5 respectively.

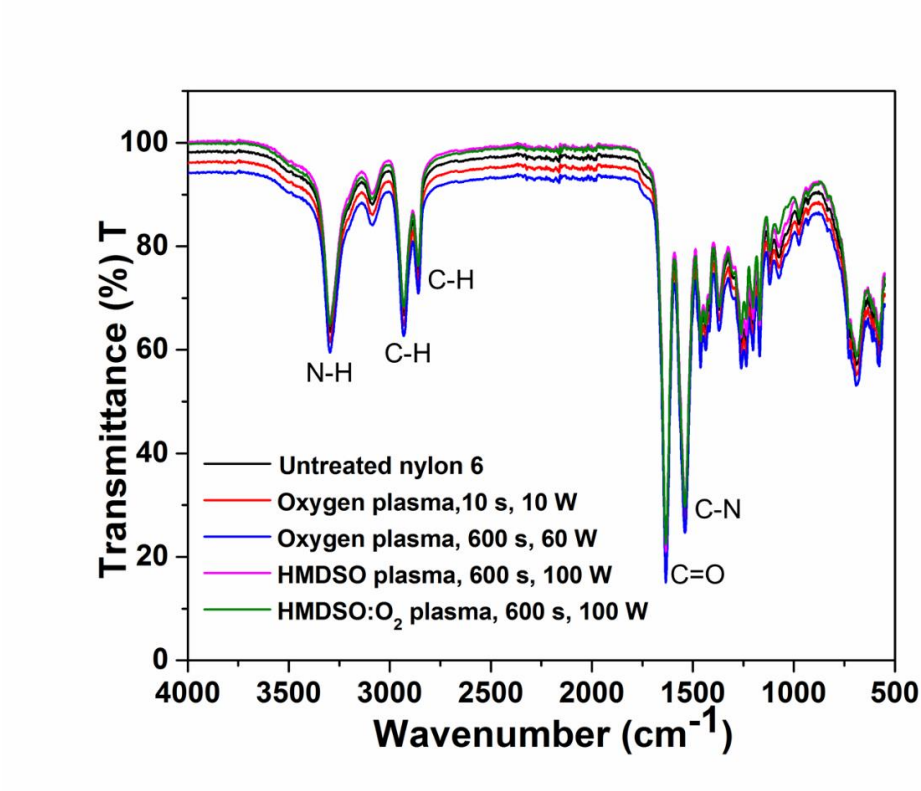

Figure 3-4. The FT-IR spectra of untreated and plasma treated nylon 6 under a range of different conditions in this study.

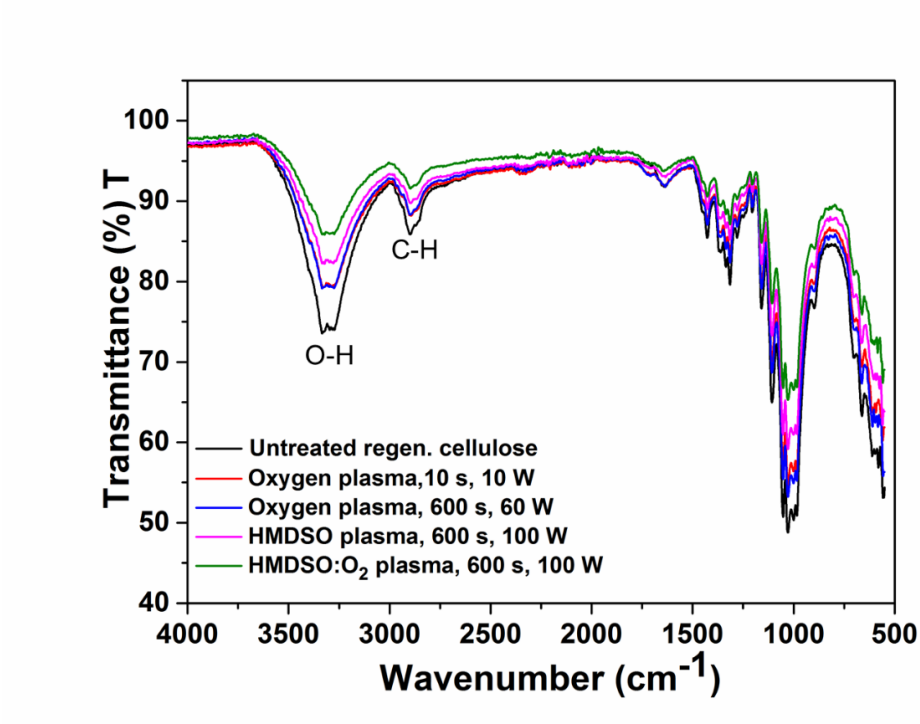

Figure 3-5. The FT-IR spectra of untreated and plasma treated regenerated cellulose under a range of different conditions in this study.

From the FT-IR spectra, it was evident that there was no obvious change in the spectra of the untreated or plasma treated under any of the different conditions. This can be attributed to the lack of sensitivity of the technique towards the nano-scale surface modifications. For this reason, the spectra were not reported in the results and discussion, and XPS and SSIMS analysis were used to characterise the surfaces in this study, as they are more sensitive than FT-IR.

3.1.8 Contact angle measurements and apparent surface free energy

Contact angles are often used to assess and quantify the wettability of solid material surfaces by specific liquids. Wettability is generally dependent on both the chemical composition of the surface, and the surface morphology. The contact angle is measured through the use of a probe liquid such as water, at the point where the liquid-vapour interface meets a solid surface. A material is classified as hydrophilic if it has a contact angle value < 90°, and described as hydrophobic if it has a contact angle value > 90°.[120] Contact angle measurements are based around Young's equation, which describes the relationship between the contact angle θ, the surface tension of the liquid σ_{lg}, the interfacial tension σ_{sl} between the liquid and solid, and the surface free energy σ_{sg} of the solid. The expression is shown in Equation 3.3[121].

$$\sigma_{sg} = \sigma_{sl} + \sigma_{lg} \cdot \cos\theta$$

Equation 3.3. Young's equation.

Static contact angles represent systems whereby the water droplet is in equilibrium with the surface (hence the surface free energy is a minimum). This means that the interface between the liquid and solid is not changed externally during the measurement, and contrasts with dynamic contact angles, whereby measurements are taken during the process of wetting (advancing contact angle) and de-wetting (receding contact angle). Static contact angles are useful in studying the homogeneity of substrates by

measuring the contact angle on multiple different positions of the same sample. An example of a static contact angle obtained on an untreated nylon 6 plastic surface is shown in Figure 3-6. The key features and interfaces of the droplet are clearly labelled to illustrate each of the terms in Young's equation.

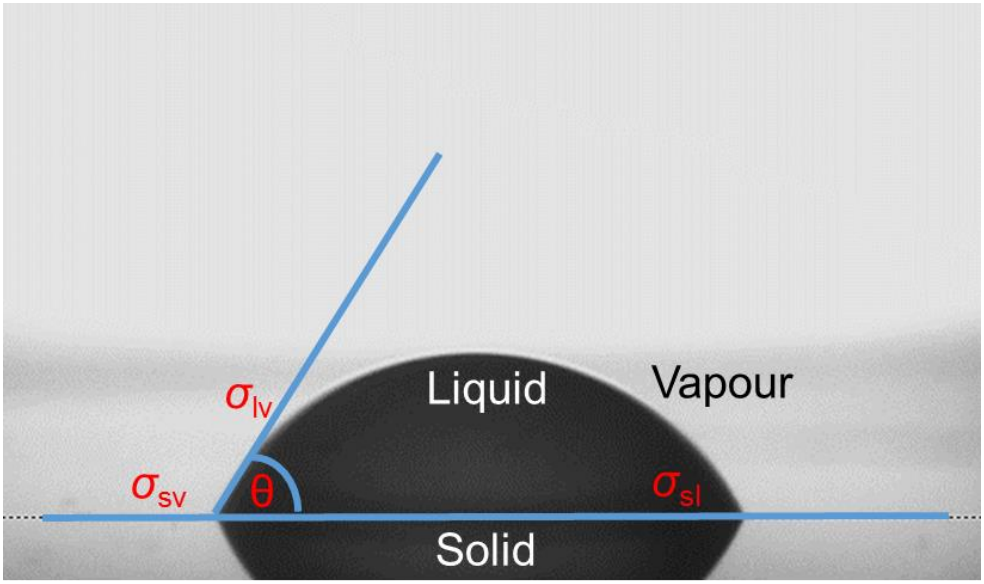

Figure 3-6. A sessile water droplet (4 µl) captured by the PGX goniometer and visualised with PGX+ software on the surface of a nylon 6 plastic substrate.

All contact angle measurements were carried out using a PGX Goniometer, in combination with PGX+ software that was used for visualising and measuring the droplets. The measurement procedures all followed the ASTM D5946 standard test method.[122] The PGX goniometer comprised a built-in pump capable of delivering accurate droplets of 4 µL, PTFE tubing to transport the pumped deionised water, an LED light for clear viewing of the water droplet, and an integrated camera that captured 80 frames/sec. This camera was used for viewing the water droplet in real-time. The main features of the goniometer are shown in Figure 3-7.

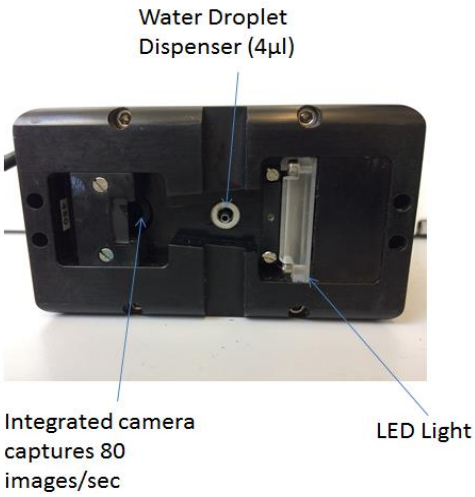

Figure 3-7. The main components of the PGX goniometer (shown on the underside of the instrument).

The PGX goniometer was calibrated before each session using a tool that utilised a steel ball to replicate the shape of a sessile water droplet with a known contact angle value. Static contact angles were then measured for the untreated and plasma treated nylon 6 plastic sheets and regenerated cellulose films by initially placing the substrates flat, ensuring there was no wrinkle or crease. A 4 µL pendant droplet of deionised water was suspended at the end of the syringe needle that was lowered until the droplet made contact with the sample. The syringe was then carefully lifted away, ensuring that the 4 µL sessile water droplet had been transferred onto the sample surface. The droplet was left on the surface for 20 s to equilibrate. 6 different static contact angle measurements were performed at different locations of each sample, and average values for the contact angle were obtained, with standard deviations used to report the uncertainty in each set of sample measurements.

Surface free energy/surface energy/interfacial energy is a measure of the excess energy that a surface has compared to the bulk material that arises from intermolecular interactions (van der Waals, hydrogen bonding, dipole-dipole) at the surface interface; it can be considered as the surface tension of a solid. The adhesive properties of a material are governed by the surface free energy of the solid and surface tension of the liquid applied. When the surface energy is high the solid is more wettable, with low surface energy materials

having poor wettability. From the static measurements obtained, the apparent surface energies of the samples were determined using a calculator that was built into the PGX+ software based on the ASTM D5946 standard calculation model.[122]

3.1.9 SEM imaging/EDX

Scanning electron microscopy (SEM) is an imaging technique, whereby a high-energy electron beam is used to scan a sample (using a raster scan pattern) to image the sample surface. The electron beam penetrates into the sample surface to the depth of a few microns, producing signals comprising secondary electrons, backscattered electrons, and characteristic X-rays. These signals are collected by detectors to produce images that contain information about the surface topography of the sample. These SEM images, enable plasma treated materials to be analysed on the nanoscale, to show any morphological changes in the surface, including any damage or defects.[123]

In this study, samples were imaged using an FEI Nova 450 scanning electron microscope. The SEM operated with an FEG source in standard secondary electron and backscattered electron modes, operating at 3 keV. All samples were sputtered coated with an ultra-thin iridium layer (2 nm) before analysis. The EDX measurements were obtained using an EDAX (AMTEL) coupled with TEAM EDS software. These EDX measurements were primarily used to detect the presence of silicon, indicating the presence of grafted siloxane films from HMDSO and HMDSO:O_2 plasmas. Some of the plasma etched samples were imaged at a 45° angle to enable the depth of the newly formed nanopores to be determined. ImageJ image processing software was then used to measure the pore depths of the samples. The software enabled the images to be magnified and enhanced, to assist in accurately measuring the pore depth. For each sample, five separate measurements at different etched positions within the surface structure of the polymer were performed, with the mean value and standard deviations being reported.

In order to determine the film thickness of the plasma-deposited HMDSO films, cross sectional analyses of the nylon 6 and regenerated cellulose samples were performed, requiring them to be resin-embedded. Following HMDSO and HMDSO:O_2 plasma treatment, each of the samples (1 × 1 cm) were embedded by placing them vertically in a mould with a commercially available, hard-polishing, conductive two component resin (Dermotec 70), based on methyl methacrylate and electrically conductive carbon. The resin was then left to harden for approximately 30 minutes. The resultant embedded samples underwent a grinding process in three steps using 320, 400 and 600 grit silicon-carbide sandpaper sequentially, until the surface of the HMDSO coated samples were level with the surface of the resin. The embedded samples were then mechanically polished using a short-nap woven acetate cloth and 1 µm diamond paste. The cloth was lubricated using liquid soap and water during the polishing process. The polished samples were then sputtered coated with an ultra-thin iridium layer (2 nm), and cross sectional SEM images were obtained, with the nanoscale polymer films being visualised at the substrate-resin interface. To confirm the presence of the films, EDX spectra were obtained from areas of the films and compared to areas of the uncoated polymer. All film thicknesses were subsequently measured using ImageJ software. The software enabled the images to be magnified and manipulated to assist in determining the film thicknesses of the coatings. Again, each sample was measured five times at different positions in the image, enabling the mean value to be reported with the uncertainty being expressed as the standard deviation between the measurements.

3.1.10 Atomic Force Microscopy (AFM)

AFM is a powerful analytical tool that can be used to characterise the surface morphology and topography of materials. It is a type of scanning probe microscopy that uses a sharp tip at the end of a cantilever to scan over the material surfaces. When the surface is scanned, different morphological features of the surface deflect the tip and cantilever. Measuring this deflection allows 3D topographical images of the surface to be obtained, with resolution

up to the order of fractions of a nanometre.[124] A schematic showing the main components of an AFM setup is given in Figure 3-8:

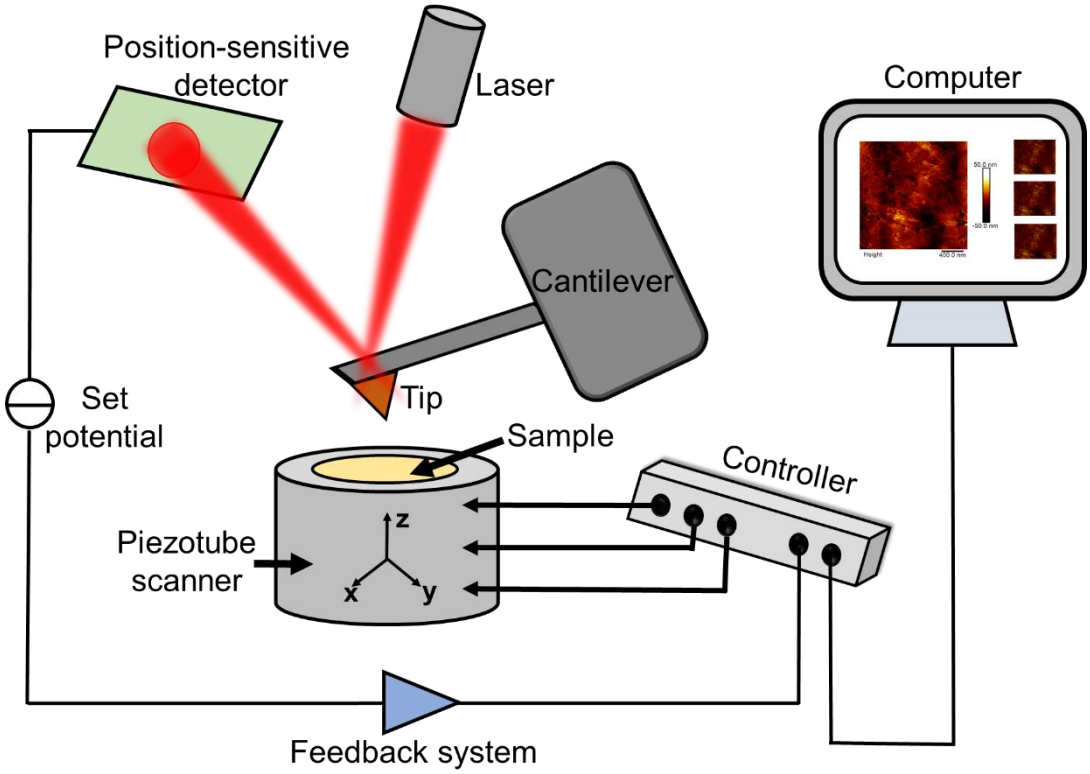

Figure 3-8: Schematic showing the main components of an AFM system.[125]

In this study, AFM images were obtained using a Bruker Innova microscope (USA) coupled with a NanoScope ADCS controller. A monolithic silicon cantilever with a resonant frequency of 300 kHz and a force constant of 40 N/m was utilised in tapping mode, and 1 × 1 µm images were obtained. The images were processed using NanoScope Analysis v1.40r1 (Bruker) Software. On each of the 1 × 1µm topographical images, three separate 300 × 300 nm areas were evaluated to calculate three roughness average (Ra) and root mean square roughness (Rq) values for each image. The mean Ra and Rq values obtained were then reported, with standard deviations also given to provide uncertainties in the measurements. For the etched samples, the depths of the pores formed from plasma etching were determined through assessing the surface roughness profiles of each of the images using the NanoScope software. The vertical distances measured in the profiles showed the depths of the etched pores.

3.1.11 X-ray photoelectron spectroscopy (XPS)

XPS is a widely used technique providing quantitative elemental analysis of the near-surface regions of materials. The technique is particularly useful for investigating the effects of plasma treatments on polymer substrates due to the ability to obtain the chemical composition of surfaces with up to approximately 10 nm depth analysis (% of elements, except hydrogen). XPS spectra are acquired through irradiating the polymer samples with an X-ray beam under ultra-high vacuum conditions, whilst simultaneously measuring the kinetic energy and number of electrons escaping from the sample surface, also enabling the binding energy of the core electron in an atom to be determined.[126] The XPS technique is fundamentally based around the first law of thermodynamics, i.e. energy conservation. This is described in Equation 3.4, through stating that the energy of the incident X-ray photon is partitioned between the binding energy ($E_{binding}$) and the kinetic energy ($E_{kinetic}$) of the ejected electron.[127]

$$E_{photon} = E_{binding} + E_{kintetic}$$

Equation 3.4. The first law of thermodynamics used to describe the fundamentals of energy conservation in XPS.

A typical schematic setup for an XPS spectrometer is presented in Figure 3-9. XPS systems generally comprise an X-ray source (an electron gun is used to excite X-ray emission from a metal anode such as aluminium), a monochromator to remove unwanted radiation from the X-ray source, a hemispherical analyser to determine the kinetic energy of ejected photoelectrons, and electron optics to transmit photoelectrons through the analyser. The ejected photoelectrons pass through two charged co-hemispherical plates; electrons with surplus energy collide with the outer plate, while electrons with too little energy collide with the inner plate, with a narrow pass-energy of electrons able to arrive at the detector. XPS

measurements are performed in ultra-high vacuum conditions to keep the sample surface free from contamination during analysis.[127]

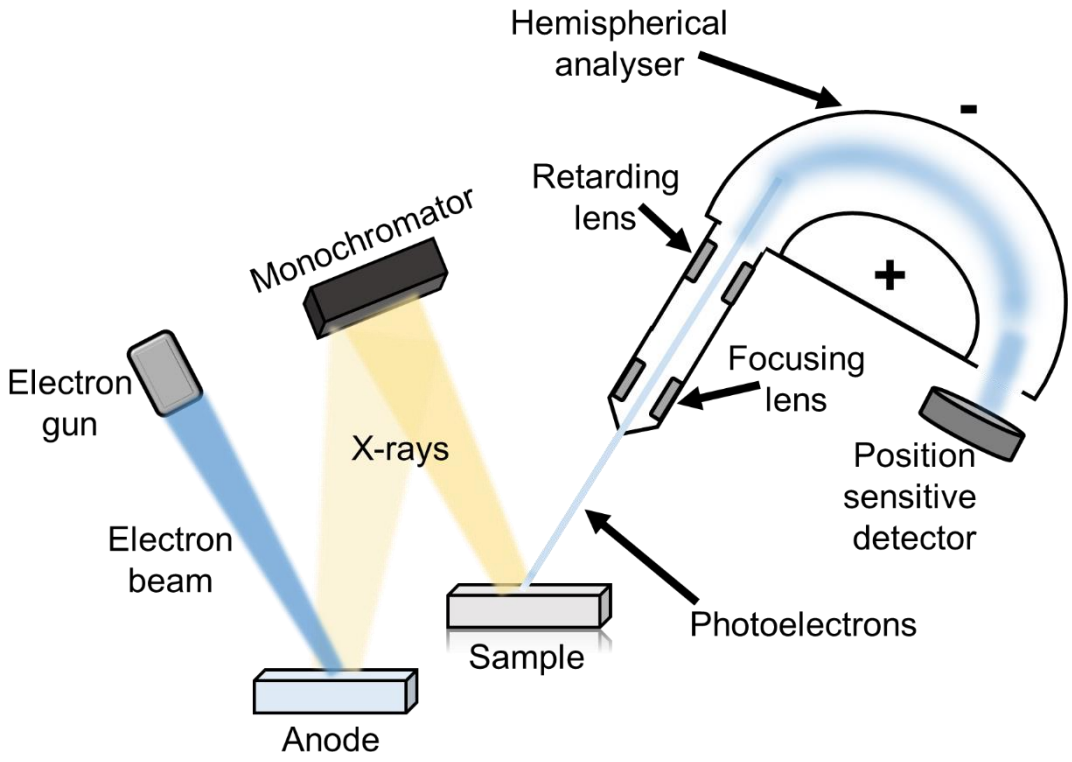

Figure 3-9. Schematic setup of a typical XPS analyser[127]

In this research, the plasma treated nylon 6 sheets and regenerated cellulose films were analysed by XPS using a Thermo Fisher Kα spectrometer, using monochromatic Al Kα radiation (72 W) at pass energies of 150 eV for survey scans, and 40 eV for high-resolution scans, with 1.0 eV and 0.1 eV step sizes respectively. The angle between the photoelectron emission direction and plane of the sample was kept constant at 45°, and an area of approximately 400 µm was scanned. The XPS utilised low energy electrons and argon ions to prevent charge build-up on the polymer surfaces. Deconvolution of the high-resolution C 1s, O 1s and Si2p spectra obtained was carried out using the line fitting function on CasaXPS 2.3.19 software, with a Shirley type background subtraction, and the full width half maximum (FWHM) set to 1.5 eV for all spectral components. For each of the plasma activated and etched nylon samples, one spot on three separate samples treated under the same

conditions was analysed to test the reproducibility of the plasma treatments. The positions of each of the spots were varied according to the positions shown in Figure 3-10, i.e. one sample was measured in the centre, one at the side and one in the corner, all having undergone the same plasma treatment. The mean values of the three measurements were then reported with the standard deviations to show the uncertainties. For the regenerated cellulose samples, one spot in the centre of each sample was analysed, meaning that the results reported were not an average of three measurements. For both the nylon and cellulose samples that were treated with HMDSO and HMDSO:O_2 plasma, multiple point XPS analysis was used to measure the distributions of chemical changes across the nylon 6 surfaces. Three different points on each sample were measured by XPS (again, according to Figure 3-10), to assess the homogeneity of the deposited siloxane films.

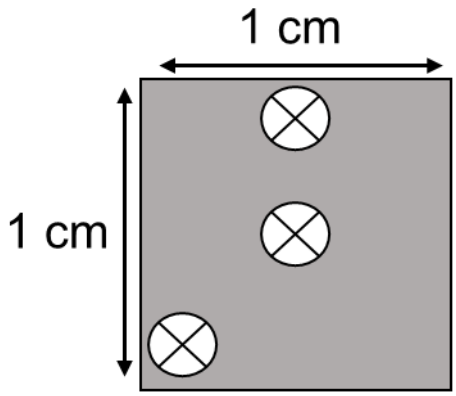

Figure 3-10. The targeted spots for measurements in the XPS multiple point analysis.

XPS depth profiles were obtained for some of the untreated, oxygen plasma treated and aged plasma treated nylon 6 samples using an argon gas cluster ion beam (energy of 4 keV, 1000 and 2000 Ar atoms) at an angle of incidence of 55° to the sample surface. The size of the sputtered area was 1.5 × 1.5 mm, with the beam current set to 6.5 nA. Polymer materials are generally susceptible to damage from monoatomic sputter sources, so an argon cluster ion beam was adopted. There is substantially less kinetic energy per atom in a cluster, meaning there is less ballistic energy per atom and less damage to the polymer chains, while maintaining sufficient energy to sputter away surface matter with minimal damage to the underlying surface.

3.1.12 Secondary ion mass spectrometry analysis (SIMS)

SIMS is a particularly useful technique when analysing the surface chemistry of materials, due to its ability to provide information on the chemical composition of solid materials. The technique works through sputtering solid surfaces with a focused primary ion beam, which then ejects secondary ions that are collected by a mass analyser.[128] There are two main analysers used in SIMS. Time-of-flight (ToF) analysers separate ions in a field-free drift path according to their velocity, meaning that the time of flight varies according to mass, as all ions have the same kinetic energy. Quadrupole analysers separate masses by resonant electric fields, only allowing certain masses to pass through.[128] The mass spectrometer can measure the mass/charge ratio of the secondary ions formed to determine the elemental, isotopic or molecular composition of the surface. SIMS has the capabilities to produce positive and negative mass spectra from the outer 1 - 20 Å of material surfaces.[129]

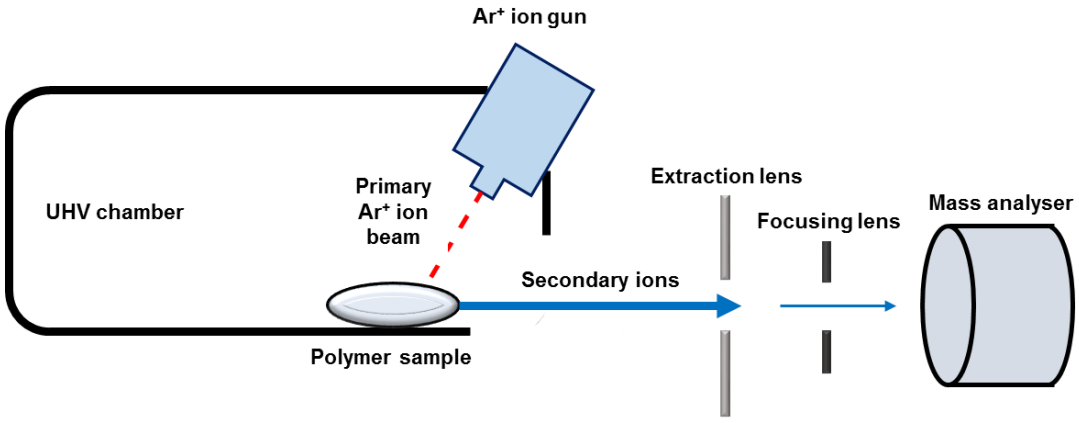

Figure 3-11. Schematic diagram showing the main components of the Compact SIMS spectrometer.

In this study, the plasma treated samples were analysed by SIMS using a Hiden Compact SIMS spectrometer, using a MAXIM-600P detector which was based around the Hiden 6mm triple quadrupole mass filter with pulse ion detection. The samples were initially placed in the sample chamber under ultra-high vacuum, to increase the mean free path of the liberated surface ions. The samples underwent Ar^+ primary ion bombardment with a 25 nA

primary current rastered over a 180 × 180 µm area at a 41° angle of incidence from normal, with a 5.5 KeV impact energy. Two separate areas of each of the samples were measured to obtain the negative and positive ion spectra. The geometry of the ion gun was set to obtain nanometre depth resolution and near surface analysis. The specific depth resolution of the Hiden Compact SIMS was 3 nm.

3.1.13 Determination of surface radical densities using 2,2-diphenyl-1-picrylhydrazyl (DPPH) and UV-vis spectrophotometry

Surface radical densities were determined through a chemical labelling method, utilising the radical scavenging molecule DPPH. A calibration graph of DPPH solutions in toluene was initially prepared (displayed in Figure 3-12), enabling the extinction coefficient, ε to be calculated.

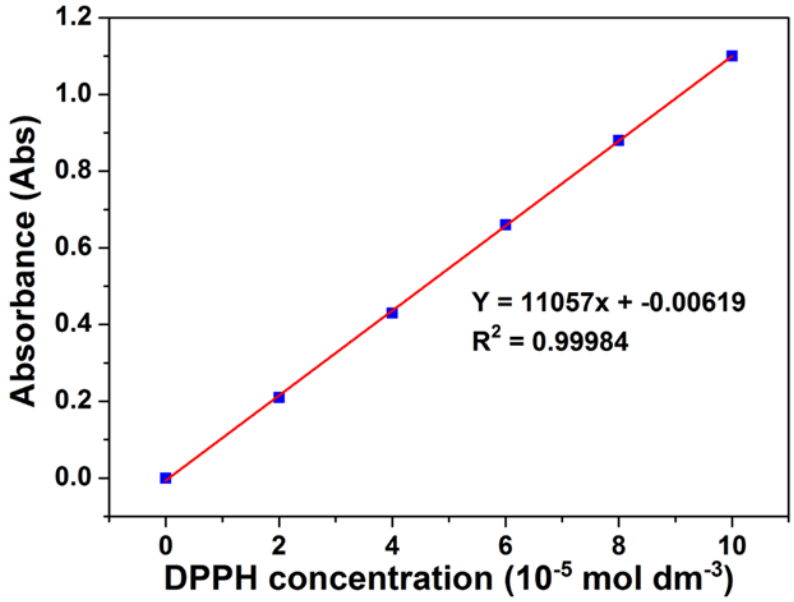

Figure 3-12. Calibration graph for DPPH in toluene. Absorbance measured at λ_{max} = 520 nm for DPPH.

1 × 1 cm untreated and plasma-treated nylon 6/regenerated cellulose samples were immersed in 10 mL solutions of DPPH (1.0×10^{-4} M) in degassed toluene. The DPPH solution was heated for 3 hours at 80°C. The samples were then cooled to room temperature, and their photoabsorptions were

measured with a Varian Cary 50 UV-vis spectrophotometer at 520 nm (the maximum absorbance for DPPH).[130] The surface radical densities of the untreated and plasma-treated samples were then calculated using Equations 3.5a and b respectively:

$$d_{Untreated} = \frac{[DPPH]_{Blank} - [DPPH]_{Treated}}{V \times S} \quad \text{(a)}$$

$$d_{Treated} = \frac{[DPPH]_{Untreated} - [DPPH]_{Treated}}{V \times S} \quad \text{(b)}$$

Equations 3.5a and b. Calculations used to determine the surface radical densities of the untreated and plasma treated polymer surfaces.

Where $d_{Untreated}$ = surface radical density of the untreated nylon 6, $d_{Treated}$ = surface radical density of the plasma treated nylon 6/regenerated cellulose substrates, $[DPPH]_{Blank}$ = concentration of DPPH remaining after heating the solution without the substrate, $[DPPH]_{Untreated}$ = concentration of DPPH remaining after heating with the untreated sample, $[DPPH]_{Treated}$ = concentration of DPPH remaining after heating with the plasma treated substrate, V = volume of DPPH solution, and S = surface area of the substrate.

3.1.14 Differential scanning calorimetry analysis (DSC)

DSC is a useful technique for determining the thermal transitions and crystallinities of polymer samples, through measuring the amount of heat required to increase the temperature of a sample in comparison to a reference that is maintained at the same temperature. The crystallinity of a polymer can be determined by measuring the enthalpy of fusion for a sample (ΔH_t), and comparing it to the enthalpy of fusion for a pure material (ΔH_f).[131] The fractional of crystallinity can be determined using Equation 3.6.

$$Fractional\ of\ crystallinity = \frac{\Delta H_t}{\Delta H_f}$$

Equation 3.6. The equation to obtain fractional crystallinity from the enthalpy of fusion of a sample and corresponding pure material.

To provide information about the crystallinity of the untreated and plasma treated nylon 6 samples, DSC analysis was carried out using a DSC Q20 model (TA Instruments, USA), with a heating rate of 10°C/min, increasing from 25 to 250°C under a nitrogen atmosphere. The nitrogen flow rate was 50 mL/min. The initial heating and controlled cooling were carried out to remove the thermal history from the samples. Values for crystallinity were derived using the literature enthalpy value of 230 J g^{-1} for 100 % nylon 6.[132] Due to the lack of changes seen in the nylon 6 samples for all treatments, DSC was not attempted on the regenerated cellulose samples.

3.1.15 X-ray diffraction (XRD)

XRD measurements are useful in investigating the atomic and molecular structures of materials, and are useful in determining the crystallinities of polymer samples. Samples are irradiated with incident X-rays, with the corresponding intensities and scattering angles of the X-rays that are scattered by the sample being measured.[133] To compliment and verify the DSC data, XRD measurements were obtained using a Bruker D8 diffractometer (USA). Copper Kα radiation (λ = 1.0541 nm) was used to obtain spectra with 2θ values ranging between 5 - 90°, with steps of 0.05° and a rate of 0.2 s/step. The samples were not rotated upon exposure to the copper radiation. Again, the technique was initially utilised for the nylon 6 samples, but was not repeated for the regenerated cellulose samples due to a lack of observed changes following plasma exposure.

3.1.16 Thermogravimetric analysis (TGA)

Thermogravimetric analysis enables the mass loss of a sample to be measured over time as a function of temperature, to provide insights into the thermal stabilities of the materials. Thermogravimetric analyses of the nylon 6

plastic sheet samples were performed using a TGA Q50 (TA Instruments, USA) under a nitrogen atmosphere. Each of the nylon samples (approximately 10 mg) were heated from 25 to 700 °C, with a heating rate of 10 °C/min. The sample purge flow rate was 60 mL/min and the balance purge flow rate was 40 mL/min.

3.2 Method for plasma activation

Following ultrasonic cleaning with acetone, the dry nylon 6 and regenerated cellulose samples were treated with a CCP low-frequency (40 kHz), low-pressure oxygen plasma at a power of 10 W, for exposure times between 10 - 60 s. The samples were placed on a glass holder in the centre of the 1.7 L plasma chamber, made of borosilicate glass. Oxygen gas was allowed to flow through the reactor for 600 s prior to the treatments, to remove any impurities. The oxygen gas flow rate was controlled using mass flow controllers and was held constant at 100 cm^3 min^{-1} for all treatments, with the working pressure kept between 0.2 - 0.5 mbar. A dummy plug was fitted in the secondary gas inlet to ensure that there was no contamination of the plasma chamber with air. After treatments, the samples were exposed to air for 30 s to enable an unavoidable, controlled post-treatment surface oxidation process before being stored under vacuum until analysis.

3.3 Method for plasma etching

The cleaned nylon 6 and regenerated cellulose samples were treated with a low-frequency (40 kHz), low-pressure oxygen plasma at a discharge power of 60 W, for exposure times that varied between 30 - 600 s. The samples were placed on a glass sample holder in the middle of the 1.7 L borosilicate glass plasma chamber. Similarly to the activated samples, oxygen gas was allowed to flow through the reactor for 600 s prior to the treatments, to remove any impurities, and the oxygen gas flow rate was controlled using mass flow controllers and was held constant at 100 cm^3 min^{-1} for all of the plasma treatments. The working pressure was kept between 0.2 - 0.5 mbar. After the plasma treatments, the samples were exposed to air for 30 s for a controlled

post-treatment surface oxidation process before being stored under vacuum until analysis.

3.4 Method for depositing and grafting functional siloxane coatings with HMDSO and HMDSO:O_2 plasmas via plasma polymerisation

The cleaned nylon 6 and regenerated cellulose samples were treated with CCP low-frequency (40 kHz), low-pressure HMDSO and HMDSO:O_2 plasmas at a discharge power of 100 W, for exposure times varying between 30 - 600 s. The samples were initially placed on a glass sample holder in the middle of the 1.7 L borosilicate glass plasma chamber. The liquid HMDSO was stored in a bottle, and the volatile vapour was dosed into the low-pressure plasma chamber through an inlet valve, with the working pressure 0.2 - 0.5 mbar. For the pure HMDSO vapour plasma treatments, the flow rate of the vapour was controlled and held constant at 100 cm^3 min^{-1}. For the HMDSO:O_2 gas mixture plasma treatments, the HMDSO vapour and oxygen gas entered the plasma chamber through two separate inlet valves, with the flow rate held at a constant ratio of 1:6 (HMDSO:O_2). This ratio was selected due to previous literature reports suggesting that for plasmas with different discharges and frequencies, flow rate ratios of >1:6 have the ability to yield films with increased oxygen content and inorganic character, with substantially different properties to pure HMDSO plasmas.[61, 66] These different treatments enabled the versatility of the deposition technique and its dependence on gas choice to be investigated, whilst also enabling comparisons to be made to previous work utilising different plasma setups/configurations. For both the HMDSO and HMDSO:O_2 treatments, the gases were allowed to flow through the reactor for 600 s prior to the treatments, to remove any impurities. Following the plasma treatments, the samples were exposed to air for 30 s before being stored under vacuum until further analysis.

3.5 Method for ageing of oxygen plasma treated nylon 6 and regenerated cellulose

The nylon 6 and regenerated cellulose samples were initially treated according to the plasma activation and plasma etching procedures described in Sections 3.2 and 3.3 respectively. In order to study the ageing properties of the polymer samples following plasma treatment, the samples were exposed to air under ambient conditions for time periods ranging between 0 and 20 days, before being stored under vacuum until being analysed (the samples treated for 0 days were still exposed to air for 30 s immediately following plasma treatment, as described earlier in the activation and etching procedures). Additionally, to study the effects of different storage conditions on the ageing of the plasma treated polymer materials, the nylon and cellulose samples treated for 40 s at 10 W (activated) and 600 s at 60 W (etched) were stored under vacuum for time periods ranging from 0 to 20 days until analysis, to test the ability of vacuum conditions to prevent the hydrophobic recovery of the materials. The nylon 6 samples were also fully immersed and stored in deionised water for time periods ranging from 0 to 20 days, with subsequent static contact angle measurements being undertaken. The regenerated samples were not stored in water due to the high level of swelling induced by immersion in water, which prevented static contact angles from being measured.

4. Characterisation of plasma treated nylon 6 and regenerated cellulose for mechanistic understandings of plasma activation

In the research described in this chapter, the chemical and physical effects of the plasma activation of nylon 6 plastic sheets and regenerated cellulose films were studied, using CCP low-frequency, low-pressure oxygen plasma. Through isolating the surface functionalisation/activation plasma process through parameter control, it was possible to quantify the effects of varying the plasma exposure time of the polymer substrates when activating the surfaces. Also, through studying both materials, it has been possible to see the importance of the chemical structure of the substrate and its corresponding susceptibility to plasma activation, through comparing aliphatic nylon 6 structures to cyclic regenerated cellulose samples that have a high initial surface saturation of oxygen functionalities.

4.1 Pre-cleaning of samples prior to plasma treatment

To establish a procedure for the sample preparation of the nylon 6 and regenerated cellulose samples prior to treatment with plasma, a series of solvent cleaning procedures were implemented to prevent any interfering species/contaminants from affecting any of the treatments or subsequent analysis performed. These cleaning procedures were then verified through the use of XPS and SEM, through the observed reduction in surface contamination (adventitious carbon) using XPS, alongside SEM images confirming that the samples had not been physically/morphologically damaged.

Nylon 6 polymers generally exhibit excellent solvent resistance to a range of organic solvents.[134] For this reason, acetone was selected as a solvent to remove any organic surface contamination from the nylon 6 plastic sheets through ultrasonic washing, without affecting the physical properties of the

plastics. This was due to acetone having the ability to remove most if not all residual oils, dusts and greases that may have been deposited on the materials during manufacturing/storage. Acetone is also fast-evaporating (boiling point of 56°C), leading to a short drying time being required for the nylon 6 samples after washing (all samples were allowed to dry at room temperature for 30 minutes following cleaning).[134]

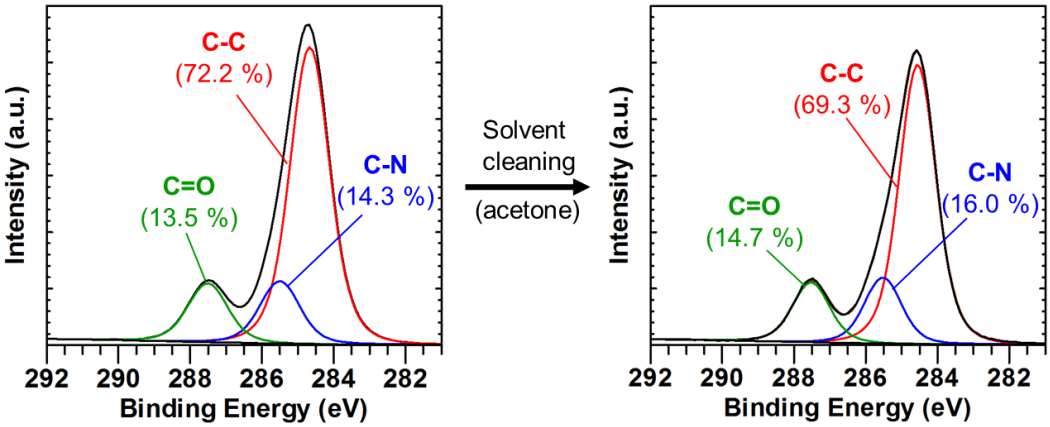

Figure 4-1. High resolution C1s XPS spectra of nylon 6 prior to and following solvent cleaning.

From the high resolution C1s XPS spectra of nylon 6 shown in Figure 4-1, the cleaning of the nylon 6 surface with acetone was shown to effectively remove some of the adventitious carbon present, which can be seen through the reduction in the C-C peak from 72.2% to 69.3% (this reduction was seen in all cleaned nylon 6 samples). The initial C-C component in the unwashed sample indicated that there was a degree of surface contamination due to the presence of hydrocarbons on the surface, with its reduction in intensity verifying the cleaning capabilities of acetone through ultrasonic washing. This simple process was therefore used to clean all nylon 6 samples prior to plasma treatment, ensuring reproducibility within experimental procedures.

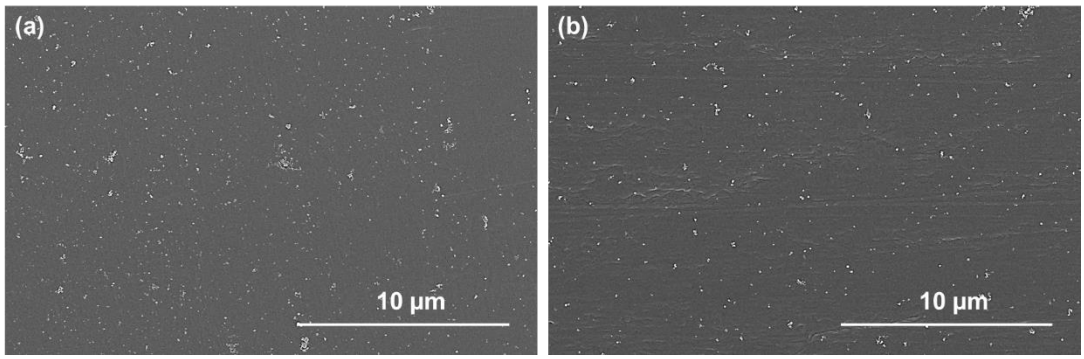

Figure 4-2. SEM images of nylon 6 (a) prior to solvent cleaning and (b) following solvent cleaning.

The SEM images displayed in Figure 4-2 show that the untreated nylon substrates were generally smooth, with a large number of surface nanoparticles/agglomerates that were likely formed during the manufacturing and processing of the sheeted plastic. Ultrasonic cleaning with acetone did not appear to alter the physical or morphological properties of the nylon 6 surfaces. Furthermore, the cleaning process did not appear to significantly reduce the number of surface nanoparticles, suggesting that they were embedded into the surface, rather than being surface contaminants that could be washed away with the solvent cleaning. To check the composition of these surface agglomerates, EDX analysis was performed on areas of the smoother surface that did not contain these surface particles, and compared against EDX spectra of areas of the surface that had a large presence of these particles. The resulting spectra are shown in Figure 4-3.

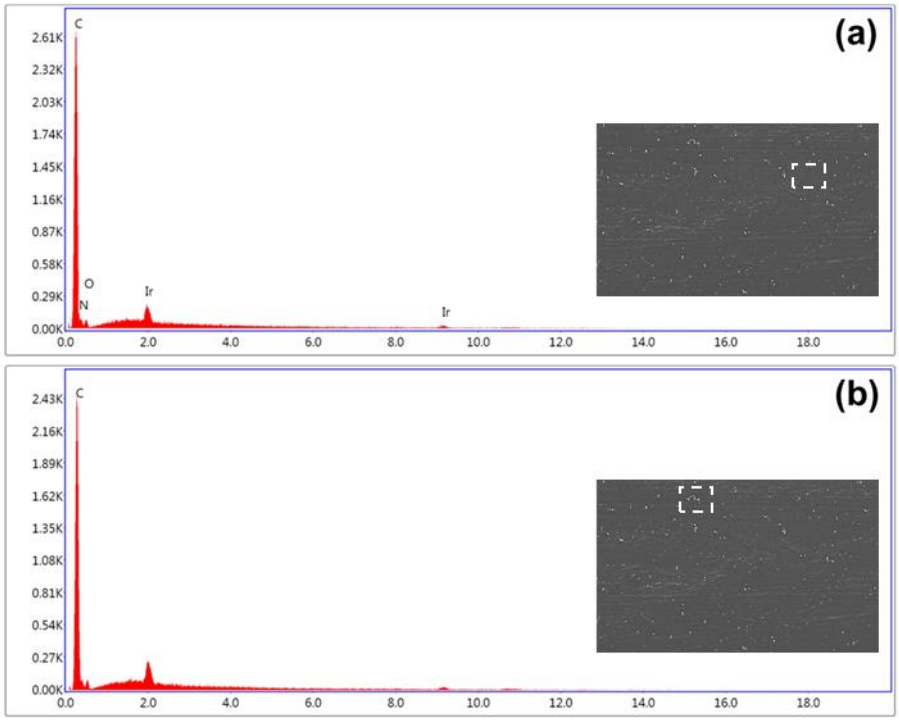

Figure 4-3. EDX spectra showing (a) the smoother areas of the cleaned nylon 6 surface and (b) the area of the cleaned nylon 6 surface containing surface nanoparticles/agglomerates.

Figure 4-3a shows the EDX spectrum of a smooth area of the cleaned nylon 6 surface, confirming that the surface is organic in nature with only carbon, nitrogen and oxygen detected (the iridium peak was seen due to the samples being sputter coated with an ultra-thin layer of iridium). Figure 4-3b confirms that the areas of the cleaned nylon 6 surface containing a number of surface nanoparticles had an essentially identical spectra when compared to the smoother areas of the surface, with primarily carbon being detected. This confirmed that the surface agglomerates were organic in nature, and were likely to have been lower molecular weight oligomeric species formed in the manufacturing/processing of the polymers. This also confirmed that these surface particles were not inorganic additives (such as silicon or calcium).

Similarly to nylon 6, cellulosic polymers also tend to exhibit good chemical resistance against acetone, so acetone was selected as a suitable candidate to be used in the cleaning of the regenerated cellulose film surfaces to remove oils/greases/dust.[135] This enabled consistency in the sample preparation of

both the nylon and cellulose samples. XPS and SEM were again used to prove that the acetone had been effective in remove any potential surface contaminants such as dusts or oils.

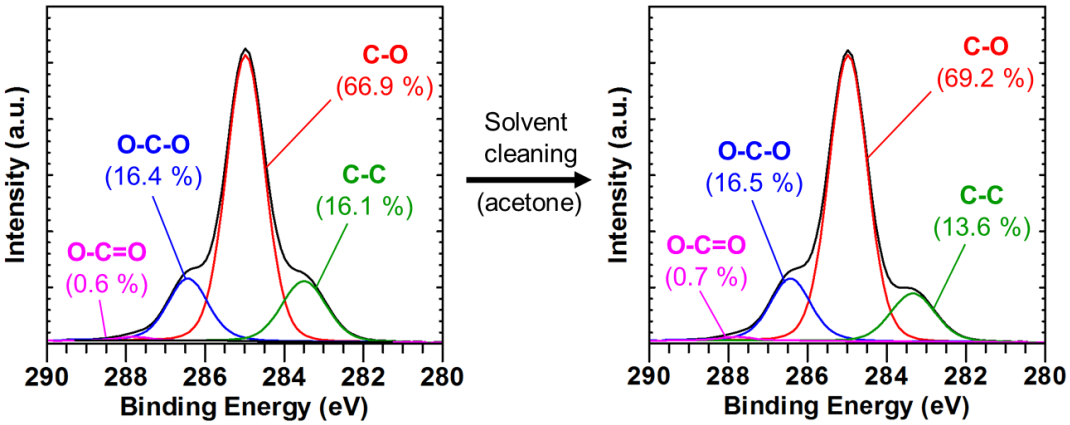

Figure 4-4. High resolution C1s XPS spectra of regenerated cellulose prior to and following solvent cleaning.

In the high resolution C1s XPS spectra of regenerated cellulose shown in Figure 4-4, there is a clear reduction in the C-C peak from 16.1 % to 13.6 %, indicating the reduction in adventitious carbon after ultrasonic washing with acetone. Due to the acetone having a clear ability to remove hydrocarbon contamination in both nylon 6 and regenerated cellulose, it was implemented as part of the systematic sample preparation for both materials, and helped to provide a baseline from which all polymer samples could be subsequently treated with various plasma treatments. The SEM images in Figure 4-5 were used to check for any potential changes in the physical and morphological properties of cleaned the cellulose surfaces.

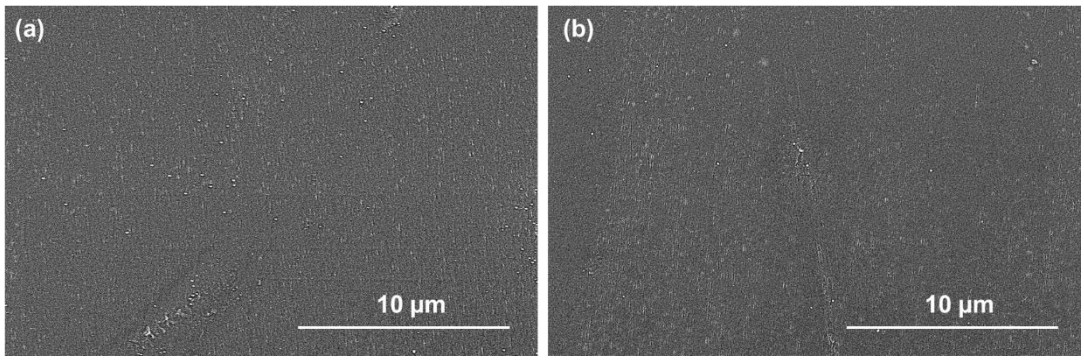

Figure 4-5. SEM images of regenerated cellulose (a) prior to solvent cleaning and (b) following solvent cleaning.

The SEM image in Figure 4-5a showing the regenerated cellulose film surface before solvent cleaning confirms that the surface was generally quite smooth but with some nanoscale defects, and a number of surface agglomerates that were similar to those present on the nylon 6 surface. Following solvent cleaning with acetone, the film surfaces remained unchanged and relatively smooth, with some defects/scratches, and no obvious alteration in morphology or swelling of the polymer film. The number of surface nanoparticles did not appear to change in any significant way, suggesting that these agglomerates were embedded into the surface of the films, and were not contaminants.

The EDX spectra in Figure 4-6 were used to confirm whether these surface particles were lower molecular weight surface oligomers formed in the processing of the materials, or from the presence of inorganic additives. It was apparent from the analysis of the smoother area of the regenerated cellulose film (Figure 4-6a) that the primary composition of the surface was carbon and oxygen; this was expected based on the repeating glucose structure of regenerated cellulose repeating units. The analysis of the area containing a large proportion of the surface particles (Figure 4-6b) remained essentially unchanged from the EDX spectra of the smoother region, confirming that similarly to the nylon 6 surface, the surface agglomerates on the regenerated cellulose films were attributed to organic matter.

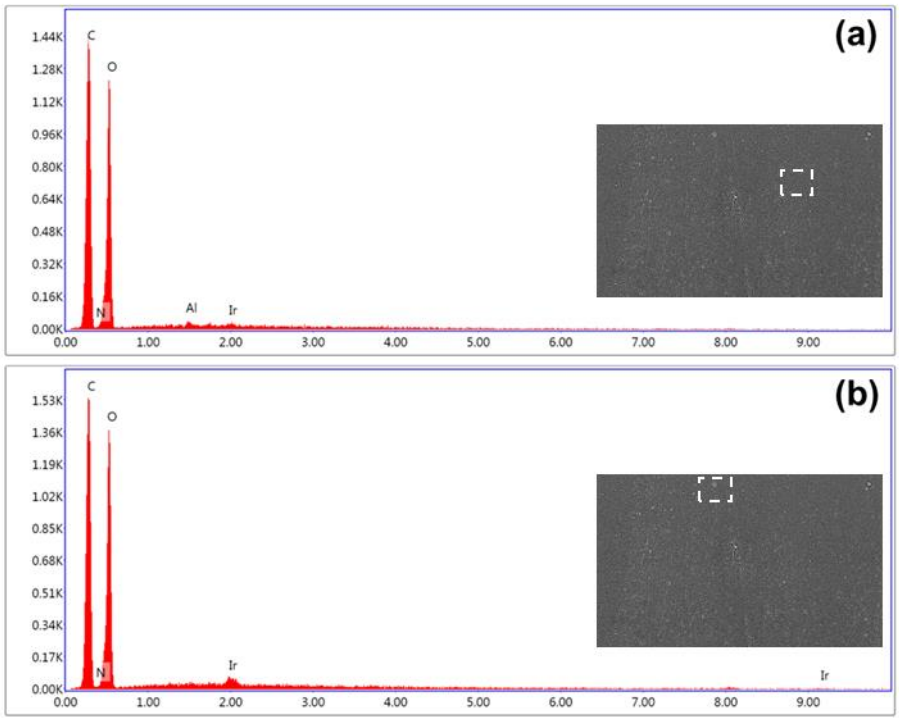

Figure 4-6. EDX spectra showing (a) the smoother areas of the cleaned regenerated cellulose surface and (b) the area of the cleaned regenerated cellulose surface containing surface nanoparticles/agglomerates.

4.2 Determination of parameters for the plasma activation of nylon 6 and regenerated cellulose

Due to the limited literature available relating to the plasma treatment of polymers with CCP low-frequency, low-pressure plasma systems, and the large variation in plasma system specifications across different plasma system manufacturers, all parameters had to be determined empirically in this work. In order to determine appropriate/representative parameters to study “plasma activation” and “plasma etching” as separate phenomena, nylon 6 and regenerated cellulose samples were initially screened through the use of mass loss measurements, as mass loss is indicative of an etching effect. Through identifying parameters that would enable the polymer materials to be treated with oxygen plasma without instigating any loss of mass, mechanisms of plasma activation could then be studied through further detailed chemical and morphological analyses of the materials under the selected conditions.

Plasma etching or “nanotexturing” could then be studied under conditions that led to varying degrees of mass loss following plasma exposure. Table 4-1 shows relevant screening data through mass loss experiments for nylon 6 and regenerated cellulose substrates following oxygen plasma treatment.

Table 4-1. Factor effects on mass loss for oxygen plasma treated nylon 6 and regenerated cellulose.

Run Order	Treatment time (s)	Power (W)	Mass Loss ± SD (mg cm^{-2})	
			Nylon 6	Regen. Cellulose
1	600	100	1.04 ± 0.05	1.71 ± 0.07
2	300	60	0.39 ± 0.04	0.76 ± 0.05
3	10	10	0.00 ± 0.00	0.00 ± 0.00
4	600	10	0.29 ± 0.05	0.67 ± 0.03
5	10	100	0.03 ± 0.02	0.08 ± 0.02

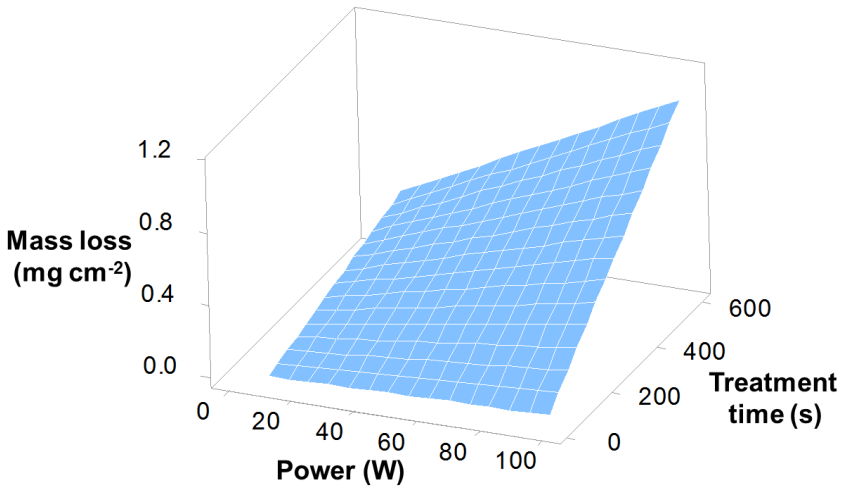

Figure 4-7. Mass loss response surface plot using DoE for oxygen plasma treated nylon 6 with varying discharge power and treatment time.

The multivariate analysis for the oxygen plasma treatment of nylon 6 is displayed in the surface plot in Figure 4-7. Alongside the data in Table 4-1, the plot shows that generally, at each of the different discharge powers ranging between 10 and 100 W, there was a predicted linear trend of increasing mass loss with increasing treatment time. Likewise, there was also

a predicted general linear increase in mass loss with increasing power at each of the different treatment times. These linear trends were indicative of a high level of control in terms of plasma uniformity and gas flow within the low-pressure plasma system. The observed trends of increasing mass loss can be rationalised by the fact that increasing the amount of energy supplied to the system, either through increased discharge power or longer exposure times increased the amount of ion bombardment by the plasma, and hence the extent of etching. It was noted that the data point obtained from the plasma treatment at 10 W for 10 s reported no mass loss, with the model also predicting that shorter treatment times up to approximately 60 s at 10 W would also have no/negligible mass loss. For this reason, these conditions were selected to investigate plasma activation in detail throughout the study reported in Chapter 4, having the potential to activate/functionalise the nylon 6 polymer sheets, without any interfering etching effects. Given that the response plot was constructed from only five data points, it was only used for screening purposes to find conditions that would induce plasma activation and plasma etching processes, rather than for obtaining accurate models for mass loss within the plasma system. The accuracy of the models was verified later in studies reported in Chapter 5.1.2, whereby etch rates for each of the different plasma powers were calculated.

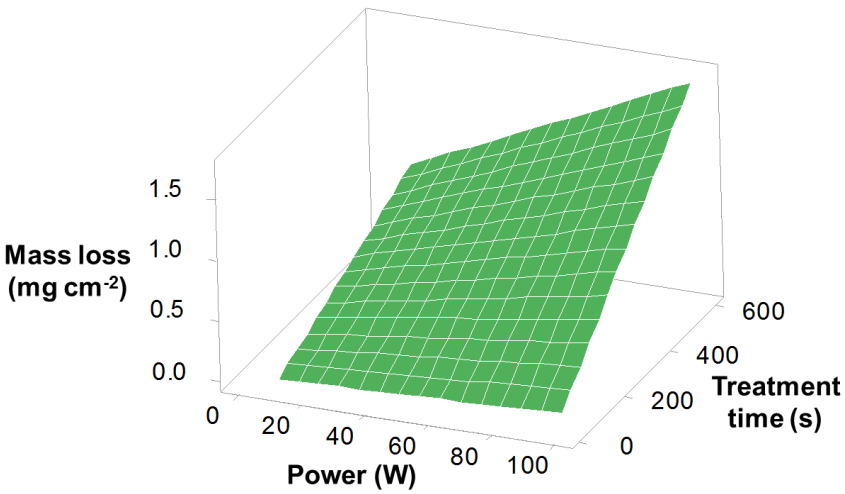

Figure 4-8. Mass loss response surface plot using DoE for oxygen plasma-treated regenerated cellulose with varying discharge power and treatment time.

The response surface plot in Figure 4-8 and data displayed in Table 4-1 confirmed that increasing the discharge power and exposure times of the oxygen plasma treatments also resulted in a linear increase in mass loss for the regenerated cellulose samples. From these mass loss models alone, it appeared that regenerated cellulose was more susceptible to the ion bombardment capabilities of the plasma than nylon 6 from the increased mass loss, resulting in chain scission and subsequent etching of the polymer chains. However, the linear trends of mass loss were effectively identical for both materials, suggesting that in terms of etching, the plasma can be considered as qualitatively “substrate-independent” for nylon 6 and regenerated cellulose.

As most of the conditions above 10 W provided at least some degree of etching/mass loss of both material samples, it was important to select a set of conditions to provide representative samples to study the phenomenon of plasma etching. In order to study the mechanisms of this plasma etching in more detail, the parameters of 60 W discharge power with varying treatment times were selected to provide representative conditions for etching for both the nylon 6 and regenerated cellulose samples, as they both had a wide variation in the degree of etching at 60 W. This ranged from very low level etching at shorter treatment times, to significantly higher levels following longer exposure to the oxygen plasma. Furthermore, the data point obtained for the treatments at 100 W for 600 s resulted in macroscopic scalding of the nylon and cellulose samples. This suggested that they had been over-treated/degraded under these conditions, meaning that 60 W was a more suitable power for the etching process. Keeping the conditions fixed with only plasma treatment time varied for both materials also enabled direct comparisons to be made between the two, through a range of surface-chemical and morphological analysis. Therefore, these conditions formed the basis of the study reported in Chapter 5.

4.3 Plasma activation of nylon 6 and regenerated cellulose

4.3.1 Enhancement of surface wettability

The wettability of the untreated and plasma-treated samples was assessed using apparent static contact angle measurements. From the contact angle measurements displayed in Figure 4-9, it can be seen that increasing the treatment times with the oxygen plasma led to a relatively linear decrease in contact angle, with the overall hydrophilicity and wettability of both the nylon 6 plastic sheets and the regenerated cellulose films increasing. Such an increase is more clearly illustrated in the linear increase shown in apparent surface energy.

The untreated nylon 6 had an average contact angle value of 63.2 ± 1.2°. Following the longest plasma exposure times, there was a significant increase in hydrophilicity, reaching the lowest value of 38.4 ± 1.4° after 40 s. Compared to the untreated nylon 6 samples, there were also gradual reductions in contact angle after 10 s, 20 s, and 30 s respectively. These measurements can be rationalised from the XPS and SIMS data shown later in this chapter, that confirm the ability of the oxygen plasma to attach a number of “active” hydrophilic groups within the polymeric structure; this increased the overall wettability of the nylon 6 substrates. The contact angle measurements were not influenced by any changes in surface morphology or roughness during these short treatment times (≤ 40 s), as confirmed by the SEM and AFM images.

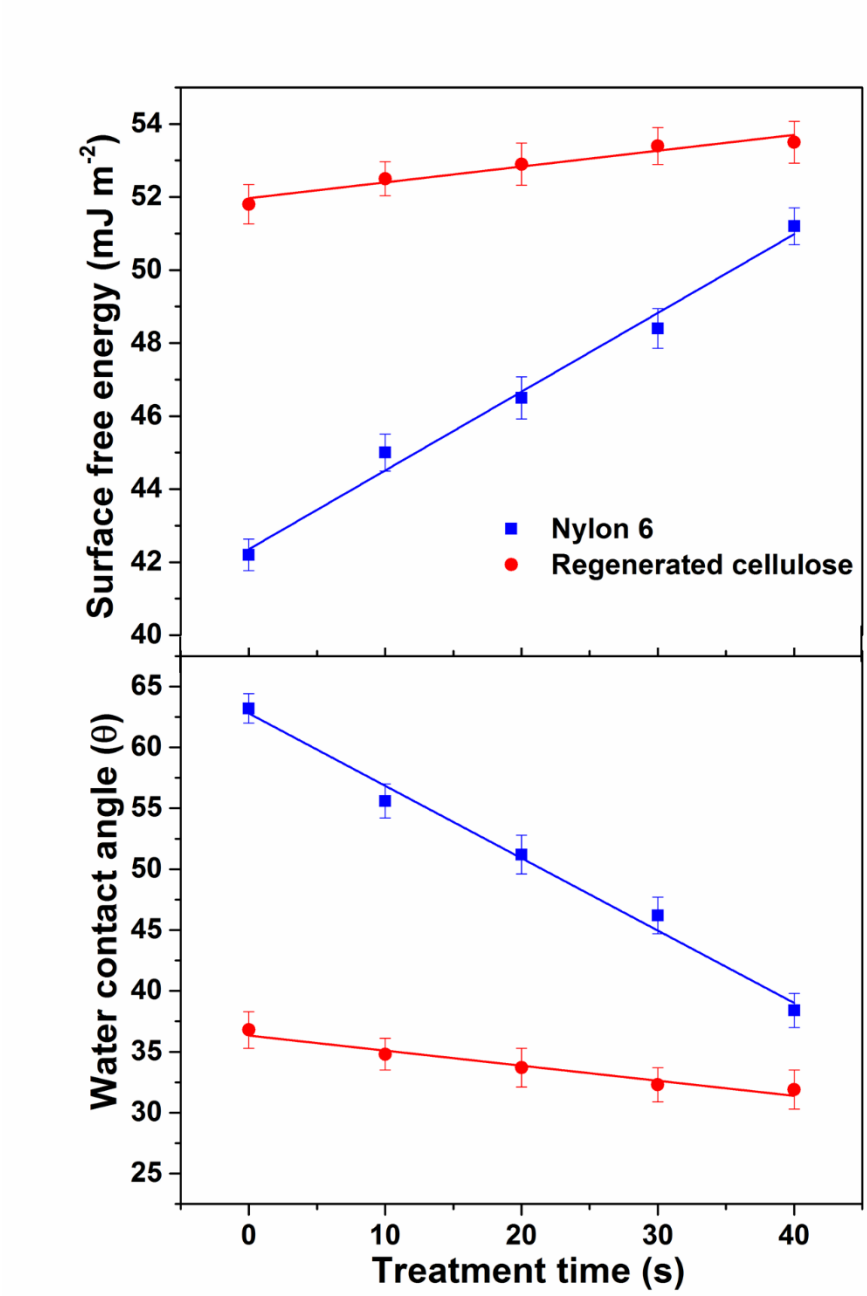

Figure 4-9. The variation in apparent surface free energy and static contact angle of nylon 6 plastic sheets and regenerated cellulose films with increasing oxygen plasma treatment time at 10 W.

Interestingly, in the oxygen plasma treatment of regenerated cellulose between 10 - 40 s, the decrease in static contact angle values (and increase in apparent surface energy) was much less substantial compared to that of nylon 6, and only saw a reduction from 36.8 ± 1.5° (untreated) to 31.9 ± 1.6° after 40 s of plasma treatment. This clearly shows that the chemical structure of the polymer surface is important when considering the substrate-plasma

interactions. As the untreated regenerated cellulose surface structure has an abundance of polar oxygen functional groups, it is already greatly hydrophilic before the plasma exposure. It also has a large degree of hydrogen bonding present in the cellulose macromolecules. The cellulose surface appears to be less receptive in accepting additional oxygen functionalities from the reactive plasma species, as the surface is already close to saturated with polar groups, and has fewer sites in which the additional functional groups can be attached. In contrast, nylon 6 has several potential sites for the oxygen plasma to attach, meaning that there is a greater potential for large increases in wettability through the surface saturation of the aliphatic polymer chains with oxygen-containing species. It is likely that the observed small decrease in contact angle in regenerated cellulose can be attributed to a slight absorption of oxygen from the plasma, while the larger decrease seen in nylon is due to a significant surface-chemical modification through the attachment of polar groups. This theory is evidenced and discussed in more detail later in the chapter when considering the XPS results of plasma activated substrates. It is also worth noting that for both plasma treated polymers, different drop positions were tested on each of the sample surfaces, and the contact angle values did not vary significantly (as shown by the relatively small errors in the measurements). This suggests that the uniform gas flow that is utilised in the low-pressure plasma treatment method had evenly distributed the surface chemical modifications across all areas of the substrates.

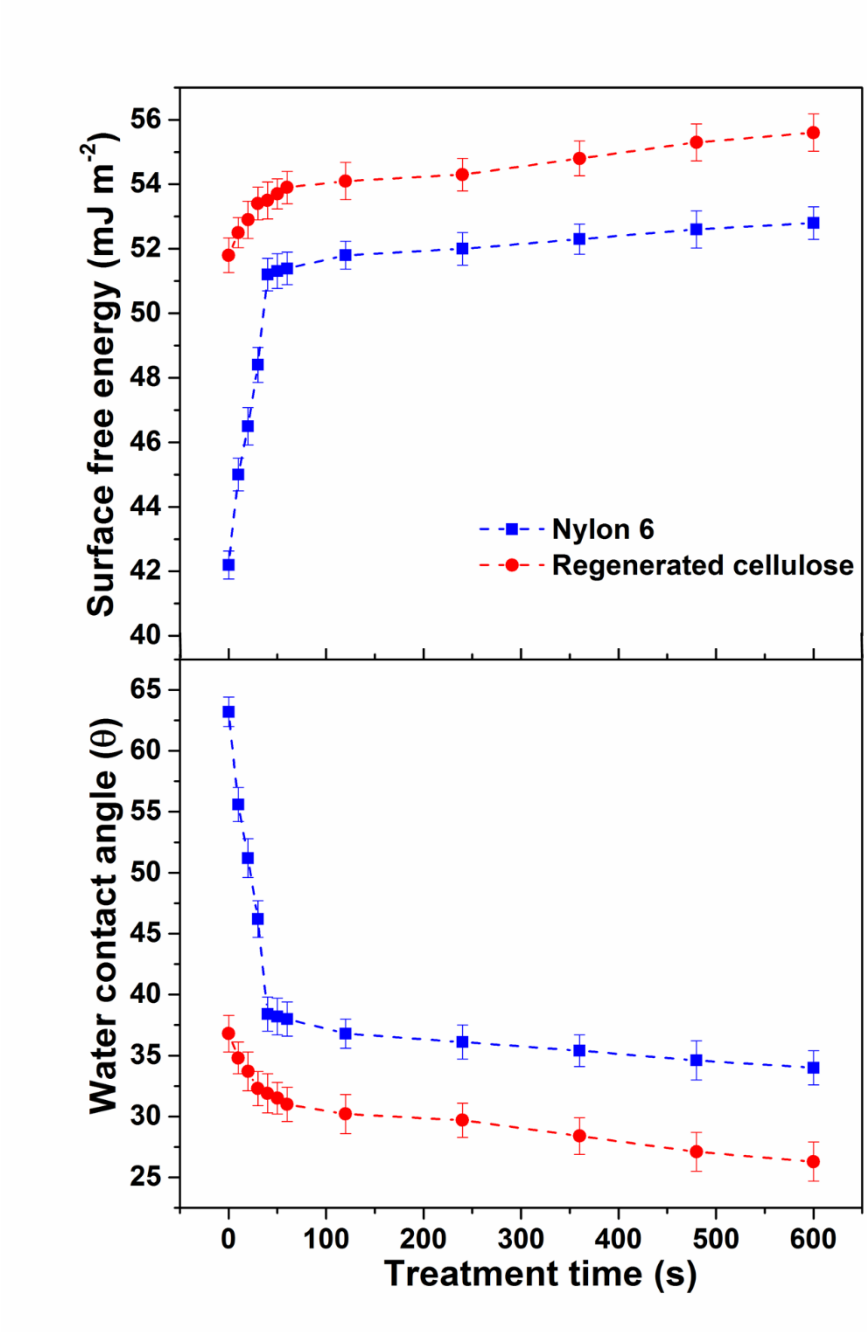

Figure 4-10. The variation in surface energy and static contact angle of nylon 6 plastic sheets and regenerated cellulose films following longer exposure times to oxygen plasma at 10 W.

Although the static contact angle and apparent surface energy values from Figure 4-9 showed that plasma activation led to a linear decrease in contact angle (and therefore linear increase in surface energy), when the treatment time was extended over a longer period of 600 s at low power (10 W), the relationship between exposure time and contact angle changed significantly and produced a non-linear fitting for both nylon 6 and regenerated cellulose.

This is illustrated in Figure 4-10. In the case of nylon 6, there was a clear rapid initial functionalisation of the material surface, which led to a sharp decrease in contact angle value between 0 and 40 s treatment time. This then appeared to level off, suggesting that the surface had reached a saturation point for functionalisation with oxygen plasma. Such a saturation of the nylon 6 repeating units with oxygen groups then prevented any further large increase in surface wettability. The mass loss surface plot modelled previously in Figure 4-7 suggested that there would be a predicted slight etching that had taken place between 60 and 600 s at 10 W that increased with treatment time, which may account for the slight decrease in contact angle and therefore increase in wettability from 60 s to 600 s, but this had much less of an effect on wettability compared to the initial rapid functionalisation.

The regenerated cellulose films did not have the same sharp decrease in contact angle values as did nylon 6, which can be attributed to the untreated cellulose repeating units already being saturated with oxygen groups prior to plasma exposure. Over time, the regenerated cellulose films experienced a gradual decrease in contact angle, with a slightly curved shape over the 600 s time period. Such a gradual decrease can be attributed to a combination of surface-chemical modifications and loss of mass through etching at longer treatment times.

4.3.2 Gravimetric analysis

Table 4-2: Mass loss results for the oxygen plasma activated nylon 6 and regenerated cellulose samples with varying treatment times at 10 W.

Treatment time (s)	Power (W)	Average Mass Loss (mg cm^{-2})	
		Nylon 6	Regen. Cellulose
10	10	0.00 ± 0.00	0.00 ± 0.00
20	10	0.00 ± 0.00	0.00 ± 0.00
30	10	0.00 ± 0.00	0.00 ± 0.00
40	10	0.00 ± 0.00	0.02 ± 0.01
50	10	0.02 ± 0.01	0.03 ± 0.01
60	10	0.02 ± 0.01	0.05 ± 0.02

The mass loss measurements of the plasma activated nylon 6 and regenerated cellulose samples shown in Table 4-2 confirm that generally, plasma activation did not involve the degradation of surface material. For low power (10 W) treatments between 10 and 30 s, there was no measureable mass loss for either material, suggesting that the observed decrease in surface wettability for these samples was primarily due to a modification in the surface chemistry through the attachment of polar oxygen functionalities or absorption of oxygen (this is explained in more detail later in this chapter when discussing XPS and SIMS data). Nylon 6 also saw no mass loss until 50 s of treatment, while regenerated cellulose exhibited mass loss after 40 s treatment, suggesting that it is more susceptible to the etching effects induced by the surface ion bombardment of the oxygen plasma species. Firstly, this can be attributed to differences in the chemical structures of the two polymers. Nylon 6 is aliphatic polymer with strong polyamide linkages, as the amide groups have a resonance structure due to conjugation from the double bonded oxygen that forms a partial double bond between the nitrogen and carbon atoms. This reduces the ability of nitrogen to act as a leaving group, hence enhancing the stability and therefore oxidation resistance of nylon 6 polyamide polymers. On the other hand, cellulose has repeating glucose units that are connected through *β*-1, 4 covalent glycosidic linkages. The ionising radiation of the oxygen plasma has the ability to degrade these linkages through chain scission.[93] The polyamide links in nylon 6 appear to be more resistant to the oxidative capabilities of the plasma than the *β*-1, 4 linkages of the repeating glucose units of regenerated cellulose, which can largely be attributed to the resonance stabilisation of the polyamide linkages of nylon.

Furthermore, due to cellulose films being substantially thinner than the nylon 6 plastic sheeting, and having more defects prior to plasma exposure shown previously in the SEM images in Figure 4-5, they have greater susceptibility to surface oxidation from the plasma. Nylon is generally a tougher, more durable material than regenerated cellulose, and has better mechanical properties including higher tensile strength and impact strength.[78] These additional factors enable nylon to be more resistant to the destructive effects of the plasma ion bombardment in combination with the structural features of

nylon 6. As only 0.02 - 0.05 mg cm^{-2} of the polymer materials had been detected to have been lost by both materials in the time range between 10 and 60 s at 10 W, it suggests that treatment times in this range generally appropriate for enhancing the surface wettability of substrates without any potentially undesired changes in morphology. The low levels of mass loss can essentially be treated as negligible, and do not affect the bulk properties of the material.

4.3.3 Morphological analysis

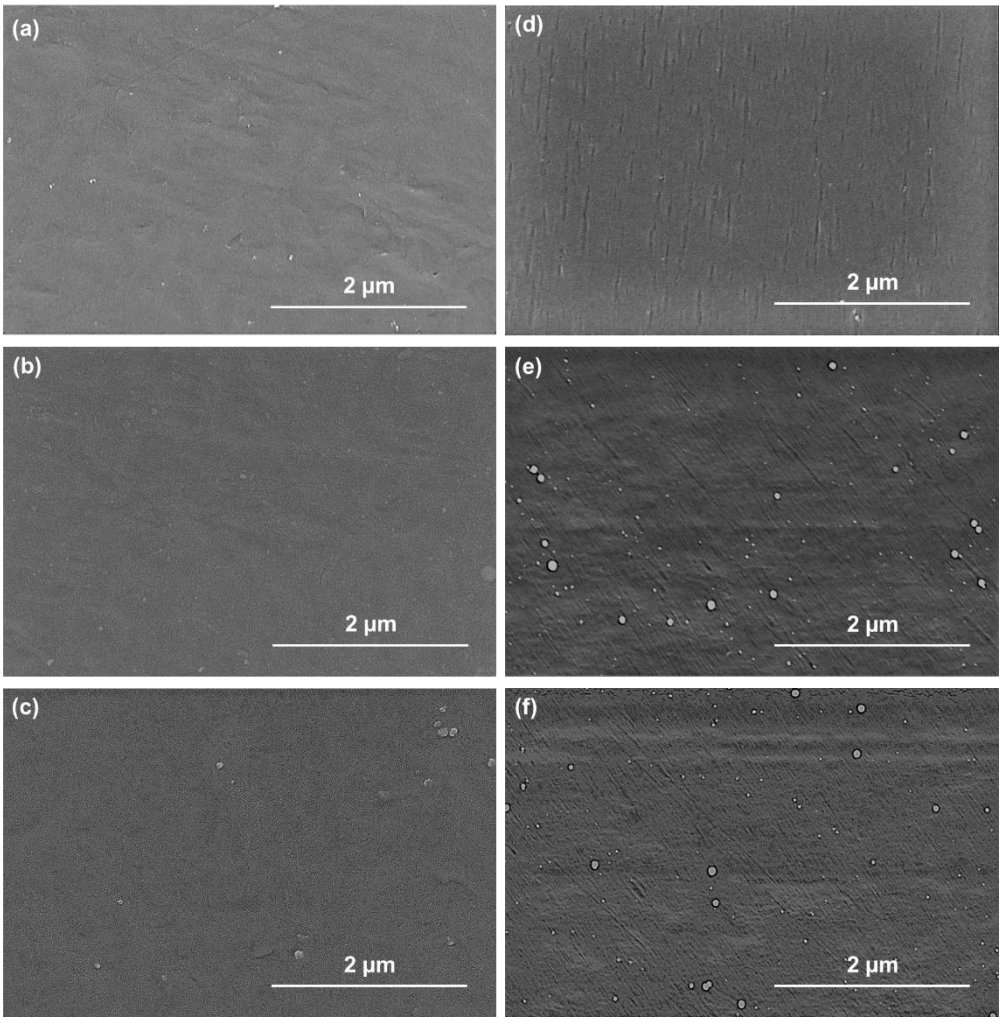

Figure 4-11. SEM images of nylon 6 treated at 10 W for (a) 0 s (untreated); (b) 10 s and (c) 40 s. Images of regenerated cellulose treated at 10 W for (d) 0 s (untreated); (e) 10 s and (f) 40 s.

The SEM images in Figure 4-11 show the surface morphology of the nylon 6 sheets and regenerated cellulose films both before and after low power (10

W) oxygen plasma exposure. The images confirm that there were no significant physical changes to the polymer surface morphology following exposure (40 s) to the plasma at 10 W. Figure 4-11a shows that the untreated nylon 6 sheets were generally smooth with occasional grooves and a number of embedded surface particles. The EDX spectra of these particles were analysed earlier in the chapter (4.1), and were attributed to surface agglomerates formed from the manufacturing and processing of the nylon sheets. After oxygen plasma treatment for 10 s and 40 s (Figure 4-11b and c respectively), the surface of the polymer sheets and embedded surface particles did not change. Almost identical findings were seen when the regenerated cellulose films were exposed to the oxygen plasma for up to 40 s.

The untreated cellulose films displayed in Figure 4-11d showed that the films were generally smooth, but with a number of nanoscale scratches and trenches; there was generally more inherent surface roughness in the cellulose film samples when compared to the nylon 6 samples. Similarly to the nylon surfaces, there were also a number of surface particles that were confirmed to have organic structures by EDX (Section 4.1), and therefore attributed to surface agglomerates formed in the manufacturing of the films. After 10 s and 40 s of plasma treatment (Figure 4-11e and f), there was no obvious change in the morphology of the surfaces. Despite there being a slight detected mass loss of 0.02 mg cm^{-2} after 40 s of treatment, there was still no obvious change in the surface from the SEM images. The lack of morphological change in the activated samples confirmed that under the conditions selected for this study, the plasma treatments were non-destructive to the outer surface layers of the nylon 6 and regenerated cellulose substrates, and the increase in hydrophilicity shown in the contact angle measurements (Figure 4-9) was caused entirely by chemical changes; further evidence for these chemical changes are illustrated in the XPS and SIMS data shown in

Section 4.3.4. In terms of morphology, the treatments can therefore be considered as substrate-independent based on nylon and cellulose.

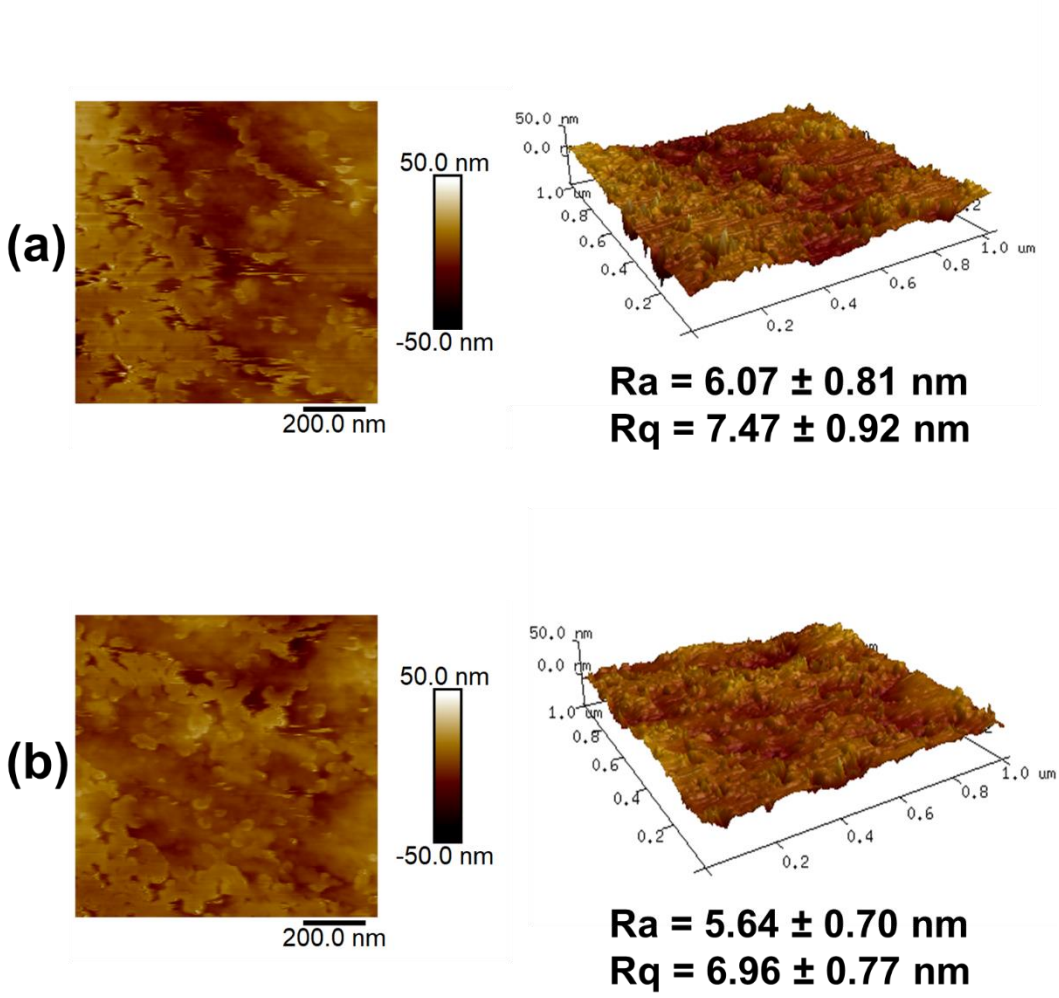

Figure 4-12. AFM images of: (a) untreated nylon 6; (b) oxygen plasma treated nylon 6 for 40 s at 10 W.

AFM was used to provide further details regarding the quantification of surface roughness of the nylon 6 samples before and after plasma activation. It is well-known that low-pressure plasma treatments of polymer materials generally have the effect of increasing the surface roughness.[136] However, under the conditions adopted for this study, the SEM images showed no obvious changes in surface morphology. The AFM images and corresponding surface roughness measurements shown in Figure 4-12 were in agreement with the information provided by the SEM images, and confirmed that there had been no induced surface roughness or notable change in the nanotopography of

the plasma-activated samples. The root mean square roughness (Rq) values for the untreated (7.47 ± 0.92 nm) and 40 s oxygen plasma-treated (6.96 ± 0.77 nm) were both very similar, and within the error limits of each measurement, confirming that the plasma had not increased the surface roughness. Although the roughness Rq value was slightly smaller for the plasma-treated surface, this difference was attributed to the general variation between different areas of the manufactured sheets that were present in all samples. The roughness average (Ra) values for the untreated (6.07 ± 0.81 nm) and 40 s plasma treated (5.64 ± 0.70 nm) were also both very similar, further confirming the lack of morphological change induced by the plasma. Both samples showed generally smooth surfaces, with small areas of slight roughness. The highest points on the AFM images were attributed to the embedded surface particles, which had heights varying between 40 and 50 nm. The AFM data further confirmed that the plasma activation process that occurred under the selected conditions was an entirely surface chemical driven process, with no observed physical change in the surface roughness or appearance.

4.3.4 Surface chemical analysis

From the XPS survey spectra for the untreated and plasma activated nylon 6 samples shown in Figure 4-13, it is evident that increasing the plasma treatment time increased the amount of oxygen present on the surface of the samples, hence increasing the O/C ratios. The amount of carbon detected reduced with treatment time, while the level of nitrogen stayed relatively constant throughout the exposure, suggesting that the amide groups were relatively unaffected by the treatments.

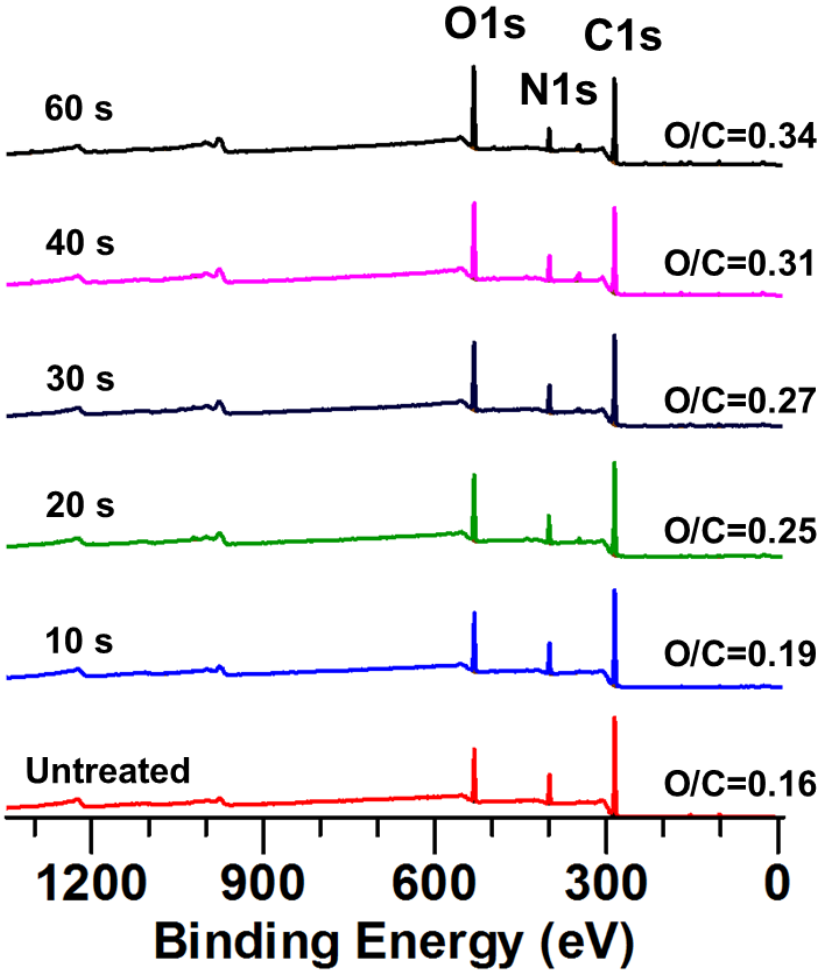

Figure 4-13. XPS survey spectra of untreated and oxygen plasma treated nylon 6 at 10 W for different treatment times.

The elemental composition data obtained from the survey spectra are summarised in Table 4-3. In addition to the detected oxygen, carbon and nitrogen peaks, there were also residual traces of silicon, calcium, sodium, and magnesium in each of the samples that are not reported in this table, due to their negligible amounts (< 1%); they were attributed to general surface contaminants, and their amounts were not altered in a significant way by plasma exposure.

Table 4-3. Elemental composition from the XPS data obtained for the untreated and oxygen plasma treated nylon 6 samples.

	Elemental composition (%)				C1s peak area (%)				
Treatment time (s)	Carbon	Oxygen	Nitrogen	O/C ratio	C-C	C-N	C=O	C-O(H)	O-C=O
0	76.0±1.1	12.3±0.3	10.0±0.4	0.16±0.01	69.0±0.4	16.3±0.2	14.7±0.4	0.0±0.0	0.0±0.0
10	75.0±1.3	14.0±1.0	10.3±0.4	0.19±0.02	62.8±0.9	16.4±0.2	15.8±0.6	4.1±0.3	0.9±0.2
20	70.5±1.1	17.7±0.9	10.1±0.2	0.25±0.02	59.9±2.6	16.2±0.9	16.4±1.5	5.9±0.3	1.6±0.6
30	69.0±1.1	18.5±1.3	10.1±0.5	0.27±0.02	59.2±1.3	15.9±0.4	15.8±0.7	7.0±0.4	2.1±0.6
40	66.8±1.4	20.8±0.7	10.2±0.7	0.31±0.02	58.5±1.9	15.6±0.3	15.4±1.6	7.2±0.7	3.3±0.3
60	66.2±0.9	22.4±1.5	10.1±0.5	0.34±0.03	58.0±1.4	15.4±0.3	15.1±1.5	7.7±1.5	3.8±0.4

After treatment for 10 s, the nylon 6 saw an increase in oxygen content of 1.7%, suggesting that the ratio of oxygen-containing functional groups to carbon atoms had increased within the polymer chains. The oxygen content then continued to increase progressively up to a maximum of 22.4% following 60 s of treatment. This increase was caused through the plasma generated oxygen radical species reacting with the surface polymer chains of the nylon 6, forming reactive radical sites through hydrogen abstractions. These reactive radical centres then rearranged/recombined or reacted with oxygen upon exposure to air following the treatments, to produce more hydrophilic functionalities such as C-OH, C=O and O–C=O. Longer exposure times increased the concentration of these newly formed functional groups, which correlated well with the increase in wettability seen through the contact angle measurements in Section 4.3.1.

In addition to showing the general trends from the plasma exposure, the XPS data obtained enabled the “spread” of chemical modifications across the treated surfaces to be analysed in terms of homogeneity. For each of the plasma treatment conditions, there were three separate samples that were measured, at different positions on each sample. From the errors shown in Table 4-3 (representing the standard deviations between the three samples under identical treatment conditions), it can be seen that the general variations

for each elemental/functional group peak area were small, with the largest deviation being ± 2.6%. The small variations in the sample data suggested that the extent of the surface modifications induced by the plasma was relatively even at different positions in the plasma chamber, confirming that low-pressure plasma systems have the ability to generate a uniform plasma within the plasma chamber.

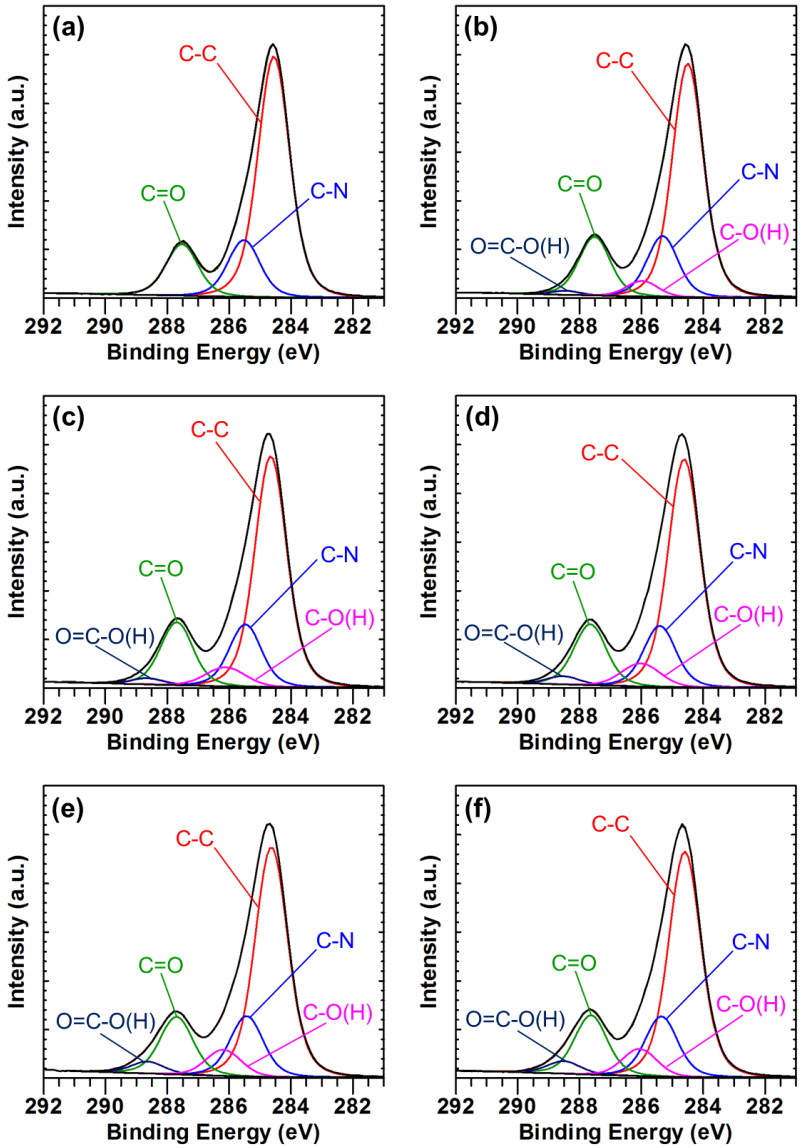

Figure 4-14. High resolution C1s XPS spectra with peak fitting of plasma treated nylon 6 at 10 W for (a) 0 s (untreated); (b) 10 s; (c) 20 s; (d) 30 s; (e) 40 s (f) 60 s.

Deconvolution of the C 1s spectra of each of the samples has enabled such an increase in oxygen to be characterised further, showing the functional

groups formed following oxygen plasma treatment. From the high-resolution C1s XPS spectra shown in Figure 4-14, the changes in surface functionalities following plasma activation can be seen. In the untreated nylon 6 spectra displayed in Figure 4-14a, it is shown that the functional groups identified as being present in the peak fitting model were C-C, C-N, and C=O. This corresponded to the functionalities present within the nylon 6 repeating unit and was consistent with peak fittings found in the literature.[137]

The ratio of each functional group also correlated with the polymer repeating unit. Following plasma treatment for 10 s, at 10 W (Figure 4-14b), there was a slight increase in the percentage of C=O groups present when compared to the untreated samples (an increase of 1.1%). Also, newly formed C-OH (4.1%) and O-C=O (0.9%) functionalities were identified. These were attributed to the formation of hydroxyl groups and more heavily oxidised species in the form of carboxylic acid groups through plasma oxidation, bond scission, and subsequent structural rearrangements/reactions with air following plasma treatment. Some of the main initiation, propagation and termination steps that led to the formation of these groups are postulated in the general mechanism:

Initiation

$O\cdot + R\text{-}C\text{-}H \rightarrow R\text{-}C\cdot + OH$

Propagation

$R\text{-}C\cdot + O \rightarrow R\text{-}C\text{-}O\cdot$

$R\text{-}C\cdot + O_2 \rightarrow R\text{-}C\text{-}O_2\cdot$

$R\text{-}C\cdot + O_3 \rightarrow R\text{-}C\text{-}O\cdot + O_2$

$R\text{-}C\text{-}O\cdot \ _{(\beta\text{-scission})} \rightarrow R\text{-}HC{=}O + HR\text{-}C\cdot$

$R\text{-}HC{=}O + O\cdot \rightarrow R\text{-}\cdot C{=}O + OH$

$HO\cdot + R\text{-}HC{=}O \rightarrow R\text{-}\cdot C{=}O + H_2O$

Termination

$H\cdot + R\text{-}C\cdot \rightarrow R\text{-}CH$

$HO\cdot + R\text{-}C\cdot \rightarrow R\text{-}C\text{-}OH$

$R\text{-}\cdot C{=}O + \cdot OH \rightarrow R\text{-}(OH)C{=}O$

Whereby initiation begins with hydrogen abstraction from the surface polymer chains by the gaseous oxygen plasma radical species, which leads to the generation of free radicals. These free radicals then further react with the oxygen species (including O_2 and O_3) and form peroxy or alkoxy radicals. Peroxy radicals have the ability to subtract hydrogen from neighbouring sites on the same polymer chain, or from different polymer chains to form hydroperoxides, which can then decompose to form various oxidised functionalities. Alkoxy radicals can produce alcohol groups, or promote *β*-chain scissions that can lead to the formation of ketones, aldehydes or heavily oxidised carboxylic acids. Termination occurs through the formation of lower energy molecules by reactions between hydrogen atoms and OH from the gas phase with other radicals, as they form more stable end products.[22] These mechanisms are not specific to nylon and can also be applied to cellulose polymers.

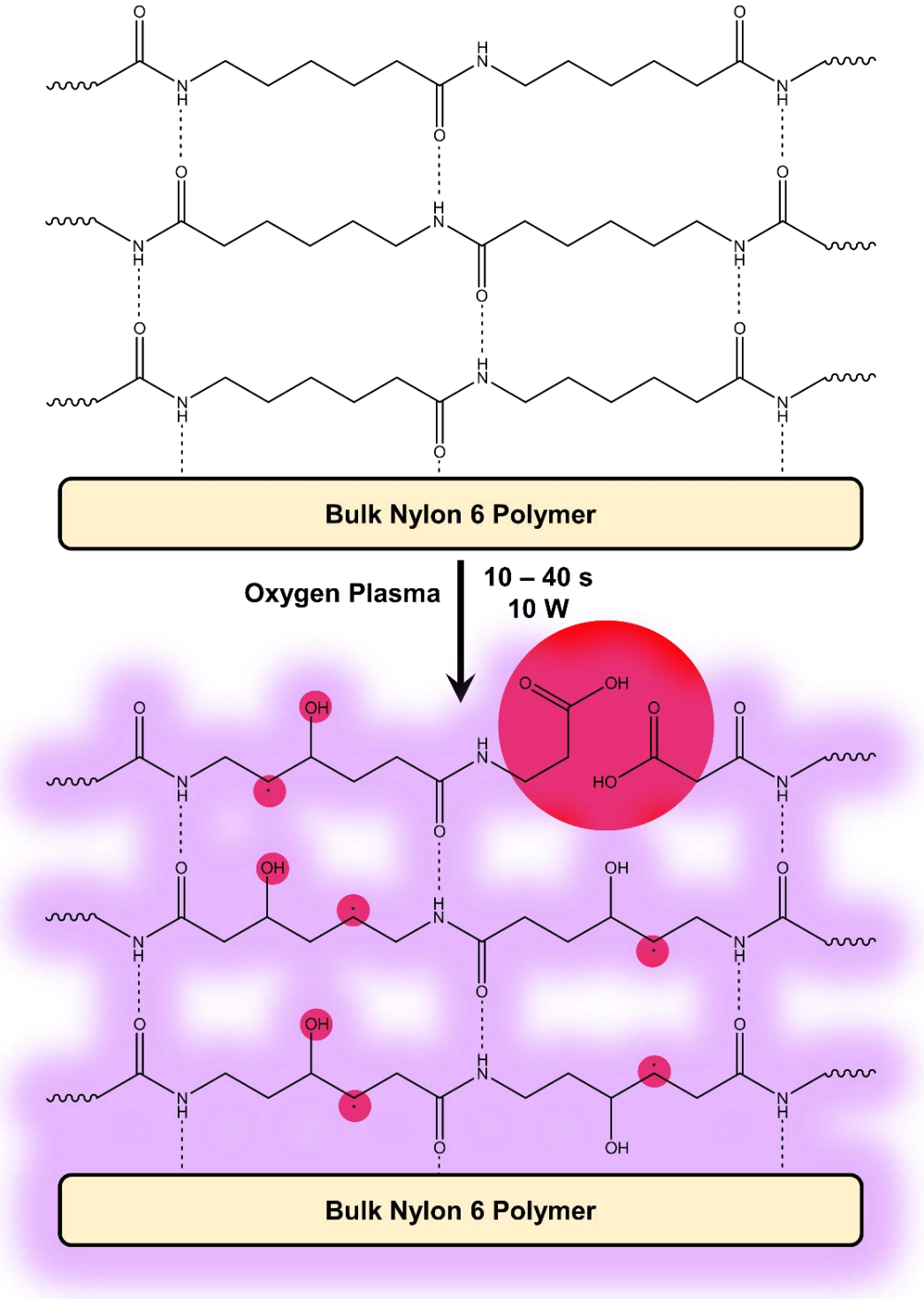

Figure 4-15. General schematic showing the structural changes induced by oxygen plasma activation on a nylon 6 polymer surface.

The schematic displayed in Figure 4-15 shows a simplification of the general groups and surface radicals formed on the surface of nylon 6 polymers following oxygen plasma treatment. The newly formed species are highlighted

in red. It was evident from the XPS data that the attachment of hydroxyl groups to the nylon 6 repeating units was the dominant mechanism of action in increasing the surface wettability of the substrates.

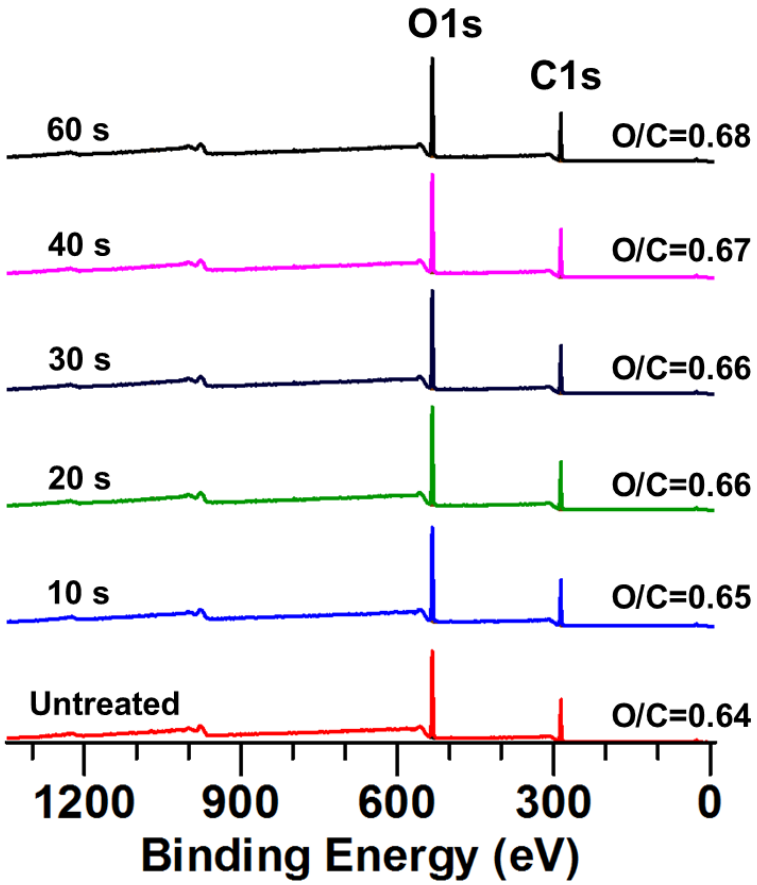

Figure 4-16. XPS survey spectra of untreated and oxygen plasma treated regenerated cellulose at 10 W for different treatment times.

From the XPS survey spectra for the untreated and plasma activated regenerated cellulose samples shown in Figure 4-16, it could be seen that increasing the plasma treatment time appeared to slightly increase the amount of oxygen present on the surface of the samples, but the increase in O/C ratio was much less substantial than that of nylon 6. The amount of carbon detected saw a minor reduction with treatment time, owing to the slight surface modification induced through exposure to the oxygen plasma. The data obtained from the survey spectra are summarised in Table 4-4.

Table 4-4. Elemental composition from the XPS data obtained for the untreated and oxygen plasma treated regenerated cellulose samples.

	Elemental composition (%)			C1s peak area (%)			
Treatment time (s)	**Carbon**	**Oxygen**	**O/C ratio**	**C-C**	**C-O(H)**	**O-C-O**	**O-C=O**
0	60.9	38.8	0.64	13.6	69.2	16.5	0.7
10	60.2	39.2	0.65	13.1	69.7	16.4	0.8
20	59.9	39.5	0.66	12.9	69.8	16.3	1.0
30	59.6	39.6	0.66	12.5	70.1	16.6	0.8
40	59.4	39.9	0.67	12.1	70.3	16.6	1.0
60	59.1	40.1	0.68	11.7	70.6	16.4	1.3

Similarly to the data obtained from the nylon 6 samples, the survey spectra for each of the regenerated cellulose samples revealed some residual traces of silicon, calcium, and magnesium (< 1%). Again, the amount of surface contaminants did not appear to change between the untreated and plasma treated films. After treatment for 10 s, the cellulose film saw a small increase in oxygen of 0.4%, which could suggest that there was slight absorption of oxygen onto the film surface, or could simply be due to errors from uncertainty in the XPS measurements. Such a small increase in the presence of oxygen is unlikely to have resulted from a chemical change to the surface due to the negligible amount of increase. As the treatment time was increased, the amount of oxygen seemed to generally increase, but all of the increases were small. It is likely that such increases had resulted from an increase in the amount of absorbed oxygen, with the possibility of the attachment of polar groups at longer treatments times, such as 60 s, whereby the amount of oxygen increased by 1.3% compared to the untreated sample. However, in comparison to the treated nylon, it was apparent that the cellulose was much less susceptible to the attachment of oxygen-containing groups, suggesting that the cellulose polymers that have a greater degree of surface oxygen present prior to plasma treatments may have fewer sites that are able to attach additional polar groups.

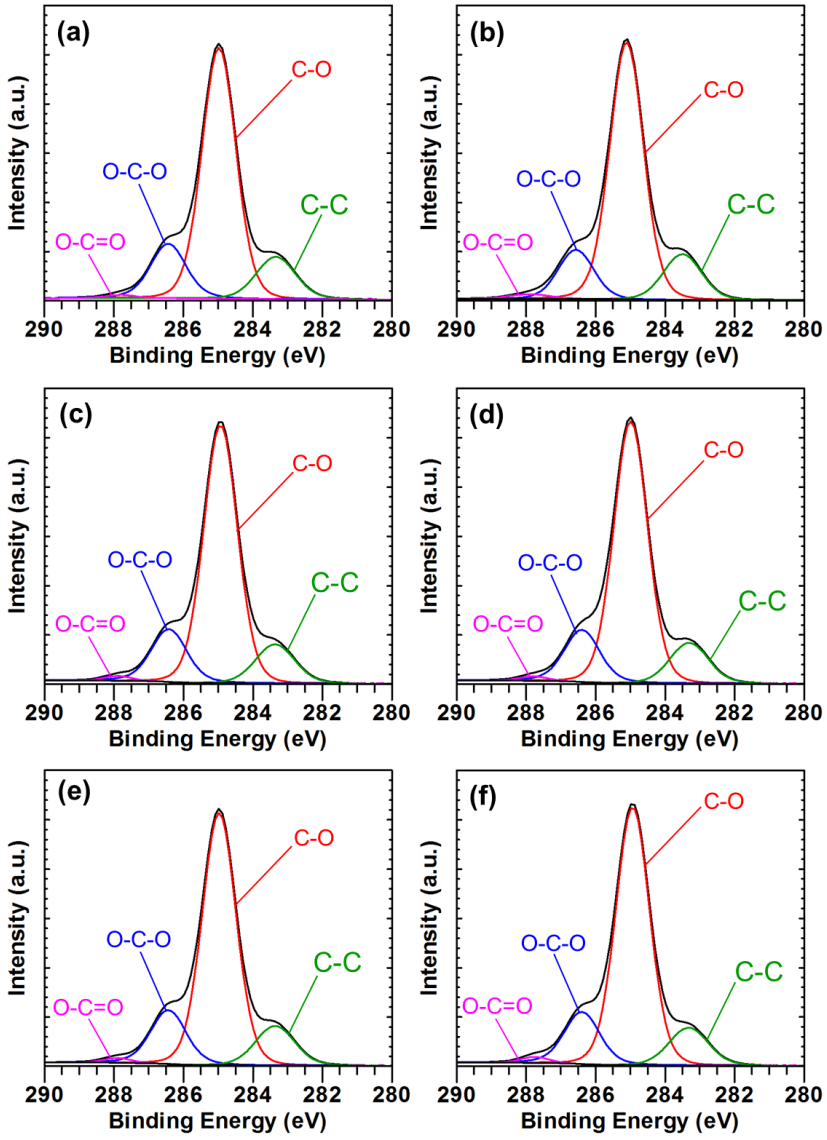

Figure 4-17. High resolution C1s XPS spectra with peak fitting of plasma treated regenerated cellulose at 10 W for (a) 0 s (untreated); (b) 10 s; (c) 20 s; (d) 30 s; (e) 40 s (f) 60 s.

Through deconvolution of the C1s spectra for each of the regenerated cellulose samples, the slight increase in surface oxygen was characterised in more depth. The high-resolution C1s spectrum for the untreated regenerated cellulose shown in Figure 4-17a confirmed that the functional groups identified as being present were C-C, C-O(H), C-O-C and O-C=O. These groups represent the carbon, hydroxyl groups, the β-1, 4 glycosidic linkages between the cellulose repeating units, and a small degree of oxidised carboxylic species in the surface structures respectively. The peak fittings were

comparable to XPS spectra of cellulose samples found in the literature.[86] 10 s of oxygen plasma treatment at 10 W (Figure 4-17b) showed that the plasma had little effect on the functionalities of the cellulose repeating units. Most notably, the C-C content was reduced by 0.5% while the C-O content increased by 0.5%. This suggests that there could have been some attachment of hydroxyl groups onto the cellulose surface. However, it is not abundantly clear if the increase was due to attachments of these groups, or simply due to uncertainties in the XPS measurements. Between 20 s and 60 s of treatment (Figure 4-17c - f), the trend of decreasing C-C content continued, with the C-O groups seeing a constant slight increase from 69.2% (untreated) to 70.6% after 60 s, while the O-C-O linkages and O-C=O groups fluctuated by a small amount with increasing treatment time. This suggested that the treatments were inducing a degree of surface attachment of hydroxyl functional groups into the surface structure, while the lack of significant changes in the O-C-O and O-C=O groups suggests that there was a lack of bond scission and surface oxidation of the polymer units.

The observed increase in surface wettability in the cellulose films can be attributed to a small extent of polar hydroxyl group attachment, and likely a degree of surface absorption of oxygen. It was clear that the regenerated cellulose films had not been chemically altered to the extent that the aplihatic nylon 6 polymers had upon exposure to these relatively short (10 - 60 s) and low powered (10 W) plasma treatments. No new groups had formed from the regenerated cellulose structures, due to the polar oxygen groups already present in the untreated materials. The schematic displayed in Figure 4-18 shows the possible groups formed on the surface polymer chains of the regenerated cellulose during oxygen plasma activation. The newly formed species, highlighted in red, resulted from the formation of surface radicals through hydrogen abstractions, absorption of oxygen, and subsequent incorporation of a small number of hydroxyl groups.

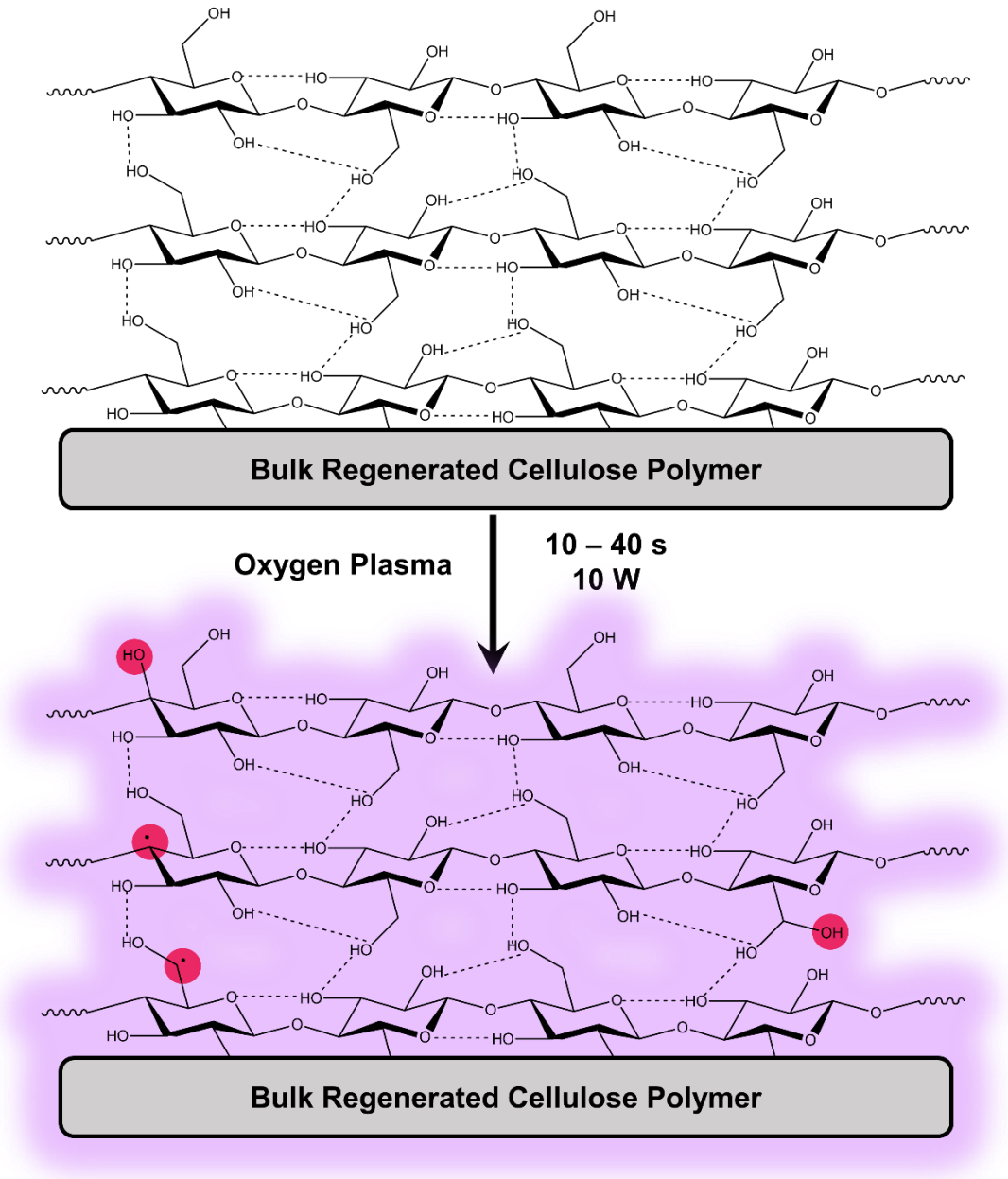

Figure 4-18. General schematic showing the structural changes induced by oxygen plasma activation on a regenerated cellulose polymer surface.

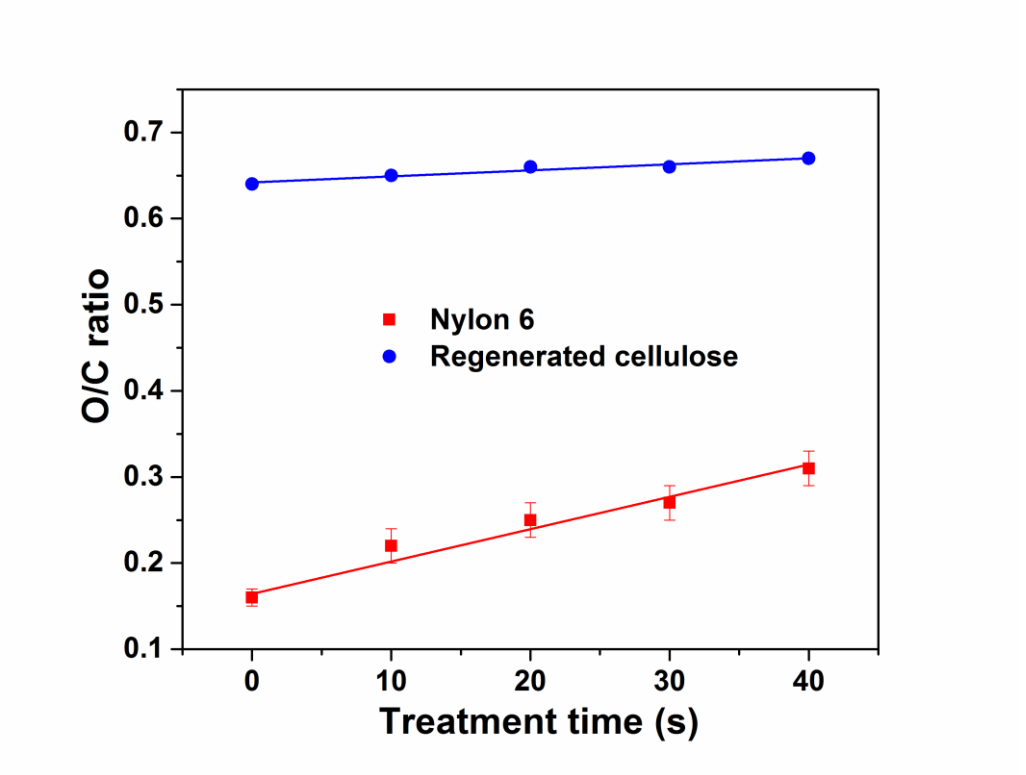

Figure 4-19. O/C ratios of the plasma treated nylon 6 and regenerated cellulose samples as a function of treatment time between 0 and 40 s at 10 W.

From the O/C ratios shown in Figure 4-19, a linear increase can be observed for both nylon 6 and regenerated cellulose. Due to the increase in oxygen content for both materials following plasma treatment, the increase in O/C ratio directly accounts for the linear decrease in measured contact angle values, and therefore increase in surface energy/hydrophilicity. For the nylon samples, there were some minor deviations from the linear trend of increasing O/C ratio at 10 s and 20 s exposure times. These were attributed to minor differences in the plasma-induced surface chemical changes between the different treated samples that were analysed (these differences were also observable when analysing the surface compositions of different untreated samples). These minor deviations are represented by the error bars showing the standard deviations of the measurements. It is notable that the increase in O/C ratio is much greater in the nylon 6 samples than in the regenerated cellulose samples. It is clear that the amount of surface oxygen present in the untreated polymer structure clearly has implications on the extent to which it can be oxidised by the plasma. As in the case of regenerated cellulose, the

greater the extent of surface oxygen saturation prior to plasma exposure, the less likely the plasma is to be able to attach polar functionalities to the surface, hence the less likely the surface wettability is to be substantially altered. From the perspective of surface chemistry, the low-frequency oxygen plasma activation process cannot be considered as substrate-independent based on the two materials studied.

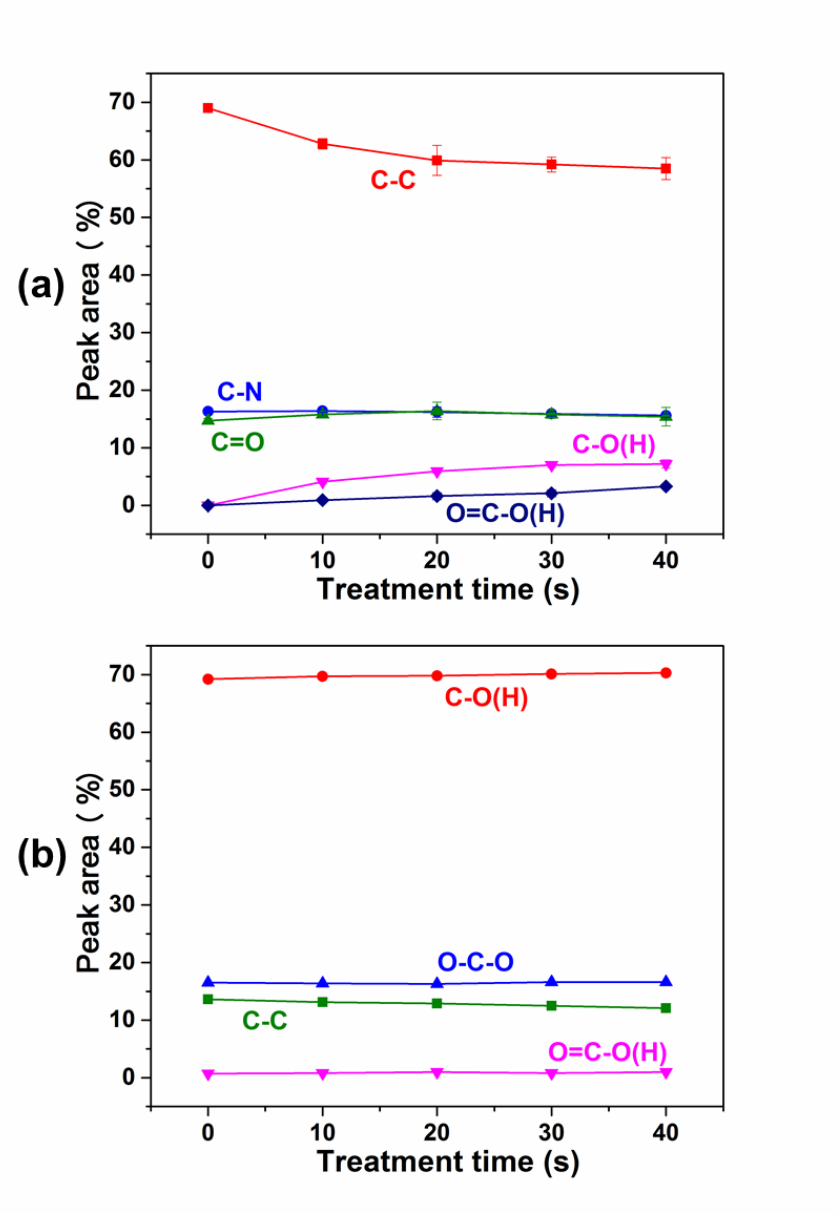

Figure 4-20. The observed changes in peak area (%) for the different XPS C1s spectra for (a) nylon 6 and (b) regenerated cellulose treated with oxygen plasma for different treatment times at 10 W.

When considering the changes in peak area graphically for each of the functional groups detected using XPS (Figure 4-20), some clear trends are

observed. For the nylon 6 samples, there is a clear decrease in the peak area of the C-C bonds, with an obvious increase in C-O(H) groups and a minor increase in O-C=O groups. Therefore, it is apparent that the increase in surface wettability with increasing plasma exposure time is primarily instigated by the attachment of polar hydroxyl groups to the hydrocarbon backbones of the nylon 6 polymer chains. The C=O peak appeared to increase slightly after 10 s of treatment, but effectively remained constant for longer treatments between 20 - 40 s. Generally, the C=O and C-N groups remained unchanged, indicating that the polyamide linkages within the nylon 6 repeating units were unaffected by the oxygen plasma surface activation. The formation and subsequent small increase in the more heavily oxidised O-C=O species were indicative of a small extent of chain scission by the reactive plasma species, forming carboxylic acid chain end groups. However, this appeared to be at a low level.

For the regenerated cellulose samples, the graphical representation of the peak areas for the detected functional groups remained largely unchanged between the untreated and plasma activated samples. There was a subtle decrease in C-C peak area alongside a slight increase in the C-O(H) areas, again suggesting that a low level of hydroxyl attachment had occurred (this was more apparent after 30 – 40 s of plasma exposure). The O-C-O and O-C=O groups remained effectively unchanged, suggesting that the plasma had not induced chain scission of the polymer chains, as the integrity of the O-C-O linkages remained unaffected. It is likely that the oxidised carboxylic species (O-C=O) were not formed by the reactive species of the oxygen plasma, as they were already present in the untreated samples. The regenerated cellulose films were hardly chemically altered by the plasma activation process, when compared to the aliphatic nylon 6 polymers.

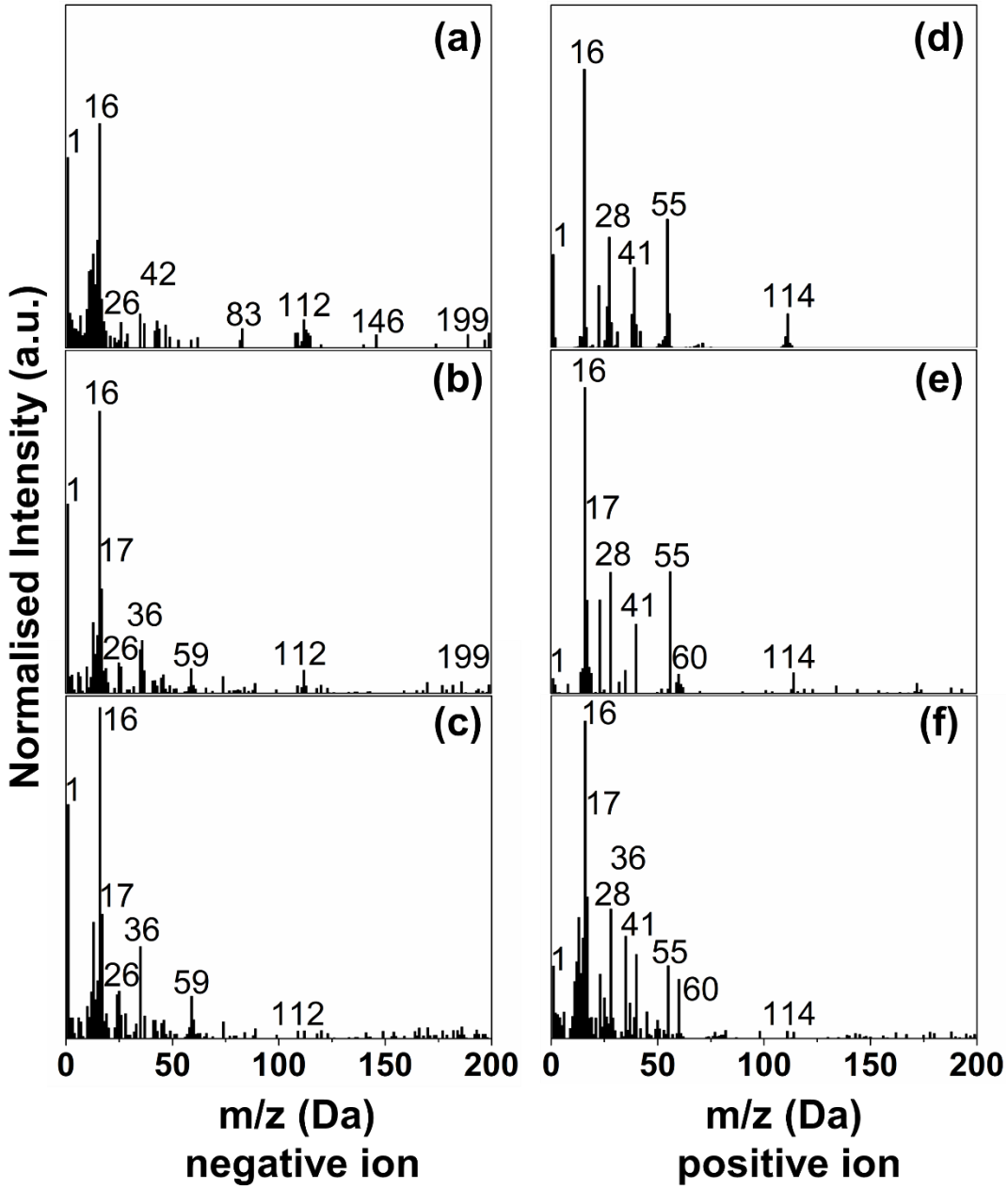

Figure 4-21. SSIMS negative ion spectrum of plasma treated nylon 6 at 10 W for (a) 0 s (untreated); (b) 10 s and (c) 40 s. SSIMS positive ion spectrum of nylon 6 at 10 W for (d) 0 s (untreated); (e) 10 s and (f) 40 s.

To complement the quantitative XPS data, SSIMS analysis was performed (Figure 4-21) to provide further details on the chemical species present on the nylon 6 surfaces following oxygen plasma exposure. From the untreated nylon 6 negative ion spectrum shown in Figure 4-21a, it can be seen that the major peaks observed with the highest normalised intensities appeared at m/z = 1^- (H^-), 16^- (O^-), 26^- (CN^-), 42^- (CNO^-), 83^- ($C_5H_7O^-$), 112^- ($C_6H_{10}NO^-$, M^-H^-), 146^-

($C_7H_{16}NO_2^-$), and 199 ($C_{12}H_{25}NO^-$). The major assigned peaks in the positive ion spectra (Figure 4-21d) appeared at m/z = 1^+ (H^+), 16^+ (O^+), 28^+ (CO^+), 41^+ ($C_2H_3N^+$), 55^+ ($C_3H_3O^+$) and 114^+ ($C_6H_{12}NO^+$, M^+H^+). All of these peaks can be considered to be expected fragments from the polyamide structure of the nylon 6 repeating unit, correlating to the functionalities present within the polymer. The peaks at m/z = 112 and 114 corresponded to the polymer repeating units as M^-H^- and M^+H^+ respectively. The negative ion spectrum obtained for the 10 s plasma activated nylon 6 samples shown in Figure 4-21b had major peaks at m/z = 1^- (H^-), 16^- (O^-), $17^=$(OH^-), 26^- (CN^-), 36^- (C_3^-), 59^- ($C_2H_3O_2^-$), 112^- ($C_6H_{10}NO^-$, M^-H^-), and 199 ($C_{12}H_{25}NO^-$). The positive ion spectrum (Figure 4-21e) had major peaks at m/z = 1^+ (H^+), 16^+ (O^+), 17^+ (OH^+), 28^+ (CO^+), 41^+ ($C_2H_3N^+$), 55^+ ($C_3H_3O^+$), 60^+ ($C_2H_4O_2^+$), and 114^+ ($C_6H_{12}NO^+$, M^+H^+).

In both spectra, the most notable newly found peak was the OH^- peak at 17 Da, confirming that the oxygen plasma had attached hydroxyl functional groups onto the repeating units of the nylon 6 polymers. Additionally, the new peaks at m/z = 59^- ($C_2H_3O_2^-$), and 60^+ ($C_2H_4O_2^+$) were attributed to the formation of carboxylic acid groups in their deprotonated and protonated forms respectively. The spectra seemed to confirm the peak model used in quantifying the functional groups present on the plasma activated nylon 6 samples, as both newly incorporated functional groups were detected by the SIMS analysis. It was also noted that the relative intensity of the oxygen peak seemed to have increased in both the negative and positive ion spectra, suggesting that the amount of surface oxygen on the nylon 6 samples had indeed increased through surface functionalisation through oxygen plasma activation.

The nylon 6 oxygen plasma treated negative ion spectra for 40 s of plasma exposure at 10 W is displayed in Figure 4-21c. The major peaks observed were shown at m/z = 1^- (H^-), 16^- (O^-), 17^- (OH^-), 26^- (CN^-), 36^- (C_3^-), 59^- ($C_2H_3O_2^-$), and 112^- ($C_6H_{10}NO^-$, M^-H^-). There were also a large number of new peaks with very low intensities that were present in the negative ion spectrum.

The assigned peaks in the positive ion spectra (Figure 4-21f) appeared at m/z = 1^+ (H^+), 16^+ (O^+), 17^+ (OH^+), 28^+ (CO^+), 36^+ (C_3^+), 41^+ ($C_2H_3N^+$), 55^+ ($C_3H_3O^+$), 60^+ ($C_2H_4O_2^+$), and 114^+ ($C_6H_{12}NO^+$, M^+H^+). Similarly to the negative ion spectrum, a large number of new fragments with low relative intensities were also observed. Interestingly, in both the negative and positive ion spectra, the intensity of the oxygen peak at m/z = 16 increased following plasma exposure for 40 s. This aids in rationalising the increase in O/C ratio observed in the XPS spectra, and the increase in wettability. It also confirms that the oxygen plasma incorporated polar oxygen-containing functionalities into the surface structure of the nylon 6 polymer.

Similarly to the samples treated for 10 s, the peak at m/z = 17 that was observed in both the positive and negative ion spectra with high intensity confirmed the presence of a significant number of hydroxyl groups that had been incorporated into the nylon structure. The m/z = 112^- (M^-H^-) and 114^+ (M^+H^+) peaks in the negative and positive ion spectra respectively were both still present in the plasma-treated samples, but their intensities had been vastly reduced. Although peaks with these intensities would not normally be assigned as significant peaks, they provided evidence that a small portion of the original unmodified nylon 6 surface structure was still present in the samples following plasma exposure. This suggested that under these low powered and short timescale treatments, the plasma action was not substantial enough to completely eradicate the original surface structure, with a small number of the nylon 6 chains remaining intact.

The peaks at m/z = 59^- ($C_2H_3O_2^-$), and 60^+ ($C_2H_4O_2^+$) were attributed to the formation of carboxylic acid groups in their deprotonated and protonated forms respectively; they were also present in the 10 s treated samples. These polar groups were formed as chain end groups on the polymer chains following plasma-induced chain scission and surface oxidation. They also confirmed that the formed O-C=O bonds shown in the XPS data can be attributed to carboxylic acid groups. It was evident from both the positive and negative ion spectra of the 40 s plasma-treated surfaces that there was no intense peak

with a m/z value > 100. However, a large number of newly formed, low-intensity peaks with m/z > 100 were indicative of chain scission of the polymer chains, disrupting the long-range order in the polymer structures and increasing the extent of fragmentation. The large number of new peaks with low intensity also suggested that the chain scissions induced by the plasma treatments were not selective, and created a large number of new species with different chain lengths. The SSIMS data largely corroborated the XPS data for the untreated and plasma treated nylon 6 samples.

From the negative ion and positive ion SSIMS spectra shown in Figure 4-22a and d respectively, it can be seen that there were a large number of characteristic peaks that can be attributed to the untreated regenerated cellulose surface structure. In the negative ion spectrum, these include the peaks at m/z = 1^- (H^-), 13^- (CH^-), 17^- (OH^-), 27^-($C_2H_3^-$), 31^-(CH_3O^-), 45^-($C_2H_5O^-$), 59^- ($C_2H_3O_2^-$), 61^-($C_2H_5O_2^-$), 81^-($C_5H_5O^-$), 85^-($C_4H_5O_2^-$), 113^- ($C_5H_5O_3^-$) and 145^- ($C_6H_9O_4^-$). There were also peaks above 145 Da that were difficult to assign due to the multiple possibilities for molecular ion fragments formed. In the positive ion spectrum, the characteristic peaks were found at m/z = 16^+ (16^+), 27^+ ($C_2H_3^+$), 39^+ ($C_3H_3^+$), 57^+ ($C_2HO_2^+$), 71^+ ($C_3H_3O_2^+$), 85^+ ($C_4H_5O_2^+$), 91^+ ($C_2H_3O_4^+$), 105^+ ($C_3H_5O_4^+$) and 115^+ ($C_5H_7O_3^+$). Following 10 s of plasma exposure at 10 W, the negative and positive ion SIMS spectra (Figure 4-22b and e respectively) showed few changes compared with the untreated spectra. Most of the characteristic peaks that were present in the untreated spectra were also present in the 10 s plasma treated samples, with similar relative intensities. The slight deviation in peaks between the untreated and 10 s treated samples were not surprising when bearing in mind the error that is likely to arise both in the configurations used in the SIMS analysis, and in general variations between each of the different cellulose film samples.

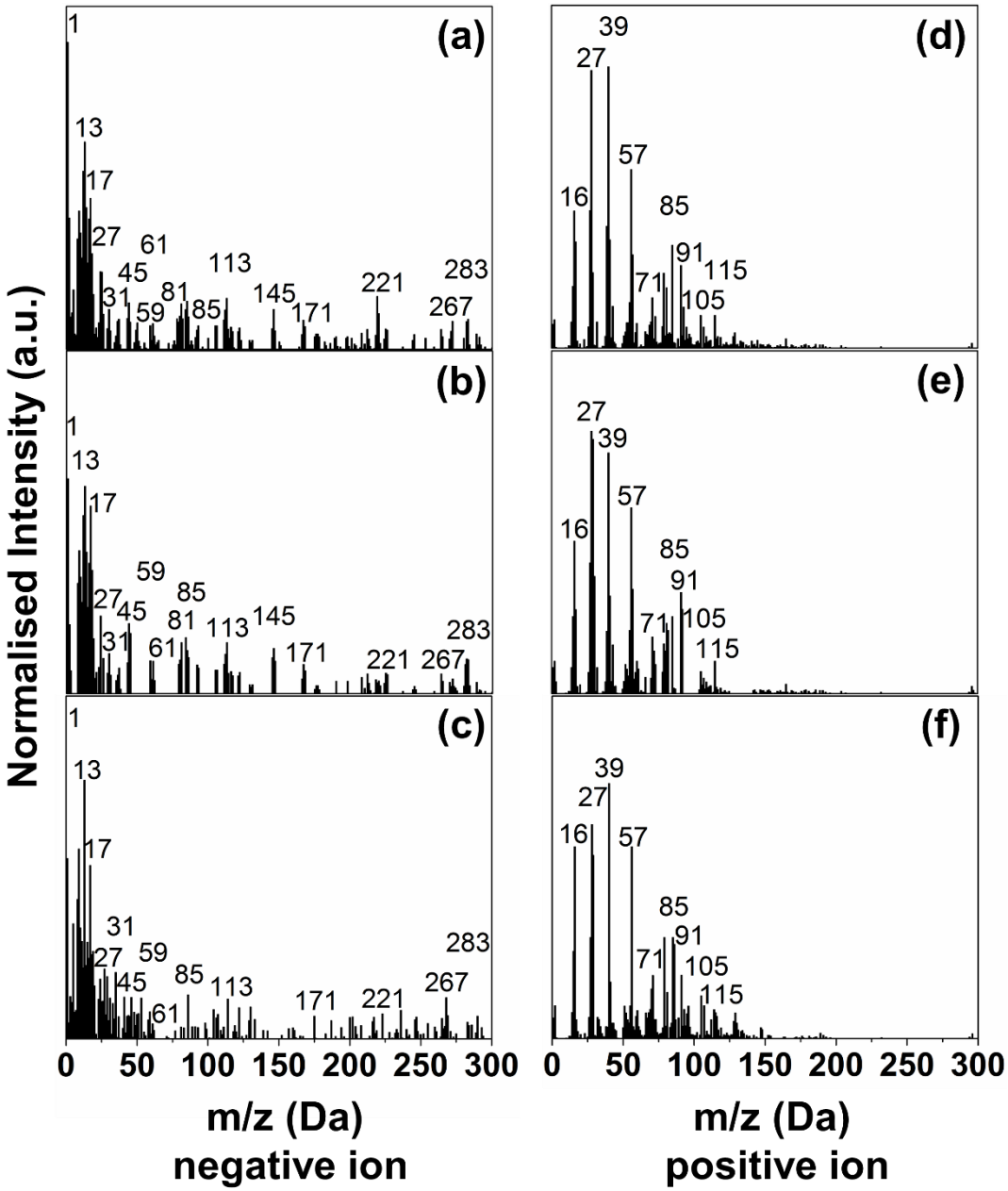

Figure 4-22. SSIMS negative ion spectrum of plasma treated regenerated cellulose at 10 W for (a) 0 s (untreated); (b) 10 s and (c) 40 s. SSIMS positive ion spectrum of regenerated cellulose at 10 W for (d) 0 s (untreated); (e) 10 s and (f) 40 s.

After the regenerated cellulose samples were exposed to oxygen plasma for 40 s of treatment, the negative ion spectra (Figure 4-22c) saw a small increase in the peak at 17^- (OH^-), with the positive ion spectra (Figure 4-22f) seeing a similar increase in the 16^+ (O^+) peak. This supported the trend of increasing O/C ratios with increasing plasma exposure time seen from the XPS measurements. Unlike the SSIMS spectra obtained for the nylon 6

measurements, the measurements showed that the surface chemistry of the regenerated cellulose films was largely unchanged (with the exception of the increase in surface oxygen and hydroxyl groups). This supported the XPS data presented earlier for the regenerated cellulose film samples, suggesting that the plasma may have increased the number of hydroxyl groups present, hence increasing the surface wettability of the substrates. The SIMS results for both materials reinforced the information derived from the XPS measurements, and proved useful as a supplementary surface analytical tool for the surface analysis of the plasma treated polymers.

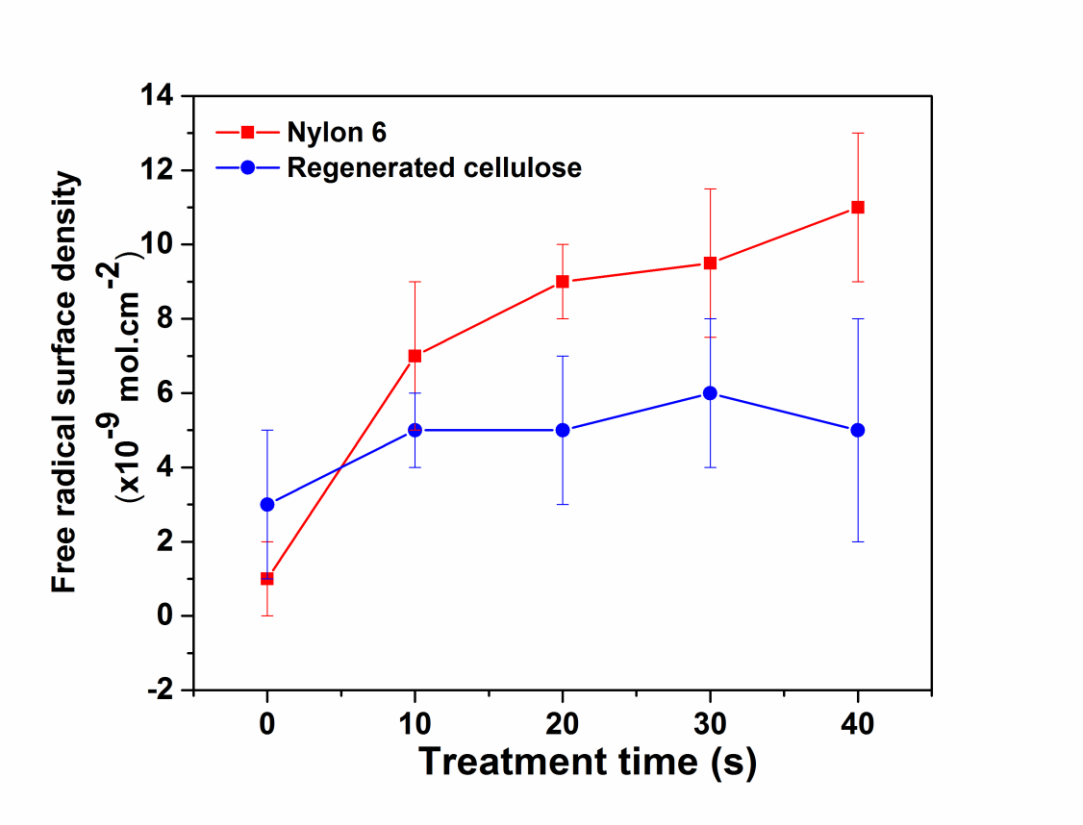

Figure 4-23. The free radical surface densities of untreated and oxygen plasma treated nylon 6 and regenerated cellulose samples between 0 - 40 s at 10 W.

The surface densities of free radicals, including post-oxidation products such as peroxy radicals formed after exposure of the plasma activated samples to air immediately after plasma treatment were quantified using a chemical labelling method, which utilised the radical scavenging molecule DPPH. The extinction coefficient for DPPH in toluene was measured to be 11057 L mol^{-1} cm^{-1}, which is similar to values previously reported in the literature.[138] From

the calculated values for the surface density of free radicals on the nylon 6 samples shown in Figure 4-23, it could be seen that there was a general trend of increasing radical density with increasing plasma treatment time. In the case of regenerated cellulose, there was a slight increase in the radical densities with the plasma treated samples compared to the untreated sample, but these increases were minimal. There were some initial surface radicals detected in both untreated nylon 6 and regenerated cellulose samples, which could be attributed to the DPPH undergoing undesired side reactions with the amide functional groups present in the nylon structure and the hydroxyl groups in the cellulose structure.

For nylon 6 samples that were exposed to treatments between 10 s and 40 s, their radical surface densities were all in the range of 7.0 - 11.0 × 10^{-9} mol cm^{-2}. Those of the treated regenerated cellulose samples were in a considerably smaller range of 5.0 – 6.0 × 10^{-9} mol cm^{-2}, suggesting that the plasma activation had generated fewer surface radicals than on the nylon plastic sheets. For both materials, the values obtained were of a similar order to that of previously reported radical densities for plasma treated polymer materials.[130, 139] For the nylon 6 samples, the presence of radicals on the surface confirmed that plasma activation led to the formation of reactive radical sites (and post oxidation products following exposure to air). This aided in explaining the incorporation of oxygen-containing hydroxyl and carbonyl groups, due to reactions of oxygen plasma species with these radical sites through the free radical mechanisms mentioned earlier (p.82), including the formation of carboxylic acid chain end groups (detected in XPS and SSIMS analysis).

The error bars were particularly large for each of the treated samples, which could be attributed to a variety of potential interfering factors in the DPPH radical scavenging method, such as the swelling effects of the toluene solvent on the nylon and cellulose polymer surfaces, and potential side reactions that can occur between the highly reactive DPPH and some of the structural features (amide groups/hydroxyls/hydrocarbon chains) within the polymer

structures. Although it had several limitations, such as the radical scavenger DPPH not having the ability to distinguish between specific radical species and the aforementioned interfering chemical species, this chemical labelling method of detecting and quantifying surface radicals is still useful in providing mechanistic insights into the complex surface modification induced by plasma activation. Despite the method not being conclusive as an independent method of analysis, it is effective in complimenting to the XPS and SIMS data, providing information about the scale of the radical surface densities following plasma activation. It also showed the general trend of increasing radical density with increasing treatment time for nylon, with minimal changes seen with increasing treatment time for regenerated cellulose.

4.4 Conclusions

Through studying the effects of oxygen low-frequency, low-pressure plasma treatments on nylon 6 plastic sheets and regenerated cellulose films, mechanistic understandings of plasma activation in terms of physical properties, surface chemistry, and morphology/roughness have been formed which can then be applied for use in the industrial plasma treatment processing of polymer materials. In addition to the processing of plastics and films, the materials tested also prove to provide excellent model surfaces to study the effects of the oxygen plasma that could be applied to nylon 6 and cellulose textiles, which are inherently difficult to analyse and often incompatible with several surface analytical techniques due to their fibrous and inhomogeneous surfaces. This makes it almost impossible to retain uniform analysis conditions across a set of samples with techniques such as XPS, SIMS, SEM, and AFM.

It has been found that oxygen plasma activation substantially increases the hydrophilicity of nylon 6 surfaces, with increasing treatment time also enhancing this increase. XPS, SSIMS, and chemical labelling methods were used to rationalise this increase in wettability in terms of surface chemistry, revealing that due to the combination of 1) oxygen plasma increasing the number of attached polar functional groups (C=O, COOH, C-OH); 2) the

plasma increasing the fragmentation of nylon 6 polymer chains through oxidation and chain scission; 3) the plasma increasing the surface radical density with increasing treatment time, the hydrophilicity of the substrates increased. SEM imaging and AFM imaging were then used to confirm that under the conditions chosen for this study, there was no change to the surface morphology or roughness, unlike relevant results reported in many previous studies on low-pressure plasma treatments. Gravimetric analysis also confirmed that between 10 and 40 s of plasma exposure, there had been no loss of mass of the samples.

Similarly to nylon 6, the cellulose films saw an increase in hydrophilicity with increasing plasma treatment time between 10 and 60 s. However, this increase was much less extensive. XPS and SSIMS analyses indicated that the treatments had increased the oxygen content on the surfaces of the films, but the surface structures of the polymers had not been significantly altered in the same way as had the nylon 6 samples. Absorption of oxygen onto the cellulose film surfaces, and the introduction of a small number of newly attached hydroxyl groups seemed to be the main driving force for the increase in substrate wettability for the cellulose samples. Chemical labelling methods showed that the amount of surface radicals present on the surface of the regenerated cellulose films seemed to be generally lower than that of the nylon samples, and had similar values to the untreated cellulose samples. It was not clear why the fewer radicals were generated on cellulose compared to nylon, confirming that the activation process was not substrate independent. SEM imaging confirmed that the surface morphology of the samples was not significantly altered, while gravimetric analysis showed that there had been a slight loss of mass due to etching by the plasma between 40 and 60 s of treatment; this indicated that the cellulose films were more sensitive to the etching capabilities of the plasma species.

Potential applications for the investigated plasma activation process include being used as a prerequisite for applying coatings to enhance coating adhesion, or as a general method for increasing the wettability of materials,

without inducing surface degradation or alterations in morphology. From the results presented in this chapter, it is apparent that plasma activation is more suitable for aliphatic polymers that have a relatively low initial surface concentration of oxygen, with several hydrocarbon sites for which polar groups can be readily attached.

5. Physical, chemical and morphological characterisation of plasma etching

This chapter focusses on the surface-chemical and morphological analyses of nylon 6 plastic sheets and regenerated cellulose films following nanotexturing/etching by exposure to CCP low-frequency (40 kHz) discharge, low-pressure oxygen plasma for treatment times varied between 30 s and 600 s. The wettability and crystallinities of the plasma-treated polymers are also explored. The chapter aims to provide detailed understandings of the effects of varying plasma treatment time on the extent of surface modification attained on the nylon 6 and regenerated cellulose samples.

5.1 Plasma etching of nylon 6 plastic sheets and regenerated cellulose films

5.1.1 Surface wettability

From the apparent surface free energies and measured static contact angle values shown in Figure 5-1, it can be seen that for both nylon 6 and regenerated cellulose substrates, the surface free energy increased with oxygen plasma treatment time at 60 W, with the contact angles decreasing. The highest surface energies were obtained after 10 minutes of plasma treatment for both materials, with values of 60.6 mJ m^{-2} and 63.0 mJ m^{-2} being achieved for nylon 6 and regenerated cellulose respectively. This was a large increase when compared to the untreated polymer samples that had the lowest surface energy values of 42.2 mJ m^{-2} (for nylon) and 51.8 mJ m^{-2} (for cellulose). The surface energy values were directly related to the measured

static contact angles; these contact angles saw an overall larger decrease in both materials than in the study on lower powered, shorter treatment times for plasma activation reported in Chapter 4, suggesting that the etching had a greater impact on wettability compared to functionalisation with polar groups.

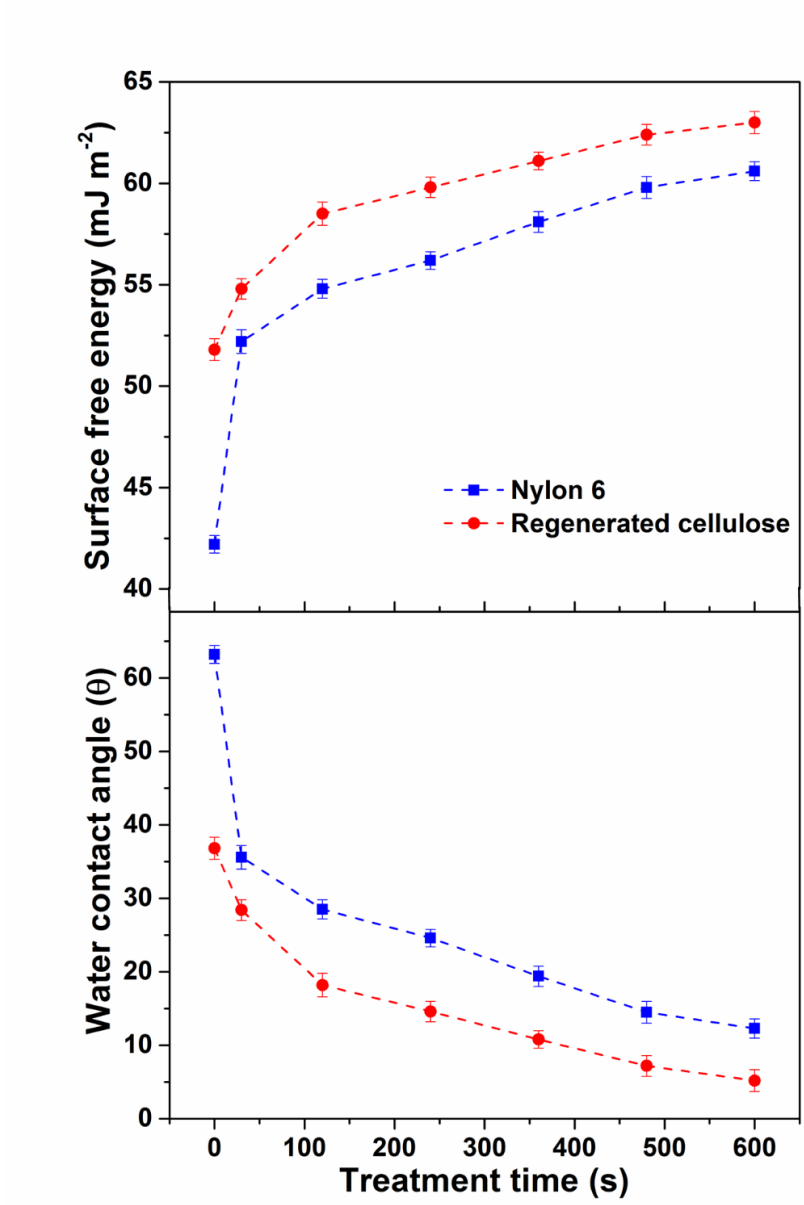

Figure 5-1. The variation in apparent surface free energy and static contact angle of nylon 6 plastic sheets and regenerated cellulose films with increasing oxygen plasma treatment time at 60 W.

For nylon 6, there was an initial large decrease in contact angle after only 30 s of plasma exposure, from 63.2° (untreated) to 35.6°. Such a decrease was primarily attributed to a similar plasma activation process to that reported in Chapter 4, but with some slight etching effects also roughening the material

surface, as determined by the mass loss (gravimetric) analysis (5.1.2). This also appeared to be the case for the regenerated cellulose samples, but the decrease was much smaller, due to the cellulose surfaces having a higher initial oxygen concentration, with fewer sites in the surface structure that could create free radicals for further oxidation. The etching at this point was also only slight, so it had a minimal effect on the contact angle value.

From 120 s of treatment up to 600 s, both the nylon 6 and regenerated cellulose samples saw a relatively linear decrease in contact angle value. The increase in wettability was caused primarily by plasma etching, but also combined with some synergistic surface-chemical effects. At 60 W, the energy reaching the reactive plasma species was high enough to enable the ions present to bombard the polymer surfaces, breaking the polymer chains into low molecular weight or volatile species that were transferred into the gas phase and then removed by the vacuum system. The roughening of the surface by plasma etching increased as a function of time, with longer treatment times leading to more mass loss. Also, due to simultaneous activation effects increasing the number of hydrophilic polar functionalities, the newly formed polar groups could interact with moisture through hydrogen bonding, hence having a greater affinity for water. When combined with the increase in surface roughness from the plasma etching effects, this process led to an overall increase in wettability.

5.1.2 Gravimetric analysis

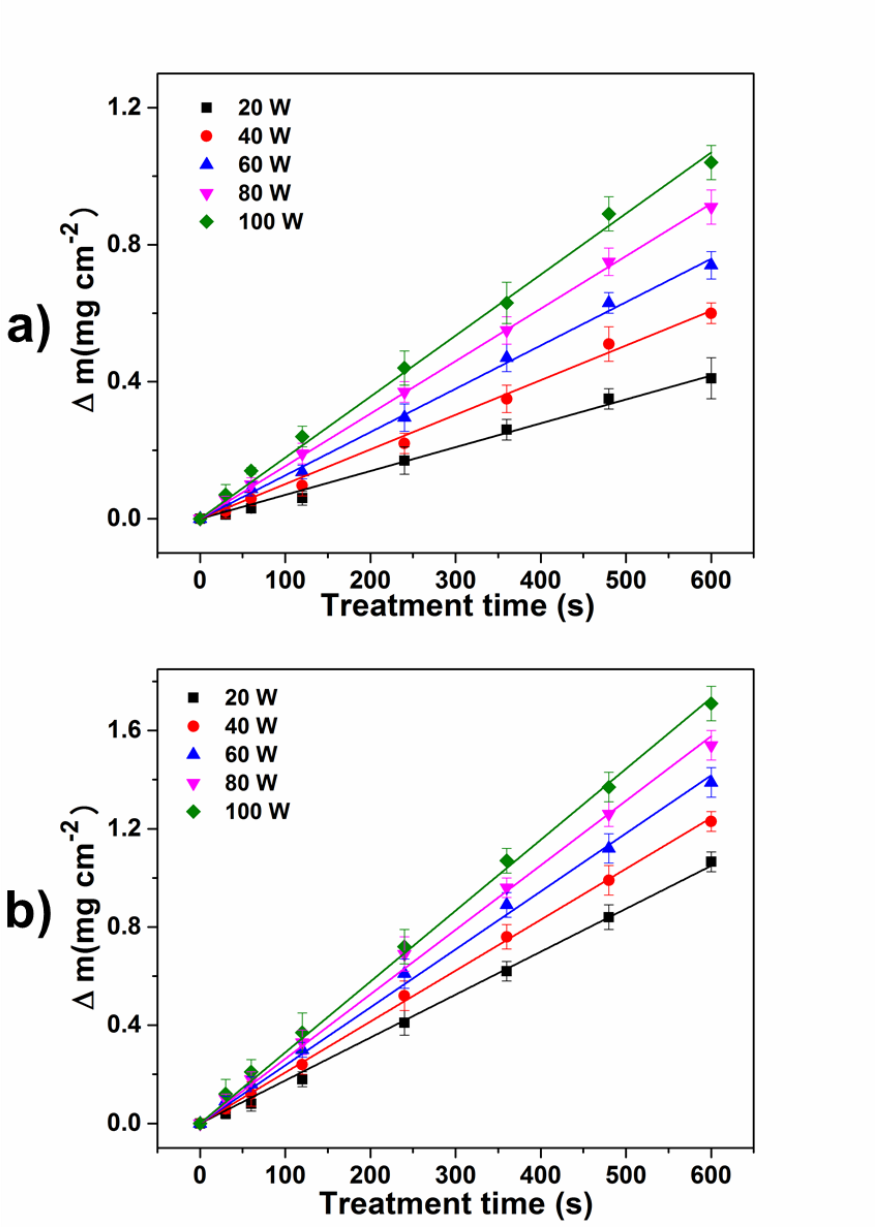

Figure 5-2. Mass loss measurements of a) nylon 6 plastic sheets and b) regenerated cellulose films treated with oxygen plasma with varying discharge power and treatment time.

The mass loss measurements shown in Figure 5-2 confirm that the earlier linear models obtained in the response-surface plots in Figure 4.2 predicted the behaviour of the oxygen plasma system accurately, owing to the large degree of control available over the gas flow and plasma gas uniformity with the low-frequency, low-pressure plasma system. For both the nylon 6 and regenerated cellulose samples, there was a linear increase in mass loss with

both treatment time and plasma power, due to the availability of large quantities of the energetic oxygen plasma species to bombard and subsequently etch the polymer surfaces. The regenerated cellulose samples were more susceptible to this etching processes, and had greater mass loss than the nylon 6 samples at all treatment time/power combinations. This can be seen through the calculated etch rates shown in Figure 5-3, which takes into consideration the polymer densities.

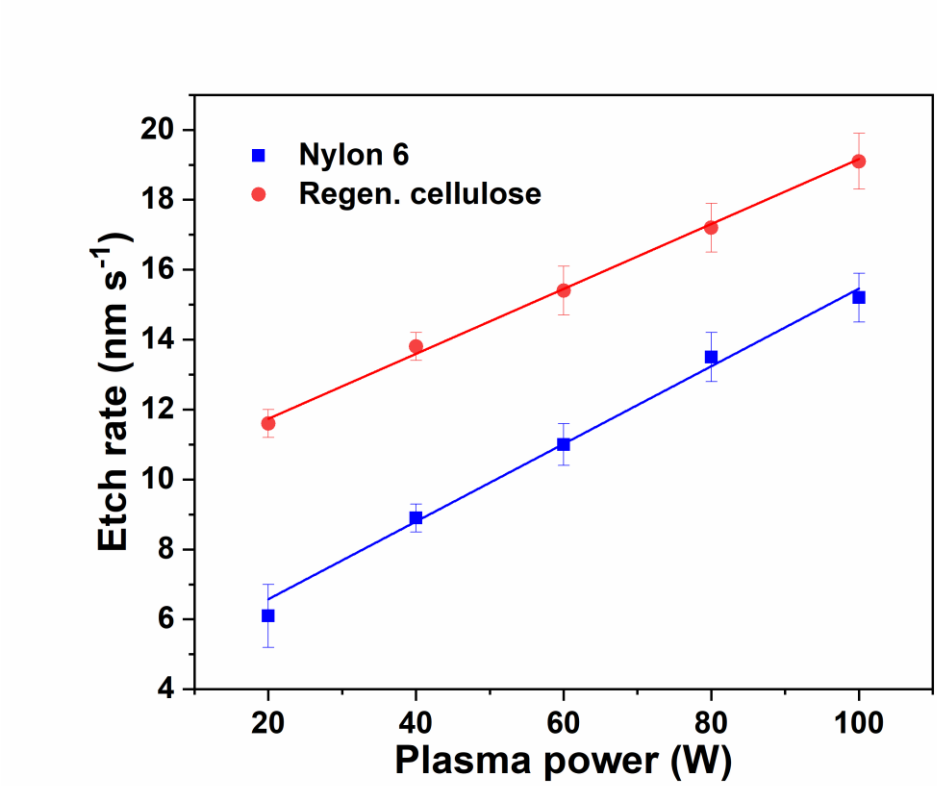

Figure 5-3. Calculated etch rates for nylon 6 and regenerated cellulose samples with varying plasma power.

It can be seen, from Figure 5-3, that the etch rates of both nylon 6 and regenerated cellulose samples increased with increasing plasma power, due to the increased energy available to break up the polymer chains through bond scission. The etch rates were also higher for regenerated cellulose than nylon 6, which can be attributed to the increased number of heteroatoms in the cellulose structures. This means that during exposure to the plasma, the breaking up of bonds within the polymer repeat units leads to a release of O or OH radicals from the cellulose surfaces that can further react with the polymer backbone, providing higher etch rates.[140] Due to the difference in etch

rates between the two materials, plasma treatments cannot be considered as fully “substrate-independent” in terms of the quantitative resultant effects obtained; clearly the chemical structures of the polymer has implications on the plasma-surface interactions.

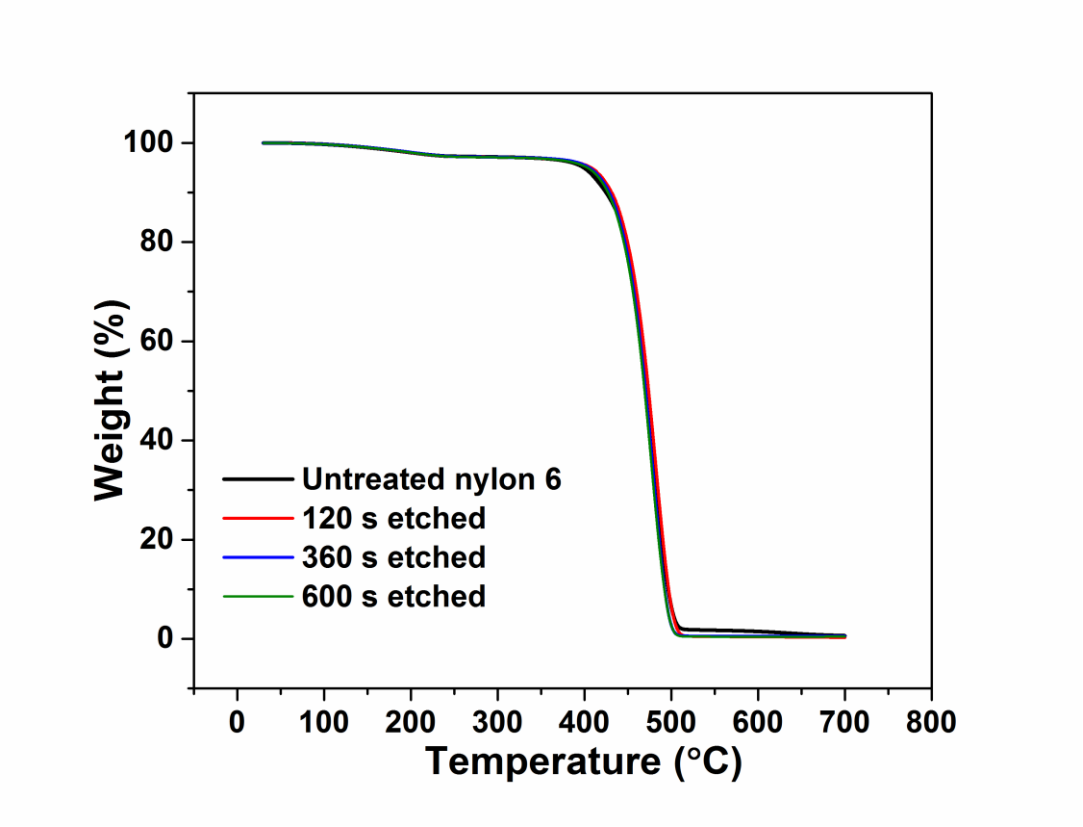

Figure 5-4. TGA curves for untreated and oxygen plasma treated nylon 6 samples between 120 - 600 s at 60 W.

The TGA curves shown in Figure 5-4 were used to assess the effects of oxygen plasma exposure on the thermal stabilities of nylon 6 plastic sheets, and investigate any potential changes in thermal properties of the oxygen plasma treated materials. Through tracking the *in-situ* weight changes of the nylon samples during heating, detailed information relating to the thermal degradation of the samples was obtained. The curve for the untreated sample showed that the nylon 6 sheets had excellent thermal stability, with no significant weight loss observed in the TGA curve below 397°C, at which point the polymer chains degraded. This thermal stability was replicated across the series of plasma-treated samples, with no obvious differences between the untreated and plasma treated sample curves. The plasma treatments had not affected the thermal stabilities of the plastic sheets, owing to the plasma

treatments only modifying the outer nanoscale layers of the surface, having no effects on the bulk thermal properties of the material. The analysis was not repeated for cellulose, as it was evident that the plasma did not alter the bulk thermal properties of the nylon polymers.

5.1.3 Morphological characterisation of plasma etched surface nanopores

The SEM images in Figure 5-5 show the plasma-induced morphological changes in the nylon 6 and regenerated cellulose material surfaces, and support the mass loss experiments described earlier in Section 5.1.2. Figure 5-5a shows that the untreated nylon 6 sheets were relatively smooth, with occasional grooves and a small number of surface particles. These particles were analysed by EDX and had nearly identical spectra to the nylon surface; for this reason they were not identified as contaminants. Similarly, Figure 5-5e shows that the untreated regenerated cellulose films were generally smooth, but with a number of nanoscale cracks and scratches. There were also a small number of surface particles on the untreated surface.

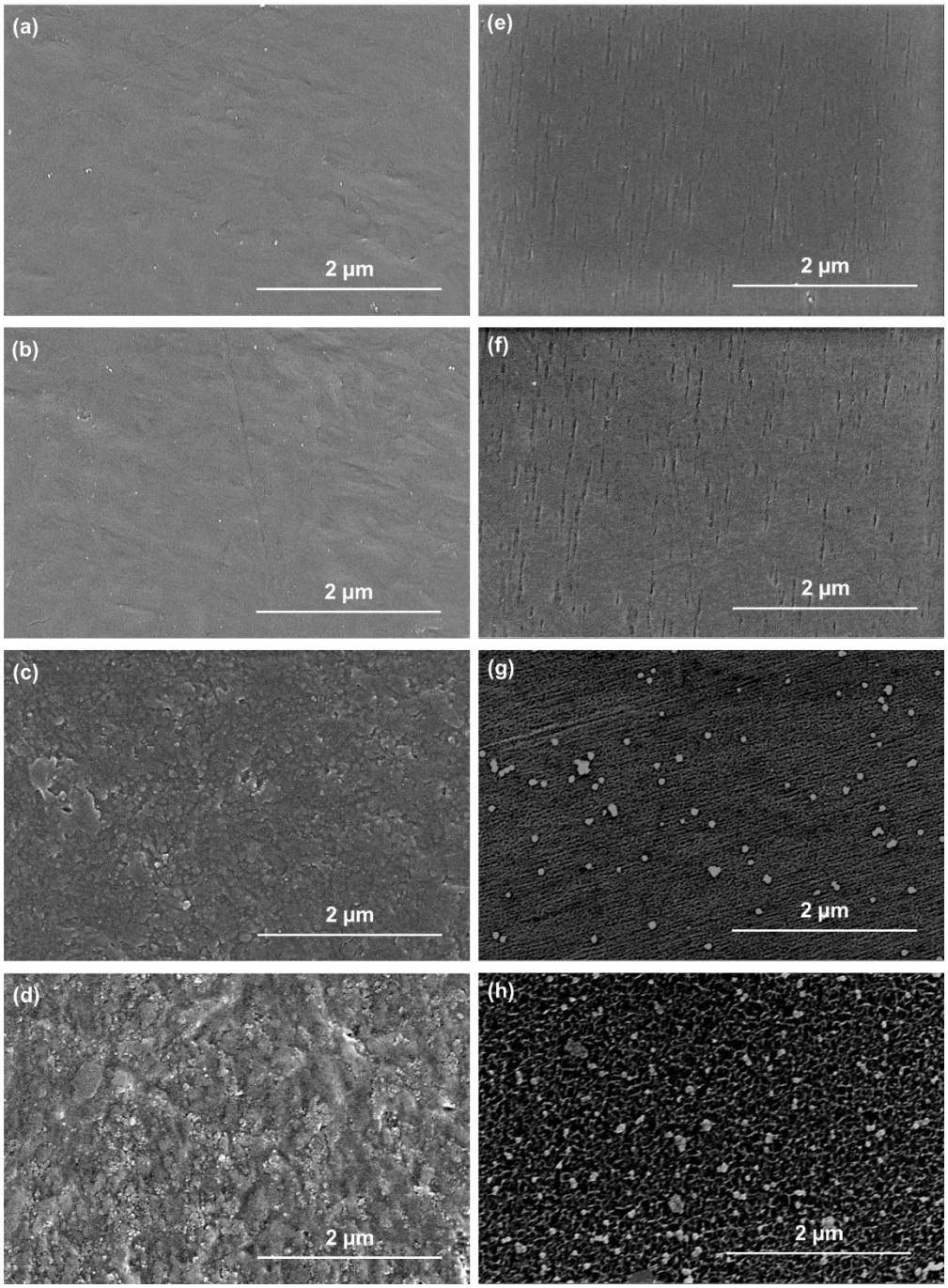

Figure 5-5. SEM images of nylon 6 treated at 60 W for (a) 0 s (untreated); (b) 30 s; (c) 120 s and (d) 600 s. Images of regenerated cellulose treated at 60 W for (e) 0 s (untreated); (f) 30 s; (g) 120 s and (h) 600 s.

Following 30 s of plasma treatment at 60 W, both the nylon 6 (Figure 5-5b) and regenerated cellulose (Figure 5-5f) surfaces appeared to be generally unchanged, with no significant alteration in morphology. Some of the scratches that were originally visible in the untreated samples appeared to be slightly more defined in the cellulose samples after 30 s, which could account

for the slight mass loss observed in these samples. Plasma etching was visible in both samples following 120 s of treatment, with a clear increase in surface roughness of the nylon 6 surface shown in Figure 5-5c. Such an increase in surface roughness was also seen in the regenerated cellulose samples shown in Figure 5-5g, in addition to the formation of a number of surface agglomerates. The surface roughness substantially increased further in both samples following 600 s of treatment. Both samples showed heavily damaged surfaces with many distinct nanoscale pores and trenches formed. This can be attributed to the ability of the oxygen plasma to etch the sample surfaces, leading to a dramatic increase in surface area of the nylon and cellulose samples. The etching of both samples was isotropic due to the diffusion of reactive species occurring in all directions within the low pressure chamber. Isotopic etching is typically selective, with atomic oxygen initiating the etching process through hydrogen abstraction, and subsequent bond scission of the polymer chains. Such a rupture of the polymer chains then forms low molecular weight species that can be removed by the vacuum system.

Again, in the cellulose samples, there was a larger number of agglomerates that had formed on the surfaces after 600 s of treatment compared to 120 s, with a number of large clusters of these surface particles that had formed. This indicated that the plasma etching of cellulose had led to the thermodynamically-driven nucleation of the surface particles formed through the etching process that increased with increasing treatment time. These agglomerates were likely to have also been formed from the decomposition of lower molecular weight samples induced by the etching ability of the plasma, through ion bombardment, chain scission and oxidative mechanisms.

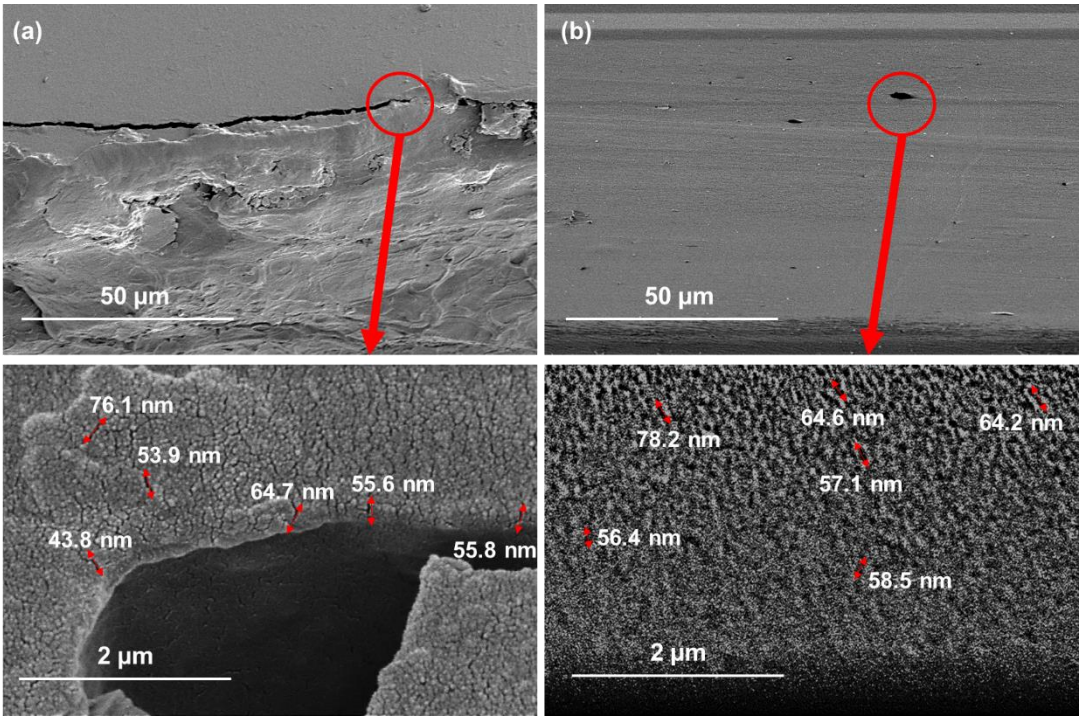

Figure 5-6. SEM images taken with a 45° view of (a) 600 s, 60 W oxygen plasma-treated nylon 6 and (b) 600 s, 60 W oxygen plasma-treated regenerated cellulose.

SEM images obtained from a 45° angled view of some imperfections found within the nylon 6 and regenerated cellulose samples were obtained to enable the depth of the nanopores formed through plasma etching to be measured. Relevant images are shown in Figure 5-6 for samples treated for 600 s at 60 W. The images confirmed that the etching of both material surfaces was isotropic, which can be attributed to low-frequency, low-pressure systems having the ability to create high-density and uniform plasmas. In addition, oxygen is considered as a reactive plasma, meaning that it forms reactive ions that can subject polymer samples to chemical etching, whereby the ions formed can react with, and remove the polymer substrate material. It is clear that the etching across both surfaces had a degree of homogeneity, with uniform etching patterns across both material surfaces. When considering the extent of etching across the samples, both showed a distribution of different depths. For nylon 6, this ranged from 43.8 to 76.1 nm, while the regenerated cellulose samples ranged from 56.4 to 78.2 nm. The ranges for both materials were comparable, with the etched pores in the cellulose film samples being moderately deeper than those in the nylon 6 plastic sheets, suggesting that

the etching capabilities of low-pressure oxygen plasma are effectively substrate-independent when only considering nylon 6 and regenerated cellulose polymers.

Table 5-1. The mean pore depths of the plasma etched nylon 6 and regenerated cellulose samples determined through SEM analysis.

	Mean pore depth (nm)
Nylon 6	58.3 ± 4.09
Regenerated cellulose	63.2 ± 7.46

The calculated mean pore depths and their uncertainties based on standard deviations from the measured values are shown in Table 5-1. It is clear that the values for nylon and cellulose were similar, especially when considering the greater uncertainty in the cellulose measurements. As can be seen from the images of etched samples at different magnifications in Figure 5-6, the bulk material for both nylon 6 and regenerated cellulose had clearly remained unchanged in the lower magnification images, with the higher magnification images showing a high level of surface degradation, with a clear increase in surface area. This increase in surface area aids in explaining the increase in wettability seen with increasing treatment time as reported in Section 5.1.1.

The AFM images presented in Figure 5-7 were used to obtain quantitative information based on the increase of surface roughness following etching with low-frequency, low-pressure oxygen plasma. The untreated nylon 6 samples were characterised by low surface roughness, with a root mean square roughness (Rq) value of 7.47 ± 0.92 nm, and a roughness average (Ra) value of 6.07 ± 0.81 nm.

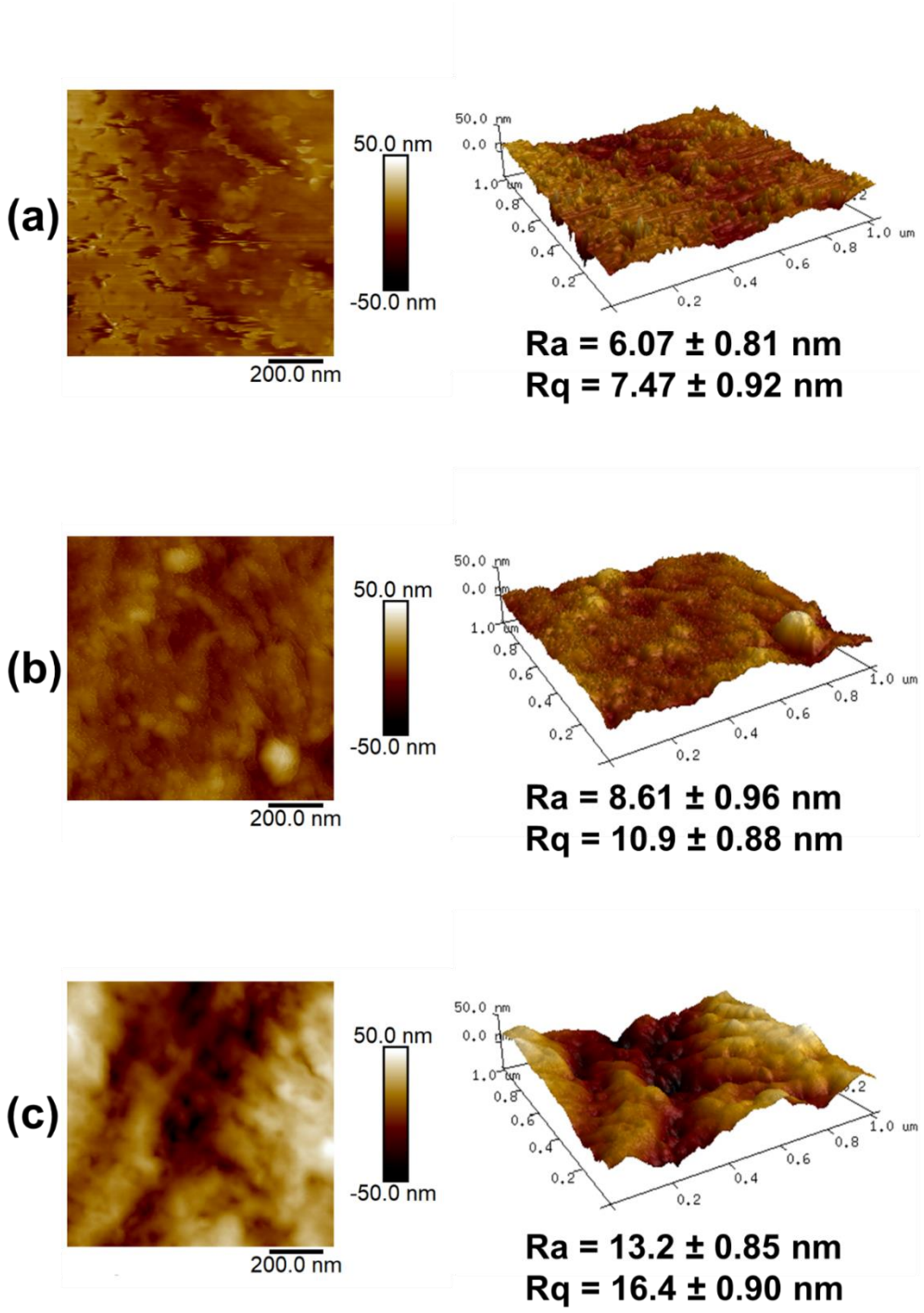

Figure 5-7. AFM images of: (a) untreated nylon 6; (b) oxygen plasma treated nylon 6 for 120 s at 60 W and (c) oxygen plasma treated nylon 6 for 600 s at 60 W.

The image shown in Figure 5-7a confirms that the untreated surface is generally smooth. After 120 s of oxygen plasma exposure, there is clearly an increase in Rq and Ra value, to 10.9 ± 0.88 nm and 8.61 ± 0.96 nm respectively. Such an increase in roughness is also visualised in the 3D image

shown in Figure 5-7b. After the longer plasma treatment of 600 s, a major alteration in surface morphology and topography was obtained, as shown in Figure 5-7c. The Rq and Ra values increased further to 16.4 ± 0.90 nm and 13.2 ± 0.85 nm respectively. The AFM images obtained verified the significant increase in surface roughness due to plasma etching/nanotexturing shown in the SEM images in Figure 5-5. It was evident that with increasing treatment time at 60 W, the degree of etching increased, with a general increase in irregularities shown in the sample after 120 s of treatment, and the generation of well-defined pores and trenches after 600 s. The depths of the nanopores generated following 600 s of treatment were determined based on roughness profiles, through measuring the vertical distance between the maxima and minima of the AFM image. The values for pore depth obtained using AFM were compared to the values attained using 45° angled SEM images. Both sets of data are presented in Table 5-2.

Table 5-2. The mean pore depths of the plasma etched nylon 6 samples determined by SEM and AFM analysis.

Imaging method	Nylon 6 mean pore depth (nm)
SEM	58.3 ± 4.09
AFM	63.1 ± 6.31

The SEM and AFM data both show similar values for pore depth, suggesting that both methods are valid and useful in quantifying the physical effects of plasma etching on polymer materials such as nylon 6. The greater uncertainty in the AFM value means that the determined pore depth using SEM was within the errors limit of the AFM samples. Through creating pore depths in the region of 58.3 nm to 63.1 nm, the oxygen plasma etching had the ability to dramatically alter the surface morphology. It is intuitive that the increase in surface roughness/surface area with increasing oxygen plasma treatment time directly correlated to the increase in surface wettability with time.

5.1.4 Surface chemical analysis

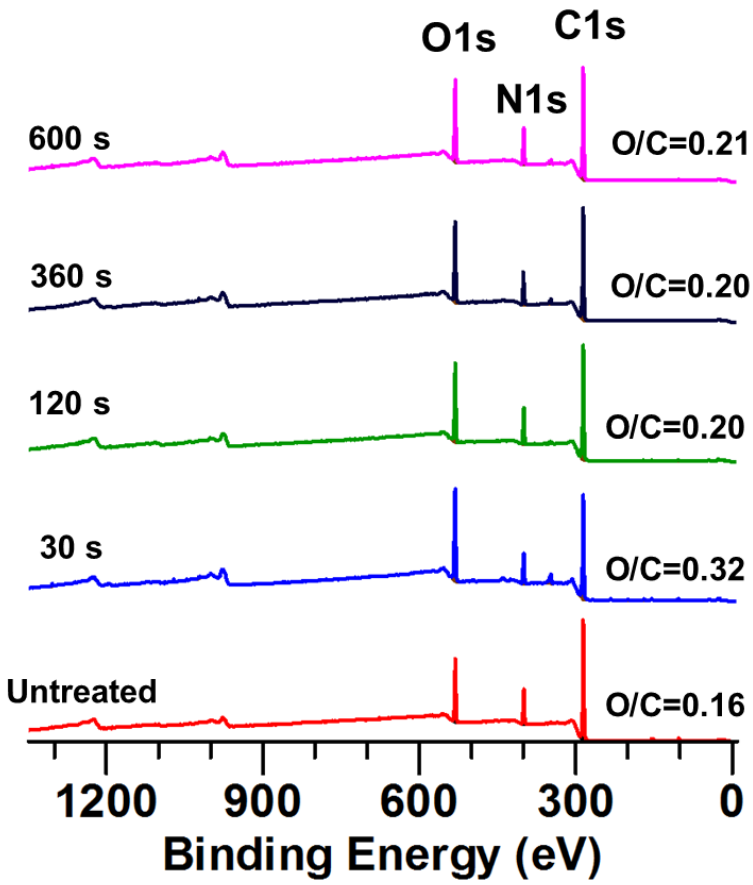

Figure 5-8. XPS survey spectra of untreated and oxygen plasma treated nylon 6 at 60 W for different treatment times.

The XPS survey spectra presented in Figure 5-8 concern the untreated and oxygen plasma treated samples at 60 W, for treatment times varying between 30 s (inducing low levels of plasma etching) and 600 s (inducing high levels of plasma etching). From Figure 5-8, it was evident that the shorter 30 s treatment times induced a similar increase in O/C ratio that was seen in the plasma activated nylon 6 samples at 10 W, with treatment times ranging between 40 and 60 s as reported in Chapter 4. The O/C decreased from 0.32 at 30 s, to 0.20 at 120 s, showing that the extent of attachment of oxygen containing functionalities had decreased with the longer treatment (primarily due to the etching of the surface removing some of the newly functionalised groups). At treatment times ranging from 120 s to 600 s, there was a similar level of surface-chemical modification to the nylon 6 samples, with little change in the O/C ratios. Therefore, the increase in surface wettability seen

through the contact angle values discussed earlier in this chapter in Figure 5-1 were primarily attributed to the increase in physical etching (loss of mass and surface roughening) with increasing treatment time at 60 W.

Table 5-3. Elemental composition from the XPS data obtained for the untreated and oxygen plasma-etched nylon 6 samples.

	Elemental composition (%)				C1s peak area (%)				
Treatment time (s)	**Carbon**	**Oxygen**	**Nitrogen**	**O/C ratio**	**C-C**	**C-N**	**C=O**	**C-O(H)**	**O-C=O**
0	76.0±1.1	12.3±0.3	10.0±0.4	0.16±0.01	69.0±0.4	16.3±0.2	14.7±0.4	0.0±0.0	0.0±0.0
30	67.1±1.3	21.4±1.3	10.1±0.5	0.32±0.03	57.9±1.3	15.8±0.4	15.1±0.9	7.8±0.4	3.4±0.4
120	74.6±1.1	14.7±1.1	9.9±0.3	0.20±0.02	62.0±1.6	16.0±0.6	15.7±0.7	3.8±0.7	2.5±0.9
360	74.2±1.8	15.0±0.8	10.4±0.4	0.20±0.02	61.5±1.0	15.9±0.9	15.9±0.4	4.2±1.2	2.5±0.7
600	73.8±0.5	15.8±0.7	10.0±0.2	0.21±0.01	60.7±1.2	16.0±0.7	16.2±0.6	4.3±1.1	2.8±0.6

Table 5-3 presents the elemental composition data obtained from the XPS survey spectra, and details the functional group quantification from the high resolution C1s spectra for the different untreated and oxygen plasma treated samples. Various inorganic contaminants such as silicon, calcium, sodium, and magnesium were found in trace quantities in all samples; these were not included in the table due to their negligible quantities. The survey spectra revealed an initial large increase in surface oxygen content after 30 s of plasma exposure, from 12.3% (untreated) to 21.4%. This was attributed to an activation effect, with the oxygen plasma species attaching polar hydroxyl groups, whilst also oxidising the surface to form carbonyl species. Furthermore, it was shown from the SEM images presented in 5.1.3 that there was no substantial etching at this treatment time. Following 120 s of plasma treatment, the oxygen plasma had again increased the surface oxygen content from 12.3% (untreated) to 14.7%, but the increase was much smaller than that of the 30 s plasma-treated sample. This is likely due to the increased etching effects that were more prevalent after 120 s. The oxygen content of the nylon 6 surfaces then increased to a similar extent of the 120 s treated

sample following both 360 s and 600 s of exposure, with a small increase with increasing treatment time. Two simultaneous activation and etching processes occurred at these treatment times, with the etching process removing some of the newly activated areas of the surface through ion bombardment as they were formed. These processes appeared to be competing, with the activation process being dominant after 30 s of treatment, while the etching process was more dominant between 120 and 600 s of plasma treatment.

When considering the distributions of the chemical changes across the treated nylon surfaces, it can be seen that the general variations for each elemental/functional group peak area were small, with all of the deviations being less than ± 2%. Uncertainty in XPS measurements would generally be expected due to a wide range of variables such as X-ray flux and aperture settings[141], meaning that the small variations found in the sample data suggested that the surface-chemical modifications seen on the nylon 6 surfaces appeared to be evenly distributed across the surfaces. This verified the small deviations that were also seen in the XPS data for the plasma activated nylon 6 samples reported in Section 4.3.4.

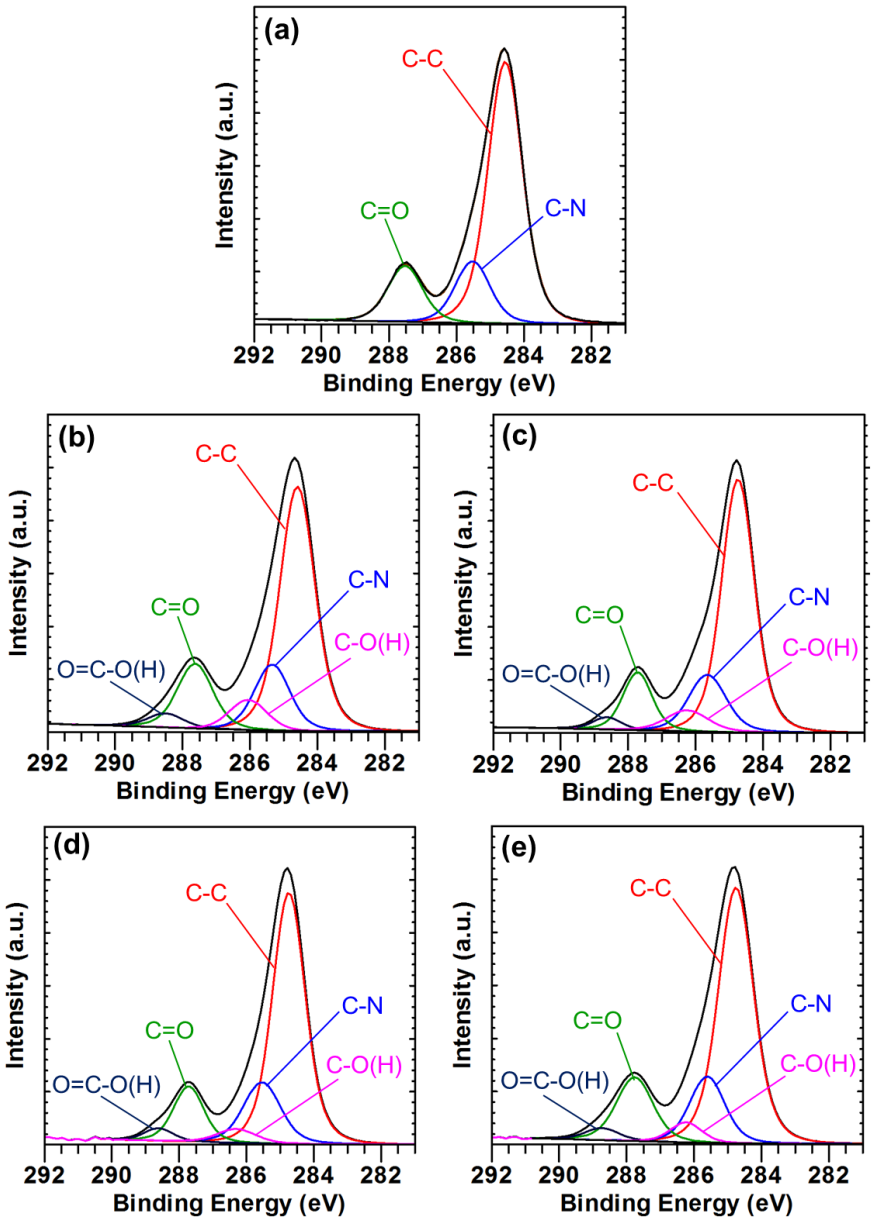

Figure 5-9. High resolution C1s XPS spectra with peak fitting of plasma treated nylon 6 at 60 W for: (a) 0 s (untreated); (b) 30 s; (c) 120 s; (d) 360 s and (e) 600 s.

The XPS peak fittings, through deconvolution of the C1s regions for each of the untreated and plasma treated samples between 30 s and 600 s at 60 W are shown in Figure 5-9. As mentioned previously in Chapter 4, the untreated nylon 6 C1s spectrum displayed in Figure 5-9a shows the characteristic C-C, C-N and C=O peaks that correlated well to the structure of nylon 6 polymers, as did their quantified peak areas. Following 30 s of treatment at 60 W, the C1s spectra in Figure 5-9b show a comparable surface modification to those

seen previously in the nylon 6 plasma activated samples reported in Chapter 4. The same newly formed C-O(H) and (H)O-C=O groups were present, indicating that the plasma had oxidised the surfaces of the nylon 6 samples, through the attachment of polar groups, hence increasing the wettability of the surfaces. Samples that had been treated for 30 s had the largest quantity of both hydroxyl and carboxylic species than all other treatment times that were studied at 60 W. This was attributed to the lack of etching at this short treatment time, resulting in the newly formed polar groups remaining at the surface, rather than being removed by the etching of the plasma.

After 120 s of treatment, the same newly formed groups were found on the surface, but to a lesser extent, with a reduction in C-O(H) from 7.8% (30 s) to 3.8% (120 s), and (H)O-C=O from 3.4% (30 s) to 2.5% (120 s). This was largely due to the etching of the outer surface of the nylon 6 material that included the removal of both the original nylon 6 surface structure, and the newly functionalised areas of the surface. This etching effect led to similar levels of chemical modifications to the nylon surfaces after 360 s and 600 s, again with the introduction of hydroxyl and carboxylic species. Interestingly, the C-N peak remained relatively constant throughout all of the treatments, suggesting that the amide groups and C-N bonds had remained intact, while the C=O peak saw a gradual increase with increasing exposure time up to 600 s. This suggests that the plasma surface oxidation includes the introduction of additional C=O groups into the surface structure. Due to the similar levels of chemical modifications between 120 s and 600 s, the increase in wettability with increasing treatment time seen through the contact angle measurements was primarily attributed to an increase in the extent of etching, rather than an increase in attachment of polar functional groups. This was further supported by the SEM and AFM images discussed in Section 5.1.3. A simplified schematic of the general etching process of nylon 6 polymers with the subsequent formation of nanopores is shown in Figure 5-10.

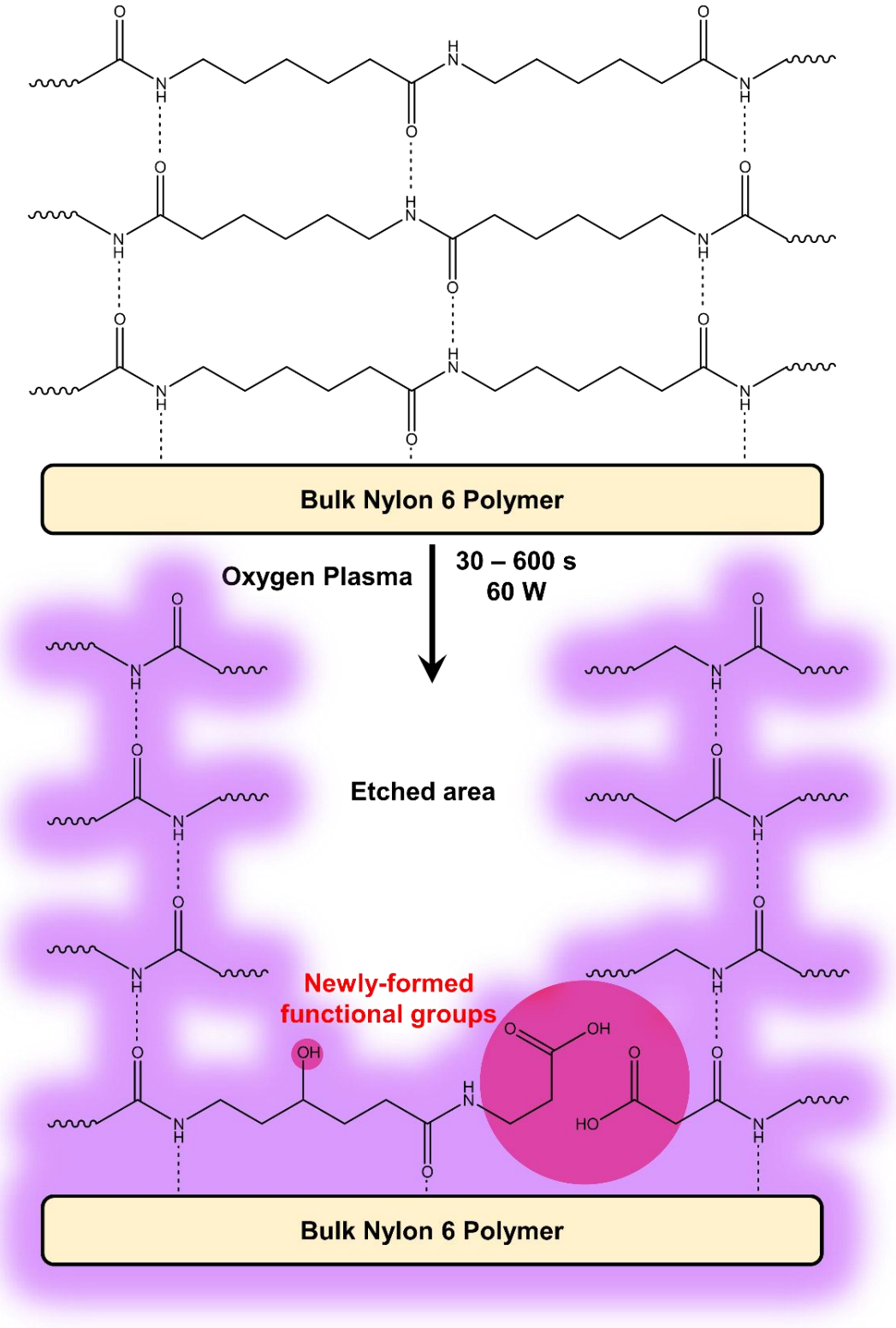

Figure 5-10. General schematic showing the etching of nylon 6 polymer chains induced by oxygen plasma.

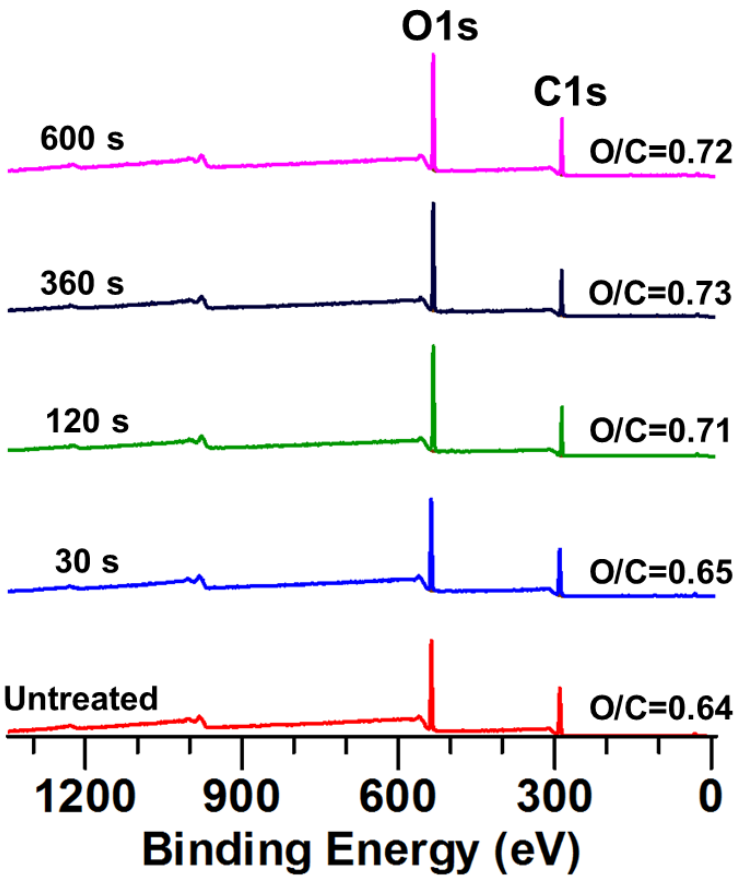

Figure 5-11. XPS survey spectra of untreated and oxygen plasma treated regenerated cellulose at 60 W for different treatment times.

The XPS survey spectra for the untreated and oxygen plasma treated regenerated cellulose films are shown in Figure 5-11. From these wide-scan spectra, it can be seen that the elemental composition of the untreated regenerated cellulose films confirmed the presence of carbon and oxygen as expected. The data showed that the chemical composition of oxygen plasma-treated regenerated cellulose samples saw an overall increase in oxygen-containing species with increasing treatment time, with the O/C ratio increasing from 0.64 (untreated) to 0.65, 0.71, 0.73 and 0.72 for the samples treated for 30 s, 120 s, 360 s and 600 s respectively. It was apparent that the initial extent of surface modification after 30 s of plasma exposure was slight, suggesting that 30 s of plasma treatment was not sufficient to significantly alter the surface chemistry of the regenerated cellulose film, although some oxygen had likely been absorbed onto the surface. Similarly to the nylon 6 samples, the level of surface oxidation increased to a similar degree following

120 s, 360 s and 600 s of treatment, suggesting that increasing the treatment time to longer than 120 s did not result in a significant difference in chemical effect created, and the incorporation of oxygen species into the cellulose structure became nearly saturated after this point.

Table 5-4. Elemental composition from the XPS data obtained for the untreated and oxygen plasma-etched regenerated cellulose samples.

	Elemental composition (%)			C1s peak area (%)			
Treatment time (s)	**Carbon**	**Oxygen**	**O/C ratio**	**C-C**	**C-O**	**O-C-O**	**O-C=O**
0	60.9	38.8	0.64	13.6	69.2	16.5	0.7
30	60.0	39.3	0.65	12.9	69.6	16.7	0.8
120	57.7	41.1	0.71	9.1	71.1	18.5	1.3
360	57.3	42.0	0.73	8.7	74.0	15.5	1.8
600	58.0	41.5	0.72	8.9	73.6	14.7	2.8

Table 5-4 shows the quantified elemental compositions of the untreated and oxygen plasma treated regenerated cellulose films. The table further confirms that oxygen and carbon were the only prevalent elements found on the surfaces of the films. There were also residual traces of silicon and calcium in each of the untreated and plasma treated samples that were not reported in this study due to their trace amounts (< 1 %), and they did not appear to be altered in any significant way by the plasma. After 30 s of plasma exposure, the increase in O/C ratio was very small, suggesting that there had been little surface oxidation by the plasma following this treatment. Similarly to the nylon 6 samples, the oxygen content did not vary significantly between 120 s and 600 s of plasma exposure. Again, this was attributed to the ion bombardment of the oxygen plasma species removing the outer layers of the films, including some of the newly functionalised polymer chains. However, unlike nylon 6, the cellulose film surfaces had greater chemical modifications at longer treatment times between 120 s and 600 s, with only a very slight increase in surface oxygen content after 30 s. This was also observed as reported in Chapter 4,

whereby the cellulose samples had fewer polar groups attached to the surface through plasma activation. The cellulose samples did not see the formation of any new functional polar groups, but instead an increase in the number of those already present. This was due to cellulose surfaces already being relatively saturated with oxygen-containing functionalities such as hydroxyls.

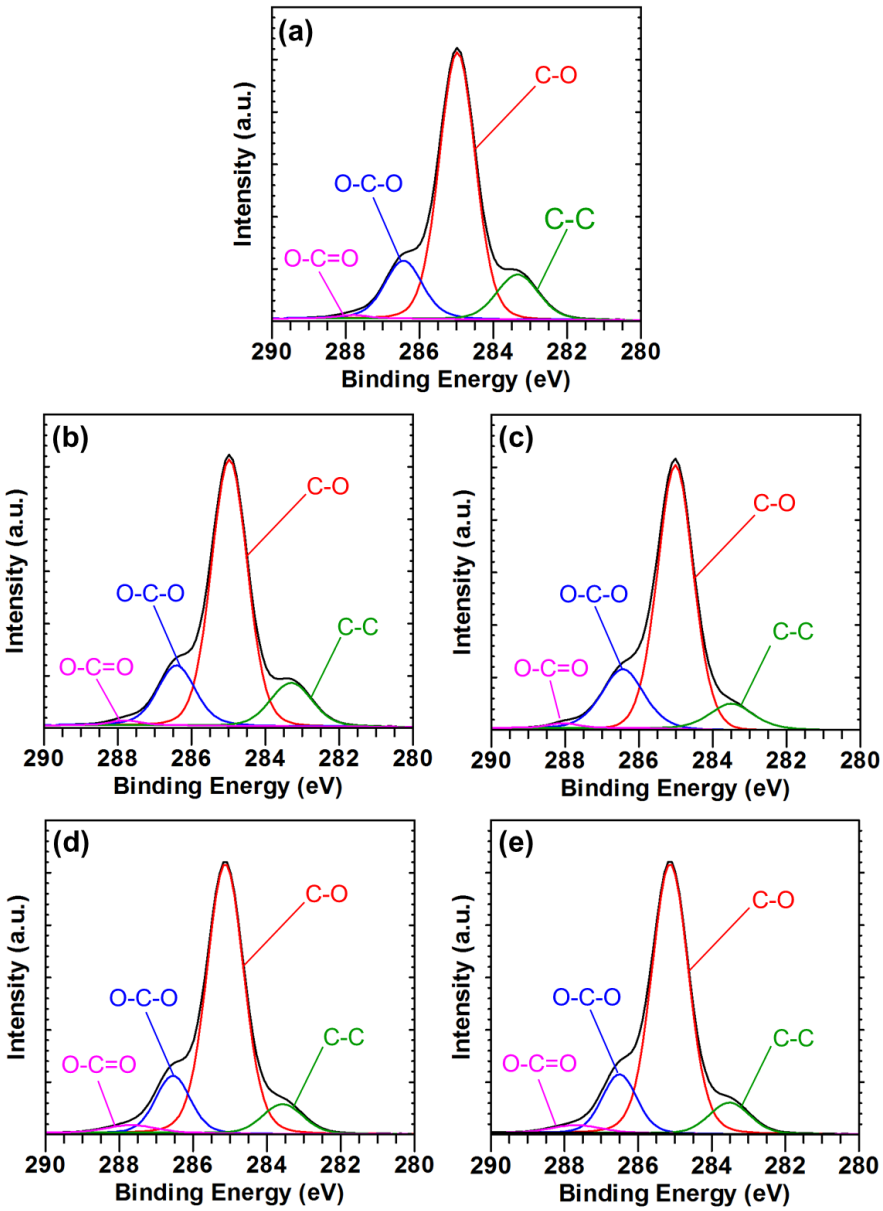

Figure 5-12. High resolution C1s XPS spectra with peak fitting of plasma treated regenerated cellulose at 60 W for: (a) 0 s (untreated); (b) 30 s; (c) 120 s; (d) 360 s and (e) 600 s.

Deconvolution of the C1s peak for the regenerated cellulose films provided a more detailed analysis relating to the chemical functionalities present in both

the untreated and plasma-treated samples (Figure 5-12). The groups identified as being present in each of the samples were C-C, C-O, O-C-O and O-C=O. The C-C peak (with an area of 13.6%) was attributed to a combination of the C-C backbone within the cyclic repeating units of the polymer films, and to adventitious carbon, formed from surface contamination (although most of this was removed through solvent cleaning). The expected C-O/C-OH groups from the cellulose repeating unit were also present in the untreated samples with peak areas of 69.2% and 16.5% respectively. Upon exposure to the oxygen plasma for 30 s, the regenerated cellulose saw minor changes to its surface chemistry, with a reduction in the C-C peak from 13.6% to 12.6% (that was partially attributed to the cleaning effects of the plasma), and an increase in each of the oxygen-containing functionalities, with the C-O peak increasing by 0.7%, the O-C-O by 0.2% and O-C=O by 0.1%. It is worth noting that slight changes in surface composition of this magnitude would often be considered as negligible, and indicative that the apparent changes observed in the surface composition of the cellulose samples could be attributed to associated errors with the XPS measurements, rather than plasma surface-oxidation. Hence, 30 s cannot be considered a long enough time to reliably alter the surface chemistry of cellulose at a discharge power of 60 W. It is likely that the O/C ratio also increased following this treatment due to the absorption of oxygen, and incorporation of a small amount of new hydroxyl groups.

Following 120 s of plasma exposure, the C-C peak saw a more pronounced decrease by 3.2% compared to the untreated cellulose. The C-O/C-OH peak saw an increase of 1.9%, with the O-C-O and O-C=O groups also increasing by 2.0% and 0.6% respectively. The increase in O-C=O was indicative of bond scission, through the formation of heavily oxidised carboxylic acid chain end groups. Such a general trend of decreasing C-C surface functionalities with increasing O/C ratio also continued following plasma treatment for 360 s, but then appeared to decrease slightly after 600 s. However, the magnitude of this decrease was very small, and could be attributed to errors in the XPS measurements. After both 360 s and 600 s, the extent of modification remained similar to 120 s treatment, with a slightly larger decrease in C-C

groups, with the C-O/C-OH and O-C=O groups having marginally larger increases in concentration respectively. This suggested that the plasma action increased the concentration of incorporated oxygen surface functional groups formed, but the increase in treatment time between 120 s and 600 s did not appear to have a major effect on the final concentrations of these species, or the O/C ratios.

After plasma treatment for 360 s and 600 s there was an increase in the formation of heavily oxidised species (O-C=O), which includes both carboxylic and carbonic acids. The formation of these species was indicative of chain scission of the cellulose repeating units at the bridging group, and increased between 360 s - 600 s, due to the increased scission at longer treatment times. This ultimately led to decomposition and etching/nanotexturing of the surface structure that was seen in the SEM and AFM images reported in Section 5.1.3. A general schematic of this etching process for regenerated cellulose is shown in Figure 5-13.

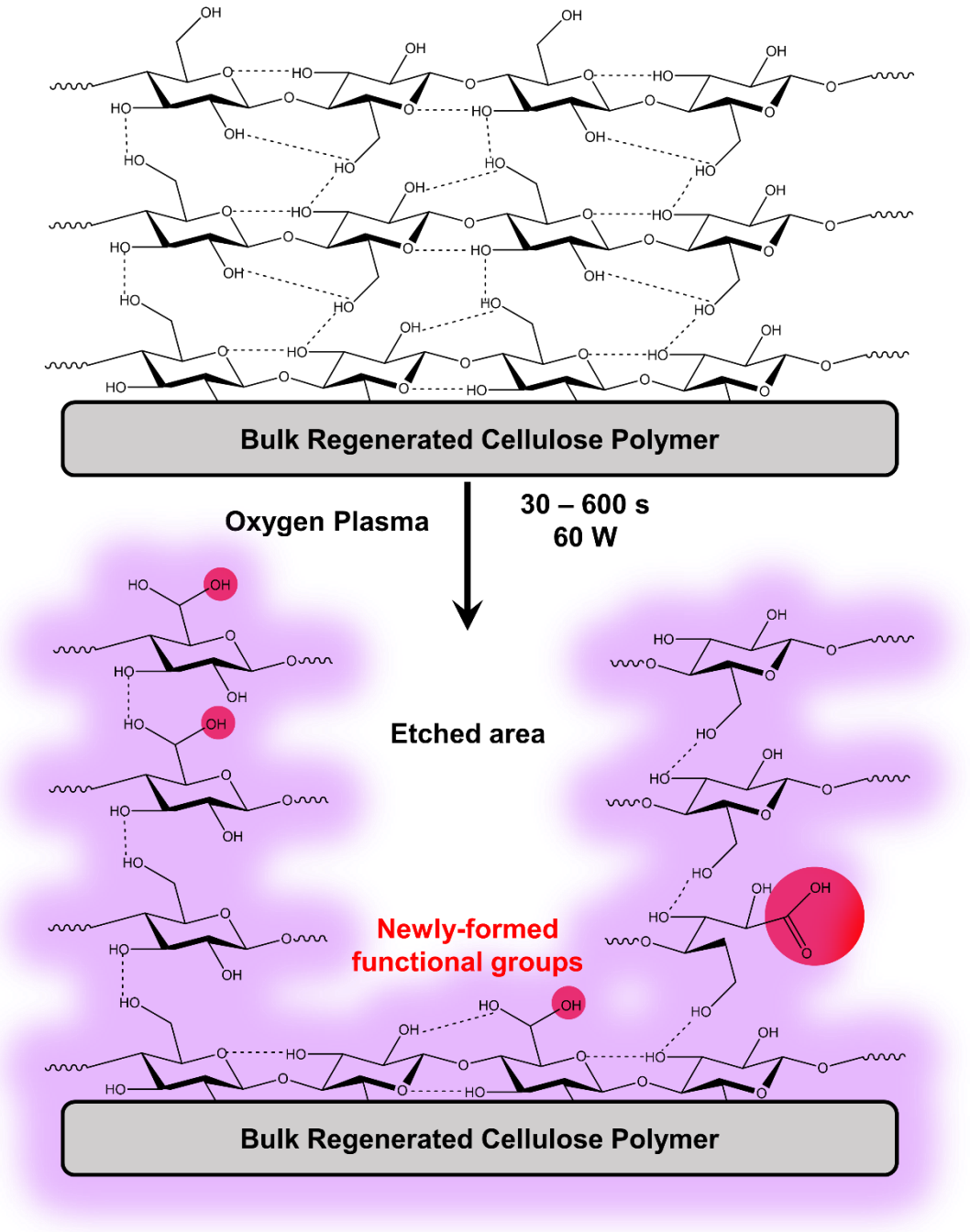

Figure 5-13. General schematic showing the etching of regenerated cellulose polymer chains induced by oxygen plasma.

The O/C ratios presented in Figure 5-14 show differing trends between the nylon 6 plastic sheets and regenerated cellulose films that were treated with oxygen plasma under the same conditions. Firstly, considering nylon 6, the O/C ratio saw an initially large increase after 30 s of exposure to the plasma, resulting in an O/C ratio of 0.32 (compared to 0.16 for the untreated nylon 6 samples). Such an increase was attributed to the attachment of polar groups,

with minimal mass loss or etching. The short treatment time did not allow the plasma to transfer enough energy to the nylon 6 sheets to significantly degrade the polymer chains through scission.

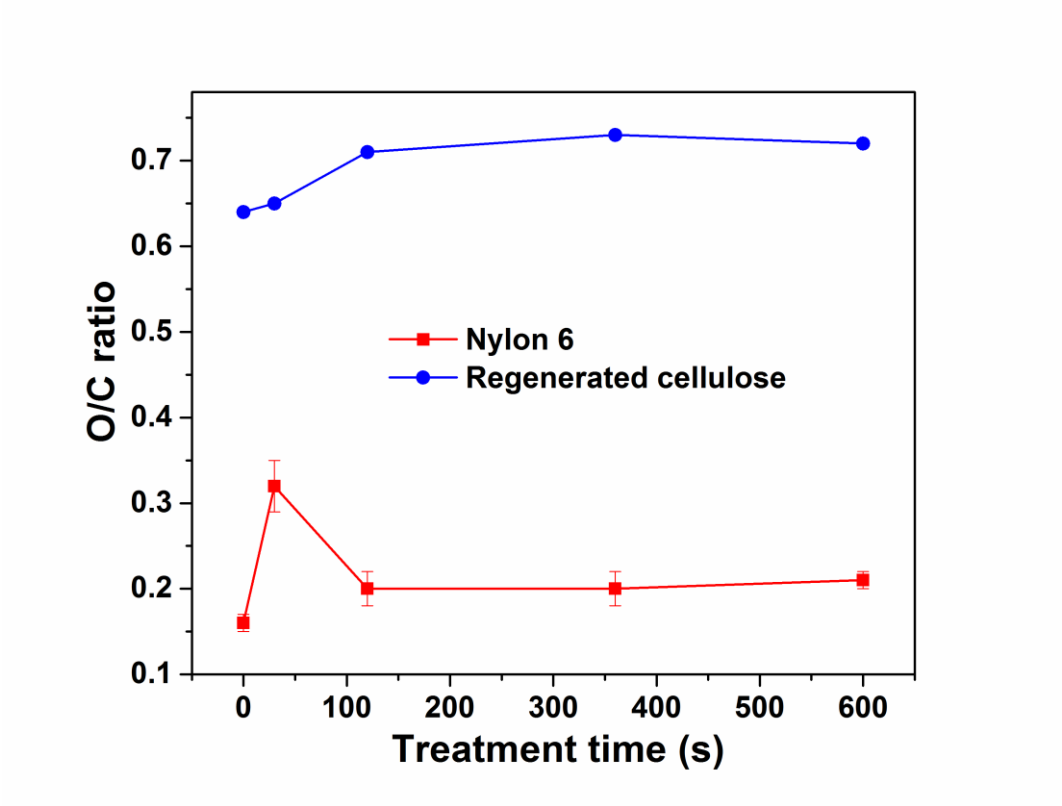

Figure 5-14. O/C ratios of the plasma treated nylon 6 and regenerated cellulose samples as a function of treatment time between 0 and 600 s at 60 W.

The increase was comparable to the increase seen after 40 - 60 s of treatment at 10 W that was reported in Chapter 4. It was evident that shorter treatment times favoured high levels of surface functionalisation on the aliphatic nylon 6 polymer samples, with low levels of etching. The regenerated cellulose samples had a much smaller increase after 30 s of plasma exposure, confirming that the surface-oxygen content had not increased after the short treatment time. The small increase was attributed to a combination of some low levels of oxygen being absorbed onto the surface, and to a cleaning effect from the plasma, removing any hydrocarbon contaminants from the surface, hence increasing the ratio of oxygen to carbon. Unlike the nylon 6 samples, the cellulose samples did not favour shorter treatment times to achieve high

levels of surface functionalisation, but both samples saw little mass loss after 30 s of plasmas exposure.

The trend of the O/C ratios of nylon 6 then had a large decrease from 30 s to 120 s of treatment, to a ratio of 0.20. Such a decrease was attributed to the newly functionalised nylon surfaces being bombarded by the ions in the plasma species with sufficient energy to induce a large extent of chain scission. This led to the outer layers of the material being etched away, meaning that the samples were only partially functionalised when compared to those treated for 30 s. In the case of regenerated cellulose, the O/C had quite a large increase from 30 s to 120 s, to a ratio of 0.71. Although the cellulose samples were subjected to the same etching processes as the nylon samples, the degree of surface functionalisation appeared to be higher at longer treatment times, suggesting that the increased exposure time enabled polar groups (primarily hydroxyls) to be attached to the surfaces.

The O/C of both samples appeared to level off from 120 s of treatment up to 600 s. This was attributed to the constant synergistic activation/functionalisation and etching processes, attaching polar groups to the outer layers of the surface before a proportion of these were removed through etching. The resultant samples in both cases were polymers that had significantly increased surface roughness, with an increased number of polar functional groups compared to the original untreated materials.

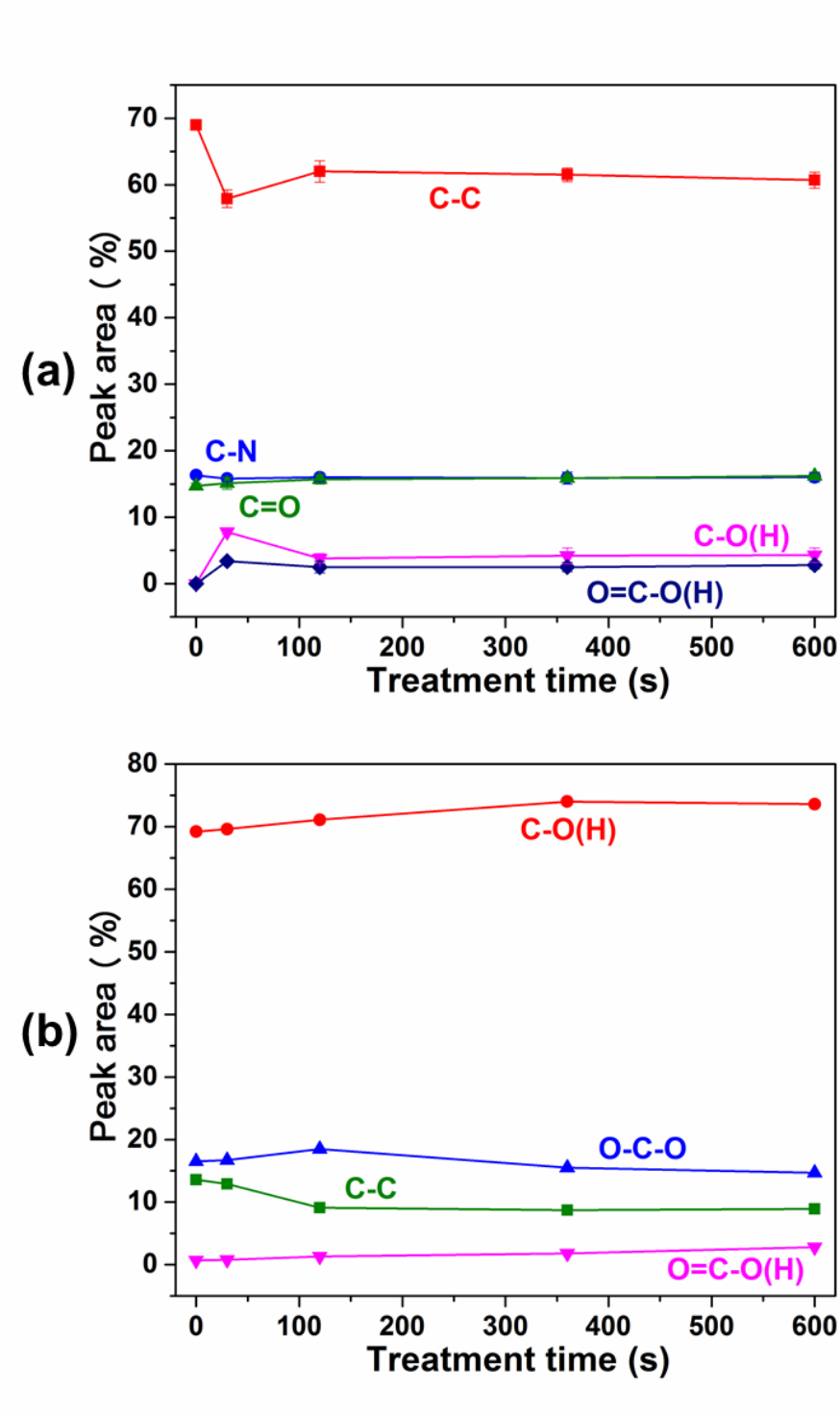

Figure 5-15. The observed changes in peak area (%) for the different XPS C1s spectra for (a) nylon 6 and (b) regenerated cellulose treated with oxygen plasma for different treatment times at 60 W.

The changes in peak areas for each of the functional groups present on the surfaces of the nylon 6 and regenerated cellulose samples analysed in this

study of plasma etching are shown in the graphs in Figure 5-15, enabling direct comparisons to be made. For the nylon 6 samples shown in Figure 5-15a, the major change in the surface functionalities occurred after 30 s of plasma treatment. There was a clear reduction in the C-C groups, with a large increase in C-O(H) groups and small increase in O=C-O(H) groups. This confirmed the aforementioned surface functionalisation that occurred after the short 30 s treatment time at 60 W. Therefore, the increase in wettability at this treatment time was primarily down to the attachment of hydroxyl groups, with some heavily oxidised carboxylic acid groups also formed. After 120 s of plasma treatment, the C-C peak area increased from that after 30 s treatment, with a large reduction in the hydroxyl groups, and slight reduction in carboxylic acid groups. This then stayed fairly constant from 120 s to 600 s, with a slight decrease in C-C groups and slight increase in C-O(H) groups. Although logically, this would indicate that the wettability of the samples should have decreased, the surface roughening processes through etching seen in the SEM and AFM images reported in Section 5.1.3 increased the surface wettability further.

For the observed changes in peak area (%) for the different XPS C1s spectra of the regenerated cellulose film samples shown in Figure 5-15b, the most notable trend was an increase in C-O(H) groups with increasing treatment time, confirming that the plasma had attached additional polar hydroxyl groups onto the already polar regenerated cellulose surfaces. Additionally, the C-C content decreased with increasing treatment time, with the largest decrease seen between 30 s and 120 s of treatment, due to the large increase in polar groups. The peak area of the O-C-O linkages had slightly increased as the C-C groups decreased with 120 s of treatment, before dropping after 360 s and 600 s, indicating that the longer treatment times had induced a greater degree of bond scission, degrading the polymer chains. The carboxylic acid species seemed to slightly increase with increasing treatment time, indicating that the largest degree of scission was experienced after 600 s. The cellulose samples experienced the same synergistic etching and surface functionalisation processes as the nylon 6 samples, but the cellulose surfaces were not

functionalised as rapidly or as much, meaning that there were not a large number of newly functionalised groups removed from the plasma etching.

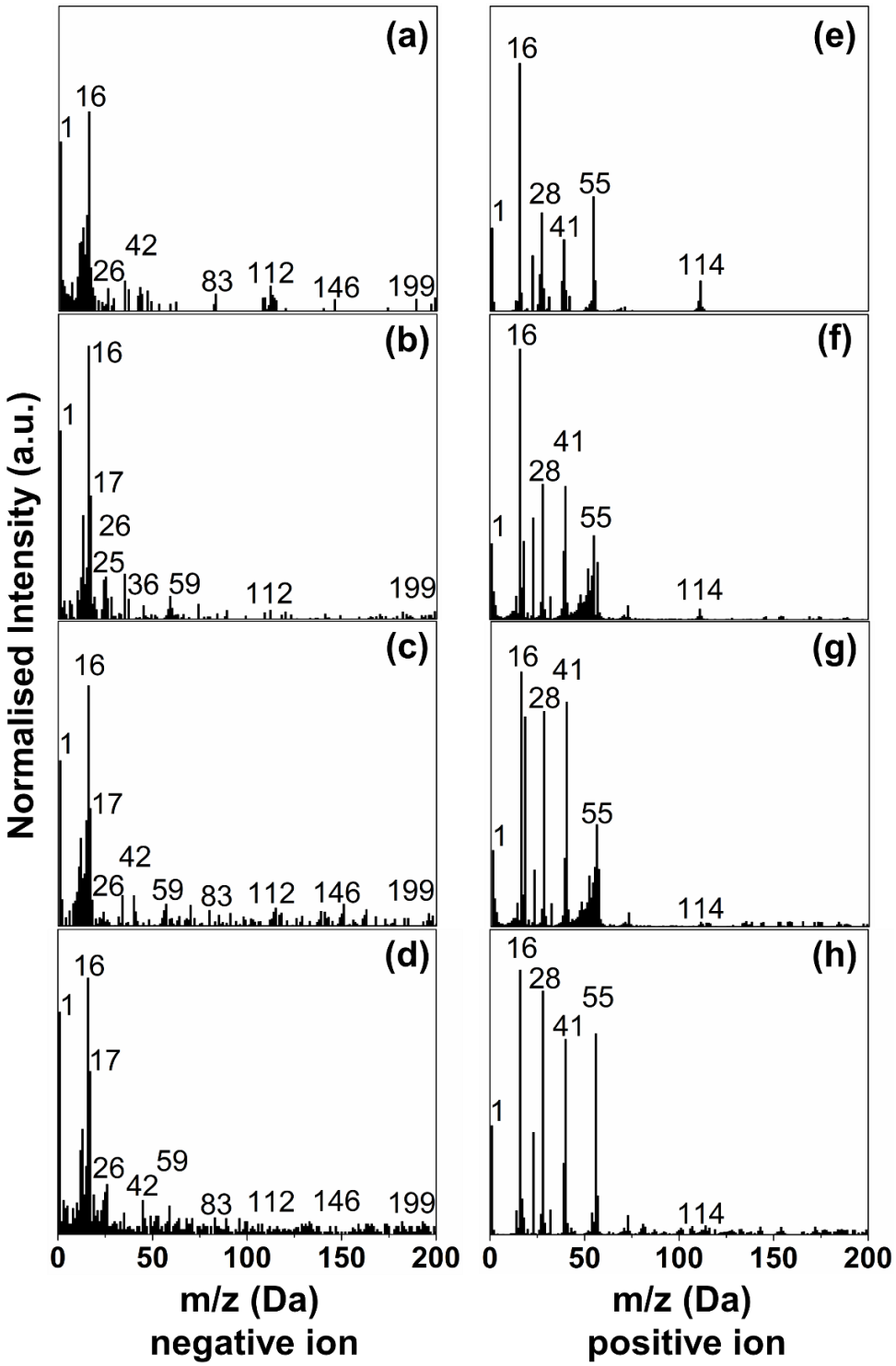

Figure 5-16. SSIMS negative ion spectrum of plasma treated nylon 6 at 60 W for (a) 0 s (untreated); (b) 30 s,; (c) 120 s and (d) 600 s. SSIMS positive ion spectrum of nylon 6 treated for (e) 0 s (untreated); (f) 30 s; (g) 120 s and (h) 600 s.

The SSIMS data presented in Figure 5-16 aids in understanding the surface-chemical modifications induced by the plasma at a range of treatment times at 60 W. As mentioned earlier in Chapter 4, the peaks shown in the untreated nylon spectra (Figure 5-16a) had the following assignment: m/z = 1^- (H^-), 16^- (O^-), 26^- (CN^-), 42^- (CNO^-), 83^- ($C_5H_7O^-$), 112^- ($C_6H_{10}NO^-$, M^-H^-), 146^- ($C_7H_{16}NO_2^-$), and 199 ($C_{12}H_{25}NO^-$). The peaks in the positive ion spectra (Figure 5-16e) were assigned as m/z = 1^+ (H^+), 16^+ (O^+), 28^+ (CO^+), 41^+ ($C_2H_3N^+$), 55^+ ($C_3H_3O^+$) and 114^+ ($C_6H_{12}NO^+$, M^+H^+). These characteristic peaks were consistent with the structure of the nylon 6 polymers, with the peaks at 112^- and 114^+ corresponding to the polymer repeating units as M^-H^- and M^+H^+ respectively.

After 30 s of oxygen plasma treatment at 60 W, the main peaks were seen at m/z = 1^- (H^-), 16^- (O^-), 17^- (OH^-), 25^- (C_2H^-), 26^- (CN^-), 36^- (C_3^-), 59^- ($C_2H_3O_2^-$), and 112^- ($C_6H_{10}NO^-$, M^-H^-) for the negative ion spectra shown in Figure 5-16b, and m/z = 1^+ (H^+), 16^+ (O^+), 28^+ (CO^+), 41^+ ($C_2H_3N^+$), 55^+ ($C_3H_3O^+$) and 114^+ ($C_6H_{12}NO^+$, M^+H^+) from the positive ion spectra shown in Figure 5-16f. The peaks present in both of these spectra confirmed that newly formed hydroxyl groups seen in the XPS data had been attached, and there appeared to be an increase in surface oxygen content relative to the untreated sample. The peaks at 112^- and 114^+ both remained after the plasma exposure for 30s, showing that some of the original nylon 6 structures remained intact, due to the short exposure to the plasma that did not supply enough energy to the surfaces to disrupt the structures further. The peak seen at 59^- in the negative ion spectra also verified the XPS peak model through showing the presence of the O-C=O group, hence indicating a level of chain scission and surface oxidation by the plasma.

Following 120 s of plasma exposure, the negative ion spectra (Figure 5-16c) had notable peaks at m/z = 1^- (H^-), 16^- (O^-), 17^- (OH^-), 26^- (CN^-), 42^- (CNO^-), 59^- ($C_2H_3O_2^-$), 83^- ($C_5H_7O^-$) and 112^- ($C_6H_{10}NO^-$, M^-H^-), with the positive ion spectra (Figure 5-16g) having peaks at m/z = 1^+ (H^+), 16^+ (O^+), 28^+ (CO^+), 41^+

($C_2H_3N^+$), 55^+ ($C_3H_3O^+$) and 114^+ ($C_6H_{12}NO^+$, M^+H^+). The peaks greater than 112^- and 114^+ were not assigned as specific fragments, due to the multiple possibilities for different molecular ion fragments. The two spectra showed that the same hydroxyl and carboxylic acid groups had been attached by the plasma as seen in the 30 s treated sample, in addition to a large number of new peaks being detected. More specifically, there was a large increase in the number of new peaks with low intensity at m/z > 100 in both the negative and positive ion spectra, suggesting that the long range order had been significantly disrupted by plasma-induced oxidative degradation of the polymer chains. Again, the peaks at 112^- and 114^+ suggested that despite the etching and surface-chemical alterations to the sample, some of the original nylon 6 structure remained. This was likely due to some deeper, unmodified areas of the nylon 6 samples being exposed to the surface, having had the original outer surface layer being removed through etching.

After 600 s of treatment, the negative ion spectra for the nylon 6 samples shown in Figure 5-16d showed peaks that were the same as those seen in the 120 s treated samples, but with different relative intensities. Furthermore, the positive ion spectra in Figure 5-16d also showed the same major peaks as the 120 s treated samples. These similarities in both spectra verified the XPS analysis, confirming that the extent of chemical modification was similar for both samples. This was attributed to the samples being rapidly functionalised, but with a simultaneous etching process that stripped away some of the outer layers of the samples, including some of the newly functionalised structures. Again, the dominant feature in both the negative and positive ion spectra was the large number of peaks with low intensities, particularly above 100 Da, indicating a high level of fragmentation due to chain scission from surface ion bombardment of the plasma species. The peaks at 112^- and 114^+ still remained in both spectra, but had very low intensity, suggesting that the original nylon 6 structure had been more significantly disrupted/damaged after 600 s of treatment than after 120 s.

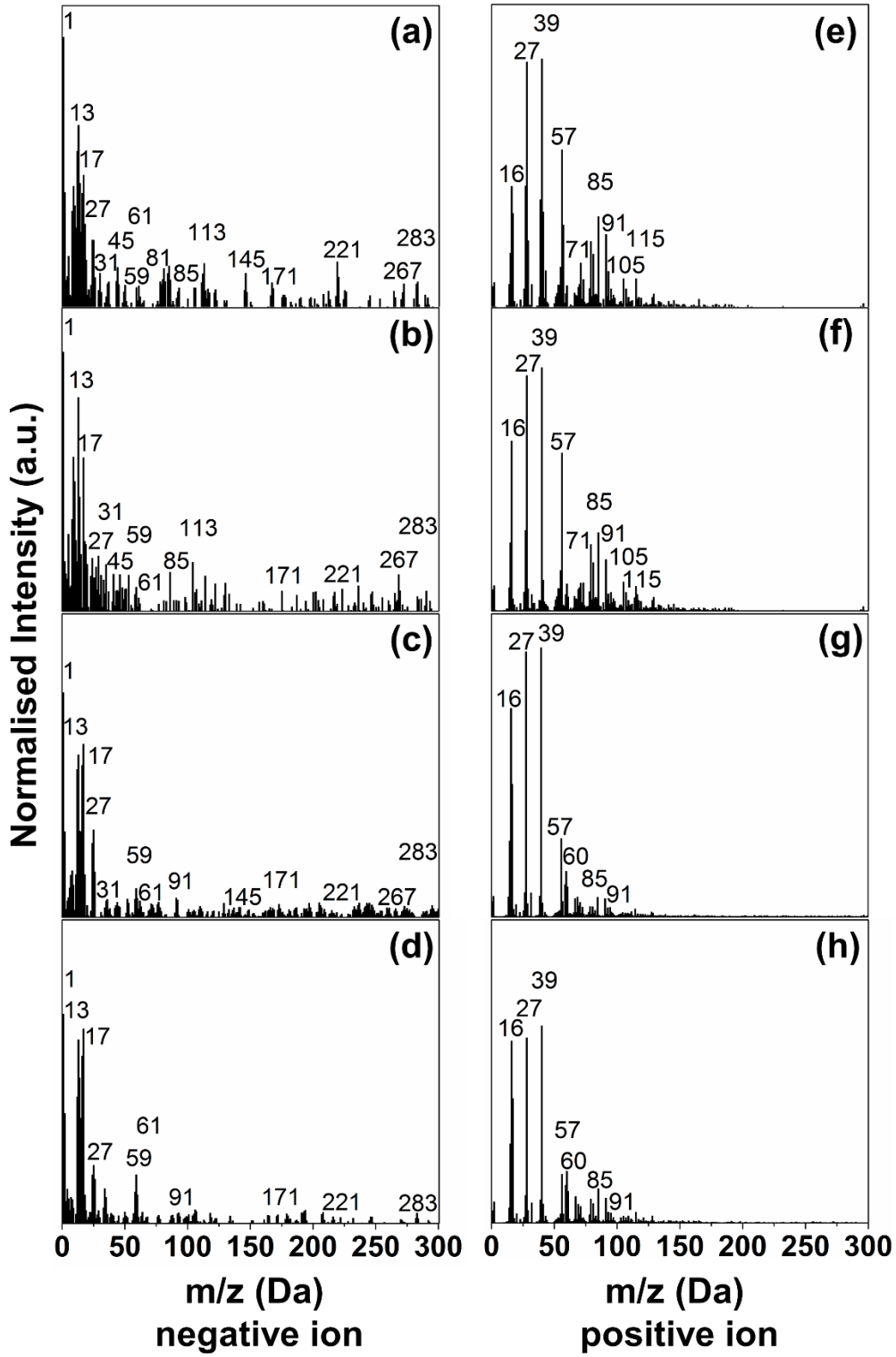

Figure 5-17. SSIMS negative ion spectrum of plasma treated regenerated cellulose at 60 W for (a) 0 s (untreated); (b) 30 s,; (c) 120 s and (d) 600 s. SSIMS positive ion spectrum of regenerated cellulose treated for (e) 0 s (untreated); (f) 30 s; (g) 120 s and (h) 600 s.

From Figure 5-17a and e, it can be seen that there were a large number of characteristic peaks that were attributed to the untreated regenerated

cellulose surface structure. In the negative ion spectrum, these included the peaks at m/z = 1^- (H^-), 13^- (CH^-), 17^- (OH^-), 27^- ($C_2H_3^-$), 31^- (CH_3O^-), 45^- ($C_2H_5O^-$), 61^- ($C_2H_5O_2^-$), 81^- ($C_5H_5O^-$), 85^- ($C_4H_5O_2^-$), 113^- ($C_5H_5O_3^-$) and 145^- ($C_6H_9O_4^-$). Peaks above 145 Da were difficult to assign due to the multiple possibilities for molecular ion fragments formed. In the positive ion spectrum, the characteristic peaks were found at m/z = 16^+ (16^+), 27^+ ($C_2H_3^+$), 39^+ ($C_3H_3^+$), 57^+ ($C_2HO_2^+$), 71^+ ($C_3H_3O_2^+$), 85^+ ($C_4H_5O_2^+$), 91^+ ($C_2H_3O_4^+$), 105^+ ($C_3H_5O_4^+$) and 115^+ ($C_5H_7O_3^+$). After 30 s of plasma exposure, the negative and positive ion SIMS spectra (Figure 5-17b and f respectively) showed few changes compared with the untreated spectra.

Most of the characteristic peaks that were present in the untreated spectra were also present in the 30 s plasma treated samples, with similar relative intensities. Some of the slight deviation in peaks between the untreated and 30 s treated samples would be expected due to the general variations between the cellulose samples, combined with any associated error in the SIMS measurements. This further supported the XPS data in showing that any surface-chemical modification induced by the 30 s plasma treatment was marginal, with 30 s failing to induce any significant change in the functional groups present on the surface of the regenerated cellulose films.

Following oxygen plasma exposure for both 120 s and 600 s of treatment, the resultant spectra had similar peaks, suggesting that both samples had been subjected to a similar chemical modification. The negative ion spectra saw an increase in the peak at 17^- (OH^-), with the positive ion spectra seeing a similar increase at the 16^+ (O^+) peak. This supports the increasing O/C ratio obtained from the XPS data. There was also a substantial decrease in the relative intensity of the characteristic peaks >80 Da shown in the untreated sample. This can be attributed to the etching power of the plasma breaking up the cellulose chains through chain scission, hence lowering the concentration of the higher molecular weight fragments. Furthermore, peaks at m/z = 59^- ($C_2H_3O_2^-$) and 60^+ ($C_2H_4O_2^+$) respectively were found in both the untreated and plasma treated samples. These peaks were attributed to carboxylic acid

species, with their intensities increasing with increasing treatment time after having an initially low concentration in the untreated samples, hence confirming the XPS data. Similarly, in the positive ion spectra, a small number of peaks >100 Da with relatively low intensity were present in the untreated spectra (e), but were either significantly reduced or completely removed following plasma exposure. This suggests that similarly to the nylon 6 samples, the plasma had disrupted the long-range order within the cellulose repeating units, through bond scission and oxidation, hence accounting for the increase in the concentration of highly oxidised carbonic and carboxylic acid species present. Although the complexity of the spectra obtained makes a definitive assessment of the surface-chemical changes induced by the plasma difficult to obtain by SIMS alone, it was still possible to extract key information from the data to support the XPS information.

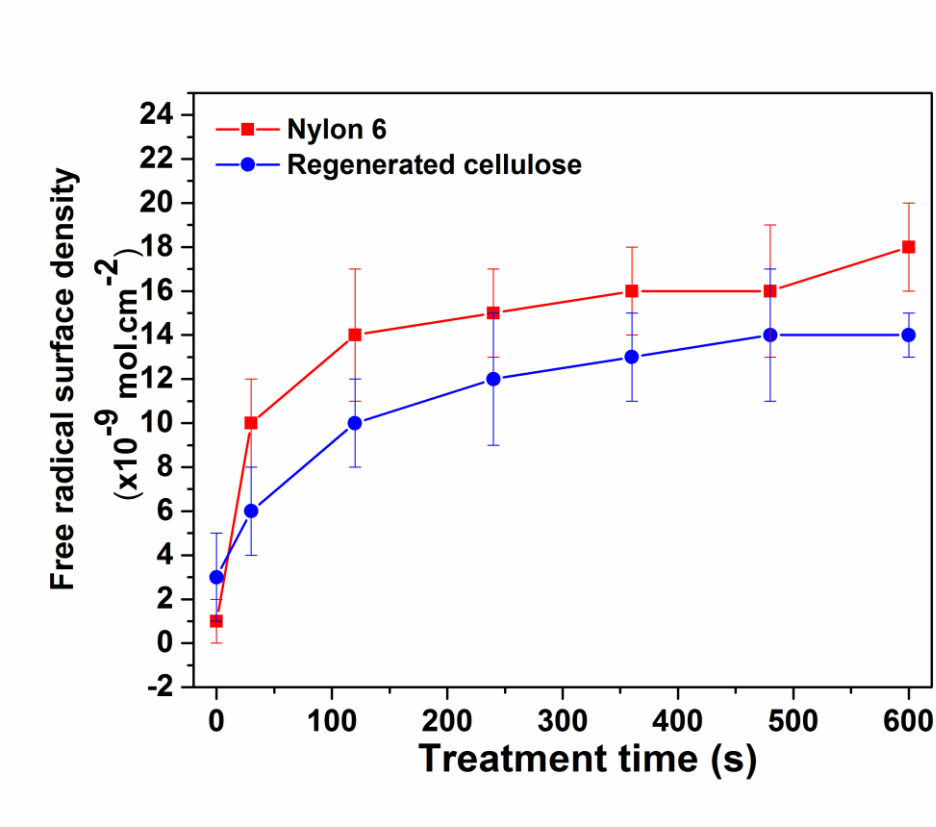

Figure 5-18. The free radical surface densities of untreated and oxygen plasma treated nylon 6 and regenerated cellulose samples between 0 - 600 s at 60 W.

To provide further insights into the effects of plasma etching on the surface chemistry of the plasma treated nylon 6 plastic sheets and regenerated cellulose films, the surface densities of free radicals were determined using a chemical labelling method with the radical scavenger DPPH. As mentioned previously in Chapter 4, the extinction coefficient for DPPH in toluene was determined to be 11057 L mol^{-1} cm^{-1}. Figure 5-18 shows the values obtained for the surface densities of free radicals (including post-oxidation products from exposure of the samples to air following plasma treatment) for the nylon 6 and regenerated cellulose samples for treatment times between 0 and 600 s at 60 W. There was a clear trend of increasing surface radical density with increasing treatment time for both samples, with the increase being initially large at shorter treatment times between 0 and 120 s. The increase in radical density then levelled off slightly at longer treatment times between 240 and 600 s, producing curve fittings on the data points. This suggested that the increase in surface radical density was slowed by a higher degree of etching that was seen in the samples that had undergone longer treatments. For both materials, there were low levels of surface radicals detected in the untreated samples that were attributed to the hydrocarbon chains of nylon, and hydroxyl groups of cellulose undergoing side reactions with the DPPH molecules.

The initially large increase in surface radical densities seen after 30 s was primarily attributed to the surface activation process described in Chapter 4, generating surface radicals through surface-plasma interactions (specifically H-abstractions), with minimal etching following 30 s of treatment. Between 240 s and 600 s, the surface radical densities had similar values, ranging from 15.0 to 18.0 × 10^{-9} mol cm^{-2} for nylon 6, and 12.0 to 14.0 × 10^{-9} mol cm^{-2} for cellulose. This supported the theory that through removing the outer surface layers through etching, newly exposed areas would have then been functionalised and bombarded by the reactive plasma species, hence generating new functional groups and surface radicals. The synergistic etching and functionalisation processes ultimately resulted in similar extents of chemical modification between 240 s and 600 s. Generally, the samples treated for these times generated more surface radicals due to the increase

in chain scission that was also seen in the SIMS data, in addition to some surface radical generation through hydrogen abstraction by the oxygen plasmas species. For the nylon 6 samples, there appeared to be an unexpectedly large value after 600 s of treatment, which showed the data point to be a slight outlier from the general curve trend. However, the error in the surface radical density quantifications was generally quite large due to the highly reactive nature of the DPPH molecule, which is prone to side reactions with a large range of functional groups.[139] Therefore, this slightly higher than expected value was attributed to experimental errors at 600 s of treatment. Despite having a higher initial surface radical density in the cellulose samples (due to the large number of hydroxyl groups present in the surface of the cellulose repeating units that could react with DPPH), each of the plasma treated samples had smaller radical densities compared to the nylon samples. This indicated that the oxygen plasma had generated more radical sites in the aliphatic hydrocarbon chains than in the cellulose cyclic repeating units, due to nylon 6 having longer hydrocarbon chains that have more available sites that are susceptible to hydrogen abstraction by the oxygen plasma.

5.1.5 Penetration depth of oxygen plasma

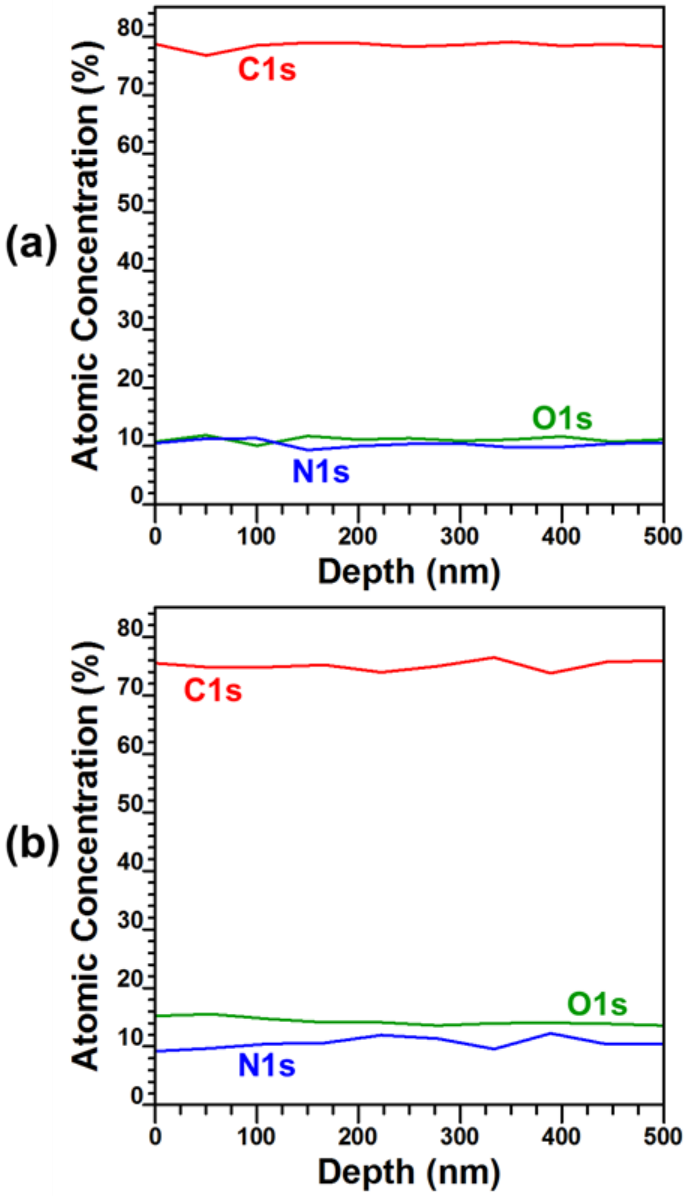

Figure 5-19. XPS depth profiles of (a) untreated nylon 6 and (b) oxygen plasma treated nylon 6 for 600 s at 60 W.

Using nylon 6 as a case study, the XPS depth profiles shown in Figure 5-19 were used to assess the untreated and plasma treated samples, to monitor the depth of modification induced by plasma treatments at extended exposure times of 600 s. The depth profile for the untreated nylon 6 plastic sheets presented in Figure 5-19a shows the expected at% for the samples that have similar elemental composition, both at the surface and into the subsurface due to the uniformity of the material.

Following exposure to plasma for 600 s at 60 W, the depth profile for the oxygen plasma treated sample shown in Figure 5-19b confirmed that the oxygen plasma had increased the surface oxygen content from approximately 11% to 16% through the attachment of polar hydroxyl groups (discussed in detail in Section 5.1.4), with the at% of carbon decreasing. At depths below 100 nm, the oxygen at% decreased slightly compared to that of the surface. Following this slight decrease, the oxygen content remained relatively constant until a depth of 500 nm. It was evident that the oxygen content for the range of depths surveyed in this profile was higher than that displayed in the untreated spectra. Given that oxygen plasma typically functionalises the outmost atomic layers of a surface, it is likely that during the prolonged 600 s of plasma treatment, there had been diffusion of polar species into the sub-surface through the amorphous regions of the polymer chains. There were also nanopores that were formed through etching of the plasma under these conditions that could have enabled a more efficient absorption of oxygen into the sub-surface layers.

5.1.6 Crystallinity

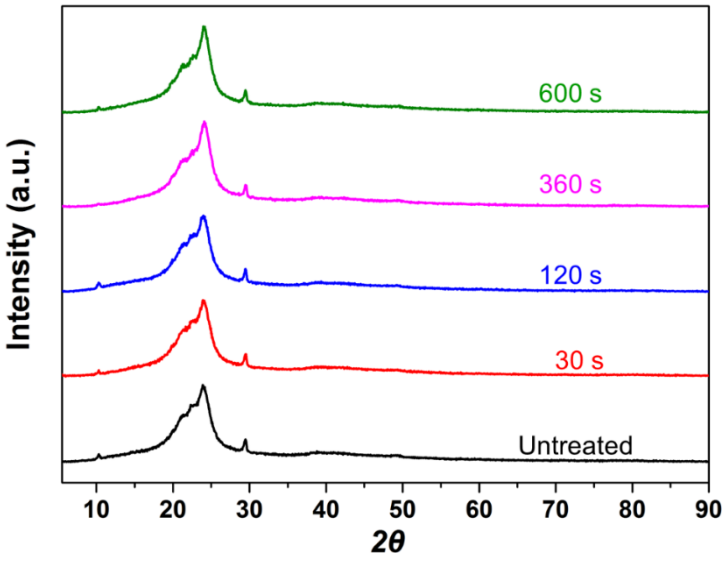

Figure 5-20. XRD spectra of the untreated and oxygen plasma treated nylon 6 samples between 30 - 600 s at 60 W.

Using nylon 6 as an example, the effects of plasma etching on crystallinity were investigated. From the XRD data displayed in Figure 5-20, it was

apparent that there was no change in the crystallinity of the plasma-treated nylon 6 samples. Under the selected conditions, oxygen plasma surface etching did not alter the degree of crystallinity or result in the formation of new crystalline species. The major 2θ peak shown in the XRD spectra for nylon 6 appeared as a broad peak at 24°, confirming the sheets to be mostly amorphous. There was no major shift or change in the spectra for the etched samples compared against the untreated samples. The crystallinities of all of the untreated and oxygen plasma-treated samples ranged between 39.3 and 40.6%. This range can be attributed to the associated error in the XRD, in addition to the expected slight variation in each of the manufactured nylon 6 plastic sheet samples. The results confirmed that there was no significant change in crystallinity induced by plasma etching, and that the polymer chain arrangements in the nylon 6 sheets were predominantly amorphous, both before and after plasma exposure. Additional DSC measurements were performed to further confirm the lack of changes in crystallinity following plasma etching, which also showed there to be no significant change in the samples.

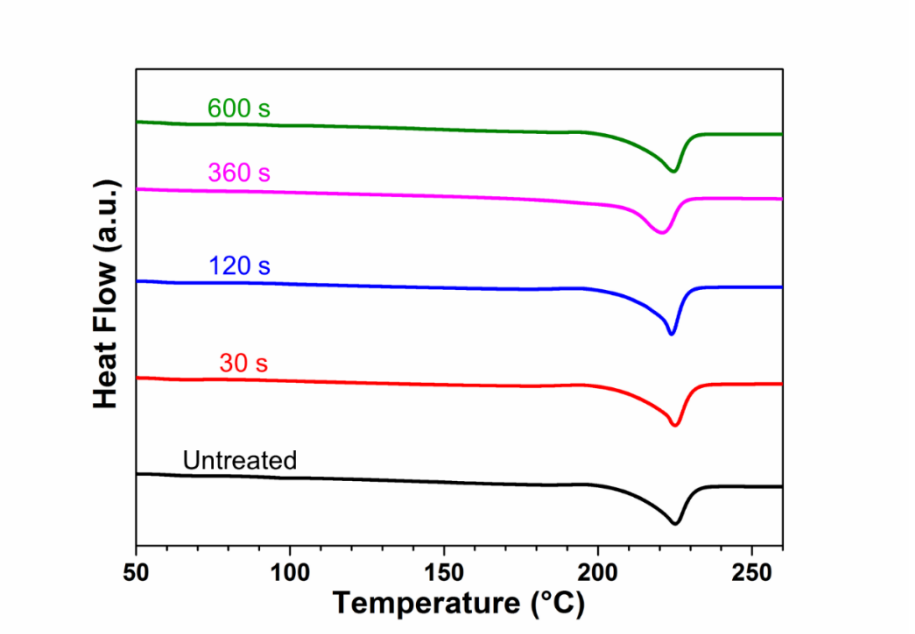

Figure 5-21. DSC curves of the untreated and oxygen plasma treated nylon 6 samples between 30 - 600 s at 60 W.

To complement the XRD data, and give further insights into the effects of plasma etching on crystallinity, DSC analyses were carried out. From the DSC

curves shown in Figure 5-21, it can be seen that there was no major change between the untreated nylon 6 and plasma-treated nylon 6 samples up to 600 s. There were slight variations in the curves, which is likely due to associated errors in the DSC measurement, or in the variations in each of the plastic sheeted samples. The DSC appeared to verify the XRD data in showing that plasma etching did not change the crystallinity of the nylon 6 sheets in any major way. The lack of any trend of major alteration in the polymer crystallinities are shown in the values displayed in Table 5-5.

Table 5-5. DSC thermal analysis data for untreated and plasma etched nylon 6.

Sample reference	**Endothermic transition energy ($J\ g^{-1}$)**	**Crystallinity (%)**
Untreated / As received	86.85	38.43
Untreated / Following thermal treatment	63.04	27.89
30 s, 60 W / As received	86.94	38.47
30 s, 60 W / Following thermal treatment	61.61	27.26
120 s, 60 W / As received	86.14	38.12
120 s, 60 W / Following thermal treatment	59.27	26.23
360 s, 60 W / As received	81.28	35.97
360 s, 60 W / Following thermal treatment	59.27	26.23
600 s, 60 W / As received	82.21	36.38
600 s, 60 W / Following thermal treatment	60.45	26.75

5.2 Conclusions

The data presented in this chapter confirm that CCP low-frequency (40 kHz), low-pressure oxygen plasma had a nanotexturing ability to increase the surface area of both nylon 6 and regenerated cellulose polymers through plasma etching, yielding results similar to those previously reported using RF (13.56 MHz) and microwave (2.46 GHz) plasma discharges.[93, 115, 142] Through the use of surface-chemical XPS and SSIMS analyses, it was evident that nylon 6 saw increased degrees of functionalisation after shorter treatment times (30 s at 60 W), with a lesser extent of further functionalisation seen between 120 s and 600 s of plasma exposure. In comparison, the regenerated cellulose samples saw a general increase in the degree of surface functionalisation with increasing plasma treatment time. For both materials, plasma treatment with the low-frequency, low-pressure oxygen plasma resulted in an increase in the presence of polar functionalities, primarily comprising -COOH and -C-OH groups. The plasma also appeared to increase the amount of fragmentation of the polymer chains, whilst also increasing the surface radical densities of both materials with increasing treatment time.

However, the main alterations in the nylon 6 and regenerated cellulose surfaces were seen in the morphology and topography through the SEM and AFM images. Both techniques revealed that the surface area of the substrates increased with increasing plasma treatment time, due to the bombardment of plasma species upon the polymer chains, resulting in -C-C- bond scission and the subsequent removal of the resultant volatile degradation products (low molecular weight species). This increase in surface area was particularly prevalent after 600 s of treatment, at which point both materials had formed trenches and pores due to the etching of the plasma. This increase in surface area through etching ultimately resulted in the hydrophilicity of the substrates increasing; this trend was seen through the measured contact angle values and calculated surface energies. Gravimetric analysis confirmed that the etching of the substrates increased with increasing treatment time through mass loss experiments, with TGA analysis showing no obvious changes in the thermal stabilities of the nylon 6 samples. XRD and DSC analyses further

confirmed that plasma etching under these conditions had no observed changes in crystallinity. It was evident that between 30 s and 600 s of low-frequency plasma treatment at 60 W, a synergistic combination of surface activation and etching led to an increase in surface wettability, with etching being the predominant process between 120 s and 600 s.

6. Ageing/hydrophobic recovery of post-plasma treated polymers

6.1 Ageing of nylon 6 plastic sheets and regenerated cellulose films

This chapter details a study on the loss of hydrophilicity of oxygen plasma activated and etched nylon 6 and regenerated cellulose samples due to plasma ageing. Plasma ageing occurs due to the thermodynamically-driven lowering of surface energy from a newly-formed unstable high energy state (induced by plasma treatment) to a more stable lower energy state.[72] The main focus of the chapter is the observed change in surface wettability of the plasma treated samples following exposure to air for a number of weeks. Static contact angle measurements are primarily used in monitoring the alterations in surface wettability in air, and under a range of different storage conditions. These included storage under vacuum and in water. The static contact angle values obtained for the samples aged in air were rationalised by surface-chemical XPS measurements.

6.1.1 Surface wettability of aged plasma-treated samples

The graphs displayed in Figure 6-1a and b show the observed decrease in surface wettability in the oxygen plasma activated nylon 6 and regenerated cellulose samples respectively, with subsequent ageing in air for 20 days. It is worth noting that each of the values presented in the graphs represent mean

values, but the uncertainties were omitted to allow the graphs to be legible, and the displayed trends to be clearly visible.

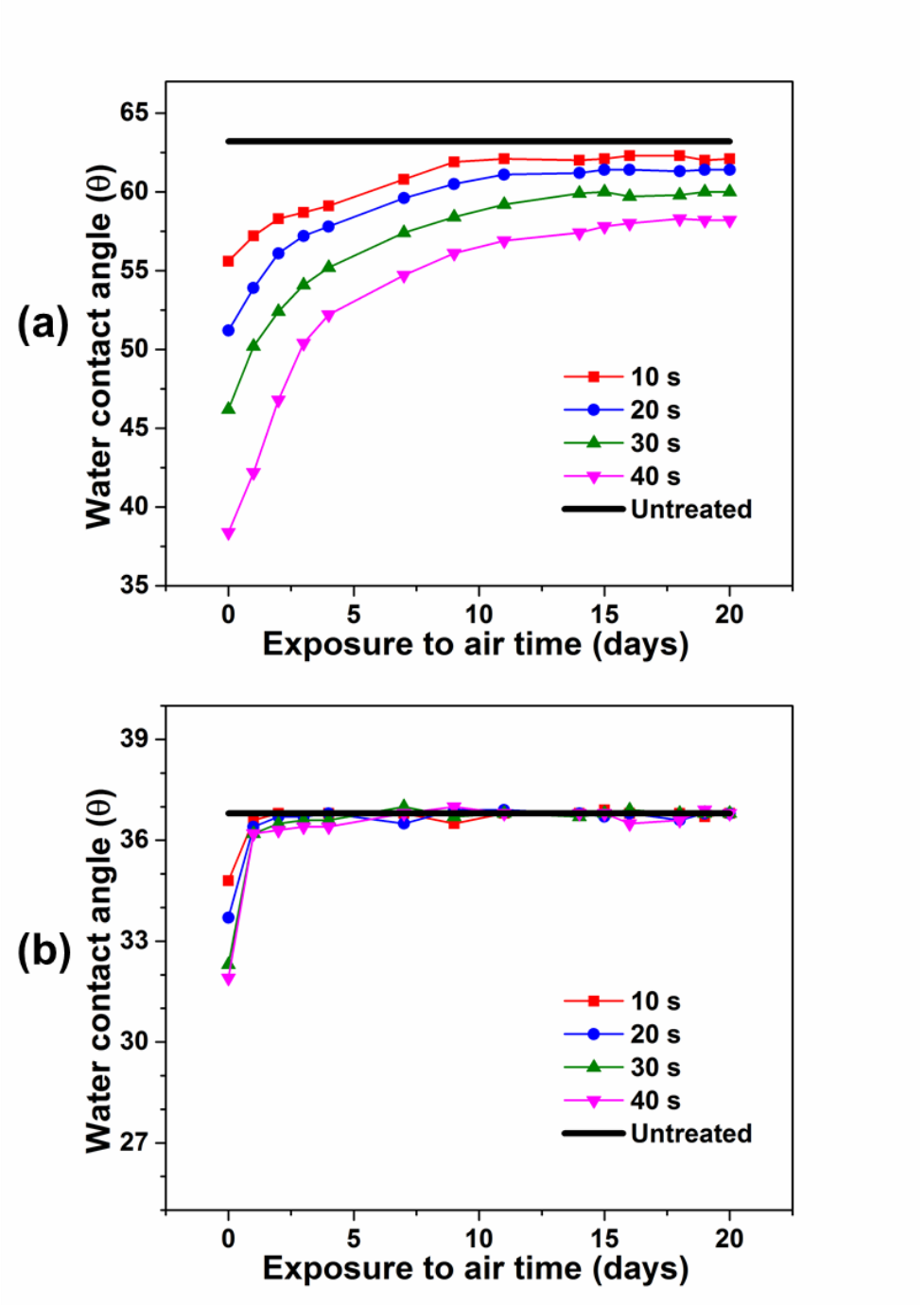

Figure 6-1. Static contact angle measurements of plasma activated samples (oxygen plasma treated for 10 - 40 s) with increasing exposure time to air following plasma exposure, for (a) nylon 6 and (b) regenerated cellulose.

In the case of nylon 6, the samples initially saw a sharp increase in hydrophobic recovery, particularly following 1 - 5 days of ageing. Such an

increase in hydrophobicity then started to become more gradual and levelled off after approximately 14 days, with prolonged exposure to air. The samples that had undergone shorter treatment times (10 - 20 s) showed a slower initial hydrophobic recovery than the longer treatments (30 - 40 s), but the final contact values obtained were much higher for the shorter treatment times, indicating a higher degree of hydrophobicity. However, the samples treated for 40 s, had an overall increase in contact angle of 19.8° over the 20 day period, while the samples treated for 10 s only increased by 6.5°, indicating that larger degrees of plasma-surface functionalisation resulted in larger increases in the extent of hydrophobic recovery. The hydrophobic recovery was attributed to the reorientation of the attached polar surface functionalities, through the diffusion of the oxidised low molecular weight species into the bulk material, and rotations of the polar moieties away from the surface. This is a thermodynamically driven process that shifted the surface energy from a high energy (polar) state to a lower energy, and more stable state.[73] It was clear that none of the plasma activated nylon samples had fully reverted back to their initial surface wettability, suggesting that some of the attached polar functionalities present on the modified surfaces had remained. This is likely to have been due to some of the attached polar groups having intermolecular interactions with the water molecules in the air, which kept the groups at the surface.

For the regenerated cellulose samples, the sample's surfaces initially reverted back to their original contact angle values within 1 - 5 days of ageing. It was clear that the initial change in surface wettability induced by the oxygen plasma was small for all of the samples, and was attributed to the absorption of oxygen onto the cellulose surfaces. The release of this absorbed oxygen from the surface then resulted in a full, rapid hydrophobic recovery of the samples back to their original untreated surface wettability.

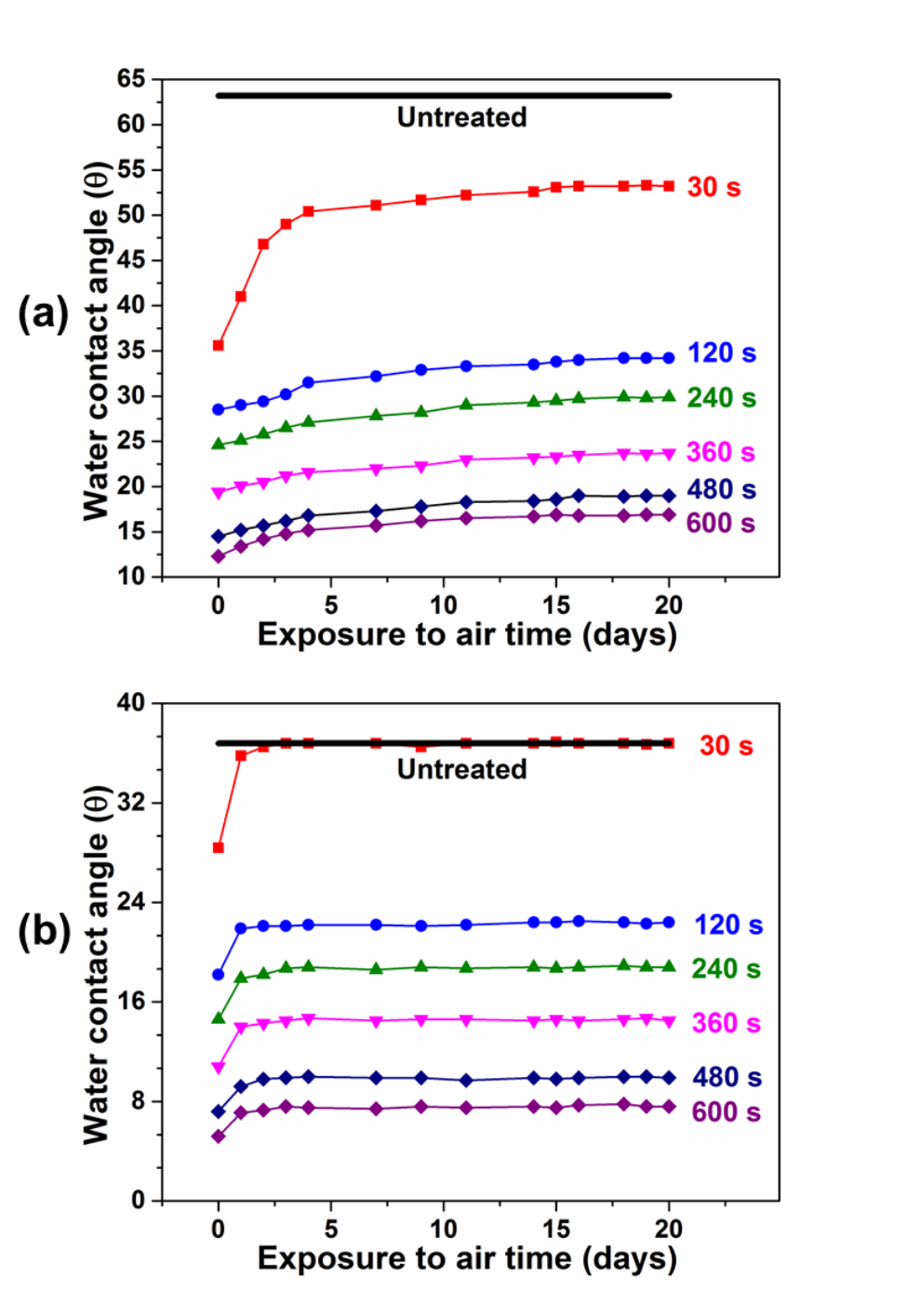

Figure 6-2. Static contact angle measurements of plasma etched samples (oxygen plasma treated for 30 – 600 s) with increasing exposure time to air following plasma exposure, for (a) nylon 6 and (b) regenerated cellulose.

The ageing effects of plasma etched nylon 6 and regenerated cellulose samples in air are presented in Figure 6-2a and b respectively, again through static contact angle measurements. The nylon 6 sample treated for 30 s at 60 W showed a similar hydrophobic recovery to the activated samples treated at

10 W, suggesting that short plasma treatment times have a similar surface-chemical activation effect at multiple different plasma powers, with a negligible increase in surface roughness. This results in a similar ageing effect being observed. Between 120 and 600 s of treatment, the etching of the samples described in 5 had significantly inhibited the hydrophobic recovery of the samples following exposure to air, due to the permanent increase in surface roughness/surface area inflicted by the oxygen plasma, through particle bombardment of the surface. The hydrophobic recovery of these samples was generally slow, with a slight increase in contact angle value appearing to level off after approximately 9 days of ageing in air. This slight hydrophobic recovery was explained by the reorientation and diffusion of the polar functional groups away from the surface. Polymer chains generally have much greater mobility on the material surface than in the bulk material, which gives rise for the surface functionalities to reorient away from the surface.[143] Highly crystalline polymers are better at averting the loss of hydrophilicity through ageing, as the mobility of crystalline polymer chains is restricted due to the highly ordered and packed structures. This can limit rotational and translational motions of the polar groups, hence limiting the ageing of the plasma treated polymers.[73] However, as shown by the XRD and DSC measurements described earlier in Chapter 5.1.6, the nylon 6 samples had low crystallinities of approximately 38 - 39%. The reorientation of polymer chains primarily occurred in the disordered amorphous region of the nylon polymers, due to the increased number microstructural spaces for diffusion of the polar species. A general schematic for this ageing process is displayed in Figure 6-3.

For the regenerated cellulose samples, there appeared to have been an initial increase in contact angle for the etched samples (treated for 120 – 600 s) after 1 day of exposure to air, which was attributed to the release of oxygen from the surface. Again, the drastic increase in surface area from the etching of the oxygen plasma through particle bombardment of the surface structures led to a permanent increase in surface wettability of the cellulose samples, even after ageing in air for 20 days.

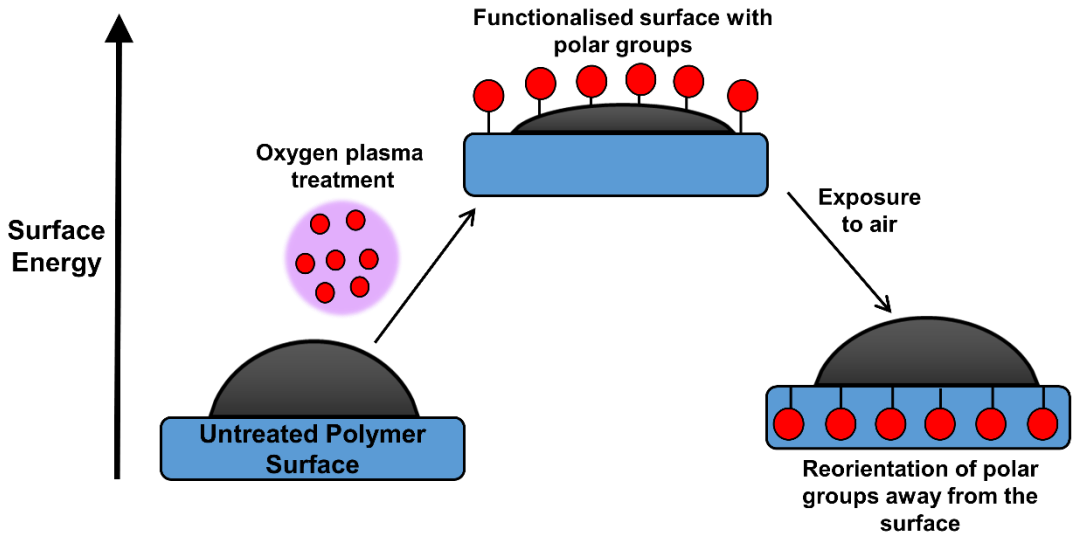

Figure 6-3. General schematic showing the reorientation of newly formed polar groups away from the polymer surface following ageing in air.

6.1.2 Surface chemical changes

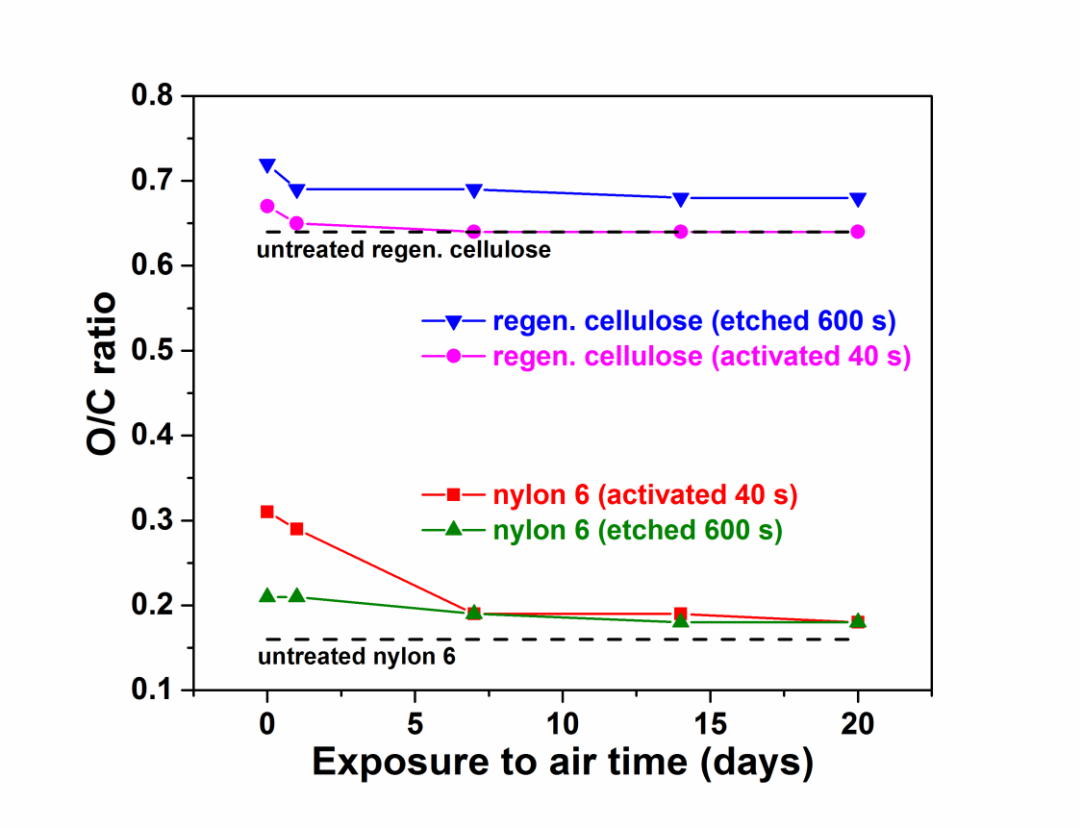

Figure 6-4. O/C ratios of plasma treated nylon 6 and regenerated cellulose samples, determined through XPS measurements.

In order to rationalise the decrease in wettability shown through the aforementioned contact angle measurements, XPS analysis was used to aid in explaining the hydrophobic recoveries of the oxygen plasma treated nylon 6 and regenerated cellulose samples. The obtained O/C ratios for the plasma treated and aged samples are shown in Figure 6-4. The O/C ratios provide further details about the hydrophobic recovery of the oxygen plasma treated samples seen through the gradual increase in contact angle value with increasing ageing time through exposure to air.

For the activated nylon 6 samples, the initial reduction in O/C ratio was slight after 1 day of ageing, from 0.31 to 0.29. This decrease was much greater after 7 days to 0.19, at which point the O/C ratio levelled off, which appeared to mirror the trend of increasing hydrophobic recovery seen through the contact angle measurements. In comparison, the etched nylon samples had a lower O/C ratio than the activated sample after plasma treatment, and saw no obvious ageing after 1 day of exposure to air. However, following 7 days, the O/C ratio had reduced slightly from 0.21 to 0.18, due to the reduction in the number of polar groups present on the surface. It was clear for both samples that the polar groups had been released from the surface, through the thermodynamically favourable reorientation of the high energy polar groups away from the surface. The oxygen content did not drop to its initial untreated at% following 20 days of ageing for either the activated or etched nylon samples, which is likely to be attributed to the small amount of moisture present in air, which could have interacted with some of the polar groups through hydrogen bonding, preventing them from reorienting away from the surface, hence keeping interfacial energy higher than the unmodified surface.

The regenerated cellulose samples had a different trend in ageing to the nylon 6 samples, primarily due to the modification induced by plasma activation being far less substantial than the nylon sheets. The O/C ratio for the activated samples had a slight decrease from 0.67 to 0.65 following 1 day of ageing, before fully reverting to the original untreated surface O/C ratio following 7 days of ageing. This was attributed to the release of absorbed oxygen onto

the surface. For the plasma etched cellulose samples, there was again a slight decrease in O/C ratio following 1 day of ageing in air from 0.72 to 0.69, but the O/C remained fairly constant between 0.69 and 0.68 following 7 - 20 days of ageing. The aged samples did not reach the original cellulose untreated surface O/C ratio. This suggested that the oxygen plasma had induced a permanent increase in the surface oxygen content of the cellulose films through longer, higher powered treatments, due to the increased energy available to the reactive plasma species. It is likely that some of this oxygen had also been absorbed onto the surface, as in the case of the activated cellulose, and was quickly released after 1 day of ageing. Generally, the diffusion/release of oxygen away from the polymer surfaces was the primary factor in the hydrophobic recoveries of the plasma activated and etched samples, with the surface energies decreasing to a more energetically favourable low energy (low polarity) state.

6.1.3 Modes of storage post-treatment

In addition to studying the phenomenon of plasma ageing for the nylon 6 and regenerated cellulose samples in air, the contact angle values were also monitored to compare the ageing effects in air with samples stored in water and under vacuum conditions. These measurements are displayed in the graphs in Figure 6-5. The largest increases in hydrophobicity due to plasma ageing were seen in the samples exposed to air, for the reasons discussed previously in Section 6.1.1. Interestingly, under vacuum conditions both the nylon 6 (Figure 6-5a) and the regenerated cellulose (Figure 6-5b) samples showed very little hydrophobic recovery.

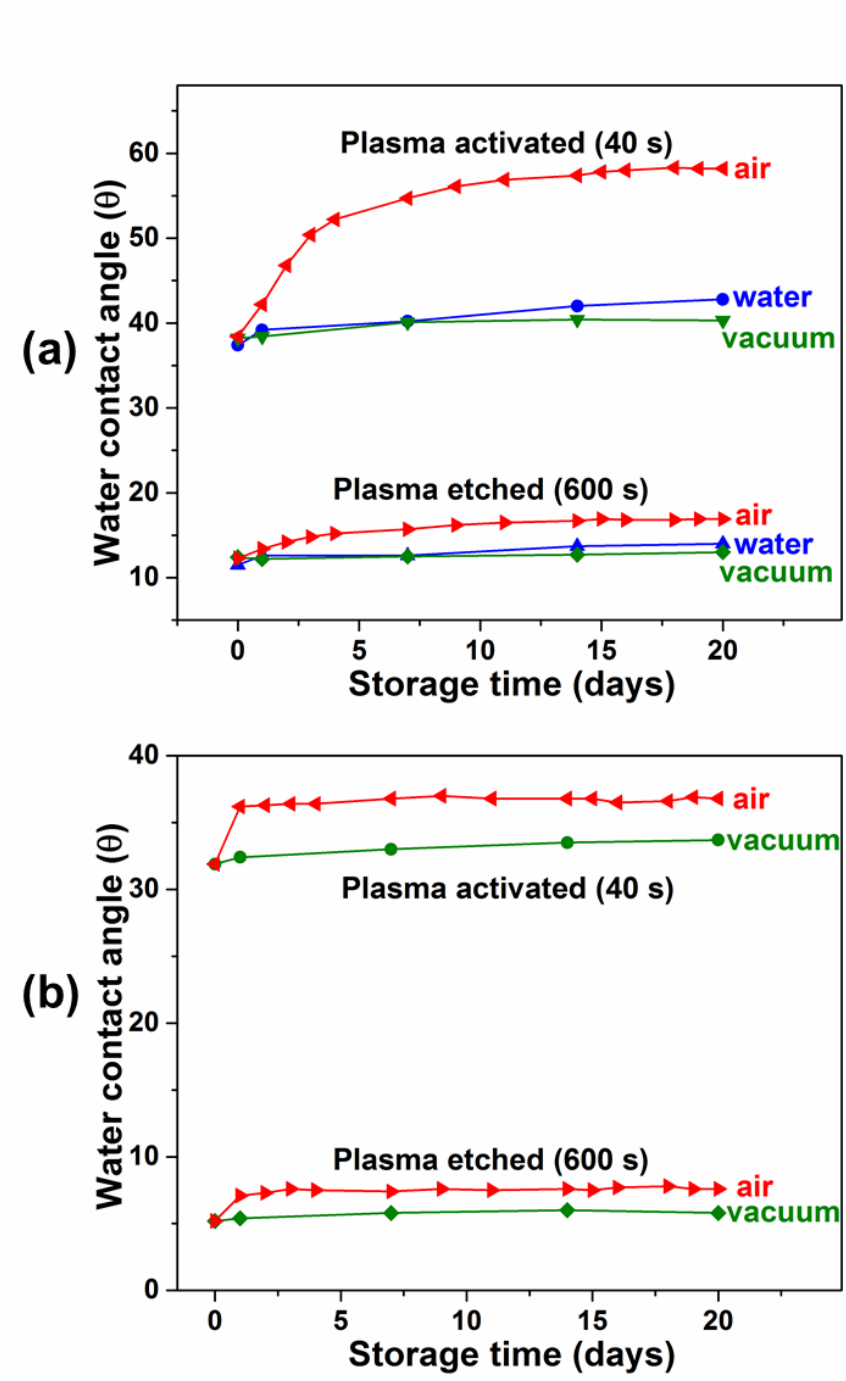

Figure 6-5. Static contact angle measurements of oxygen post-plasma treated samples with increasing storage time under different conditions for (a) nylon 6 and (b) regenerated cellulose.

A major reason for such a lack of ageing observed under vacuum is due to the absence of humidity/moisture and surrounding air. Water vapour in the air has a plasticising effect on the polymer chains, particularly in the amorphous regions of the polymer. Such a plasticising effect enables the polymer chains

to rotate more freely, enabling the polar groups to reorient away from the surface, and revert the surface back into a thermodynamically favourable lower energy state. Therefore, under vacuum conditions, the polymer chains are rigidly held in position, hindering the movements of the polymers.[16]

Similarly, when the nylon 6 samples were stored in water, there was a slight observed ageing effect, but the increase in contact angle value was small. When stored in water, the attached polar groups (through oxygen plasma treatment) of the nylon 6 surfaces interacted with the water molecules through hydrogen bonding; this affinity of the polar groups for the water molecules kept the surface in a higher energy state, forcing the polar groups to stay on the surface. It was evident that when the samples were in a saturated water environment through immersion in water, the polar groups interacted with the water molecules and remained on the surface, but when the samples were exposed to a low concentration of water in the air, the water predominantly had a plasticising effect that encouraged reorientation and diffusion of polar groups away from the surface. The slight hydrophobic recovery observed in the samples stored in water was attributed to the water having a slight plasticising effect, whilst simultaneously interacting with polar groups at the polymer surface. The regenerated cellulose samples were not stored in water due to the high level of swelling induced by immersion in water, which prevented static contact angles from being measured. Generally, similar ageing effects were observed for both nylon 6 and regenerated cellulose samples stored in air and under vacuum, with storage in air showing the most substantial hydrophobic recoveries for oxygen plasma treated polymers. The lack of ageing seen with the samples stored under vacuum meant that the plasma treated samples could be stored under vacuum conditions between being plasma treated and undergoing surface analysis.

6.2 Conclusions

To conclude, the study reported in this chapter has investigated the ageing/hydrophobic recovery of oxygen plasma treated nylon 6 plastic sheets and regenerated cellulose films. Through the use of static contact angle

measurements, the ageing behaviours of the oxygen plasma activated and etched materials have been monitored. The contact angle values for the plasma activated nylon 6 samples showed that the samples underwent an initially rapid hydrophobic recovery after being exposed to air over a period of 5 days that levelled off into a much more gradual recovery up to 20 days. In each case, for the different plasma treatment times, the activated nylon samples did not fully revert to their original surface wettability, owing to the large degree of permanence induced by the attachment of polar groups. Meanwhile, the plasma activated regenerated cellulose samples had a rapid hydrophobic recovery after 1 day that resulted in all of the treated samples at 10 W reverting back to the original untreated surface wettability. For both materials, the plasma etched samples had slight hydrophobic recoveries, but the contact angle values remained substantially lower than the original untreated materials, due to the large permanent increase in surface area caused by the etching of the plasma. XPS analysis was employed to rationalise the ageing of the samples, through monitoring the changes in O/C ratio with increasing exposure time to air. In both the activated and etched samples, nylon 6 and regenerated cellulose had decreasing O/C ratios over time, due to the release/reorientation of oxygen away from the sample surfaces. The largest decrease in O/C ratio was seen in the plasma activated nylon 6 samples. For both nylon 6 and regenerated cellulose, storage under vacuum conditions appeared to hinder the hydrophobic recovery of the samples, through limiting the amount of chain mobility within the polymer structures, preventing the newly attached polar groups from reorienting away from the surface. Storing the nylon 6 samples in water also appeared to substantially limit the extent of hydrophobic recovery, due to intermolecular interactions between the newly attached polar groups and the water molecules. These interactions kept the polar groups at the surface, averting the thermodynamically favourable diffusion of polar groups into the bulk material.

7. Deposition and grafting of siloxane films using low-frequency HMDSO and HMDSO:O_2 plasmas

7.1 Deposition and grafting of siloxane nanofilms to nylon 6 plastic sheets and regenerated cellulose films

In the work recorded in this chapter, the deposition and grafting of functional films to nylon 6 and regenerated cellulose polymer surfaces through plasma-enhanced chemical vapour deposition was studied using the hydrophobic monomer HMDSO as an example. Thus, pure HMDSO vapours and gaseous mixtures of HMDSO:O_2 (1:6 ratio) were dosed into the low-pressure plasma chamber, to study the effects of integrating oxygen gas into the plasma feed on the resultant chemical structures and properties of the deposited plasma-polymerised films. These properties included surface wettability, morphology, film thickness, chemical composition, and homogeneity. Additionally, the effects of plasma power and treatment time were also studied in an attempt to find the optimum conditions to produce films of varying thicknesses and hydrophobicity.

The schematic diagrams shown in Figure 7-1 and Figure 7-2 illuminate the general polymerisation processes and resulting structures of HMDSO and HMDSO:O_2 deposited films formed through plasma enhanced chemical vapour deposition. The polymerisations occur through dissociation of the Si-O bond of the HMDSO monomers, forming $(CH_3)_3$–Si–O· and $(CH_3)_3$–Si· radicals. These radicals abstract hydrogens and attack surface radicals formed on the polymer substrates, depositing siloxane groups that leads to continuous film growth while the plasma is ignited.[66] Electron impact dissociation also leads to abstraction of the methyl groups from the Si-CH_3 bonds of the deposited structures, yielding radicals that assist in the film growth.[61] When oxygen is including into the plasma feed in the HMDSO:O_2 plasma treated samples, the oxygen radicals generated also react with the

monomer fragments and radicals formed on the substrate surface, incorporating additional oxygen-rich groups. The oxygen ions also bombard the surface to give a degree of surface etching.[71] The main features of the HMDSO deposited films were the retention of alkyl groups with a $[(CH_3)_2\text{-Si-O}]_n$ repeating unit, while the HMDSO:O_2 films had an increased number of SiO_2 linkages (highlighted in red and blue), with a small extent of alkyl group retention. For this reason, the HMDSO films had a much greater hydrophobicity than that of the HMDSO:O_2 films.

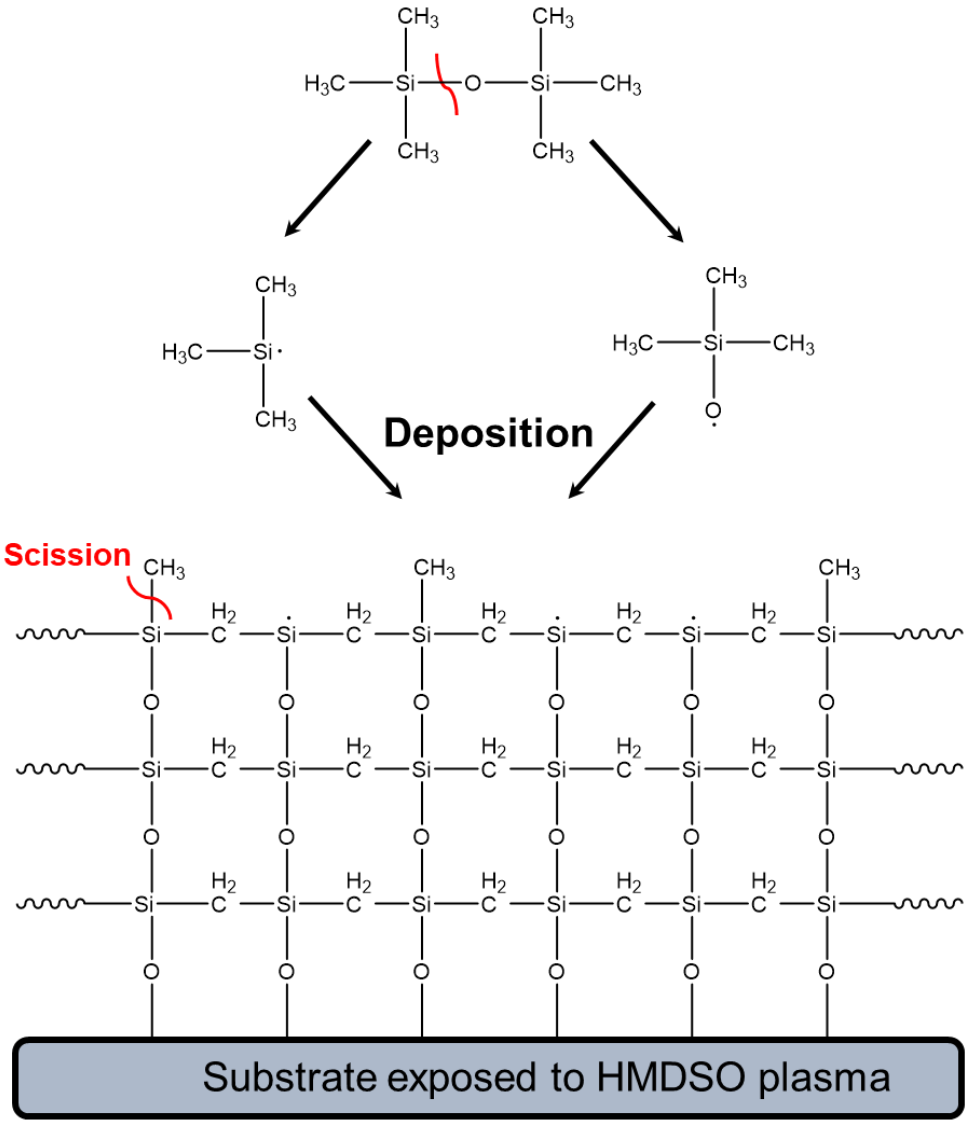

Figure 7-1. General schematic showing the plasma-enhanced chemical vapour deposition of HMDSO polymer films.

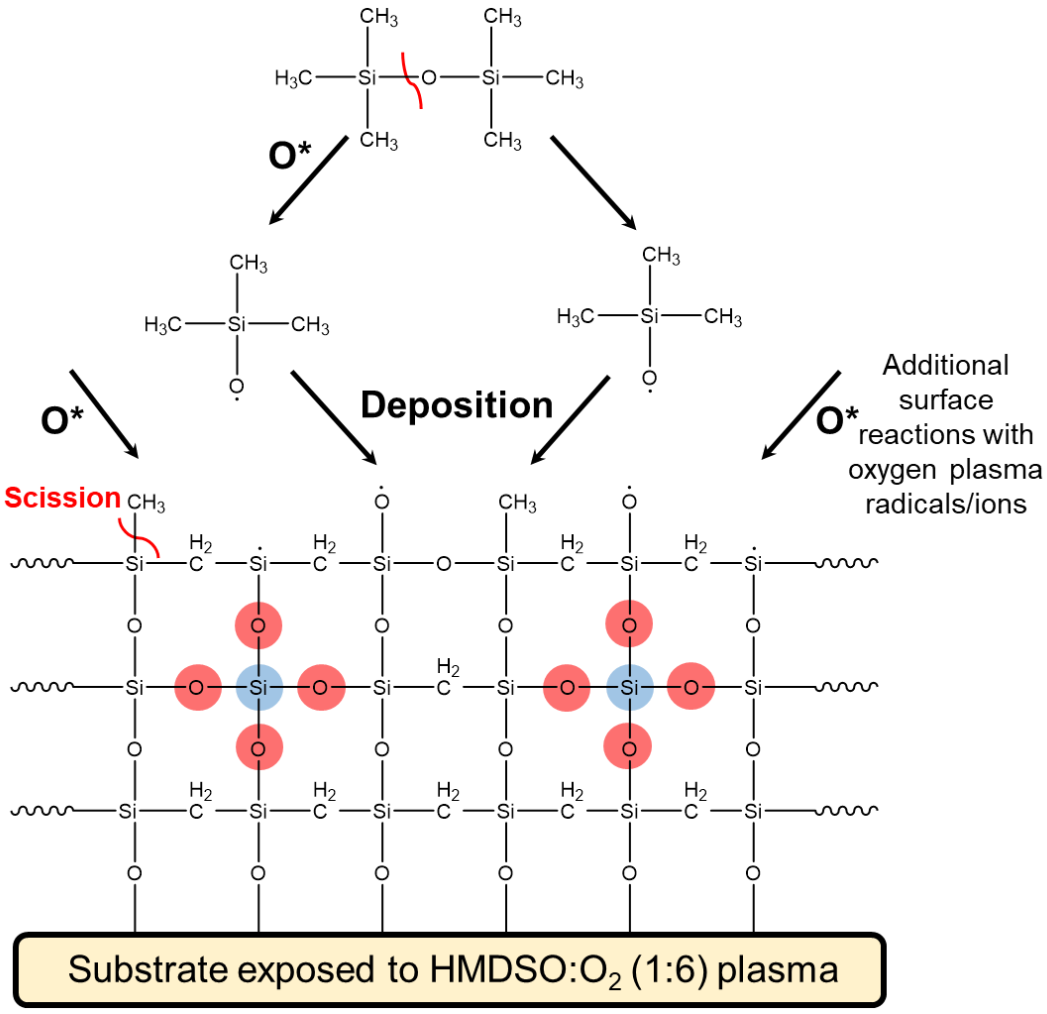

Figure 7-2. General schematic showing the plasma-enhanced chemical vapour deposition of siloxane polymer films using HMDSO:O_2 (1:6) plasma.

7.1.1 Deposition rates of HMDSO and HMDSO:O_2 grafted polymer films

From the graph shown in Figure 7-3, the masses of the deposited HMDSO polymer films (determined through measuring the difference in mass between the untreated and HMDSO plasma treated substrates) that were subsequently grafted onto nylon 6 and regenerated cellulose substrates can be seen as a function of time. The increase in film thickness for both substrates is generally linear, confirming that increasing the exposure time of the nylon 6 substrates to HMDSO plasma increased the thickness of the film, due to the plasma polymerisation process occurring over a longer period, encouraging growth of the films. Increasing the discharge power was also shown to increase mass

deposited. This mass deposited was small at lower powers, but large at higher powers such as 100 W, showing that higher powers provided more energy to the systems, leading to an increased extent of reaction between the plasma species and the substrate surface.

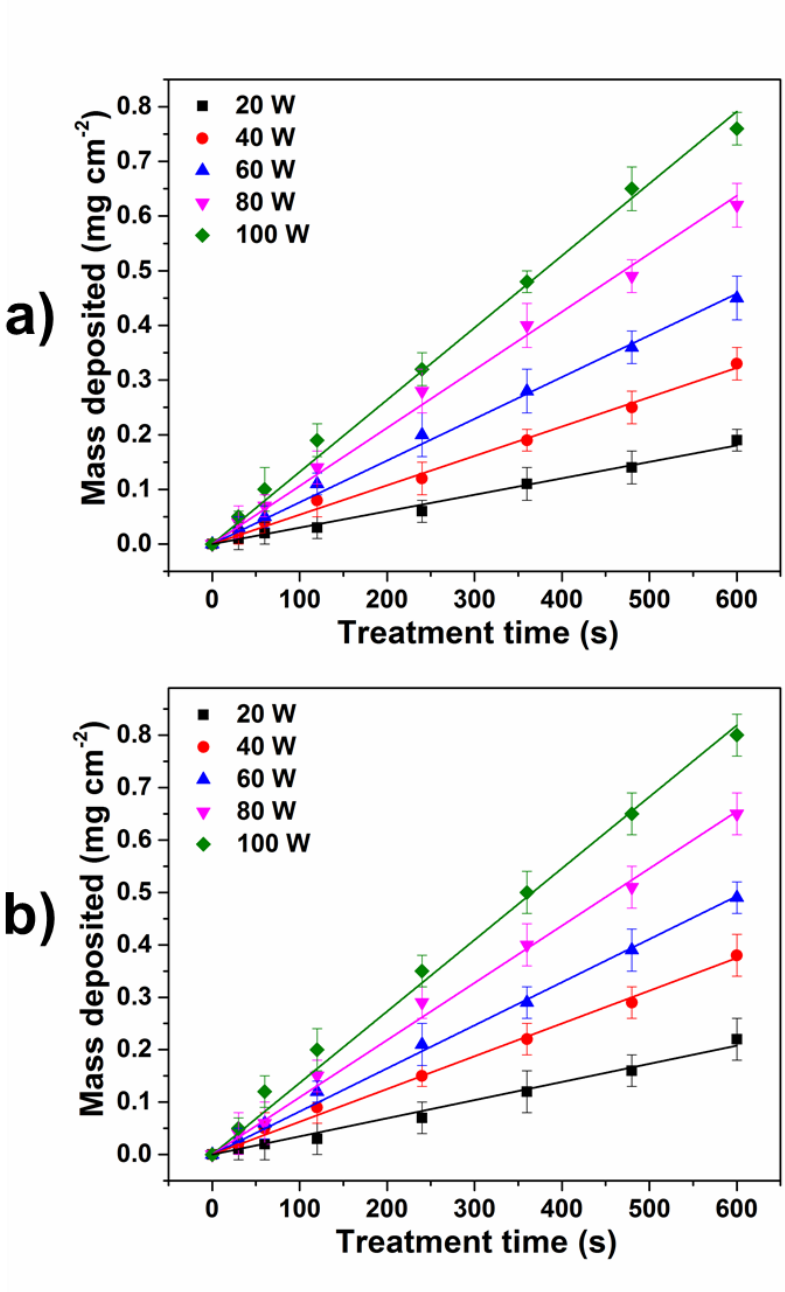

Figure 7-3. The mass of the HMDSO films deposited on a) nylon 6 and b) regenerated cellulose substrates using a pure HMDSO plasma feed with varying discharge power and treatment time.

For both substrates, the level of deposition was nearly identical, suggesting that the chemical structure of the substrate does not significantly affect the

deposition of HMDSO. The observed linearity at all plasma powers can be attributed to the high level of control that can be achieved with low-pressure plasma systems, due to the ability to have a uniform plasma glow with full control over the gas flowing into and out of the chamber. The treatments at 100 W were selected to be studied further and reported in this chapter, to provide a large range of film thicknesses and achieve the thickest siloxane film, of which the properties could be investigated further.

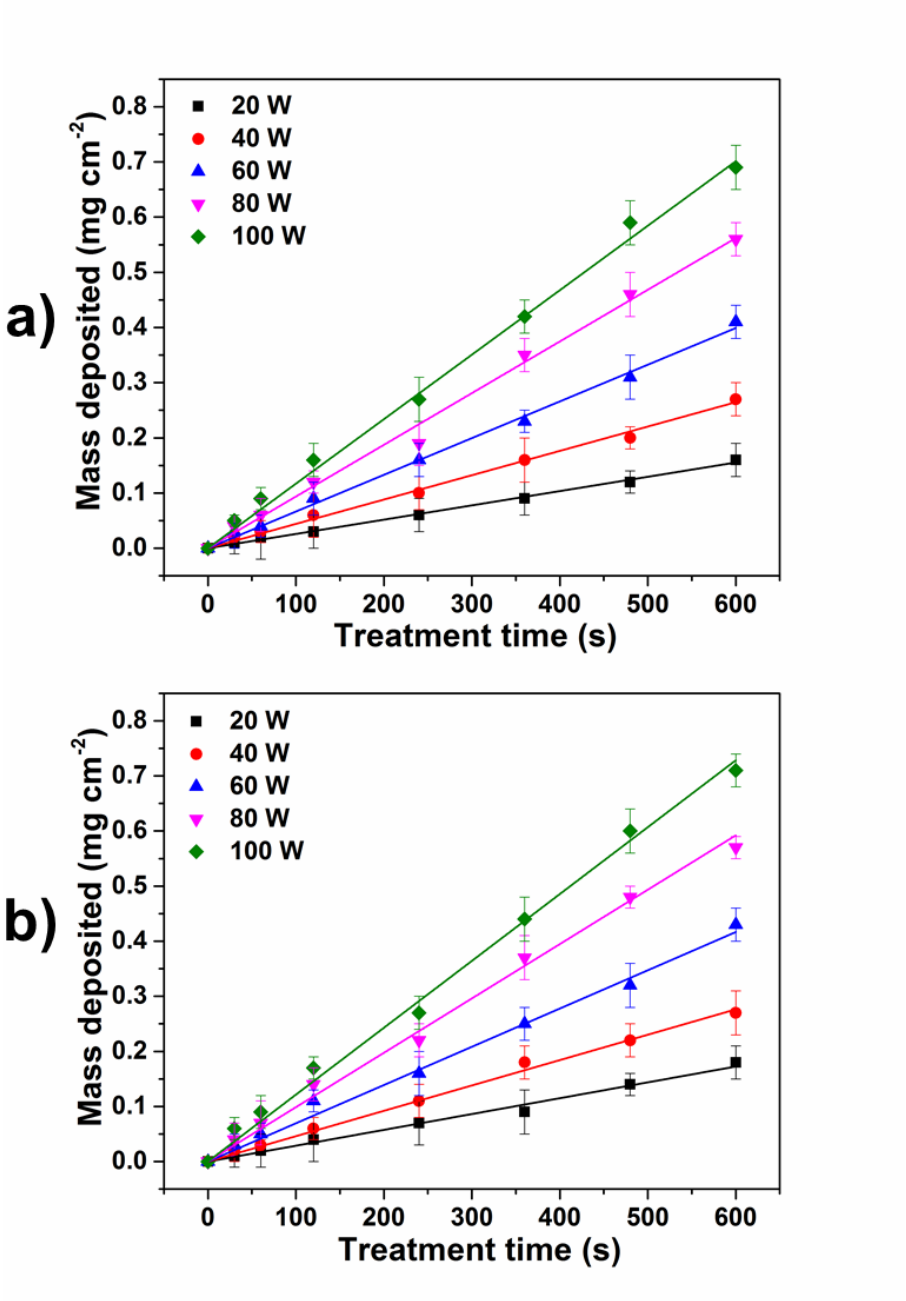

Figure 7-4. The mass of the siloxane films deposited on a) nylon 6 and b) regenerated cellulose substrates using a HMDSO:O_2 (1:6) plasma combination with varying discharge power and treatment time.

The graph showing the mass depositions of HMDSO:O_2 films in Figure 7-4 confirms that the deposition rates of the silicon-based films were similar on regenerated cellulose substrates when compared to the deposition rates on nylon 6 substrates. Again, the same linear features were observed in the gravimetric measurements as the HMDSO vapour deposited films, with a linear increase with increasing treatment time, and an increase with plasma power. The combined results of the mass-gain measurements of the nylon 6 and regenerated cellulose substrates suggested that the deposition of both the HMDSO and HMDSO:O_2 films was largely a substrate-independent process in terms of the masses of thin films produced. It was evident that the plasma conditions govern the deposition-rates of the process rather than the substrate structure.

Table 7-1. Deposition rates of films formed through the use of pure HMDSO vapour and HMDSO:O_2 (1:6) plasmas on nylon 6 and regenerated cellulose substrates.

Plasma Power (W)	**Deposition rate (μg cm^{-2} s^{-1}) (Pure HMDSO Vapour)**		**Deposition rate (μg cm^{-2} s^{-1}) (HMDSO:O_2 (1:6) gas mixture)**	
	Nylon 6	**Regen. cellulose**	**Nylon 6**	**Regen. Cellulose**
20	0.30 ± 0.01	0.35 ± 0.01	0.26 ± 0.01	0.29 ± 0.01
40	0.54 ± 0.01	0.62 ± 0.01	0.44 ± 0.01	0.46 ± 0.01
60	0.76 ± 0.01	0.82 ± 0.01	0.67 ± 0.01	0.69 ± 0.01
80	1.06 ± 0.03	1.09 ± 0.05	0.94 ± 0.02	0.99 ± 0.02
100	1.32 ± 0.02	1.36 ± 0.03	1.17 ± 0.02	1.21 ± 0.02

From the linear plots obtained for the HMDSO and HMDSO:O_2 plasma-deposited films, it was possible to calculate the deposition rates of the processes at different powers; these deposition rates are displayed in Table 7-1. From the data shown in Table 7-1, it was evident that the deposition rates of the HMDSO vapour plasma were larger than the HMDSO:O_2, indicating that

the oxygen species had partially inhibited the polymerisation process, which can be attributed to the oxygen etching the films during the process, removing some of the newly grafted co-polymer layers. For both HMDSO and HMDSO:O_2 plasmas, the deposition rates were marginally higher on regenerated cellulose substrates than nylon 6 samples, which can in part be attributed to the uncertainty in the measurements. Another possibility is that the polar $(CH_3)_3$–Si–O· radicals formed through dissociation of the HMDSO monomers had a slightly higher affinity to the highly polar surfaces of the regenerated cellulose films compared to the less polar nylon 6 surfaces.

7.1.2 Assessment of the hydrophobicity of grafted films

The plots showing the variation in apparent surface energy and static contact angle values with increasing plasma treatment time with pure HMDSO vapour and HMDSO:O_2 (1:6) plasmas on nylon 6 and regenerated cellulose films are provided in Figure 7-5. Generally, in the case of both plasmas, the films deposited resulted in the surface energy decreasing with increasing treatment time, due to the grafting of the hydrophobic siloxane films that increased in thickness with increasing time. Such a decrease was initially slow after 30 s of treatment due to the poor surface coverage of the deposited HMDSO films, but became rapid beyond 120 s of treatment due to the increase in coverage. The surface energy then appeared to decrease further between 120 and 360 s of treatment, before levelling off somewhat between 360 and 600 s. Again, this was attributed to the increase in film thickness that resulted in better surface coverage. Consequently, there was a greater influence from the increased number of non-polar functional groups present within the thicker deposited siloxane films, resulting in an increase in contact angle values.

Generally, between 30 and 360 s of plasma exposure, the nylon 6 and regenerated cellulose samples had substantially different surface energies, due to the aforementioned poor surface coverage of the films, with the native functionalities of the original substrates still having an influence on the surface wettability. However, between 360 and 600 s of plasma treatment, both substrates had similar surface energies, due to the increase in film thickness

and hence full surface coverage of the deposited films that had almost identical properties, irrespective of the substrate.

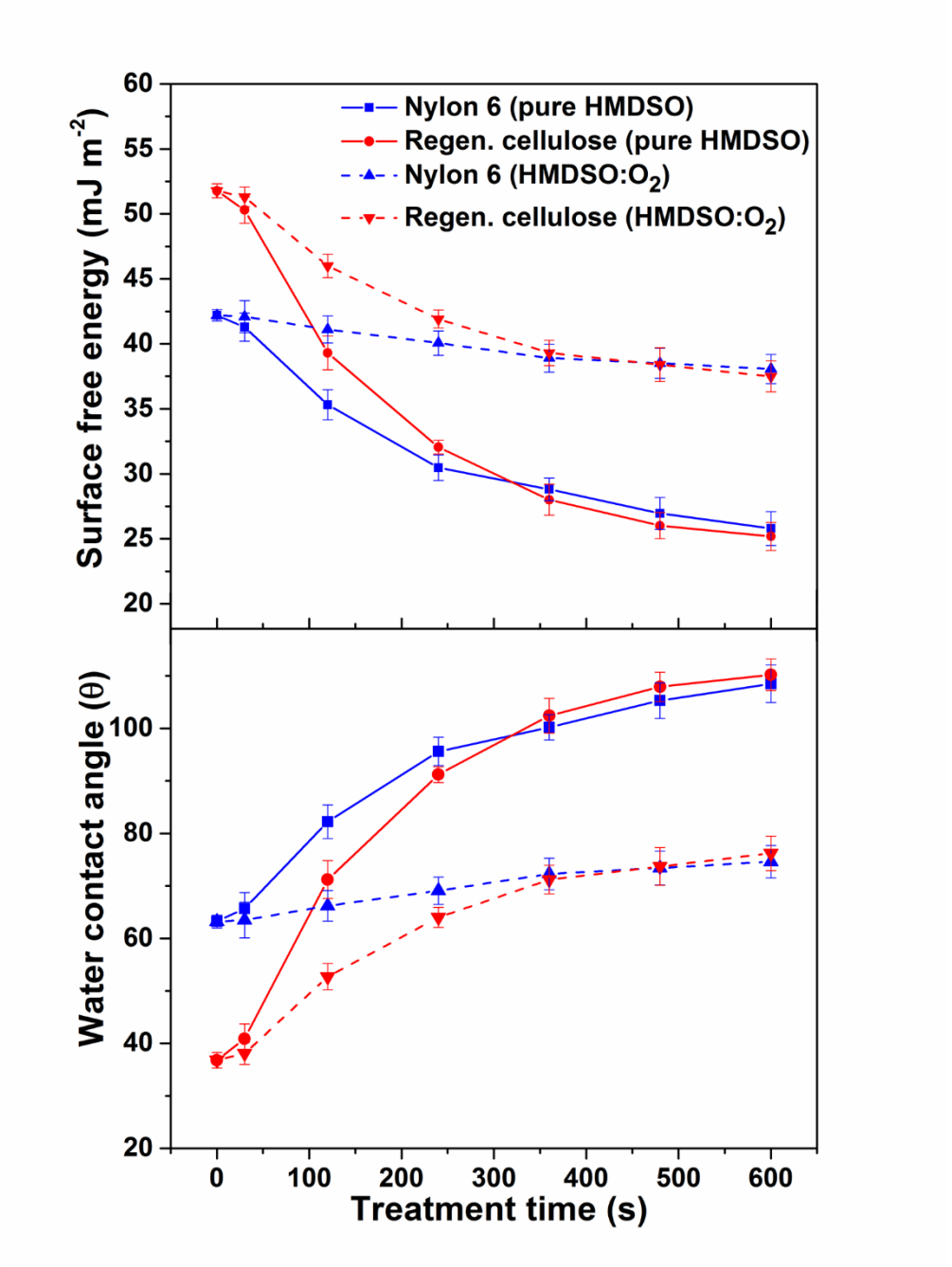

Figure 7-5. The variation in apparent surface free energy and static contact angle of nylon 6 plastic sheets and regenerated cellulose films following the plasma deposition of HMDSO and HMDSO:O_2 films.

The pure HMDSO vapour deposited films exhibited a high degree of hydrophobicity after longer treatment times due to a combination of

morphological and surface-chemical features, with the resultant films being generally smooth with predominantly non-polar structures. These properties are elucidated further in Sections 7.1.3 and 7.1.4 respectively. In comparison, the HMDSO:O_2 films all had substantially lower contact angle values than the pure HMDSO vapour films, due to the oxygen radical species in the plasma feed. The presence of these oxygen plasma species led to the occurrence of oxidative reactions with the HMDSO monomers, resulting in a high degree of fragmentation, with oligomeric species containing polar oxygen groups being deposited on the surfaces of the nylon 6 and regenerated cellulose substrates. Given that contact angles of <90° are classified as hydrophilic, this meant that all of the plasma deposited HMDSO:O_2 films on both substrates were hydrophilic in nature, despite being less wettable than the original nylon 6 and regenerated cellulose surfaces.

7.1.3 Morphology and film thickness

The SEM images in Figure 7-6 show the surface morphologies of nylon 6 plastic sheets and regenerated cellulose films both prior to and following the plasma-enhanced chemical vapour deposition of siloxane polymer films for 600 s. These films were deposited through the use of the pure HMDSO monomer vapour, and a blend of HMDSO:O_2 plasma, in the ratio 1:6. HMDSO is generally an excellent candidate for chemical vapour deposition processes due to its low toxicity, volatility and ability to form polymer films with hydrophobic properties, alongside scratch and corrosion resistance.[144] For both the untreated nylon 6 (Figure 7-6a) and untreated regenerated cellulose (Figure 7-6d), the sample surfaces were generally smooth, with occasional grooves and a number of surface particles (EDX confirmed these particles to be organic matter, with similar EDX spectra to those of the sample surfaces). The untreated regenerated cellulose also had a larger number of scratches compared to the nylon 6 surface. The images displayed in Figure 7-6b and e clearly show that polymer films had been grafted across both substrates, as the initial cracks and scratches present on the untreated surfaces were no longer visible. Some of the surface particles were still visible, but they are

covered in a film that had the appearance of blurring the images slightly, due to the transparent nature of the films formed.

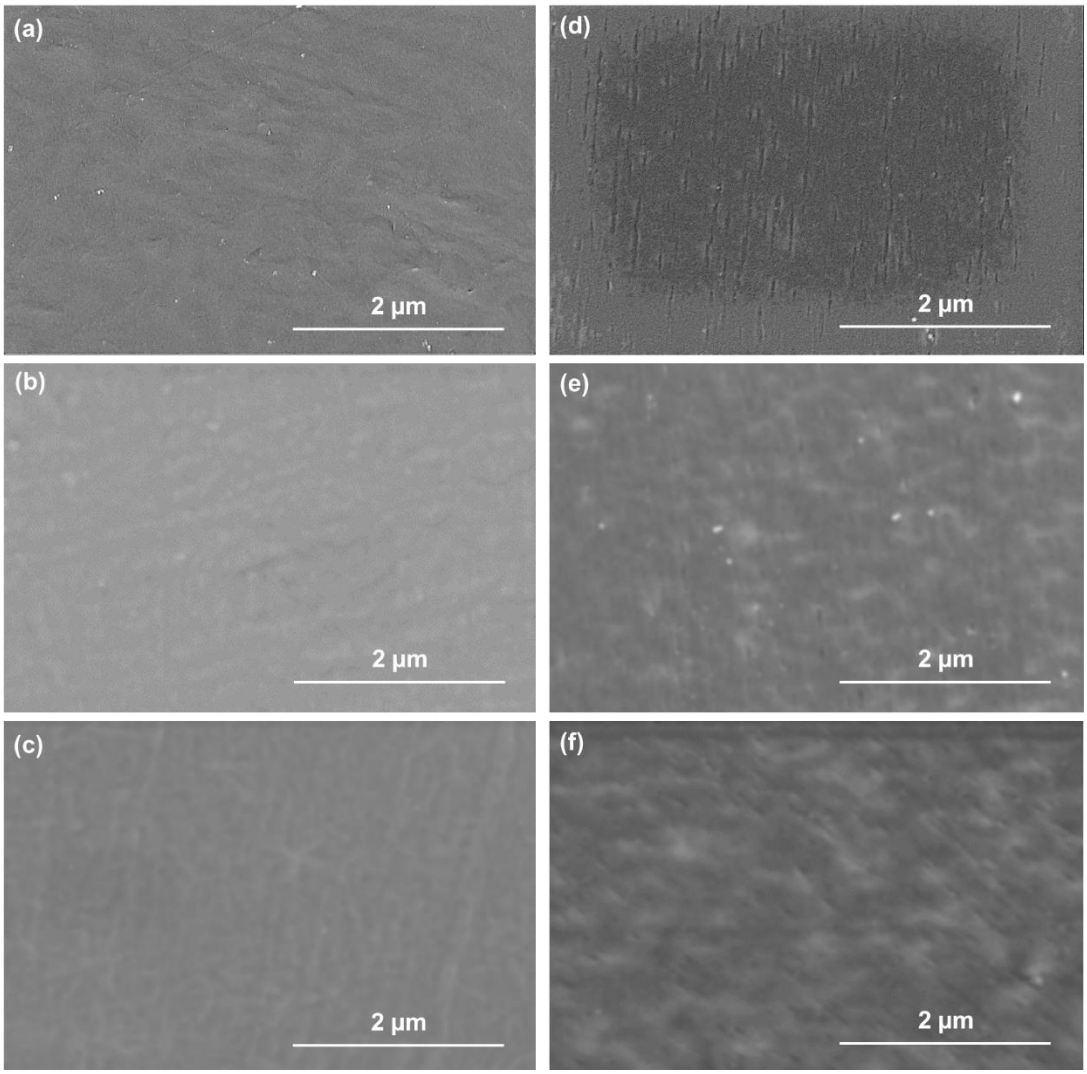

Figure 7-6. SEM images of (a) untreated nylon 6; (b) HMDSO deposited film on the nylon 6 substrate; (c) HMDSO:O_2 deposited film on the nylon 6 substrate; (d) untreated regenerated cellulose; (e) HMDSO deposited film on the regenerated cellulose substrate and (f) HMDSO:O_2 deposited film on the regenerated cellulose substrate.

Figure 7-6c and f show that the films deposited from HMDSO:O_2 plasma had similar features in the SEM images as the pure HMDSO films. Again, there was a clear distortion of the images due to the material surfaces being covered in polymer films. There appeared to be a fairly even coverage of the deposited films across the nylon and cellulose substrates for all of the polymer films investigated.

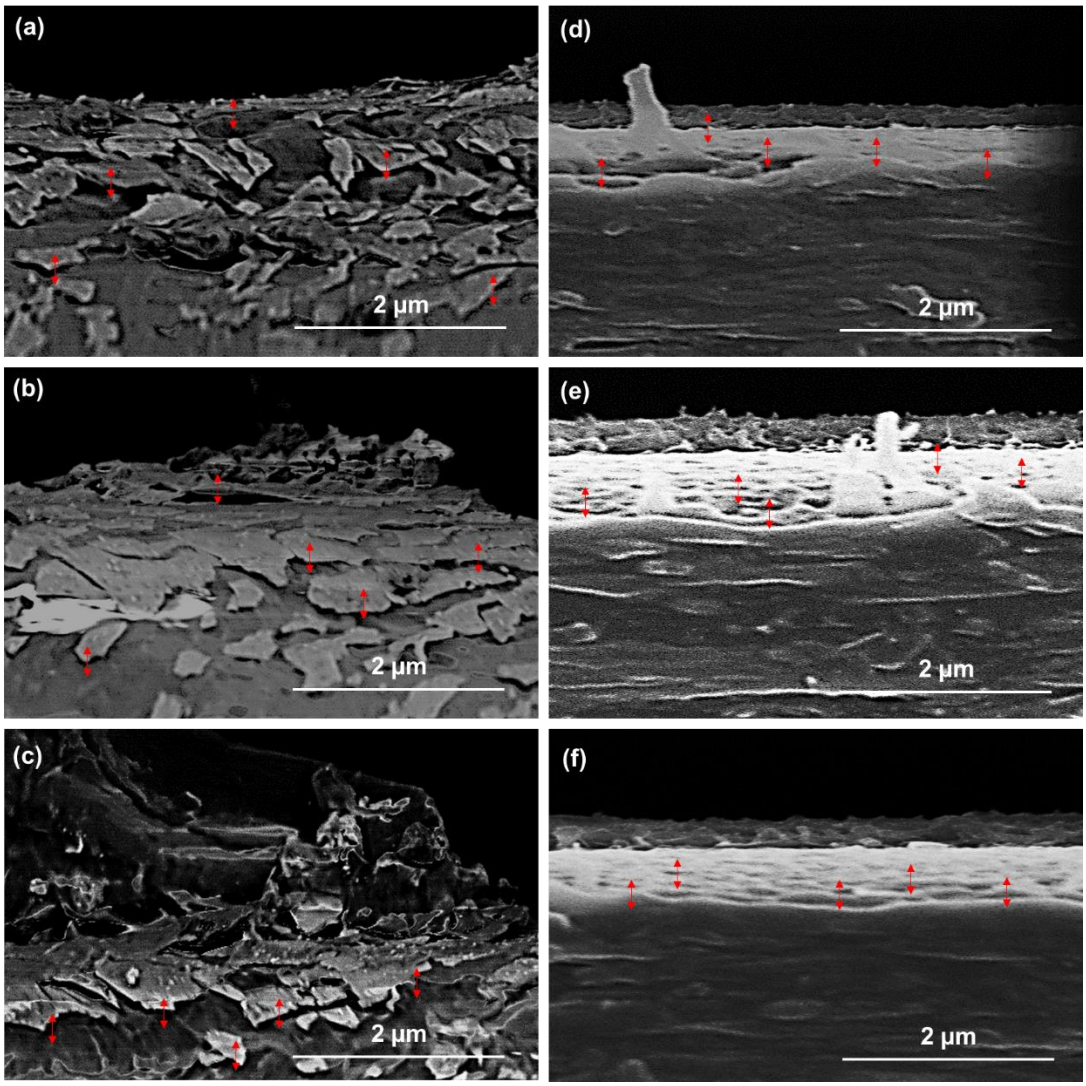

Figure 7-7. SEM images showing cross sections of deposited HMDSO films using pure HMDSO vapour plasma on (a) nylon 6 substrate for 120 s; (b) nylon 6 substrate for 300 s; (c) nylon 6 substrate for 600 s; (d) regenerated cellullose substrate for 120 s; (e) regenerated cellullose substrate for 300 s and (f) regenerated cellullose substrate for 600 s.

The SEM images showing cross sections of resin-embedded nylon 6 and regenerated cellulose samples coated through pure HMDSO vapour plasma enhanced chemical vapour deposition are shown in Figure 7-7. From these images, it was possible to measure the film thicknesses of the resultant deposited films using the computational image processing software, ImageJ. Similarly, the images used to measure the film thicknesses for the HMDSO:O_2 (1:6 ratio) plasma coated samples are shown in Figure 7-8. Some of the films appeared to be broken up into platelets and also had some unknown

disordered structures on the surfaces of the films (such as those seen in the top half of the image in Figure 7-7c); this was attributed to the abrasive polishing and resultant damage of the epoxy resin and resin-embedded materials during the sample preparation, rather than to the plasma-process.

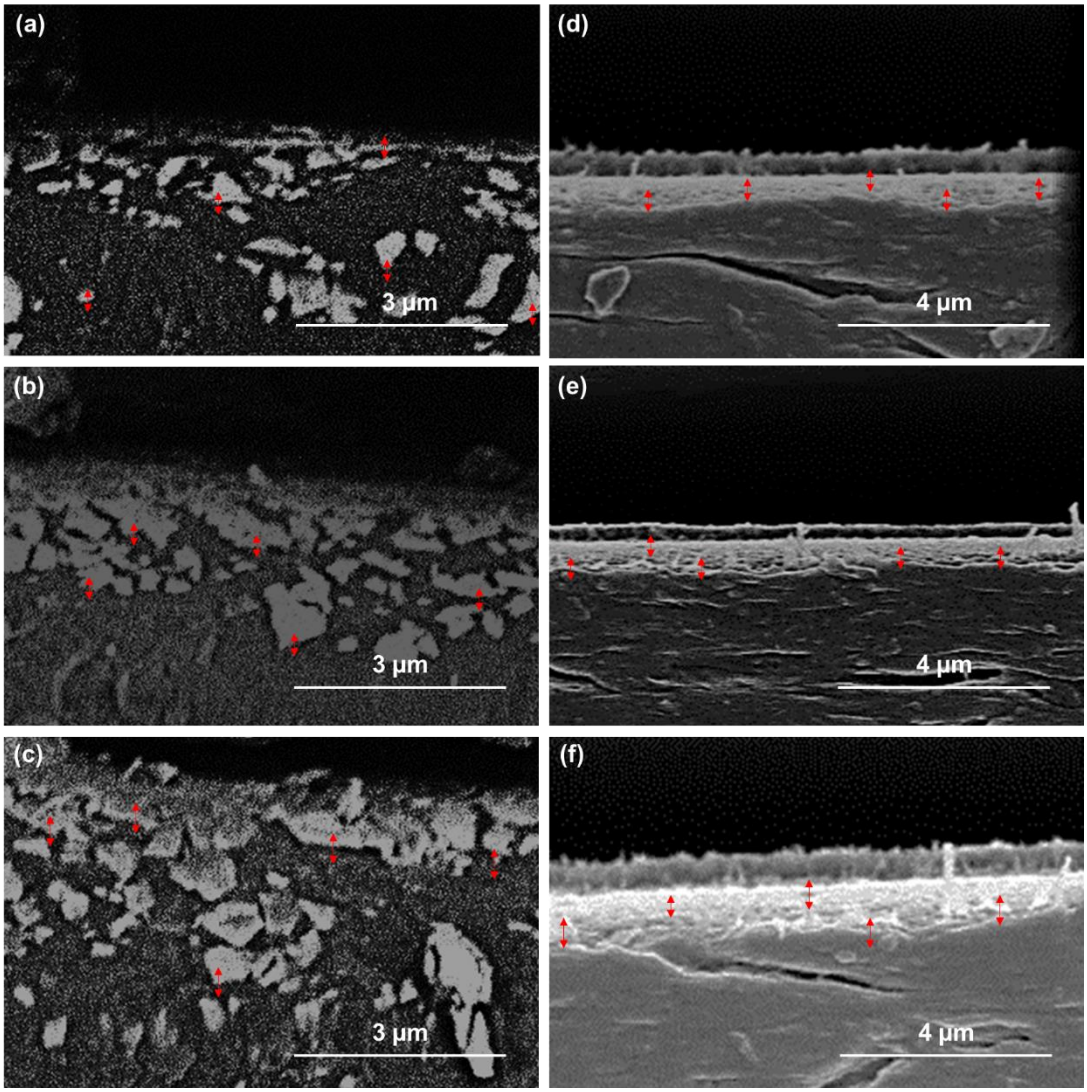

Figure 7-8. SEM images showing cross sections of deposited silicon-based films using a HMDSO:O_2 (1:6 ratio) plasma on (a) nylon 6 substrate for 120 s; (b) nylon 6 substrate for 300 s; (c) nylon 6 substrate for 600 s; (d) regenerated cellullose substrate for 120 s; (e) regenerated cellullose substrate for 300 s and (f) regenerated cellullose substrate for 600 s.

The measured film thicknesses for both sets of plasma-treated samples are summarised in Table 7-2, based on the measurements taken from the cross sectional SEM images in Figure 7-7 and Figure 7-8.

Table 7-2. Measured film thicknesses for HMDSO vapour and HMDSO:O_2 plasma deposited polymer films on nylon 6 and regenerated cellulose substrates for 600 s at 100 W.

Treatment time (s)	Average film thickness (nm) (Pure HMDSO Vapour)		Average film thickness (nm) (HMDSO:O_2 (1:6) gas mixture)	
	Nylon 6	Regen. cellulose	Nylon 6	Regen. Cellulose
120	21.8 ± 10.3	25.6 ± 8.8	27.7 ± 9.5	36.2 ± 12.3
300	36.6 ± 10.9	43.2 ± 9.2	61.9 ± 11.1	66.9 ± 8.9
600	82.9 ± 8.8	90.7 ± 11.7	93.3 ± 9.3	101.6 ± 10.0

As expected, from the increasing mass-depositions of the polymer coatings with increasing plasma exposure time (displayed earlier in Figure 7-3 and Figure 7-4, when discussing relevant gravimetric measurements), the film thicknesses of each of the deposited silicon-based films increased with increasing treatment time for both pure HMDSO plasma and HMDSO:O_2 plasma. Generally, HMDSO:O_2 films appeared to yield thicker films than the pure HMDSO vapour plasma, which can be attributed to the oxygen species producing an abundance of $(CH_3)_3$–Si–O· radicals and forming SiO_2 species through oxidative reactions between the oxygen and HMDSO fragmented molecules. This ultimately resulted in the deposition of thicker quartz-like deposits compared to pure HMDSO films that were flatter and more homogenous. Both plasmas generally deposited slightly thicker films on the regenerated cellulose substrates than on the nylon 6 sheets, although the uncertainty in the measurements were quite high, suggesting the difference in films deposited on the two materials could have been marginal. For both plasmas, the resultant films deposited had greater hydrophobicity with increased film thickness, which is intuitive considering the increased surface coverage, and increased number of available hydrophobic Si-CH_3 groups. This method for determining film thickness does have several limitations, hence resulting in large uncertainties. However, traditional optical measurement techniques for film thicknesses such as ellipsometry failed in this research, due to the nylon 6 substrates producing uninterpretable signals due to excess noise from light scattering, and the regenerated cellulose

substrates being transparent and hence unable to produce discernible signals. This cross-sectional SEM technique had several limitations in accurately measuring the film thickness of the grafted films, such as the polishing sample preparation process damaging the film surfaces, and the SEM electron beam rapidly damaging the polymer materials when being analysed, meaning that images of high quality were difficult to obtain. However, despite these limitations the film thicknesses of the HMDSO-grafted films were still comparable to those found in the literature (that were in the region of approximately 40 - 50 nm),[67] suggesting that this SEM method is effective in measuring the thickness of plasma-deposited polymer nanofilms.

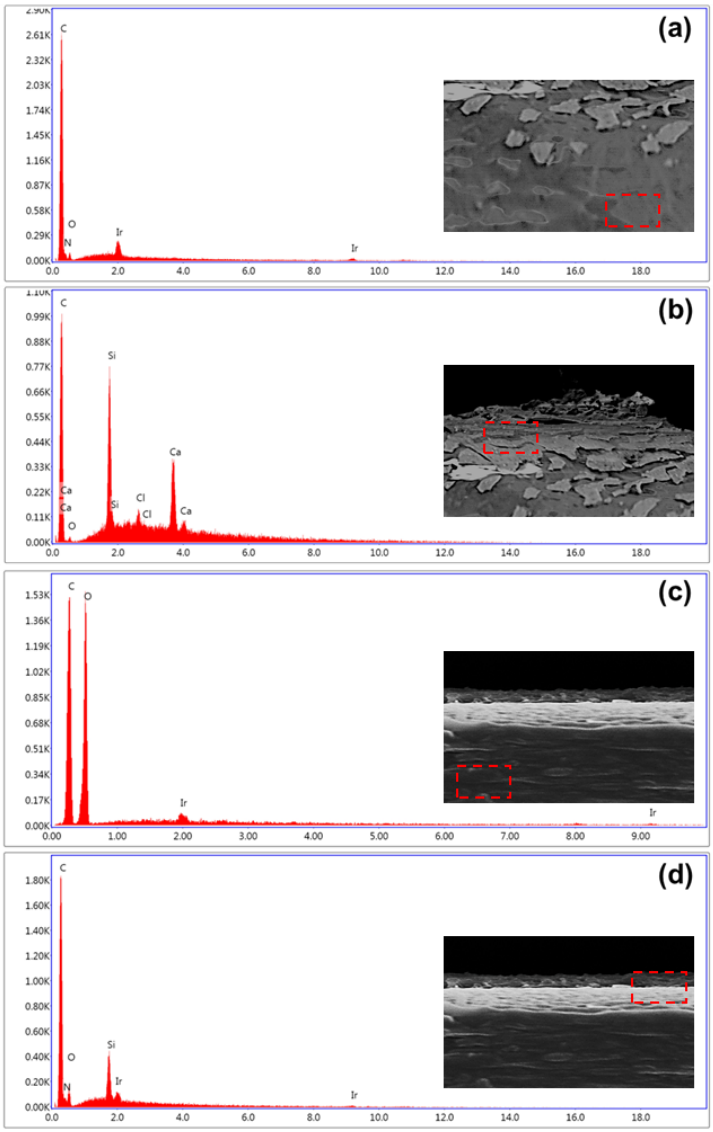

Figure 7-9. EDX spectra showing (a) uncoated area of the nylon 6 surface; (b) HMDSO coated area on the nylon 6 surface; (c) uncoated area of the regenerated cellulose surface and (d) HMDSO coated area of the regenerated cellullose surface.

The EDX spectra shown in Figure 7-9 were used to confirm that the films being measured in the SEM cross sectional images for the pure HMDSO vapour plasma were silicon-based coatings. The presence of the large silicon peak in the Figure 7-9b and d both confirmed that siloxane films had been grafted onto the surfaces of the nylon 6 and regenerated cellulose substrates, with the untreated samples not showing a silicon peak. There also appeared to be a level of contamination in the SEM sample chamber from calcium in some of the samples. The iridium peak was present in all samples due to the samples being coated in iridium prior to imaging.

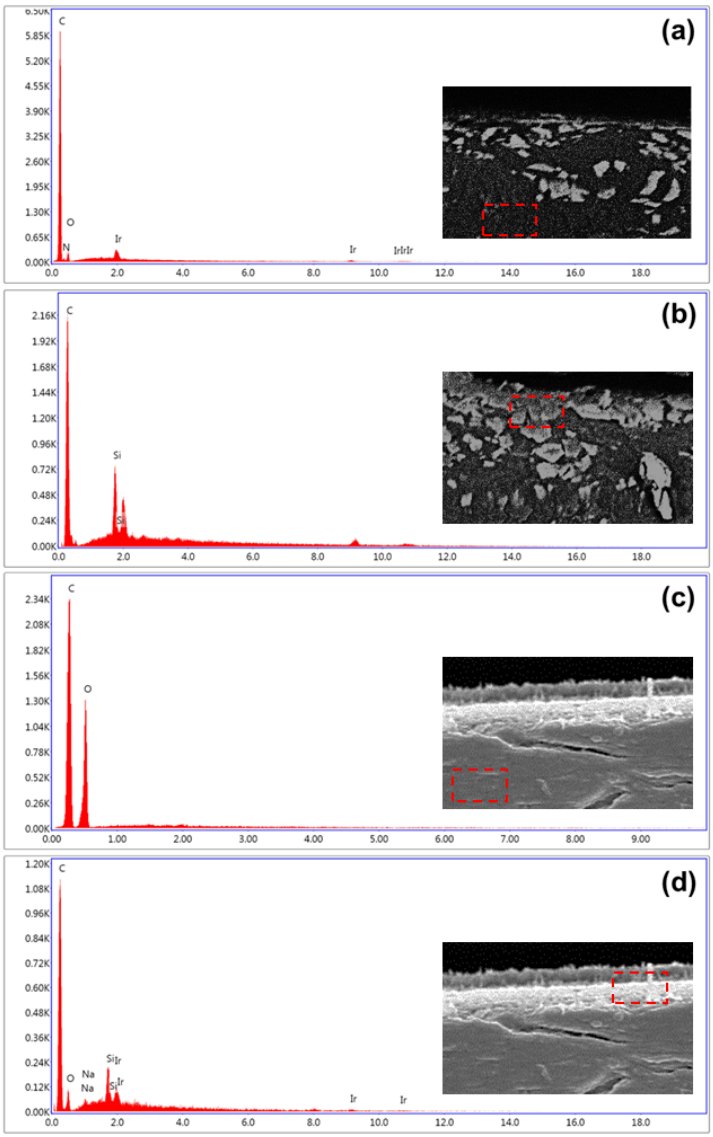

Figure 7-10. EDX spectra showing (a) uncoated area of the nylon 6 surface; (b) HMDSO:O_2 coated area on the nylon 6 surface; (c) uncoated area of the regenerated cellulose surface and (d) HMDSO:O_2 coated area of the regenerated cellullose surface.

Similarly, the EDX spectra displayed in Figure 7-10 showed that the films being measured for the HMDSO:O_2 plasma deposited films using cross-sectional SEM imaging were also silicon-based coatings, due to the presence of silicon peaks in Figure 7-10b and d. These silicon peaks were not present in the uncoated areas of the nylon and cellulose surfaces. It was expected that these coatings would also have a high oxygen content due to the O_2 component of the gaseous plasma mixture, however there was no major oxygen peak from the films. This was due to the deposited polymer films being sensitive to beam damage from the EDX analysis, hence limiting the reliability of the technique. For this reason EDX was used to provide a qualitative confirmation for the presence of the silicon-based films in this research, rather than as an absolute tool for quantitative analysis.

From the AFM images displayed in Figure 7-11, the morphologies of the HMDSO and HMDSO:O_2 films were able to be investigated further, due to the limited information that was able to be extracted from the SEMs, owing to the transparency and nanoscale properties of the films. From Figure 7-11b, it was evident that pure HMDSO vapour plasmas deposited smooth coatings, with platelet-like structures that decreased the roughness parameters Ra (roughness average) and Rq (root mean square roughness) from 6.07 ± 0.81 nm and 7.47 ± 0.92 nm (untreated nylon 6 surface) to 5.77 ± 0.69 nm and 6.95 ± 0.80 nm respectively. The films were also homogenous, which can be attributed to the uniform glow of the low-frequency, low-pressure plasma. The combination of having flat, smooth surfaces and hydrophobic Si-CH_3 branches explains the hydrophobic properties of the films seen through the contact angle measurements, with low surface energies. The HMDSO did not appear to decompose in the gas phase, meaning that it formed smooth polydimethylsiloxane (PDMS)-like coatings, with structural retention of the HMDSO monomer, rather than a series of separately distributed deposits of lower molecular weight units. This is supported further by the XPS and SIMS data discussed in the following section (Section 7.1.4).

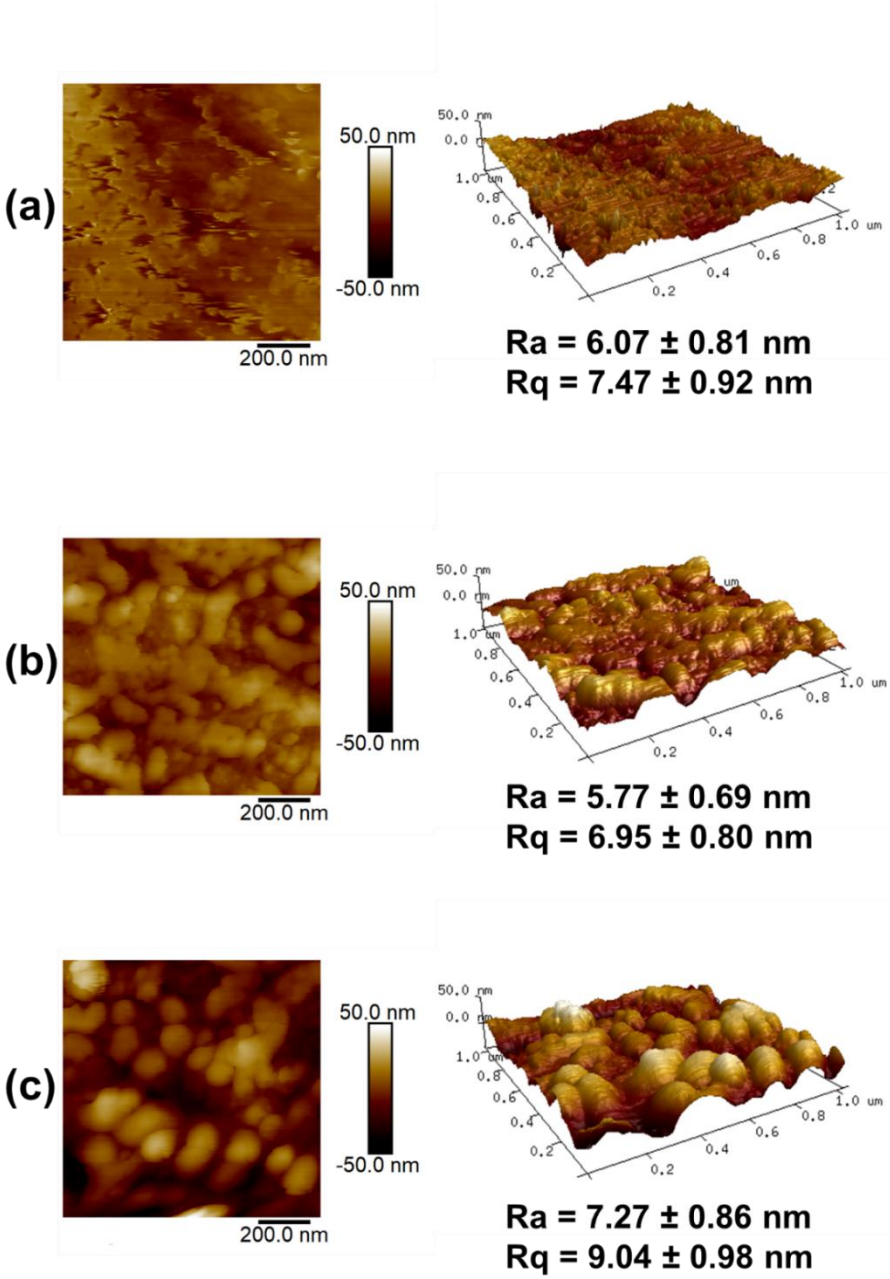

Figure 7-11. AFM images of: (a) untreated nylon 6; (b) coating deposited with pure HMDSO plasma on nylon 6 for 600 s at 100 W and (c) coating deposited with HMDSO:O_2 (1:6 ratio) plasma on nylon 6 for 600 s at 100 W.

When oxygen was introduced into the gas feed, the resultant HMDSO:O_2 films that were grafted onto the surface of the nylon substrates were quartz-like deposits, due to the reactive oxygen plasma radical species being able to react with the HMDSO moieties, leading to increasing monomer fragmentation, and the formation of SiO_2 species/linkages. These SiO_2

species provided more inorganic character than the pure HMDSO polymer films. These deposits appeared like evenly distributed globules on the surface, rather than a smooth continuous film. These had the overall effect of increasing the surface roughness parameters, with Ra and Rq increasing to 7.27 ± 0.86 nm and 9.04 ± 0.98 nm respectively, due to the increase in the range of height distribution of the coatings compared to the relatively flat untreated surface and pure HMDSO polymerised coatings. In addition to altering the surface composition of the films deposited, it is also likely that the presence of oxygen in the gaseous plasma feed led to a degree of etching of the deposited film, hence accounting for the large differences in height seen in the coatings.

7.1.4 Surface chemical analysis and mapping

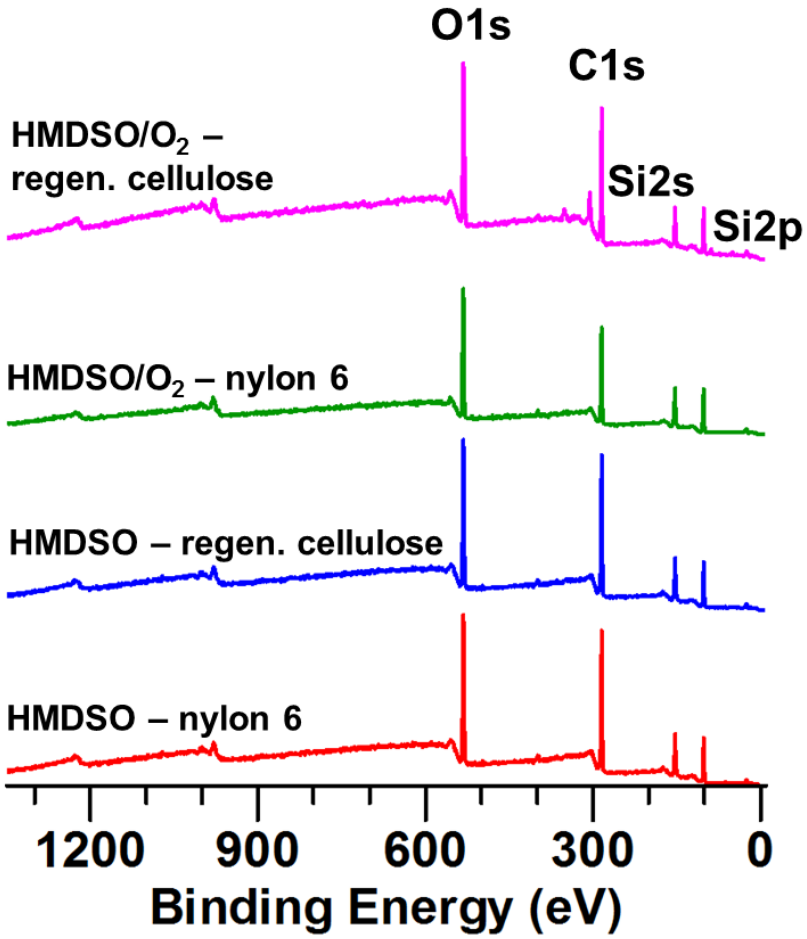

Figure 7-12. XPS survey spectra of plasma-enhanced chemical vapour deposited HMDSO and HMDSO:O_2 films on nylon 6 and regenerated cellulose surfaces.

Figure 7-12 shows the XPS survey spectra for the HMDSO and HMDSO:O_2 (1:6) films deposited on both nylon 6 plastic sheet and regenerated cellulose film substrates. In each case, the elements detected were as expected, with the films comprising silicon, carbon and oxygen. There were also some residual peaks for nitrogen, calcium and magnesium, from general contamination inside the XPS sample chamber. The HMDSO:O_2 deposited films generally had larger O/C ratios than the pure HMDSO films, which was anticipated given the inclusion of oxygen into the plasma species. The detailed elemental compositions of each of the deposited films with their respective O/C and O/Si ratios are summarised in Table 7-3. Multiple point analysis was used to determine the homogeneity of the deposited films, with each sample being measured at three different areas on the surfaces of the samples.

Multiple point XPS analysis was used to show the “spread” of chemical change induced by the plasma through grafting of silicon-based films onto the nylon 6 and regenerated cellulose surfaces. There were trace calcium, magnesium and nitrogen contaminants found in all of the samples; the quantities of these elements were not reported in Table 7-3 due to their negligible quantities (< 1%). HMDSO:O_2 films had higher O/C ratios than the pure HMDSO vapour plasma deposited films, which was intuitive due to the oxygen species incorporating polar functionalities into the surface structures of the deposited films. The higher oxygen content also appeared to result in increased fragmentation of the HMDSO monomers, due to the oxygen plasma species having the ability to bombard the silicon-based molecules, which accounts for the slight etching seen in the resultant films.

Table 7-3. Elemental composition from the XPS data obtained for the deposited HMDSO and HMDSO:O_2 films on nylon 6 and regenerated cellulose substrates for 600 s at 100 W.

		Elemental composition (%)				
	Treatment	**Carbon**	**Oxygen**	**Silicon**	**O/C ratio**	**O/Si ratio**
Nylon 6	**HMDSO**	57.6	19.5	21.3	0.34	0.92
	HMDSO	57.3	18.2	24.0	0.32	0.76
	HMDSO	59.1	16.9	23.2	0.29	0.73
	HMDSO (mean)	**58.0±0.8**	**18.2±1.1**	**22.8±1.1**	**0.31±0.02**	**0.80±0.08**
	HMDSO:O_2	53.5	28.5	18.6	0.53	1.53
	HMDSO:O_2	50.2	27.4	20.0	0.55	1.37
	HMDSO:O_2	49.4	29.2	19.1	0.59	1.53
	HMDSO:O_2 (mean)	**51.0±1.8**	**28.4±0.7**	**19.2±0.6**	**0.56±0.03**	**1.47±0.08**
Regenerated Cellulose	**HMDSO**	58.4	20.4	20.7	0.35	0.99
	HMDSO	60.4	19.2	20.1	0.32	0.96
	HMDSO	58.0	21.7	19.8	0.37	1.10
	HMDSO (mean)	**58.9±1.0**	**20.4±1.0**	**20.2±0.4**	**0.35±0.02**	**1.01±0.06**
	HMDSO:O_2	50.4	30.2	18.8	0.57	1.61
	HMDSO:O_2	48.0	34.3	17.2	0.69	1.99
	HMDSO:O_2	49.7	30.1	19.8	0.60	1.52
	HMDSO:O_2 (mean)	**49.4±1.0**	**31.5±2.0**	**18.6±1.1**	**0.64±0.05**	**1.70±0.21**

Both the HMDSO and HMDSO:O_2 deposited films had a similar silicon at%, confirming that both films had siloxane structures. The HMDSO films generally all had O/Si values close to 1.00, while the O/Si values of HMDSO:O_2 films varied between 1.37 and 1.99. This suggests that the increased fragmentation caused by the introduction of oxygen gas into the plasma feed had increased the number of different polymeric species deposited on the surface, likely

forming a range of lower molecular weight species than the pure HMDSO plasma, with SiO and SiO_2 characteristics.

In general, the multiple point analysis for the HMDSO films suggested that the structures of the films were similar across both nylon 6 and regenerated cellulose surfaces, resulting in evenly distributed homogenous films. The HMDSO:O_2 films deposited on nylon 6 substrates appeared to have similar at% concentrations, with the films deposited on regenerated cellulose substrates having a larger variation, and hence greater uncertainty in the mean value. The increased oxygen incorporated into the deposited HMDSO:O_2 films accounted for the increased hydrophilic character seen in these films compared to the pure HMDSO films. The increased carbon content in the pure HMDSO films deposited on both substrates accounted for the hydrophobic properties of the films, and was indicative of an increased surface concentration of non-polar Si-CH_3 branches, lowering the surface energies of the films.

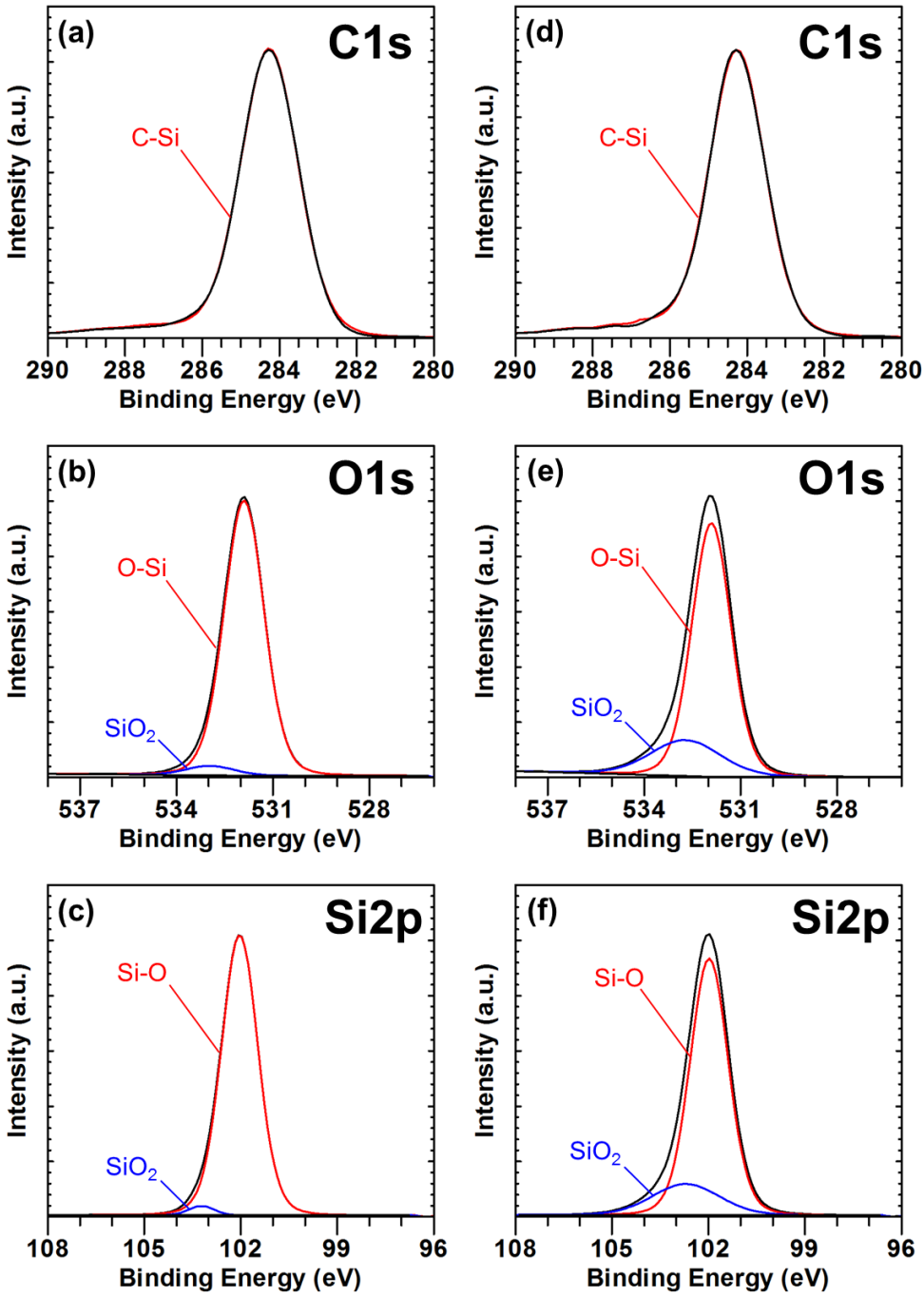

Figure 7-13. High resolution XPS spectra of plasma treated nylon 6 for 600 s at 100 W showing: (a) C1s peak of pure HMDSO deposited film; (b) O1s peak of pure HMDSO deposited film; (c) Si2p peak of pure HMDSO deposited film; (d) C1s peak of HMDSO:O_2 deposited film; (e) O1s peak of HMDSO:O_2 deposited film and (f) Si2p peak of HMDSO:O_2 deposited film.

Deconvolution of the high resolution XPS spectra for the C1s, O1s, and Si2p peaks revealed further details about the surface structures of the polymer films

formed. The pure HMDSO C1s spectra (Figure 7-13a) confirmed the structure of the films to be similar to PDMS, primarily composed of Si-CH_3 branches, with a general $[(CH_3)_2\text{-Si-O}]_n$ repeating unit. This explains the hydrophobic nature of the films, through the presence of the non-polar methyl groups. The absence of oxygen in the pure HMDSO plasma gas feed prevented the HMDSO species from reacting with the highly reactive oxygen radical species, leading to increased retention of the original monomer structures when polymerised onto the surfaces of the nylon 6 polymers. However, a small amount of SiO_2 was detected in the O1s and Si2p peaks (Figure 7-13b and c, indicating a degree of fragmentation and loss of the original HMDSO structure. However, there was a higher concentration of SiO groups than SiO_2.

Although the spectra for the HMDSO:O_2 films were similar to those formed from the pure HMDSO plasma, the most notable differences were seen in the O1s and Si2p spectra displayed in Figure 7-13e and f respectively. Both peaks had a higher concentration of SiO_2 groups/linkages formed in the resultant plasma-deposited films, due to the reactivity of the oxygen plasma in attaching polar moieties into the HMDSO film structure, consequently increasing the extent of fragmentation in the films, and ultimately resulting a large number of SiO_2 structures. This aided in rationalising both the hydrophilic nature of the siloxane films formed from the HMDSO:O_2 plasma feed, and the quartz like morphologies seen from the AFM data.

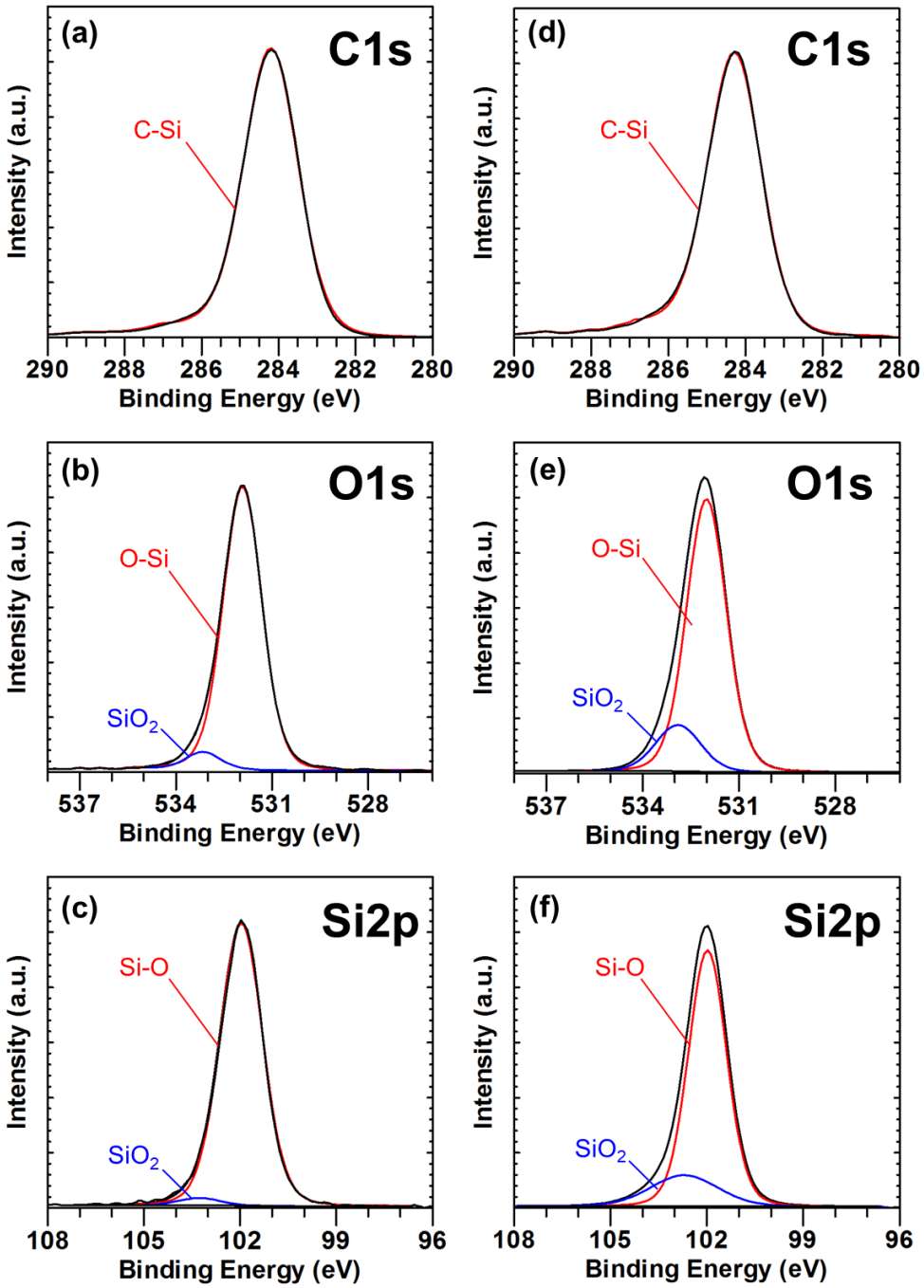

Figure 7-14. High resolution XPS spectra of plasma treated regenerated cellulose for 600 s at 100 W showing: (a) C1s peak of pure HMDSO deposited film; (b) O1s peak of pure HMDSO deposited film; (c) Si2p peak of pure HMDSO deposited film; (d) C1s peak of HMDSO:O_2 deposited film; (e) O1s peak of HMDSO:O_2 deposited film and (f) Si2p peak of HMDSO:O_2 deposited film.

From the deconvoluted high resolution C1s, O1s and Si2p spectra of the deposited HMDSO and HMDSO:O_2 films on regenerated cellulose substrates shown in Figure 7-14, it was apparent that the surface chemistry of the films

was almost identical to those formed on nylon 6 substrates. The spectra confirmed that the deposited pure HMDSO and HMDSO:O_2 films on regenerated cellulose substrates produced similar surface-chemical features, again with the HMDSO:O_2 films having an increased concentration of SiO_2 species present in the O1s and Si2p spectra. The similarities in XPS spectra between the films deposited on both nylon 6 and regenerated cellulose substrates suggest that plasma-enhanced chemical vapour deposition was a substrate-independent process, and the resultant siloxane polymer films deposited from HMDSO-based plasmas were nearly identical on aliphatic nylon 6 polymers and cyclic regenerated cellulose structures.

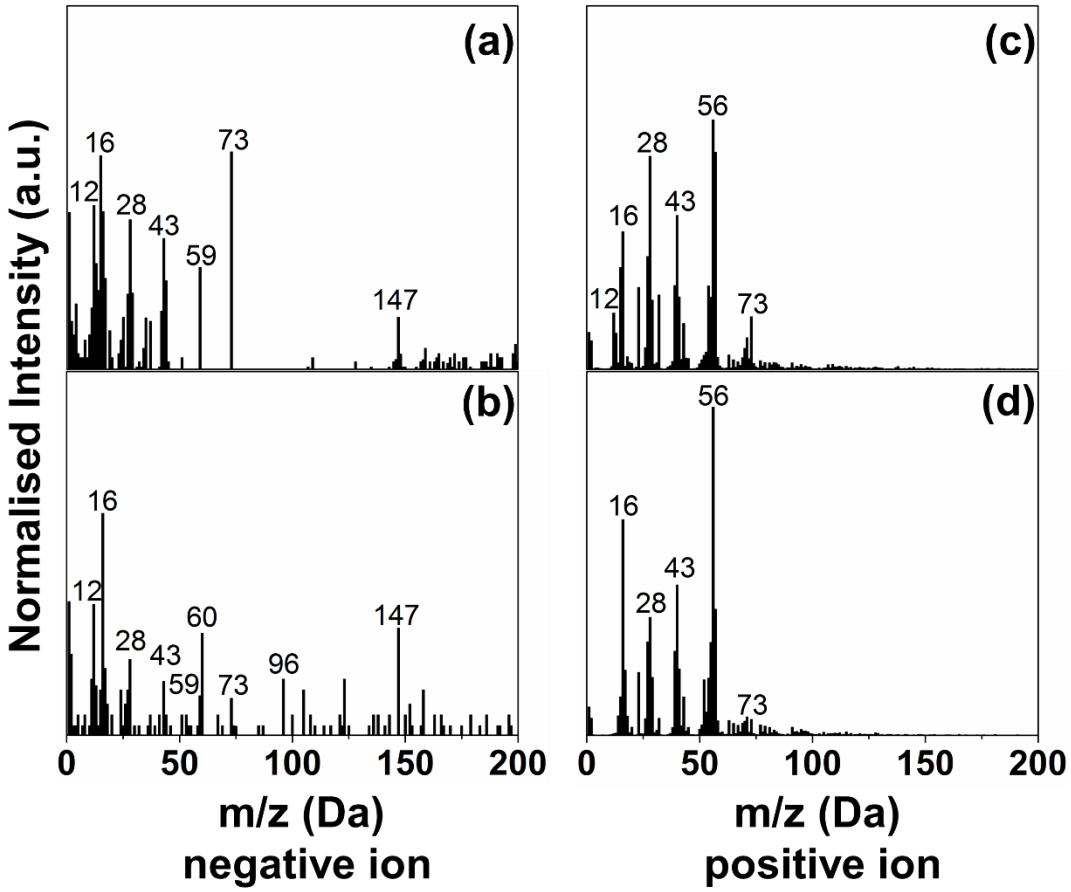

Figure 7-15. SIMS negative ion spectrum of plasma treated nylon 6 for 600 s at 100 W for (a) pure HMDSO deposited film and (b) HMDSO:O_2 deposited film. SIMS positive ion spectrum for (c) pure HMDSO deposited film and (d) HMDSO:O_2 deposited film.

The negative and positive ion SSIMS spectra for films deposited from pure HMDSO vapour and HMDSO:O_2 (1:6) plasmas are presented in Figure 7-15. The main peaks found in the negative ion spectra for the HMDSO deposited film at 100 W for 60 s were m/z = 12^- (C^-), 16^- (O^-), 28^- (Si^-), 43^- ($SiCH_3^-$), 59^- ($SiC_2H_7^-$), 73^- ($SiC_3H_9^-$) and 147^- ($Si_2C_5H_{15}O^-$). In the positive ion spectra for the HMDSO vapour plasma deposited film, the main peaks were observed at m/z = 12^+ (C^+), 16^+ (O^+), 28^+ (Si^+), 43^+ ($SiCH_3^+$), 56^+ ($SiC_2H_4^+$) and 73^+ ($SiC_3H_9^+$). The SIMS analysis confirmed the surface to be composed of silicon, carbon and oxygen fragments, with the peaks being typical with that of a polydimethylsiloxane spectra.[145] The findings were consistent with the XPS spectra from Figure 7-12, with all peaks representing fragments of the HMDSO monomer structure. The spectra obtained for the pure HMDSO vapour plasma deposited films were generally clean, with low levels of fragmentation, indicating that the main HMDSO structures were well preserved when grafted to the nylon 6 substrates. The peaks showing the $SiCH_3$, SiC_2H_4, SiC_2H_7 and SiC_3H_9 fragments accounted for the hydrophobic properties of the films, due to the non-polar Si-CH_3 bonds that have the effect of lowering the surface energy.

In comparison, the negative ion spectra for the HMDSO:O_2 deposited film showed major peaks at m/z = 12^- (C^-), 16^- (O^-), 28^- (Si^-), 43^- ($SiCH_3^-$), 59^- ($SiC_2H_7^-$), 60^- (SiO_2^-), 73^- ($SiC_3H_9^-$), 96^- ($SiO_4H_4^-$) and 147^- ($Si_2C_5H_{15}O^-$). The positive ion spectra had peaks at m/z = 16^+ (O^+), 28^+ (Si^+), 43^+ ($SiCH_3^+$), 56^+ ($SiC_2H_4^+$) and 73^+ ($SiC_3H_9^+$). Many of the peaks were identical to the pure HMDSO vapour deposited samples, but with new peaks in the negative ion spectra at 60^- (SiO_2^-) and 96^- ($SiO_4H_4^-$). These peaks confirmed that the oxygen plasma species had undergone oxidative reactions with the HMDSO plasma species, resulting in the siloxane structures being formed as quartz-like deposits. These oxidative reactions ultimately resulted in the deposited films having hydrophilic character. The spectra also showed an increased degree of fragmentation of the HMDSO:O_2 deposited films, particularly in the negative ion spectra. This was due to the oxidative reactions between the oxygen and HMDSO radical species, which led directly to an increase in the extent of fragmentation. As the treatments were undertaken at a plasma

power of 100 W, the energy was sufficient induce the ion bombardment of the oxygen species, breaking up the HMDSO units both in the gaseous phase, and following deposition onto the substrate. The peak at 60 Da in Figure 7-15b confirmed the presence of SiO_2 deposits seen earlier in the XPS measurements in Figure 7-13, explaining the increase hydrophilic character of the deposited films compared to the hydrophobic HMDSO vapour deposited films. The main structures of the fragments obtained from analysis of the polymer films for both HMDSO and HMDSO:O_2 grafted structures are shown in Figure 7-16.

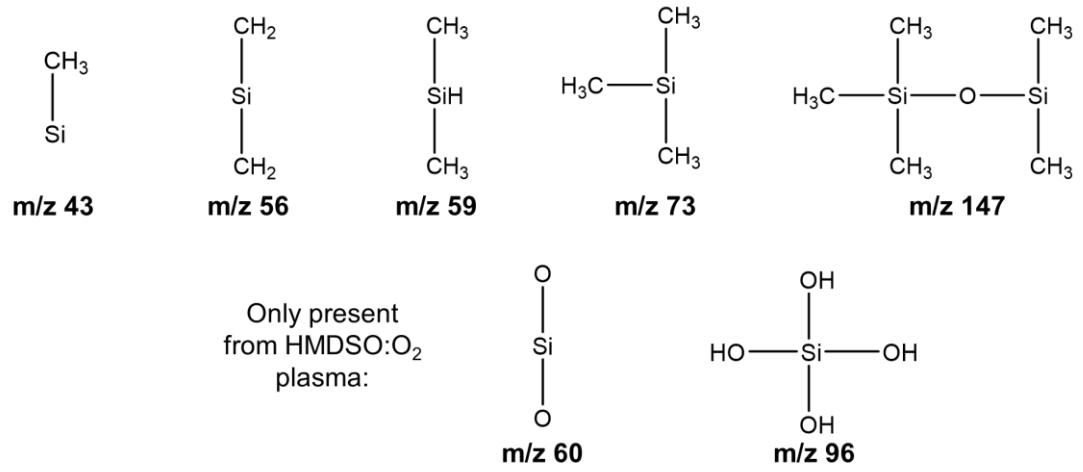

Figure 7-16. The chemical structures of the main ions found in the negative and positive SIMS spectra for the nylon 6 and regenerated cellulose samples treated with HMDSO and HMDSO:O_2 plasma.

The SIMS spectra for the HMDSO and HMDSO:O_2 plasma deposited films on regenerated cellulose substrates are displayed in Figure 7-17. The spectra obtained were nearly identical to those of the films grafted onto nylon 6 substrates, with the main peaks found in the negative ion spectra for the HMDSO deposited films found at m/z = 12^- (C^-), 16^- (O^-), 28^- (Si^-), 43^- ($SiCH_3^-$), 59^- ($SiC_2H_7^-$), 73^- ($SiC_3H_9^-$), and 147^- ($Si_2C_5H_{15}O^-$). The positive ion spectra had major peaks at m/z = 12^+ (C^+), 16^+ (O^+), 28^+ (Si^+), 43^+ ($SiCH_3^+$), 56^+ ($SiC_2H_4^+$) and 73^+ ($SiC_3H_9^+$). Again, clean spectra were obtained with minimal fragmentation, indicating that the HMDSO structures were well retained, with non-polar Si-CH_3 groups being responsible for the hydrophobic characteristics of the films.

Similarly, the SIMS spectra for the HMDSO:O_2 deposited films on regenerated cellulose had the same major peaks as the films deposited on nylon 6 substrates. The negative ion spectra for the HMDSO:O_2 deposited film showed major peaks at m/z = 12^- (C^-), 16^- (O^-), 28^- (Si^-), 43^- ($SiCH_3^-$), 59^- ($SiC_2H_7^-$), 60^- (SiO_2^-), 73^- ($SiC_3H_9^-$) and 147^- ($Si_2C_5H_{15}O^-$). The positive ion spectra had peaks at m/z = 12^+ (C^+), 16^+ (O^+), 28^+ (Si^+), 43^+ ($SiCH_3^+$), 56^+ ($SiC_2H_4^+$) and 73^+ ($SiC_3H_9^+$).

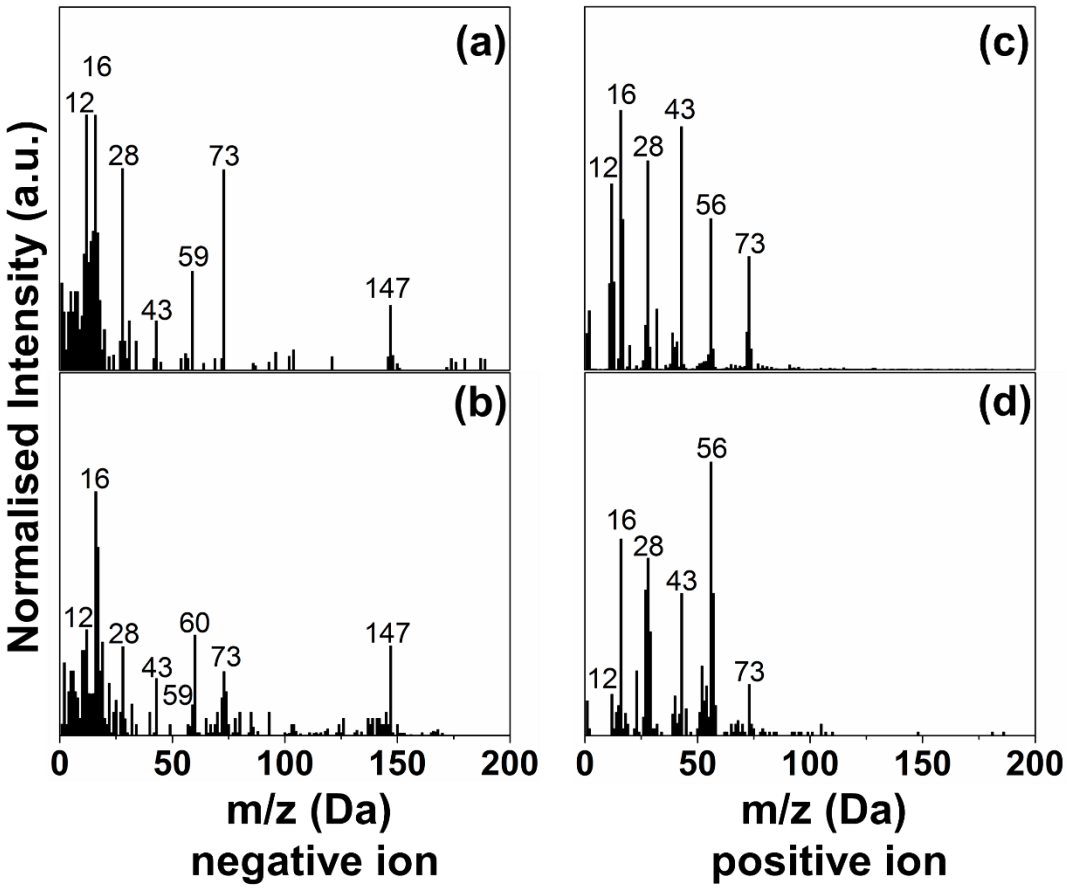

Figure 7-17. SIMS negative ion spectrum of plasma treated regenerated cellulose for 600 s at 100 W for (a) pure HMDSO deposited film and (b) HMDSO:O_2 deposited film. SIMS positive ion spectrum for (c) pure HMDSO deposited film and (d) HMDSO:O_2 deposited film.

Again, the inclusion of oxygen in the plasma feed resulted in oxidative reactions through collisions between the oxygen radical species and the HMDSO moieties, forming oligomeric deposits with polar oxygen groups, resulting in hydrophilic films being obtained. The chemical structure of the substrate did not appear to have a significant impact on the resultant structures of the deposited films, confirming that the deposition of films using both HMDSO and HMDSO:O_2 plasmas was a substrate-independent process on the nylon 6 and regenerated cellulose surfaces.

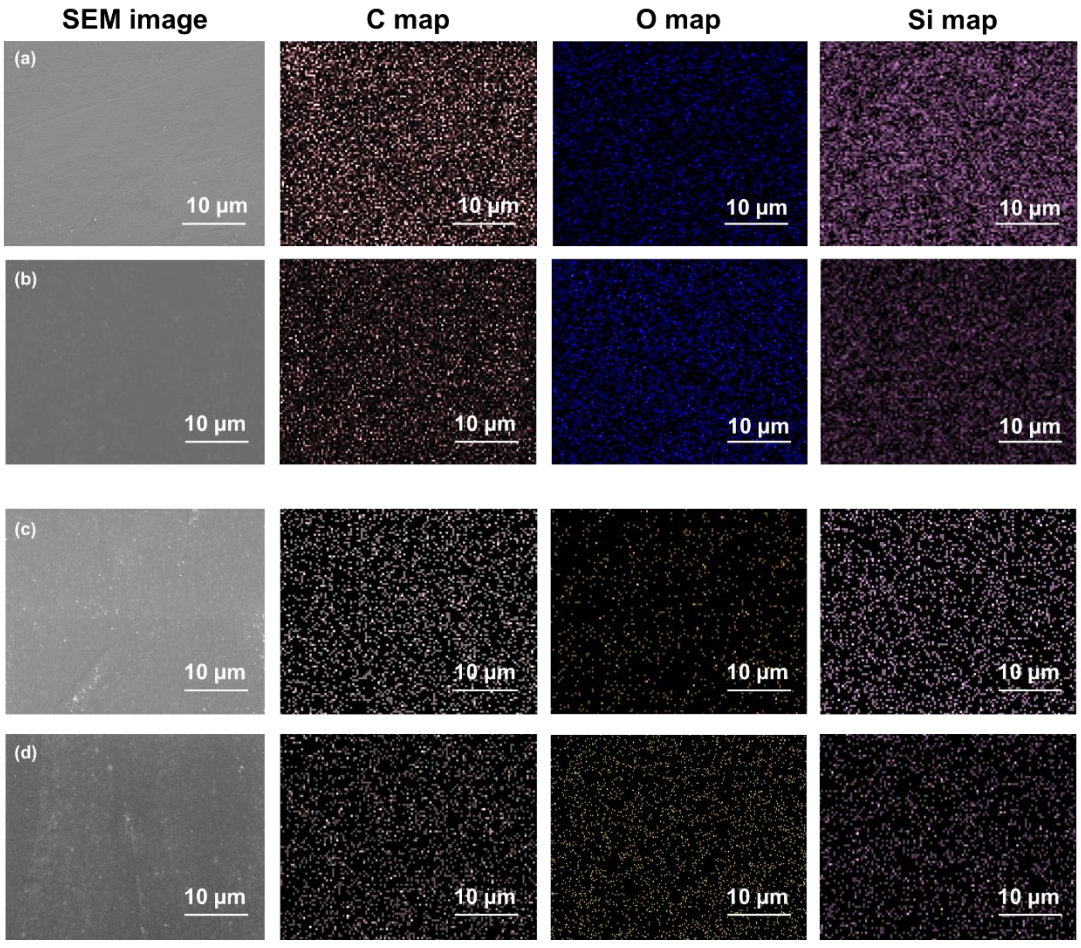

Figure 7-18. EDX maps of elemental carbon, oxygen and silicon for: (a) deposited HMDSO films on nylon 6; (b) deposited HMDSO:O_2 films on nylon 6; (c) deposited HMDSO films on regenerated cellulose and (d) deposited HMDSO:O_2 films on regenerated cellulose.

The EDX maps shown in Figure 7-18 show the elemental distributions of carbon, oxygen and silicon across the polymer surfaces, providing insight into the homogeneity of the deposited films. Firstly, focussing on the elemental

silicon is useful as a marker in identifying the presence of the plasma-enhanced chemical-vapour deposited siloxane films. In each of the samples, the elemental silicon was distributed quite evenly across the polymer surface image. The same even distribution was seen with the carbon and oxygen elemental at%, suggesting that the films were homogenous in structure across the 10 × 10 µm area. There was also a small level of nitrogen found across each of the samples that was attributed to contamination. To confirm that the carbon and oxygen groups were from the deposited siloxane films, and not the native nylon 6 and regenerated cellulose materials, the mapped surface elemental compositions presented in Table 7-4 were assessed.

Table 7-4. Surface elemental compositions obtained from the EDX mapping of the deposited HMDSO and HMDSO:O_2 films on nylon 6 and regenerated cellulose substrates for 600 s at 100 W.

		Mapped surface elemental composition (%)			
	Treatment	**Carbon**	**Oxygen**	**Silicon**	**Nitrogen**
Nylon 6	**HMDSO**	61	11	25	3
	HMDSO:O_2	49	29	16	6
Regenerated cellulose	**HMDSO**	64	7	28	1
	HMDSO:O_2	45	35	17	3

The mapped surface elemental compositions of the films corroborated the data from the XPS elemental compositions shown earlier in Table 7-3, confirming that the pure HMDSO vapour plasma-deposited films generally had higher concentrations of carbon on the surface (61% for nylon 6 and 64% for regenerated cellulose respectively), due to the presence of non-polar Si-CH_3 groups. Additionally, the lower levels of surface oxygen obtained in the pure HMDSO films were also shown from the EDX mapping, due to the lack of oxidative reactions occurring in the absence of oxygen plasma species. The EDX also confirmed that the compositions of both HMDSO and HMDSO:O_2 films were similar on both nylon 6 and regenerated cellulose structures, showing that the choice of precursor gases used was the predominant factor

that affected the resultant films obtained, rather than the choice of substrate. The data did diverge slightly from the XPS elemental compositions obtained through multiple point analysis, particularly with the underreporting of surface oxygen content in the pure HMDSO deposited films. The mapped elemental surface compositions obtained can be considered as non-standardised, semi-quantitative data, primarily because the data was being used to verify the XPS and SIMS analysis through showing the relative at% of each element, and also due to a range of factors that cause variation in the measurements. These included the polymer films and substrates being susceptible to beam damage from the electron beam, and EDX generally having poor accuracy for light elements such as oxygen, due to lighter ions being difficult to ionise and generate a characteristic X-ray, meaning a weak signal is obtained, with limited sensitivity.[146] The EDX analysis was primarily used as a complimentary analytical technique in conjunction with the XPS and SIMS data, and was able to verify the presence of evenly distributed siloxane polymer films. The EDX data also confirmed that the HMDSO:O_2 plasma deposited samples had an increased surface oxygen content compared to the pure HMDSO vapour deposited samples. Such an increase in polar oxygen content helped to rationalise the contact angle measurements discussed earlier in Section 7.1.2.

7.2 Conclusions

This chapter has explored the grafting of silicon-based polymer nanofilms onto nylon 6 and regenerated cellulose substrates through plasma-enhanced chemical vapour deposition utilising pure HMDSO vapour and HMDSO:O_2 (1:6) plasmas. Gravimetric measurements showed the linear relationship of the mass of polymer deposited with increasing plasma treatment time, due to the increasing film thicknesses. Contact angle measurements were then employed to show the increase in hydrophobicity/decrease in surface free energy of the substrates following deposition of the siloxane films. It was found that films deposited using HMDSO vapour plasma had low surface energies, with high degrees of hydrophobicity, while the HMDSO:O_2 plasma deposited films were slightly hydrophilic (although substantially less wettable than the

original nylon 6 and regenerated cellulose surfaces). Morphological assessments through SEM and AFM imaging showed that the pure HMDSO grafted films were generally smooth, while the HMDSO:O_2 films had a comparatively large surface roughness, in part due to the etching of the substrate from the oxygen component of the gaseous plasma mixture. Additionally, due to the oxygen plasma species bombarding the HMDSO monomer units, the deposited HMDSO:O_2 films largely consisted of quartz-like structures, rather than a smooth continuous PDMS-like film that was obtained from HMDSO vapour. Cross-sectional SEM imaging also enabled the film thicknesses of the grafted films to be determined, with film thickness increasing with treatment time. The surface-chemical properties of the films were investigated using XPS and SSIMS analysis, with the data showing that the HMDSO deposited films retained a high degree of the original monomer structure, with little fragmentation, resulting in the deposition of continuous polymer films with a large number of non-polar Si-CH_3 groups. On the other hand, the HMDSO:O_2 films had a higher degree of fragmentation, with a larger quantity of low molecular weight species being deposited on the surface with polar oxygen-containing groups, hence accounting for the hydrophilic properties of the films. EDX mapping confirmed that the films produced were evenly distributed across the surface, with the HMDSO:O_2 having a larger concentration of surface oxygen. The versatility of plasma-enhanced chemical vapour deposition was demonstrated in this chapter, through showcasing the capabilities of plasma to tailor specific surface properties of grafted films through carefully selecting appropriate precursor gases with specific functional properties (such as hydrophobicity or hydrophilicity in the case of HMDSO and HMDSO:O_2).

8. Conclusions and Future Work

The research presented in this thesis has investigated three plasma processes, namely plasma activation, plasma etching and plasma-enhanced chemical vapour deposition, with nylon 6 plastic sheets and regenerated cellulose films being studied as model surfaces that were exposed to the plasma. The phenomenon of ageing of the plasma treated polymer samples was also explored.

To study the plasma activation of nylon 6 and regenerated cellulose samples, a series of reproducible conditions were identified to activate the surfaces using a simple, commercially available low-pressure plasma system, without altering the surface roughness or morphology of the substrates. These treatments were carried out using low frequency (40 kHz) oxygen plasma, for treatment times between 10 and 60 s at 10 W. It was found that plasma activation increased the hydrophilicity of the nylon 6 surfaces, with increasing treatment time also enhancing such an increase. The increase in hydrophilicity of the substrates was attributed entirely to a surface-chemical change, with the oxygen plasma increasing the number of attached polar functional groups (C=O, COOH, C-OH). Nylon 6 samples had a much larger increase in the quantity of polar oxygen-containing groups compared to the regenerated cellulose samples that only saw a small increase in wettability.

The surface-chemical and morphological effects of plasma etching on nylon 6 and regenerated cellulose substrates were studied, again utilising a low-frequency, low-pressure oxygen plasma, with treatment times ranging from 30 to 600 s at 60 W. It was found that under these conditions, the plasma had a nanotexturing ability that increased wettability of both nylon 6 and regenerated cellulose polymers, primarily through increasing the surface area of the substrates though plasma etching. Such an etching effect was characterised through gravimetry, SEM and AFM imaging. The effect was slight following shorter treatment times (30 s), but increased with increasing treatment time, with the longer treatments resulting in a substantial degree of mass loss from

the surfaces of the samples. Through surface-chemical analyses, it was found that the nylon 6 samples had increased degrees of functionalisation after shorter treatment times (30 s at 60 W), but this decreased between 120 s and 600 s of plasma exposure, with a reduced extent of functionalisation. In comparison, the regenerated cellulose samples saw a general increase in the amount of surface functionalisation through the increase in surface-oxygen content with increasing plasma treatment time. For both polymers, the plasma etching process resulted in a synergistic increase in the presence of polar functionalities (including C=O, COOH, C-OH), with a combined increase in surface roughness through particle bombardment of the plasma species onto the surfaces.

Following the earlier investigations into plasma activation and etching, the subsequent ageing of the oxygen plasma activated and etched polymer samples was studied, primarily through the use of static contact angle measurements. The plasma activated nylon 6 samples showed an initial rapid hydrophobic recovery after being exposed to air over a period of 5 days, which then levelled off into a gradual recovery up to 20 days. Each of the plasma activated nylon samples did not fully revert to their original surface wettability, confirming that there was a degree of permanence that was induced by the attachment of polar groups. In comparison, the plasma activated regenerated cellulose samples had a rapid hydrophobic recovery after 1 day that resulted in all of the samples reverting back to the original untreated surface wettability, suggesting there was no permanent change induced in the plasma activation of cellulose. Both of the oxygen plasma etched materials had slight hydrophobic recoveries, but the contact angle values remained substantially lower than the original untreated materials, due to the large permanent increase in surface area/roughness induced by the etching of the plasma. XPS analysis was used to rationalise the ageing of the samples, and confirmed that the decrease in O/C ratio was primarily responsible for the hydrophobic recoveries. Different modes of storage of the samples were also investigated and compared to the samples stored in air post-plasma treatment. Both the nylon 6 and regenerated cellulose samples were stored under vacuum, with the nylon 6 samples also being stored in deionised water. The findings suggested that vacuum storage substantially hindered the ageing process of

both materials. This was attributed to the limited chain mobility of the polymer chains under vacuum. Storage in deionised water also reduced the ageing, due to the water molecules keeping the newly-formed polar groups at the surface of the polymers, but this reduction in ageing was to a lesser extent compared to the vacuum storage.

The process of plasma-enhanced chemical vapour deposition was explored through the treatment of nylon 6 and regenerated cellulose substrates using HMDSO precursor monomers, and HMDSO:O_2 (1:6) gaseous mixtures. Both plasmas deposited siloxane films, with the film thickness of the deposits increasing with increasing treatment time. The HMDSO vapour-deposited films significantly increased the hydrophobicity of the nylon 6 and regenerated cellulose substrates to a similar extent after 600 s of plasma exposure at 100 W. The HMDSO:O_2 films also increased the hydrophobicity of the substrates, but were still slightly hydrophilic in character, owing to a larger oxygen content compared to the pure HMDSO vapour deposited films. Morphological analyses showed that the pure HMDSO deposited films were generally smooth, while the HMDSO:O_2 films had a larger surface roughness that was attributed to etching from the oxygen radical plasma species. Surface-chemical analyses of the deposited films found that the HMDSO films formed structures similar to polydimethylsiloxane, with retention of a large number of non-polar Si-CH_3 groups. In comparison, the HMDSO:O_2 films had a number of quartz-like SiO_2 structures, with the oxygen plasma species increasing the degree of fragmentation of the HMDSO monomer molecules. Generally, it was found that both plasmas deposited films uniformly across the nylon and cellulose substrates, through a substrate-independent plasma-enhanced deposition process.

There are several different research strategies that could be utilised in future work relating to the studies presented in this thesis. In terms of expanding the specific study of the low-frequency, low-pressure oxygen plasma treatment of nylon 6 and regenerated cellulose polymers, further surface characterisation could be undertaken using atomic force microscope infrared spectroscopy

(AFM-IR) analysis. This analysis has much greater sensitivity than traditional FTIR, and would enable the surface-chemical functionalities formed on the nanoscale to be determined and mapped, developing further the insights obtained from the multiple-point XPS analysis into the uniformity of the plasma treatments. It would also be useful to progress the current study from model surfaces such as plastic sheets and polymer films onto textile materials, to observe how the plasma-induced surface modifications differ on substrates with similar surface chemistry, but different morphologies. Additionally, through using the range of analytical techniques exploited in this thesis, it would be appropriate to expand the study to a range of different polymers with different structural features, to investigate the compatibility of different structures in being functionalised/etched with oxygen plasma. Such polymers could include the fluoropolymer poly(tetrafluoroethylene) (PTFE), or the polyester PET to investigate the effects of ester linkages and aromaticity.

From a general perspective, an important development and challenge in the research of functional plasma treatments for polymers will involve determining the order in which specific functional groups are formed on polymer surfaces when exposed to plasma. There have been some reported simulations of polymer surface/plasma interactions that have been used to postulate mechanisms for plasma-induced surface functionalisation[147-148], but there is a further need to provide empirical evidence for the functionalisation process. To provide experimental evidence for the different stages of surface functionalisation, there will be a requirement for *in-situ* XPS and SIMS analysis, to monitor the process in real-time. This will require complex experimental setups in which the plasma chamber is attached to these ultra-high-vacuum analytical systems for in-line analysis, but will solve a major problem in determining the mechanisms of surface functionalisation with plasma, completely removing the post-oxidation reactions from the treatment process.

9. References

1. Palaskar, S. S.; Desai, A. N.; Shukla, S. R., Plasma induced nano-finish for multifunctional properties on cotton fabric. *Indian J. Fibre Text. Tes.* **2016,** *41* (3), 325-330.

2. Holmquist, H.; Schellenberger, S.; van der Veen, I.; Peters, G. M.; Leonards, P. E. G.; Cousins, I. T., Properties, performance and associated hazards of state-of-the-art durable water repellent (DWR) chemistry for textile finishing. *Environment International* **2016,** *91*, 251-264.

3. Vetter, J.; Barbezat, G.; Crummenauer, J.; Avissar, J., Surface treatment selections for automotive applications. *Surface and Coatings Technology* **2005,** *200* (5), 1962-1968.

4. Pankaj, S. K.; Bueno-Ferrer, C.; Misra, N. N.; Milosavljević, V.; O'Donnell, C. P.; Bourke, P.; Keener, K. M.; Cullen, P. J., Applications of cold plasma technology in food packaging. *Trends in Food Science & Technology* **2014,** *35* (1), 5-17.

5. Tippayawong, N.; Khongkrapan, P., Development of a laboratory scale air plasma torch and its application to electronic waste treatment. *International Journal of Environmental Science & Technology* **2009,** *6* (3), 407-414.

6. Stegmaier, T.; Dinkelmann, A.; Von Arnim, V.; Rau, A., 5 - Corona and dielectric barrier discharge plasma treatment of textiles for technical applications. In *Plasma Technologies for Textiles*, Shishoo, R., Ed. Woodhead Publishing: 2007; pp 129-157.

7. Pezzella, C.; Giacobbe, S.; Giacobelli, V. G.; Guarino, L.; Kylic, S.; Sener, M.; Sannia, G.; Piscitelli, A., Green routes towards industrial textile dyeing: A laccase based approach. *Journal of Molecular Catalysis B: Enzymatic* **2016,** *134*, 274-279.

8. Aslanidou, D.; Karapanagiotis, I.; Panayiotou, C., Superhydrophobic, superoleophobic coatings for the protection of silk textiles. *Progress in Organic Coatings* **2016,** *97*, 44-52.

9. Szulc, J.; Urbaniak-Domagała, W.; Machnowski, W.; Wrzosek, H.; Łącka, K.; Gutarowska, B., Low temperature plasma for textiles disinfection. *International Biodeterioration & Biodegradation* **2018,** *131,* 97-106.

10. Kale, K. H.; Desai, A., Atmospheric pressure plasma treatment of textiles using non-polymerising gases. *Indian Journal of Fibre & Textile Research* **2011,** *36,* 289-299.

11. Morent, R.; De Geyter, N.; Verschuren, J.; De Clerck, K.; Kiekens, P.; Leys, C., Non-thermal plasma treatment of textiles. *Surface and Coatings Technology* **2008,** *202* (14), 3427-3449.

12. Zille, A.; Oliveira, F. R.; Souto, A. P., Plasma Treatment in Textile Industry. *Plasma Processes and Polymers* **2015,** *12* (2), 98-131.

13. Hochart, F.; De Jaeger, R.; Levalois-Grützmacher, J., Graft-polymerization of a hydrophobic monomer onto PAN textile by low-pressure plasma treatments. *Surface and Coatings Technology* **2003,** *165* (2), 201-210.

14. Novák, I.; Pollak, V.; Chodák, I., Study of surface properties of polyolefins modified by corona discharge plasma. *Plasma Processes and Polymers* **2006,** *3* (4-5), 355-364.

15. Cui, N.-Y.; Brown, N. M., Modification of the surface properties of a polypropylene (PP) film using an air dielectric barrier discharge plasma. *Applied surface science* **2002,** *189* (1), 31-38.

16. Vesel, A.; Mozetic, M., New developments in surface functionalization of polymers using controlled plasma treatments. *Journal of Physics D: Applied Physics* **2017,** *50* (29), 293001.

17. Vesel, A.; Mozetic, M.; Balat-Pichelin, M., Oxygen atom density in microwave oxygen plasma. *Vacuum* **2007,** *81* (9), 1088-1093.

18. Ionin, A. A.; Kochetov, I. V.; Napartovich, A. P.; Yuryshev, N. N., Physics and engineering of singlet delta oxygen production in low-temperature plasma. *Journal of Physics D: Applied Physics* **2007,** *40* (2), 25-61.

19. Vialle, M.; Touzeau, M.; Gousset, G., Kinetics of O(1S) and O(1D) metastable atoms in a DC oxygen glow discharge. *Journal of Physics D: Applied Physics* **1991,** *24* (3), 301-308.

20. Baklanov, A. V.; Janssen, L. M. C.; Parker, D. H.; Poisson, L.; Soep, B.; Mestdagh, J.-M.; Gobert, O., Direct mapping of recoil in the ion-pair dissociation of molecular oxygen by a femtosecond depletion method. **2008,** *129* (21), 214306.

21. Steffen, T. T.; Fontana, L. C.; Nahorny, J.; Becker, D., Role of nitrogen–oxygen plasma functionalization of carbon nanotubes in epoxy nanocomposites. **2019,** *40* (2), 1162-1171.

22. Dorai, R.; Kushner, M. J., A model for plasma modification of polypropylene using atmospheric pressure discharges. *Journal of Physics D: Applied Physics* **2003,** *36* (6), 666-685.

23. Greb, A.; Niemi, K.; O'Connell, D.; Gans, T., The influence of surface properties on the plasma dynamics in radio-frequency driven oxygen plasmas: Measurements and simulations. **2013,** *103* (24), 244101.

24. Yan, X.; Lin, Y.; Huang, R.; Hang, W.; Harrison, W. W., A spectroscopic investigation of the afterglow and recombination process in a microsecond pulsed glow discharge. *Journal of Analytical Atomic Spectrometry* **2010,** *25* (4), 534-543.

25. Taylor, K. J.; Tynan, G. R., Control of dissociation by varying oxygen pressure in noble gas admixtures for plasma processing. *Journal of Vacuum Science & Technology A* **2005,** *23* (4), 643-650.

26. Lu, X.; Laroussi, M.; Puech, V., On atmospheric-pressure non-equilibrium plasma jets and plasma bullets. *Plasma Sources Science and Technology* **2012,** *21* (3), 034005.

27. McCord, M. G.; Hwang, Y. J.; Hauser, P. J.; Qiu, Y.; Cuomo, J. J.; Hankins, O. E.; Bourham, M. A.; Canup, L. K., Modifying Nylon and Polypropylene Fabrics with Atmospheric Pressure Plasmas. **2002,** *72* (6), 491-498.

28. Modic, M.; Junkar, I.; Vesel, A.; Mozetic, M., Aging of plasma treated surfaces and their effects on platelet adhesion and activation. *Surface and Coatings Technology* **2012,** *213*, 98-104.

29. Gorenšek, M.; Gorjanc, M.; Bukošek, V.; Kovač, J.; Jovančić, P.; Mihailović, D., Functionalization of PET Fabrics by Corona and Nano Silver. **2010,** *80* (3), 253-262.

30. Vesel, A.; Primc, G.; Zaplotnik, R.; Mozetič, M., Applications of highly non-equilibrium low-pressure oxygen plasma for treatment of polymers and polymer composites on an industrial scale. *Plasma Physics and Controlled Fusion* **2020,** *62* (2), 024008.

31. Fu, R.; Yang, Y.; Lu, C.; Ming, Y.; Zhao, X.; Hu, Y.; Zhao, L.; Hao, J.; Chen, W., Large-Scale Fabrication of High-Performance Ionic Polymer–Metal Composite Flexible Sensors by in Situ Plasma Etching and Magnetron Sputtering. *ACS Omega* **2018,** *3* (8), 9146-9154.

32. Lei, M. K.; Liu, Y.; Li, Y. P., Controllable wettability of poly(ethylene terephthlate) film modified by oxygen combined inductively and capacitively coupled radio-frequency plasma. *Applied Surface Science* **2011,** *257* (16), 7350-7358.

33. Iza, F.; Hopwood, J., Influence of operating frequency and coupling coefficient on the efficiency of microfabricated inductively coupled plasma sources. *Plasma Sources Science and Technology* **2002,** *11* (3), 229-235.

34. Dave, H.; Ledwani, L.; Nema, S. K., 8 - Nonthermal plasma: A promising green technology to improve environmental performance of textile industries. In *The Impact and Prospects of Green Chemistry for Textile Technology*, Shahid ul, I.; Butola, B. S., Eds. Woodhead Publishing: 2019; pp 199-249.

35. Zille, A., 6 - Plasma technology in fashion and textiles. In *Sustainable Technologies for Fashion and Textiles*, Nayak, R., Ed. Woodhead Publishing: 2020; pp 117-142.

36. Ven, E. P. v. d.; Connick, I.; Harrus, A. S. In *Advantages of dual frequency PECVD for deposition of ILD and passivation films*, Seventh International IEEE Conference on VLSI Multilevel Interconnection, 12-13 June 1990; 1990; pp 194-201.

37. Wieland, F.; Bruch, R.; Bergmann, M.; Partel, S.; Urban, G. A.; Dincer, C., Enhanced Protein Immobilization on Polymers—A Plasma Surface Activation Study. **2020,** *12* (1), 104.

38. Siciński, M.; Bieliński, D. M.; Szymanowski, H.; Gozdek, T.; Piątkowska, A., Low-temperature plasma modification of carbon nanofillers for improved performance of advanced rubber composites. *Polymer Bulletin* **2020,** *77* (2), 1015-1048.

39. Cireli, A.; Kutlu, B.; Mutlu, M., Surface modification of polyester and polyamide fabrics by low frequency plasma polymerization of acrylic acid. *Journal of Applied Polymer Science* **2007,** *104* (4), 2318-2322.

40. Peran, J.; Ercegović Ražić, S.; Sutlović, A.; Ivanković, T.; Glogar, M. I., Oxygen plasma pretreatment improves dyeing and antimicrobial properties of wool fabric dyed with natural extract from pomegranate peel. *Coloration Technology* **2020,** *136* (2), 177-187.

41. Liston, E. M.; Martinu, L.; Wertheimer, M. R., Plasma surface modification of polymers for improved adhesion: a critical review. *Journal of Adhesion Science and Technology* **1993,** *7* (10), 1091-1127.

42. Schutze, A.; Jeong, J. Y.; Babayan, S. E.; Jaeyoung, P.; Selwyn, G. S.; Hicks, R. F., The atmospheric-pressure plasma jet: a review and comparison to other plasma sources. *IEEE Transactions on Plasma Science* **1998,** *26* (6), 1685-1694.

43. Bárdos, L.; Baránková, H., Cold atmospheric plasma: Sources, processes, and applications. *Thin Solid Films* **2010,** *518* (23), 6705-6713.

44. Hall, J. R.; Westerdahl Carolyn, A. L.; Bodnar Michael, J.; Levi David, W., Effect of activated gas plasma treatment time on adhesive bondability of polymers. *Journal of Applied Polymer Science* **1972,** *16* (6), 1465-1477.

45. Goossens, O.; Dekempeneer, E.; Vangeneugden, D.; Van de Leest, R.; Leys, C., Application of atmospheric pressure dielectric barrier discharges in deposition, cleaning and activation. *Surface and Coatings Technology* **2001,** *142-144*, 474-481.

46. Homola, T.; Matoušek, J.; Hergelová, B.; Kormunda, M.; Wu, L. Y. L.; Černák, M., Activation of poly(ethylene terephthalate) surfaces by atmospheric pressure plasma. *Polymer Degradation and Stability* **2012,** *97* (11), 2249-2254.

47. Vesel, A.; Zaplotnik, R.; Primc, G.; Mozetič, M., Evolution of the Surface Wettability of PET Polymer upon Treatment with an Atmospheric-Pressure Plasma Jet. *Polymers* **2020,** *12* (1), 87.

48. Pykönen, M.; Sundqvist, H.; Kaukoniemi, O.-V.; Tuominen, M.; Lahti, J.; Fardim, P.; Toivakka, M., Ageing effect in atmospheric plasma activation of paper substrates. *Surface and Coatings Technology* **2008,** *202* (16), 3777-3786.

49. Kühn, G.; Weidner, S.; Decker, R.; Ghode, A.; Friedrich, J., Selective surface functionalization of polyolefins by plasma treatment followed by chemical reduction. *Surface and Coatings Technology* **1999,** *116-119*, 796-801.

50. Gross, T.; Lippitz, A.; Unger, W. In *Improvement in polymer adhesivity by low and normal pressure plasma*, Surface & Coatings Technology: Papers Presented at the Third International Conference on Plasma Surface Engineering, Garmisch-Partenkirchen, Germany, October 26–29, 1992, Elsevier: 2016; pp 371-378.

51. Cardinaud, C.; Peignon, M.-C.; Tessier, P.-Y., Plasma etching: principles, mechanisms, application to micro- and nano-technologies. *Applied Surface Science* **2000,** *164* (1), 72-83.

52. Nabesawa, H.; Hiruma, T.; Hitobo, T.; Wakabayashi, S.; Asaji, T.; Abe, T.; Seki, M., Low-pressure plasma-etching of bulk polymer materials using gas mixture of CF4 and O2. *AIP Advances* **2013,** *3* (11), 112105.

53. Collaud Coen, M.; Lehmann, R.; Groening, P.; Schlapbach, L., Modification of the micro- and nanotopography of several polymers by plasma treatments. *Applied Surface Science* **2003,** *207* (1), 276-286.

54. Nageswaran, G.; Jothi, L.; Jagannathan, S., Chapter 4 - Plasma Assisted Polymer Modifications. In *Non-Thermal Plasma Technology for Polymeric Materials*, P., Eds. Elsevier: 2019; pp 95-127.

55. Hegemann, D.; Michlíček, M.; Blanchard, N. E.; Schütz, U.; Lohmann, D.; Vandenbossche, M.; Zajíčková, L.; Drábik, M., Deposition of Functional Plasma Polymers Influenced by Reactor Geometry in Capacitively Coupled Discharges. *Plasma Processes and Polymers* **2016,** *13* (2), 279-286.

56. Egitto, F. D., Plasma etching and modification of organic polymers. *Pure and Applied Chemistry* **1990,** *62* (9), 1699-1708.

57. Wavhal Dattatray, S.; Zhang, J.; Steen Michelle, L.; Fisher Ellen, R., Investigation of Gas Phase Species and Deposition of SiO2 Films from HMDSO/O2 Plasmas. *Plasma Processes and Polymers* **2006,** *3* (3), 276-287.

58. Cho, S. C.; Hong, Y. C.; Cho, S. G.; Ji, Y. Y.; Han, C. S.; Uhm, H. S., Surface modification of polyimide films, filter papers, and cotton clothes by HMDSO/toluene plasma at low pressure and its wettability. *Current Applied Physics* **2009,** *9* (6), 1223-1226.

59. Kale, K. H.; Palaskar, S., Atmospheric pressure plasma polymerization of hexamethyldisiloxane for imparting water repellency to cotton fabric. *Textile Research Journal* **2010,** *81* (6), 608-620.

60. Shi, D.; He, P.; Lian, J.; Wang, L.; van Ooij, W. J., Plasma deposition and characterization of acrylic acid thin film on ZnO nanoparticles. *Journal of Materials Research* **2011,** *17* (10), 2555-2560.

61. Hegemann, D.; Vohrer, U.; Oehr, C.; Riedel, R., Deposition of SiOx films from O2/HMDSO plasmas. *Surface and Coatings Technology* **1999,** *116-119*, 1033-1036.

62. Rani, k. V.; Chandwani, N.; Kikani, P.; Nema, S. K.; Sarma, A. K.; Sarma, B., hydrophobic surface modification of silk fabric using plasma-polymerized HMDSO. *Surface Review & Letters* **2018,** *25* (02), 1850060.

63. Bertaux, E.; Le Marec, E.; Crespy, D.; Rossi, R.; Hegemann, D., Effects of siloxane plasma coating on the frictional properties of polyester and polyamide fabrics. *Surface and Coatings Technology* **2009,** *204* (1), 165-171.

64. Montarsolo, A.; Mossotti, R.; Innocenti, R.; Vassallo, E., A study on washing resistance of pp-HMDSO films deposited on wool fabrics for anti-pilling purposes. *Surface and Coatings Technology* **2013,** *224*, 109-113.

65. Chojnowski, J.; Rubinsztajn, S.; Wilczek, L., Acid-catalyzed condensation of model hydroxyl-terminated dimethylsiloxane oligomers - cyclization vs. linear condensation: intra-inter catalysis. *Macromolecules* **1987,** *20* (10), 2345-2355.

66. Hegemann, D., 4.09 - Plasma Polymer Deposition and Coatings on Polymers. In *Comprehensive Materials Processing*, Hashmi, S.; Batalha, G. F.; Van Tyne, C. J.; Yilbas, B., Eds. Elsevier: Oxford, 2014; pp 201-228.

67. Blanchard, N. E.; Naik, V. V.; Geue, T.; Kahle, O.; Hegemann, D.; Heuberger, M., Response of Plasma-Polymerized Hexamethyldisiloxane Films to Aqueous Environments. *Langmuir* **2015,** *31* (47), 12944-12953.

68. Hossain, M. M.; Hegemann, D.; Fortunato, G.; Herrmann, A. S.; Heuberger, M., Plasma Deposition of Permanent Superhydrophilic a-C:H:N Films on Textiles. *Plasma Processes and Polymers* **2007,** *4* (4), 471-481.

69. Palaskar, S.; Kale, K. H.; Nadiger, G. S.; Desai, A. N., Dielectric barrier discharge plasma induced surface modification of polyester/cotton blended fabrics to impart water repellency using HMDSO. *Journal of Applied Polymer Science* **2011,** *122* (2), 1092-1100.

70. Kettle, A. P.; Jones, F. R.; Alexander, M. R.; Short, R. D.; Stollenwerk, M.; Zabold, J.; Michaeli, W.; Wu, W.; Jacobs, E.; Verpoest, I., Experimental evaluation of the interphase region in carbon fibre composites with plasma polymerised coatings. *Composites Part A: Applied Science and Manufacturing* **1998,** *29* (3), 241-250.

71. Hegemann, D.; Hossain, M.-M., Influence of Non-Polymerizable Gases Added During Plasma Polymerization. *Plasma Processes and Polymers* **2005,** *2* (7), 554-562.

72. Johansson, K. S., 20 - Surface Modification of Plastics. In *Applied Plastics Engineering Handbook (Second Edition)*, Kutz, M., Ed. William Andrew Publishing: 2017; pp 443-487.

73. Mortazavi, M.; Nosonovsky, M., A model for diffusion-driven hydrophobic recovery in plasma treated polymers. *Applied Surface Science* **2012,** *258* (18), 6876-6883.

74. López-García, J., Chapter 10 - Wettability Analysis and Water Absorption Studies of Plasma Activated Polymeric Materials. In *Non-Thermal Plasma Technology for Polymeric Materials*, Eds. Elsevier: 2019; pp 261-285.

75. Perez-Roldan, M. J.; Debarnot, D.; Poncin-Epaillard, F., Processing of plasma-modified and polymer-grafted hydrophilic PET surfaces, and study of their aging and bioadhesive properties. *RSC Advances* **2014,** *4* (59), 31409-31415.

76. Mukhopadhyay, S. K., 8 - Manufacturing, properties and tensile failure of nylon fibres. In *Handbook of Tensile Properties of Textile and Technical Fibres*, Bunsell, A. R., Ed. Woodhead Publishing: 2009; pp 197-222.

77. Sastri, V. R., Chapter 7 - Engineering Thermoplastics: Acrylics, Polycarbonates, Polyurethanes, Polyacetals, Polyesters, and Polyamides. In *Plastics in Medical Devices*, Sastri, V. R., Ed. William Andrew Publishing: Boston, 2010; pp 121-173.

78. Wang, C.; Hu, F.; Yang, K.; Hu, T.; Wang, W.; Deng, R.; Jiang, Q.; Zhang, H., Preparation and properties of nylon 6/sulfonated graphene composites by an in situ polymerization process. *RSC Advances* **2016,** *6* (51), 45014-45022.

79. Pavliňák, D.; Galmiz, O.; Pavliňáková, V.; Poláček, P.; Kelar, J.; Stupavská, M.; Černák, M., Application of dielectric barrier plasma treatment in the nanofiber processing. *Materials Today Communications* **2018,** *16*, 330-338.

80. Jelil, R., A review of low-temperature plasma treatment of textile materials. *Journal of Materials Science* **2015,** *50* (18), 5913-5943.

81. Yip, J.; Chan, K.; Sin, K. M.; Lau, K. S., Low temperature plasma-treated nylon fabrics. *Journal of Materials Processing Technology* **2002,** *123* (1), 5-12.

82. Gao, Z.; Sun, J.; Peng, S.; Yao, L.; Qiu, Y., Surface modification of nylon 6 films treated with an He/O2 atmospheric pressure plasma jet. *Journal of Applied Polymer Science* **2011,** *120* (4), 2201-2206.

83. Pappas, D.; Bujanda, A.; Demaree, J. D.; Hirvonen, J. K.; Kosik, W.; Jensen, R.; McKnight, S., Surface modification of polyamide fibers and films using atmospheric plasmas. *Surface and Coatings Technology* **2006,** *201* (7), 4384-4388.

84. Choudhury, A. K. R., 10 - Sustainable chemical technologies for textile production. In *Sustainable Fibres and Textiles*, Muthu, S. S., Ed. Woodhead Publishing: 2017; pp 267-322.

85. Wang, S.; Lu, A.; Zhang, L., Recent advances in regenerated cellulose materials. *Progress in Polymer Science* **2016,** *53*, 169-206.

86. Johansson, L.-S.; Campbell, J. M.; Rojas, O. J., Cellulose as the in situ reference for organic XPS. Why? Because it works. *Surface and Interface Analysis* **2020,** *52,* 1134-1138.

87. Wu, Y.; Luo, X.; Li, W.; Song, R.; Li, J.; Li, Y.; Li, B.; Liu, S., Green and biodegradable composite films with novel antimicrobial performance based on cellulose. *Food Chemistry* **2016,** *197*, 250-256.

88. Lee, Y. J.; Lee, S. J.; Jeong, S. W.; Kim, H.-c.; Oh, T. H.; Lee, S. G. J. F.; Polymers, Structure and Mechanical Properties of Regenerated Cellulose Fibers Wet-Spun from Ionic Liquid/Cosolvent Systems. **2019,** *20* (3), 501-511.

89. Cvelbar, U.; Walsh, J. L.; Černák, M.; de Vries, H. W.; Reuter, S.; Belmonte, T.; Corbella, C.; Miron, C.; Hojnik, N.; Jurov, A.; Puliyalil, H.; Gorjanc, M.; Portal, S.; Laurita, R.; Colombo, V.; Schäfer, J.; Nikiforov, A.; Modic, M.; Kylian, O.; Polak, M.; Labay, C.; Canal, J. M.; Canal, C.; Gherardi, M.; Bazaka, K.; Sonar, P.; Ostrikov, K. K.; Cameron, D.; Thomas, S.; Weltmann, K.-D., White paper on the future of plasma science and technology in plastics and textiles. **2019,** *16* (1), 1700228.

90. Gorjanc, M.; Mozetič, M.; Vesel, A.; Zaplotnik, R., Natural dyeing and UV protection of plasma treated cotton. *The European Physical Journal D* **2018,** *72* (3), 41.

91. Bhat, N. V.; Netravali, A. N.; Gore, A. V.; Sathianarayanan, M. P.; Arolkar, G. A.; Deshmukh, R. R., Surface modification of cotton fabrics using plasma technology. *Textile Research Journal* **2011,** *81* (10), 1014-1026.

92. Inbakumar, S.; Morent, R.; De Geyter, N.; Desmet, T.; Anukaliani, A.; Dubruel, P.; Leys, C., Chemical and physical analysis of cotton fabrics plasma-treated with a low pressure DC glow discharge. *Cellulose* **2010,** *17* (2), 417-426.

93. Calvimontes, A.; Mauersberger, P.; Nitschke, M.; Dutschk, V.; Simon, F., Effects of oxygen plasma on cellulose surface. *Cellulose* **2011,** *18*, 803-809.

94. Lam, Y. L.; Kan, C. W.; Yuen, C. W., Effect of oxygen plasma pretreatment and titanium dioxide overlay coating on flame retardant finished cotton fabrics. *BioResources* **2011,** *6* (2), 1454-1474.

95. Tsafack, M.; Levalois-Grützmacher, J., Flame retardancy of cotton textiles by plasma-induced graft-polymerization (PIGP). *Surface and coatings technology* **2006,** *201* (6), 2599-2610.

96. Gürsoy, M.; Karaman, M., Hydrophobic coating of expanded perlite particles by plasma polymerization. *Chemical Engineering Journal* **2016,** *284*, 343-350.

97. Hossain, M. M.; Herrmann, A. S.; Hegemann, D., Plasma hydrophilization effect on different textile structures. *Plasma Processes and polymers* **2006,** *3* (3), 299-307.

98. Pandiyaraj, K. N.; Selvarajan, V., Non-thermal plasma treatment for hydrophilicity improvement of grey cotton fabrics. *Journal of materials processing technology* **2008,** *199* (1), 130-139.

99. Cheng, C.; Liye, Z.; Zhan, R.-J., Surface modification of polymer fibre by the new atmospheric pressure cold plasma jet. *Surface and Coatings Technology* **2006,** *200* (24), 6659-6665.

100. Samanta, K. K.; Jassal, M.; Agrawal, A. K., Improvement in water and oil absorbency of textile substrate by atmospheric pressure cold plasma treatment. *Surface and Coatings Technology* **2009,** *203* (10), 1336-1342.

101. Hong, S. M.; Kim, S. H.; Kim, J. H.; Hwang, H. I. In *Hydrophilic surface modification of PDMS using atmospheric RF plasma*, Journal of physics: conference series, IOP Publishing: 2006; p 656.

102. Sun, Y.; Sun, G., Durable and regenerable antimicrobial textile materials prepared by a continuous grafting process. *Journal of Applied Polymer Science* **2002,** *84* (8), 1592-1599.

103. Gao, Y.; Cranston, R., Recent advances in antimicrobial treatments of textiles. *Textile research journal* **2008,** *78* (1), 60-72.

104. Shahidi, S.; Rashidi, A.; Ghoranneviss, M.; Anvari, A.; Rahimi, M.; Moghaddam, M. B.; Wiener, J., Investigation of metal absorption and antibacterial activity on cotton fabric modified by low temperature plasma. *Cellulose* **2010,** *17* (3), 627-634.

105. Štular, D.; Jerman, I.; Naglič, I.; Simončič, B.; Tomšič, B., Embedment of silver into temperature- and pH-responsive microgel for the development of smart textiles with simultaneous moisture management and controlled antimicrobial activities. *Carbohydrate Polymers* **2017,** *159*, 161-170.

106. Sun, D.; Stylios, G., Effect of low temperature plasma treatment on the scouring and dyeing of natural fabrics. *Textile research journal* **2004,** *74* (9), 751-756.

107. Long, J.-J.; Xiao, G.-D.; Xu, H.-M.; Wang, L.; Cui, C.-L.; Liu, J.; Yang, M.-Y.; Wang, K.; Chen, C.; Ren, Y.-M., Dyeing of cotton fabric with a reactive disperse dye in supercritical carbon dioxide. *The Journal of Supercritical Fluids* **2012,** *69*, 13-20.

108. Yaman, N.; Özdoğan, E.; Seventekin, N.; Ayhan, H., Plasma treatment of polypropylene fabric for improved dyeability with soluble textile dyestuff. *Applied surface science* **2009,** *255* (15), 6764-6770.

109. Raffaele-Addamo, A.; Selli, E.; Barni, R.; Riccardi, C.; Orsini, F.; Poletti, G.; Meda, L.; Massafra, M. R.; Marcandalli, B., Cold plasma-induced modification of the dyeing properties of poly (ethylene terephthalate) fibers. *Applied Surface Science* **2006,** *252* (6), 2265-2275.

110. Cai, Z.; Qiu, Y.; Zhang, C.; Hwang, Y.-J.; Mccord, M., Effect of atmospheric plasma treatment on desizing of PVA on cotton. *Textile research journal* **2003,** *73* (8), 670-674.

111. Wakida, T.; Tokino, S.; Niu, S.; Lee, M.; Uchiyama, H.; Kaneko, M., Dyeing properties of wool treated with low-temperature plasma under atmospheric pressure. *Textile research journal* **1993,** *63* (8), 438-442.

112. Ren, Y.; Ding, Z.; Wang, C.; Zang, C.; Zhang, Y.; Xu, L., Influence of DBD plasma pretreatment on the deposition of chitosan onto UHMWPE fiber surfaces for improvement of adhesion and dyeing properties. *Applied Surface Science* **2017,** *396*, 1571-1579.

113. De Smet, L.; Vancoillie, G.; Minshall, P.; Lava, K.; Steyaert, I.; Schoolaert, E.; Van De Walle, E.; Dubruel, P.; De Clerck, K.; Hoogenboom, R., Plasma dye coating as straightforward and widely applicable procedure for dye immobilization on polymeric materials. *Nature Communications* **2018,** *9* (1), 1123.

114. Khelifa, F.; Ershov, S.; Habibi, Y.; Snyders, R.; Dubois, P., Free-Radical-Induced Grafting from Plasma Polymer Surfaces. *Chemical Reviews* **2016,** *116* (6), 3975-4005.

115. Vesel, A.; Semenic, T., Etching rates of different polymers in oxygen plasma. *Materiali in Tehnologije* **2012,** *46*, 227-231.

116. Garside, P.; Wyeth, P., Identification of cellulosic fibres by FTIR spectroscopy-thread and single fibre analysis by attenuated total reflectance. *Studies in Conservation* **2003,** *48* (4), 269-275.

117. Cooke, F. W.; Lemons, J. E.; Ratner, B. D., CHAPTER 1 - Properties of Materials. In *Biomaterials Science*, Ratner, B. D.; Hoffman, A. S.; Schoen, F. J.; Lemons, J. E., Eds. Academic Press: San Diego, 1996; pp 11-35.

118. Morent, R.; De Geyter, N.; Leys, C.; Gengembre, L.; Payen, E., Comparison between XPS- and FTIR-analysis of plasma-treated polypropylene film surfaces. **2008,** *40* (3-4), 597-600.

119. De Geyter, N.; Morent, R.; Leys, C., Surface characterization of plasma-modified polyethylene by contact angle experiments and ATR-FTIR spectroscopy. **2008,** *40* (3-4), 608-611.

120. Strobel, M.; Lyons Christopher, S., An Essay on Contact Angle Measurements. *Plasma Processes and Polymers* **2010,** *8* (1), 8-13.

121. Letellier, P.; Mayaffre, A.; Turmine, M., Drop size effect on contact angle explained by nonextensive thermodynamics. Young's equation revisited. *Journal of Colloid and Interface Science* **2007,** *314* (2), 604-614.

122. International, A., Standard Test Method for Corona-Treated Polymer Films Using Water Contact Angle Measurements. In *ASTM D5946-17*, West Conshohocken, 2017.

123. Wei, Q., Surface characterization of plasma-treated polypropylene fibers. *Materials Characterization* **2004,** *52* (3), 231-235.

124. Miller, J. D.; Veeramasuneni, S.; Drelich, J.; Yalamanchili, M. R.; Yamauchi, G., Effect of roughness as determined by atomic force microscopy on the wetting properties of PTFE thin films. *Polymer Engineering & Science* **1996,** *36* (14), 1849-1855.

125. Guo, D.; Xie, G.; Luo, J., Mechanical properties of nanoparticles: Basics and applications. *Journal of Physics D Applied Physics* **2014,** *47*, 3001.

126. Sun, D.; Stylios, G., Fabric surface properties affected by low temperature plasma treatment. *Journal of materials processing technology* **2006,** *173* (2), 172-177.

127. Cushman, C.; Chatterjee, S.; Major, G.; Smith, N.; Roberts, A.; Linford, M., Trends in Advanced XPS Instrumentation. 1. Overview of the Technique, Automation, High Sensitivity, Imaging, Snapshot Spectroscopy, Gas Cluster Ion Beams, and Multiple Analytical Techniques on the Instrument. *Vacuum Technology & Coating* **2016**.

128. Baer, D. R.; Thevuthasan, S., Chapter 16 - Characterization of Thin Films and Coatings. In *Handbook of Deposition Technologies for Films and Coatings (Third Edition)*, Martin, P. M., Ed. William Andrew Publishing: Boston, 2010; pp 749-864.

129. Belu, A. M.; Graham, D. J.; Castner, D. G., Time-of-flight secondary ion mass spectrometry: techniques and applications for the characterization of biomaterial surfaces. *Biomaterials* **2003,** *24* (21), 3635-3653.

130. O H Teare, D.; Schofield, W.; P Garrod, R.; P S Badyal, J., Rapid Polymer Brush Growth by TEMPO-Mediated Controlled Free-Radical Polymerization from Swollen Plasma Deposited Poly(maleic anhydride) Initiator Surfaces. *Langmuir : the ACS journal of surfaces and colloids* **2005,** *21*, 10818-24.

131. Koshy, O.; Subramanian, L.; Thomas, S., Chapter 5 - Differential Scanning Calorimetry in Nanoscience and Nanotechnology. In *Thermal and Rheological Measurement Techniques for Nanomaterials Characterization*, Elsevier: 2017; pp 109-122.

132. Millot, C.; Fillot, L.-A.; Lame, O.; Sotta, P.; Seguela, R. J. J. o. T. A.; Calorimetry, Assessment of polyamide-6 crystallinity by DSC. **2015,** *122* (1), 307-314.

133. Murthy, N. S.; Minor, H., General procedure for evaluating amorphous scattering and crystallinity from X-ray diffraction scans of semicrystalline polymers. *Polymer* **1990,** *31* (6), 996-1002.

134. Takahagi, T.; Nakayama, Y.; Soeda, F.; Ishitani, A., Effects of surface cleaning and X-ray irradiation in XPS study of polymers. **1990,** *41* (7-8), 1451-1458.

135. Chapter 3 - Material Surface Preparation Techniques. In *Adhesives Technology Handbook (Second Edition)*, Ebnesajjad, S., Ed. William Andrew Publishing: Norwich, NY, 2009; pp 37-46.

136. Hetemi, D.; Pinson, J., Surface functionalisation of polymers. *Chemical Society Reviews* **2017,** *46* (19), 5701-5713.

137. Beamson, G.; Briggs, D., *High Resolution XPS of Organic Polymers: The Scienta ESCA300 Database*. Wiley: 1992.

138. Kedare, S. B.; Singh, R. P., Genesis and development of DPPH method of antioxidant assay. *J Food Sci Technol* **2011,** *48* (4), 412-422.

139. Teng, R.; Yasuda, H.; Polymers, Ex Situ Chemical Determination of Free Radicals and Peroxides on Plasma Treated Surfaces. *Plasmas and Polymers* **2002,** *7* (1), 57-69.

140. Puliyalil, H.; Filipič, G.; Cvelbar, U., Chapter 9 - Selective Plasma Etching of Polymers and Polymer Matrix Composites. In *Non-Thermal Plasma Technology for Polymeric Materials*, Eds. Elsevier: 2019; pp 241-259.

141. Easton, C. D.; Kinnear, C.; McArthur, S. L.; Gengenbach, T. R., Practical guides for x-ray photoelectron spectroscopy: Analysis of polymers. *Journal of Vacuum Science & Technology A* **2020,** *38* (2), 023207.

142. Riccardi, C.; Barni, R.; Selli, E.; Mazzone, G.; Massafra, M. R.; Marcandalli, B.; Poletti, G., Surface modification of poly(ethylene terephthalate) fibers induced by radio frequency air plasma treatment. *Applied Surface Science* **2003,** *211* (1), 386-397.

143. Morent, R.; De Geyter, N.; Leys, C.; Gengembre, L.; Payen, E., Study of the ageing behaviour of polymer films treated with a dielectric barrier discharge in air, helium and argon at medium pressure. *Surface and Coatings Technology* **2007,** *201* (18), 7847-7854.

144. Zanini, S.; Riccardi, C.; Orlandi, M.; Esena, P.; Tontini, M.; Milani, M.; Cassio, V., Surface properties of HMDSO plasma treated polyethylene terephthalate. *Surface and Coatings Technology* **2005,** *200* (1), 953-957.

145. Alexander, M. R.; Jones, F. R.; Short, R. D., Mass Spectral Investigation of the Radio-Frequency Plasma Deposition of Hexamethyldisiloxane. *The Journal of Physical Chemistry B* **1997,** *101* (18), 3614-3619.

146. Nasrazadani, S.; Hassani, S., Chapter 2 - Modern analytical techniques in failure analysis of aerospace, chemical, and oil and gas industries. In *Handbook of Materials Failure Analysis with Case Studies from the Oil and Gas Industry*, **2016**; pp 39-54.

147. Bhoj, A. N.; Kushner, M. J., Repetitively pulsed atmospheric pressure discharge treatment of rough polymer surfaces: I. Humid air discharges. *Plasma Sources Science and Technology* **2008,** *17* (3), 035024.

148. Bès, A.; Koo, M.; Phan, T. L.; Lacoste, A.; Pelletier, J., Oxygen plasma etching of hydrocarbon-like polymers: Part I Modeling. *Plasma Processes and Polymers* **2018,** *15* (8), 1800038.